

Expanding Dimensionality in Cinema Color:  
Impacting Observer Metamerism through Multiprimary Display

---

David L. Long

September 21, 2015



Rochester Institute of Technology

R·I·T

| *College of* SCIENCE |

POCS  
MCSL

College of Science  
Program of Color Science  
Munsell Color Science Laboratory

Ph.D. Dissertation

A dissertation submitted in partial fulfillment of the  
Requirements for the degree of Doctor of Philosophy  
In the Program of Color Science

**Expanding Dimensionality in Cinema Color:  
Impacting Observer Metamerism through Multiprimary Display**

David L. Long

B.S. University of Texas at Austin, 1997

M.S. University of Rochester, 2001

September 21, 2015

Signature of the Author \_\_\_\_\_

Accepted by \_\_\_\_\_

Director, Ph. D. Degree Program

Date

**David L. Long**

*Expanding Dimensionality in Cinema Color: Impacting Observer Metamerism  
through Multiprimary Display*

Advisor: Mark D. Fairchild

Committee Chair: David Ross

Committee Members: Jeff Pelz and Elena Fedorovskaya

**Rochester Institute of Technology**

College of Science

1 Lomb Memorial Drive

Rochester, NY 14623

PROGRAM OF COLOR SCIENCE  
COLLEGE OF SCIENCE  
ROCHESTER INSTITUTE OF TECHNOLOGY  
ROCHESTER, NEW YORK

CERTIFICATE OF APPROVAL

---

Ph.D. DEGREE DISSERTATION

---

The Ph.D. Degree Dissertation of David L. Long  
Has been examined and approved by the  
Committee as satisfactory for the  
Dissertation required for the  
Ph.D. degree in Color Science

---

Dr. David Ross, Committee Chair

---

Dr. Mark D. Fairchild, Dissertation Advisor

---

Dr. Jeff Pelz, Committee Member

---

Dr. Elena Fedorovskaya, Committee Member

---

Date



# Calvin and Hobbes

by WATTERSON

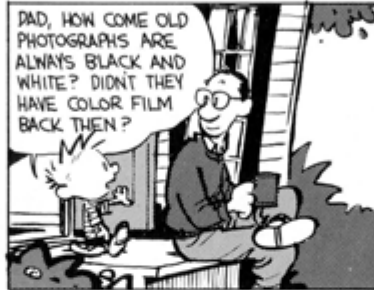
NOW, HONEY, YOU'RE MISSING A BEAUTIFUL SUNSET OUT HERE!



I'LL COUNT TO 10, AND THEN...  
**PON!**



DAD, HOW COME OLD PHOTOGRAPHS ARE ALWAYS BLACK AND WHITE? DIDN'T THEY HAVE COLOR FILM BACK THEN?



SURE THEY DID. IN FACT, THOSE OLD PHOTOGRAPHS ARE IN COLOR. IT'S JUST THE WORLD WAS BLACK AND WHITE THEN.



REALLY?

YEP. THE WORLD DIDN'T TURN COLOR UNTIL SOMETIME IN THE 1930s, AND IT WAS PRETTY GRAINY COLOR FOR A WHILE, TOO.



THAT'S REALLY WEIRD.

WELL, TRUTH IS STRANGER THAN FICTION.



BUT THEN WHY ARE OLD PAINTINGS IN COLOR? IF THE WORLD WAS BLACK AND WHITE, WOULDN'T ARTISTS HAVE PAINTED IT THAT WAY?

NOT NECESSARILY. A LOT OF GREAT ARTISTS WERE INSANE.



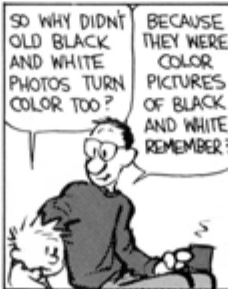
BUT...BUT HOW COULD THEY HAVE PAINTED IN COLOR ANYWAY? WOULDN'T THEIR PAINTS HAVE BEEN SHADES OF GRAY BACK THEN?

OF COURSE, BUT THEY TURNED COLORS LIKE EVERYTHING ELSE DID IN THE '30s.



SO WHY DIDN'T OLD BLACK AND WHITE PHOTOS TURN COLOR TOO?

BECAUSE THEY WERE COLOR PICTURES OF BLACK AND WHITE. REMEMBER?



THE WORLD IS A COMPLICATED PLACE, HOBBS.

WHENEVER IT SEEMS THAT WAY, I TAKE A NAP IN A TREE AND WAIT FOR DINNER.





# Abstract

---

Television and cinema display are both trending towards greater ranges and saturation of reproduced colors made possible by near-monochromatic RGB illumination technologies. Through current broadcast and digital cinema standards work, system designs employing laser light sources, narrow-band LED, quantum dots and others are being actively endorsed in promotion of Wide Color Gamut (WCG). Despite artistic benefits brought to creative content producers, spectrally selective excitations of naturally different human color response functions exacerbate variability of observer experience. An exaggerated variation in color-sensing is explicitly counter to the exhaustive controls and calibrations employed in modern motion picture pipelines. Further, singular standard observer summaries of human color vision such as found in the CIE's 1931 and 1964 color matching functions and used extensively in motion picture color management are deficient in recognizing expected human vision variability. Many researchers have confirmed the magnitude of observer metamerism in color matching in both uniform colors and imagery but few have shown explicit color management with an aim of minimized difference in observer perception variability. This research shows that not only can observer metamerism influences be quantitatively predicted and confirmed psychophysically but that intentionally engineered multiprimary displays employing more than three primaries can offer increased color gamut with drastically improved consistency of experience. To this end, a seven-channel prototype display has been constructed based on observer metamerism models and color difference indices derived from the latest color vision demographic research. This display has been further proven in forced-choice paired comparison tests to deliver superior color matching to reference stimuli versus both contemporary standard RGB cinema projection and recently ratified standard laser projection across a large population of color-normal observers.



# Acknowledgement

---

Completion of this dissertation has been a long journey, balanced carefully with requirements and expectations of serving as a full-time faculty member in the School of Film and Animation at Rochester Institute of Technology. Without the steadfast support of many dear colleagues and family, the task would have been impossible. I would like to acknowledge, first and foremost, the support of my advisor, Mark D. Fairchild, who contributed innumerable hours of consultation and support. His excellent ideas and suggestions for research direction were very much appreciated and unquestionably critical to my success. I am also grateful that he conceded me the opportunity to design a project statement equal parts engineering and science so that I could satisfy each of my academic passions.

Next, I would like to acknowledge the support of my dissertation committee, Drs. David Ross, Jeff Pelz and Elena Fedorovskaya, for their input and contributions to my work. I would also like to acknowledge Dr. Jinwei Gu for service on my committee in its earliest days.

I would also like to thank my fellow faculty and students in the School of Film and Animation who afforded me time and understanding as I balanced these two important endeavors in my professional life. I especially want to recognize the support of Malcolm Spaul, Chair of the School of Film and Animation, for his advocacy in permitting this work to represent my scholarship and academic contributions to the RIT community.

I would like to thank my parents, my wife, Karen, and my children, Morgan and Garrett, for offering me such encouragement and understanding through many long years of effort. In his short eight years, my son has only known me as a sometimes student and a sometimes teacher. This work has been impactful to all of us and they have been my biggest cheerleaders. I am so proud to be a part of my family.

Finally, I would like to recognize my grandfather, Dr. Richard H. Forsythe. He was my inspiration. I intentionally followed his path and example in life in pursuit of this goal. He passed away in the summer of 2015, but I know that he was and is with me through this very special time, providing the strength and endurance I've needed along the way.



# Preface

---

The current digital transition being experienced by the motion picture industry has afforded effective increased resolution in the domains of time and space, however, comparatively little effort has been put into expanding a rigorous treatment of color. More than 150 years after Maxwell and his contemporaries first proposed the theory of trichromatic color reproduction, all practical motion imaging systems continue to rely on metamerism wherein a particular integrated stimulation of the three cone types found on the human retina is sufficient to reproduce a tenable illusory sensation of color of any real object regardless of higher dimension spectral composition. Such treatments, though effective in a basic sense, fundamentally restrict cinema color reproduction, offering limitations in absolute color accuracy, reproducible color gamut, observer variability and consistency of creative communication.

Cinema embodies an ideal space for investigation of issues of multispectral workflow, observer metamerism and observer variability. In large part, the history of cinema technologies has been intertwined with fundamental discoveries in color science. Basic tenets of additive and subtractive imaging were confirmed and refined in early cinema systems from Kinemacolor, Gaumont Color and Kodachrome to perhaps most famously, Technicolor. Video broadcasters pioneered color management principles in transitioning content from luminance-only black-and-white television to NTSC and PAL color television. Theories of color appearance, viewing condition influence and human adaptation are explicitly engineered into cinema systems where environment variables for reproduction viewing are consistently different from those for image capture. And, finally, cinema is an art form, often a deliberate perturbation of reality. This extends from script and story to visual look and feel. Cinema has always employed professional colorists, artists who render different aesthetic design in color and tone to emphasize filmmaker intent. Support of these tasks has also bred big business in color correction, color calibration and color management. The good filmmaker purposefully controls every aspect of the stimuli presented to the cinema patron. Lighting, makeup, wardrobe and art direction are tested meticulously against camera and display technologies to evaluate the consequences to color reproduction. Few other industries are so invested in every major aspect of modern color and vision science. And few others should so intentionally examine emerging trends in spectral imaging and multiprimary display with a bent on both harnessing good science and manipulating ultimate visual content.

It is in the vein of controlling a viewer's experience in cinematic presentations that the topics of observer metamerism, observer variability and spectral video systems warrant extensive research. With the recent emergence of laser cinema projection, ITU-R Rec. 2020 broadcast color spaces and advances in high dynamic range displays, the future of color for content producers is potentially bigger than ever, but understanding consequences of such trends for the artist demands careful attention be paid to attributes of both system engineering and human visual behavior.

Within practical cinema applications, relatively little is understood of the magnitude of observer metameric variability in traditional three-primary standard and wide-gamut imaging systems. As the industry promotes larger colorimetric gamut, however, previous research suggests the consistency of viewing experience amongst a population of observers will suffer. Optimized multiprimary reproduction focused on spectral reproduction accuracy or metamerism reduction may ultimately prove a better answer to enhancing the color experience in future systems. It also promises to open new color management paradigms such as can be used for visual effects compositing of live action and computer-generated imagery or for virtual cinematography.

The following dissertation concentrates on the design and construction of an abridged multispectral video display system for evaluating potential improvements in spectral accuracy and observer metamerism versus traditional three-channel systems. Work comprises both engineering design and color science investigation to address practical application spaces in cinema color. Fundamental color vision models and observer metamerism metrics are pursued to aid in optimization of the abridged multispectral display workflows. Ultimately, the proposed topic is likely to expand beyond the confines of the dissertation process and yield continued research opportunities within the Program of Color Science and the Motion Picture Science program at RIT. A larger effort to include multispectral video capture and image processing has been envisioned with cursory work also begun. And so intentionally, aspects of this larger effort will also garner attention in the accompanying dissertation, as they are useful in communicating a comprehensive body of work applicable to the topics of observer variability and multispectral video in general.

# Contents

---

<b>Abstract</b> .....	<b>i</b>
<b>Acknowledgement</b> .....	<b>iii</b>
<b>Preface</b> .....	<b>v</b>
<b>Chapter 1</b>	
An Introduction .....	1
<b>Chapter 2</b>	
Research Objectives .....	7
Acknowledging Context for Displays in the Full Spectral Imaging Chain .....	9
<b>Chapter 3</b>	
Literature Review .....	11
Previous Efforts in Multispectral Video .....	13
Capture Spectral Sensitivity Optimization .....	21
Training Set Selection .....	26
Spectral Estimation Algorithms .....	28
RIT Prototype Multispectral Video Camera .....	36
Multispectral Displays .....	38
Driving Multispectral Displays .....	41
Observer Metamerism and Spectral Encoding .....	51
Reducing Observer Metamerism in Multiprimary Display .....	52
Multispectral Image Encoding .....	55
Metrics for Evaluating Spectral Match .....	59
Further Literature Review .....	61
<b>Chapter 4</b>	
Literature Influences on Work .....	62
Experiment #1 – Multiprimary Projector Design.....	62
<i>Categorizing Spectral Match / Metamerism Metrics</i> .....	63
<i>Identifying Candidate Projectors</i> .....	64
<i>Determining Optimized Primaries</i> .....	65
Experiment #2 – Observer Metamerism .....	66
<i>Optimizing Observer Metamerism Amongst Various Display Types</i> .....	66
Salience to Current Cinema Trends .....	67

## Chapter 5

The Two-projector Proof-of-Concept .....	68
Abstract.....	68
Native Display Models .....	68
Multiprimary Design Objectives .....	70
Building the System.....	73
Results and Discussion.....	74
<i>Baseline Display Characterization</i> .....	75
<i>Verification and Long-term Stability</i> .....	77
<i>Primary Characterization</i> .....	78
Filter Selection Models.....	80
Actual Filter Characterizations.....	81
Observer Metamerism.....	84
Conclusion .....	88

## Chapter 6

Modeling Observer Variability and Metamerism in Electronic Color Displays .....	89
Abstract.....	89
Color Vision Models.....	89
Observer Metamerism Indices.....	95
Observer Metamerism Simulations .....	99
Conclusions .....	127

## Chapter 7

The Seven-channel RIT Multiprimary Display .....	128
Abstract.....	128
Trends in the Cinema Space.....	128
Design Methodology.....	129
Optimization Results.....	133
Seven-projector MPD Prototype .....	140
The One-projector Solution.....	146
Conclusions .....	146

## Chapter 8

Validating Observer Metamerism Models and the Multiprimary Display Design.....	150
Abstract.....	150
Review of the Problem Statement.....	150
Other Experiences with Highly Metameric Color Matching.....	151
Experiment Equipment.....	152
Equipment Calibration .....	157
Experimental Procedure.....	159
Results .....	161
Conclusions .....	173

<b>Chapter 9</b>	
What We Have Learned .....	174
Contributed Publications .....	177
<b>Epilogue</b>	
Potential Future Work.....	179
<b>References.....</b>	<b>182</b>



# Chapter 1

---

## **An Introduction**

Electronic imaging technologies for cinema and television applications have evolved at an impressive pace during the course of the last 20 years. In particular three trends have dominated the story: a move from analog to digital systems, an enhancement of spatial resolution and an increase in framerate. And in each plotline, the fundamental ways in which we interact with motion content have been altered. But while the digital transition has afforded an effective increase in dimensionality in the domains of time and space, color continues to be engineered with deference to the trichromatic theory of human vision. All practical motion imaging systems continue to be founded mostly in device-dependent, three-channel color spaces with system physics similarly conforming to a three-primary or 'RGB' model. This simplified treatment, though effective, is necessarily restrictive in light of emerging trends, such as the convergence of live action and computer-generated imagery and the expansion of wide gamut display technologies. Full spectral color treatments may render improved realism in digital visual effects and enhanced uniformity of viewing experience across large audiences. Through this work, display of full spectral stimuli will be studied in the context of video applications to identify trends and limitations in spectral reconstruction accuracy and to address issues of observer metamerism. Work in display and visual perception is, further, one fundamental piece of a larger body of study in spectral workflow for cinema, including efforts in capture, color management and creative manipulation.

As analog film systems are supplanted at both capture and display by digital electronic systems, the theatrical experience is changed, in some ways obvious but others more subtle. Both analog and digital technologies have certainly established credibility with consumers over their respective lifecycles. With only minor exception, each has proven very capable in augmenting storytelling and permitting filmmakers to engage with their audience through rich visual communication. On the other hand, each also brings its peculiar restrictions. Grain, dirt and an unsteady weaving projector may be on their way out as film declines but pixilation and aliasing artifacts, limited dynamic range and increasingly complex and potentially less robust hardware are the new hallmarks of the digital cinema era. It is outside the movie theater, though, that digitization has had the most conspicuous influence. The much-anticipated switchover from analog to digital terrestrial television broadcast in the U.S. in 2009 now seems an innocuous move compared to the explosion of live and on-demand digital content distribution models via alternative means, such as TV over IP to home-based and mobile devices.

Advancing digital technologies, though have been purposed to improve the quality of the viewing experience and not just the ubiquity of motion content. Analog standard definition video at 480 or 576 lines of resolution in an interlaced presentation is now consistently replaced by high definition systems at 720 and 1080 lines of progressive scan by broadcasters throughout the world. And consumers are today able to readily invest in systems with even more pixels available for Ultra High Definition Television (UHDTV) video distribution. In the digital movie theater, 2K and 4K systems used for both capture and display allow the cinematic experience to offer something more than general television broadcast. And with standards imposed less rigorously than for broadcasters, higher resolution systems such as FilmLight's 8K film scanner and Sony's 8K F65 Digital Cinema camera push the industry towards even higher resolutions. Though there are limits in optics, bandwidth, noise and dynamic range, having more pixels does still sell. So, too, does having more frames. 24 frame per second capture as standardized in 1920s film and accompanying sound equipment remains, for now, the basis for typical creative content generation along with 30 and 60 frame per second video acquisition. However, many are experimenting with deviations from the norm. Peter Jackson produced "The Hobbit" in 2012 at 48 frames per second based partly on the findings of Doug Trumbull and the Showscan system<sup>1</sup>. James Cameron promises similar efforts for future installments of the *Avatar* series. On the display side, higher framerate systems in television sets permit expanded opportunities for advanced image processing at presentation, such as smooth motion estimation in high action content and flicker-free stereo modulation for 3D media. The trend has expanded to capture, too, where a number of groups are promoting native 120 Hz recording formats which may take advantage of frame blending algorithms to yield traditional 24, 30 and 60 fps output packages or remain as captured to offer an enhanced temporal texture with minimized motion blur and intermittency artifacts.

But again, dimensionality in color reproduction remains stagnant. Traditional image display paradigms for both still and motion picture applications are rooted in a three-primary metameric match model relying exclusively on Grassmann's laws of additivity and the fundamental quantal catch theories of the human visual system. Through the utility of color matching functions used for spectral integration of visual stimuli, the dimensional complexity of real radiometric distributions from scene colors can be simplified to finite scaled outputs in just a small number of primary channels. Problems in this model, though, are found in two principal areas: gamut limitation and observer metamerism. In the former, fully characterized scene content may constitute reproduction stimuli outside the capabilities of the traditional three-primary display device. In the latter, controlled metameric matches of color within the display for a single observer may prove to

not be matches for another observer with slightly different color matching functions or may prove inconsistent even for the single observer as they age. Or increasingly an issue for modulated stereo presentations, a single observer may experience a metameric mismatch between his or her two eyes that inhibits them resolving the binocular fusion illusion in such systems.

The solution to both problems lies, in part, in generating a full spectral-based reproduction environment. In the ideal case, narrow bandwidth, high spectral resolution systems would be conceived to accomplish the goals of controllable spectral capture and reproduction of target stimuli. By combining near monochromatic characteristics at a high sample rate across the visible electromagnetic spectrum, many sufficiently complex stimuli could be rigorously rendered. In a practical sense, however, an abridged spectral reproduction model makes more sense in both hardware design and image processing complexity, utilizing capture and display devices whose individual spectral features are purposefully optimized. In order to define terms used consistently throughout this dissertation, such abridged spectral systems with greater than three channels of controllable color are designated *multiprimary* and are engineered with intent to render explicit *multispectral* color reproduction objectives.

Successful spectral image reproduction systems require both image capture and reproduction devices capable of characterizing and representing real world scene spectra across a wide range of the spectral gamut. The intent of multispectral capture is to either directly or indirectly collect energetic profiles of scene objects under native illumination and to convey those profiles to an appropriate storage or display system. Motion-imaging systems are expected to accommodate dynamic image content often with non-uniform mixed-source lighting and with challenging high contrast ratios. Further in video applications, this must be accomplished for each pixel in each frame of a motion sequence. For spectral capture, conventional trichromatic integrating cameras can either be engineered to deliver intermediate predictions of statistical spectral behavior necessary for pixel-by-pixel spectral estimation or in a more rigorous treatment may be replaced by a much higher dimension full spectral sampling with potential temporal or spatial overhead. Other solutions invoke prismatic beam splitters and generate high spatial resolution RGB images concurrently with high spectral resolution signals at a much-reduced spatial sampling to be recombined in post-processing. Reasonably adequate systems for generating multi-spectral image data have been demonstrated by a number of researchers for both still and motion applications<sup>2</sup>.

Though not an easy problem to solve, spectral sensing is generally more straightforward to implement than spectral display, particularly because display

carries the dubious task of physically re-creating the enormous spectral gamut present in the natural world. As stated, most reproduction devices rely on colorimetric matches with finite primary sets rather than attempting to actually reconstruct full spectra. Emissive electronic display systems have historically provided very little value to the spectral reconstruction problem as optics and image processing requirements make high primary count systems impractical. Further, current industry motivations behind newer display types lie heavily in expanding colorimetric gamut via increasingly monochromatic primaries (such as found in laser-based projectors) though some groups such as Sharp<sup>3</sup>, Texas Instruments<sup>4</sup> and the Natural Vision Project<sup>5,6</sup> have promoted larger gamuts through adding more primaries to the standard RGB set. In these multiprimary devices, great care is taken with advanced color management when the display primaries no longer conform to the spectral sensitivities of the image capture device or when there is a mismatch in number of color channels between capture and display (requiring effective management of degrees of freedom). Reflective spectral attenuation systems such as those found in traditional photographic media, print media or colorant mixing (paints, textile dyes/pigments, etc.) have provided promise for static spectral re-creations, as high primary count designs are more attainable and cohesive color mixing is generally more trivial in the limit of cooperative material properties. A multispectral video system demands the flexibility of optimized multiprimary designs be expanded to an emissive display architecture with a high framerate refresh.

Further, issues of color appearance, color preference and color editing must be addressed in multispectral cinema. While much of the previous research in spectral imaging has focused on industries concerned with absolute color accuracy such as telemedicine, cultural heritage preservation and electronic commerce, the motion picture marketplace demands more creative control. In the reproduction of images for theatrical projection or television display, the artist's aesthetic intent is the paramount concern. Professionally produced images invariably are subjected to secondary color and tone manipulation by skilled colorists until the intended vision of all of the principal creatives has been realized in the post-production mastering environment. In high-end facilities, great care is taken to operate display equipment in strict adherence to industry standards promoted by the Society of Motion Picture and Television Engineers (SMPTE), the European Broadcasting Union (EBU) and the International Telecommunications Union (ITU). In this ideal model, producer, director and cinematographer can communicate in consistent visual experiences during content creation, even across disparate facilities and extended post-production schedules. A multiprimary workflow would demand equal attention to intentional color calibration.

One complication most visual artists are complacently ignorant of is the exact impact of physical and perceptual phenomena on visual appearance differences between scene and screen. As the artistic vision is refined somewhere on a well-illuminated set, motion imaging systems must be carefully engineered to account for predictable alterations in appearance during the transfer of captured images to the mastering and exhibition environments. After all, it would be unfair to ask the colorist to efficiently execute manipulations for viewing condition differences in addition to aesthetic treatments, especially if he or she were not able to be present on the set to see the original stimuli. And in the case of film-based systems, the color controls available in a traditional optical printing workflow wouldn't provide near the necessary power if fundamental reproduction appearance requirements weren't built into the media itself. Just as trichromatic motion imaging systems have been designed carefully to account for physiological and psychophysical visual phenomena across different viewing environments, multispectral image content should similarly provide color appearance accommodation in any future workflow.

Spectral content can be compatible with current best practices in image manipulation but also provide added flexibility and benefit. Multispectral capture is one key to more photorealistic compositing of live action and computer-generated content. Advanced digitization strategies for recreating virtual models of actor's facial features are already enabling enhanced visual effects work and reducing complexity otherwise required from live action visual effects shots<sup>7</sup>. Adding multispectral data to the simulation environment can permit seamless alteration of virtual lighting and surface reflectivity once the virtual actors are placed in the computer graphics (CG) environment. For example, an actor who sits to be digitized using a traditional three-channel imaging system has his skin tones forever simplified to the metameric response defined by the camera's spectral sensitivities. Trichromatic manipulation in the virtual system may not be faithful to the actual color rendition changes accompanying a lighting change on set. If the virtual actor is to be spatially intercut with other objects captured in live action across multiple lighting setups, the spectral representation permits more realistic and seamless color reproduction.

Multispectral camera systems could also be used as universal capture platforms, capable of emulating the color and tone characteristics of any electronic or film-based imaging system. Virtual cinematography has been pioneered in films such as *Avatar* in which actors, lights, and camera are all computer-tracked props on a motion capture stage. Not only is action in front of the camera choreographed somewhat virtually but so too are camera moves and lighting. If the stored CG environment used with the motion capture is characterized spectrally, the behavior

of the camera itself can be faithfully represented in rendered footage. The astute director of photography who chooses an Arri or Red camera for their engineered color reproduction on a real set could retain that benefit even on the virtual set.

Electronic multispectral displays could better emulate the color gamut and spectral profiles of motion picture print films than do current standard Digital Cinema Initiatives three-primary systems, at the same time reducing observer metamerism. A common issue for any digital intermediate suite is the quality of color match achieved between the digital grading projector and the answer print film projector (where *answer print* refers to the final color-corrected film print approved by the production team during post-production mastering). Part of this difficulty derives from the lack of similarity in color gamut and colorant spectral behavior between the two devices. A match meticulously forced for one observer may prove completely different for another. Necessity for color control like this will become even more important as film projection systems manufactured by just a few vendors using a mostly consistent optical design are replaced by a myriad of modulation technologies on the digital side such as laser, LED and LCOS, all with different spectral signatures. Some standards bodies, including SMPTE, are currently contemplating spectral definitions for future display systems as opposed to simple colorimetric definitions.

And finally, allowing colorists control over a multispectral palette affords opportunity for leaps forward in creative color manipulation. As meticulously as a director of photography and art team select wardrobe, makeup and props for explicit color appearance when rendered by the camera and display systems, post-production control of spectral pixels in a color correction session could afford equivalent power in the final mastering. Manipulation of spectral curves rather than trichromatic channel values portends ultimate artistic control over the entire visual experience for filmmakers who work to generate intentional visual stimuli for their audiences.

An expansion of color dimensionality is an obvious and compatible addition to rapidly evolving motion imaging capabilities in spatial and temporal resolution. In the attached dissertation, optimization of an abridged multispectral display will serve to explore one fundamental building block of the multispectral imaging chain. Observer experiences with multiprimary systems will generate fundamental understanding of preferred system architectures for maximizing color gamut, enforcing color accuracy and minimizing observer metamerism and variability. Special emphasis will be placed on building and confirming models of observer color vision and on engineering displayed color stimuli that yield measurable improvement in color matching across multiple observers.

## Chapter 2

---

### Research Objectives

The completed dissertation has concentrated on the design and construction of an abridged multiprimary display (MPD) intended to yield improvements in spectral image reproduction accuracy and a minimization of observer metamerism. The predominant motivation for this focus has come from experiences in the cinema industry with variable interobserver color perception in emerging near-monochromatic display technologies, trends previously predicted by Fairchild and Wyble<sup>8</sup>. Major phases of the project have included:

- 1) an investigation of color vision models and color matching function (CMF) variability across *color normal* observer populations
- 2) an establishment of interobserver color reproduction quality indices based in both spectrometry and colorimetric metamerism
- 3) a screening of existing display devices for observer metamerism and observer variability
- 4) modeled optimization of MPD prototypes intended to minimize observer metamerism against results from phases 1) and 2)
- 5) the engineering and construction of prototype MPD systems and
- 6) psychophysics experimentation across multiple display types, intended to confirm models of observer metamerism and variability

A more detailed summary of the engineering and color science challenges driving the research in these phases is presented in Table 1.

Abridged multiprimary displays utilizing some number,  $K'$ , of electro-optically controlled channels offer a more practical engineering solution for a spectral reproduction workflow than higher primary count, full-resolution spectral display systems. They, further, are critical for the color management goals of this research where color vision models, color difference indices and spectral optimization are explored to characterize and minimize observer metamerism. Paramount in the design and analysis of the MPDs described in this dissertation has been determination of the number and nature of primaries needed to reasonably reconstruct target spectral stimuli and enhance spectral gamut. Spectral reconstruction accuracy as characterized by both spectral and colorimetric metrics has been simulated on various  $K'$ -channel projection schemes and contrasted with objectives of minimized observer metamerism. Finally, metamerism experiments

Table 1. Research objectives and associated questions across project phases

<b>Color Vision Modeling</b>	<p><i>Color Science</i></p> <ol style="list-style-type: none"> <li>1. Which vision and CMF models best summarize population demographics for real 'normal' color observers?</li> </ol>
<b>Designing Color Reproduction Quality Indices</b>	<p><i>Color Science</i></p> <ol style="list-style-type: none"> <li>1. How can MPDs be objectively evaluated for spectral reconstruction quality and minimization of observer metamerism?</li> <li>2. What combination of radiometric spectral error profiling and colorimetric color difference formulae best represent observer metamerism and variability?</li> </ol>
<b>Existing Display Characterization</b>	<p><i>Color Science</i></p> <ol style="list-style-type: none"> <li>1. How well do existing display technologies perform for spectral and colorimetric variability given identified color vision models and quality indices?</li> </ol>
<b>MPD Modeling &amp; Design Optimization</b>	<p><i>Color Science</i></p> <ol style="list-style-type: none"> <li>1. How many channels are needed in cinema applications to reasonably reproduce aim spectral radiance data according to spectral and colorimetric objectives?</li> <li>2. What spectral training and optimization strategies for an MPD will maximize robustness across a wide gamut of expected spectral reproduction needs?</li> <li>3. What primary emission spectra are ideal for the number of channels selected; and is there a compromise of broad primaries suited for spectral accuracy versus narrow (monochromatic) primaries for maximizing colorimetric gamut?</li> </ol> <p><i>Engineering</i></p> <ol style="list-style-type: none"> <li>1. What visual and color artifacts are likely to be generated in any compromised MPD design strategy?</li> <li>2. How can the MPD design balance reproduction accuracy and residual color artifacts while limiting system cost and engineering complexity?</li> </ol>
<b>MPD Engineering &amp; Characterization</b>	<p><i>Engineering</i></p> <ol style="list-style-type: none"> <li>1. How best should a MPD based on <math>K'</math> channels using external optical filtration on existing three-channel RGB projectors be built?</li> <li>2. How best should an alternative MPD based on <math>K'</math> filtered projectors be built?</li> <li>3. How well can spectral and radiometric stability, screen spatial independence and display uniformity of prototype MPDs be controlled?</li> </ol>
<b>Observer Metamerism Psychophysics</b>	<p><i>Color Science</i></p> <ol style="list-style-type: none"> <li>1. How will prototype MPDs compare to existing three-channel CRT, DLP, LCOS and laser-based cinema displays in observer metamerism simulation? <ul style="list-style-type: none"> <li>• optimize each system against spectral targets for a) colorimetric accuracy and b) minimized observer metamerism</li> </ul> </li> <li>2. Will vision models and observer metamerism optimizations be confirmed using forced-choice psychophysical testing on the MPDs with real observers?</li> </ol>

have been executed with both simulated and real observers to determine benefits gained by a full multispectral display system versus standard three-channel colorimetric systems utilizing both highly saturated primaries such as found in laser displays and more typical ITU-R Rec. 709 or SMPTE-431 primaries found in DLP and LCOS cinema devices.

Chapter 5 summarizes an initial proof-of-concept display design based on delivering six unique spectral channels from external filtration applied to two traditional RGB projectors. Chapters 6 and 7 summarize subsequent improvements with a multi-projector array and seven individually optimized color channels. Chapter 8 concludes with discussion of psychophysical experiments confirming model predictions and display performance across a population of color normal observers.

### **Acknowledging Context for Displays in the Full Spectral Imaging Chain**

Multiprimary display actually sits at the end of the full multispectral imaging chain. Prior to presenting spectral reconstructions using MPDs, stimuli must be first captured and processed. These phases of research are intentionally not part of this dissertation, but it remains of value they be introduced to expand context for the benefits multiprimary display is intended to offer.

The purpose of multispectral capture is to either directly or indirectly collect spectral profiles of scene objects under native illumination and to convey those profiles to an appropriate storage or display system. Example approaches for spectral capture are included in the literature review summarized in Chapter 3, including description of a prototype multispectral video camera designed at RIT during an exploratory pre-dissertation phase of this research.

In optimizing a camera design, fundamental color science questions associated with the spectral estimation generated from the capture system must be addressed. These same questions can be extended to interpretation of the rendered display color, too. In the absence of high-resolution direct spectral measurement, several compromised reconstruction strategies are possible, optimizing results in either colorimetric, spectral or metamerism indices.

With respect to image interchange color spaces, options focused in spectral rendering, colorimetric characterization and device-dependent K-channel recording can be explored (note an intentional distinction between K-channel capture and K'-channel rendering). In some architectures, it may be preferred to extract linear

spectral signals only and do all processing on-demand for delivery to the display. In other scenarios, conversion and storage of spectral signals to display drive values may be more prudent. These questions are closely aligned with theories of profile connection spaces (PCS) addressed in modern color management research.

This introduction to characteristics of spectral capture and post processing is useful, but as stated, the completed dissertation focuses predominantly on issues of multispectral display only. For the majority of the work outlined, original multispectral content of sufficient quality and accuracy was simulated or assumed available for the display work. Further, offline image processing was employed to render content for visual experiments. Maximum attention is thus given to issues of content preparation and presentation to meet the objectives of multispectral rendering and to address issues of observer variability.

## Chapter 3

---

### Literature Review

Motivations for multispectral imaging systems, complete with strategies for capture, color management and display, have been purported by several researchers for well over a decade now. Hill summarizes the problem statement most succinctly as he outlines the limitations of three-channel imaging paradigms that don't conform to the spectral performance objectives dictated by human color matching functions.<sup>9</sup>

Trichromatic theory, whether applied to engineered devices or human observers has its foundation in the integrated spectral signature represented in Equation 1. An object with spectral reflectance,  $R(\lambda)$ , illuminated by a source with spectral power distribution  $I(\lambda)$ , is spectrally integrated through the sensitivity signature of a detector,  $SS(\lambda)_k$ , across  $k=1\dots K$  independent channels of captured response (where  $K$  is most classically 3 but is left generic in this introductory treatment for future multiprimary expansion). After appropriate normalization,  $h_k$ , the resulting quantity is generically dubbed tristimulus,  $W_k$ . A more specific replacement of  $SS(\lambda)_k$  with the CIE 1931 2° standard observer color matching functions (or any other appropriate observer color matching function) yields  $XYZ$  tristimulus values. Likewise, individual observer signal responses in the three primary cone types,  $LMS$ , are specified when  $SS(\lambda)_k$  are replaced by  $l(\lambda)$ ,  $m(\lambda)$  and  $s(\lambda)$  cone fundamentals. For film or digital image capture systems, insertion of the device's spectral sensitivities generates quantities indicative of the captured energy signal at a specific position on the image plane in each channel. And in digital systems in particular,  $h_k$  may be set variable across the response channels and even across the spatial domain in a frame, allowing for an equalization of the channels relative to a perfect white reflector with  $R(\lambda) = 1.0$  at all wavelengths (white balancing) and/or for accommodating hardware response non-uniformities.

$$W_k = h_k \int_{\lambda_{min}}^{\lambda_{max}} I(\lambda) \cdot R(\lambda) \cdot SS(\lambda)_k d\lambda \quad (1)$$

An analysis of Equation 1 suggests there are infinite combinations of spectral reflectance and illumination that may deliver integrated tristimulus values equivalent to some established target stimulus for a given detector. This principle is defined as metamerism and is the basis for most imaging systems where the generation of precise spectral matches between target and reproduction is

unnecessary for delivering an equivalent interpretation of the stimuli. This is especially useful in both soft-copy and hard-copy image display where the spectral characteristics of colorants used in either additive or subtractive mixing models do not afford a precise spectral match to the target. As Hill points out though, this also leads to several failure modes in the metamerism model.

As an elementary example, presume the goal of a designed image capture system is to mimic the responsivity of the 1931 2° standard observer or a simple linear combination thereof, an approach referred to generically as the ‘Luther’ condition, named for German physicist, Robert Luther. To accomplish this directly, the capture system should possess  $SS(\lambda)_k$  which are equivalent to either the standard observer’s color matching functions or linearly related cone fundamentals. As both of these responsivity sets are physically realizable, appropriate optical filtration could theoretically be designed to accomplish the objective. In fact, this is the typical design strategy for three-channel colorimeters used routinely for scientific and technical color measurement. However, the nature of human color vision is such that the integrated tristimulus signals from this model in three channels must be paired with rendering or display primaries that are radiometrically non-realizable if a direct full gamut reconstruction is desired. Peculiarities of the linear transforms involved in human color matching dictate that primary spectra directly driven from either *XYZ* or *LMS* must have negative energies in some portion of their spectral signatures in order to properly represent a metameric match to target stimuli captured via these sensitivity functions.<sup>55</sup>

When direct capture of human tristimulus signals becomes imprudent for practical display processing, imaging system designers typically look to compromises employing minimal color processing between capture and display. In particular, device responsivities may be chosen which are color matching functions of a chosen set of display primaries, though in a three-channel system there are no such choices where both sensitivity functions and primary spectra are all positive and realizable. This is further indication of a gamut mismatch between capture and display design when only three channels are employed. The result is that real function shapes are designed and related by statistically optimized color processing transforms instead, typically 3x3 matrices or more customized 3-dimensional look-up tables. The specification of colorimetric video cameras employing ITU-R Rec. 709 encoding characteristics and intended for display on sRGB additive displays are famously described in this approach.<sup>10</sup> Further, Hill summarizes that electronic noise considerations are often incorporated into color design strategies as image quality may be negatively affected by overaggressive attempts to generate a specific color reproduction goal.

The primary consequence of spectral responsivity compromises in real image capture equipment is that these systems are prone to failures of metamerism. In particular, multiple spectral stimuli which may integrate via Equation 1 to equivalent tristimulus signals for the standard observer may not yield equivalent response for a capture system with sensitivities that aren't linear combinations of the CIE color matching functions. Of course, the reverse scenario is also true where a camera system may fail to exhibit discrimination amongst a series of color targets that are different in appearance to the standard observer. Metamerism failure may also manifest as a function of illuminant. A particular pair of color targets may match for a given detector's response under one illuminant but not another. Finally, presumption that the standard observer represents all human response functions can cause significant issues. Just as a camera system may fail to metamERICALLY coincide with the response of the standard observer, real human observers vary significantly in their spectral response characteristics. These variations have been studied extensively with some success found in systematically characterizing average differences as a function of observer age and field-of-view<sup>11</sup> and other models based on large sets of collected physiological data<sup>76</sup>. Of course, even studies such as these can only claim to summarize the mean trends in human observers, recognizing there are still unique results found throughout real populations.

## **Previous Efforts in Multispectral Video**

Perhaps the most comprehensive collection of efforts in generating a working multispectral capture and display system for video applications to date can be attributed to the Akasaka Natural Vision project in Japan, a joint effort of the Tokyo Institute of Technology and the Japanese Ministry of Internal Affairs and Communication along with other industrial and academic partners.<sup>12</sup> Between 1999 and 2006, the Natural Vision laboratory tackled several issues of multispectral system engineering design, signal encoding, signal transmission and color science, publishing numerous significant findings. The group also built several working prototypes to confirm design principles and generate practical data.

The basic premise of the Natural Vision multispectral system design has been to change the role of color imaging from best practices metameric solutions or preferred color reproduction paradigms to absolute spectral measurement, communication and reproduction. Traditional three-channel cameras are replaced by systems employing either high dimension evenly distributed spectral transmission bands and a multi-channel modulation scheme (such as a sequential filter wheel and monochrome sensor) or simultaneous capture to multiple channels

through an optical assembly with optimized spectral responsivities. Spectral radiance, reflectance or transmittance information is then preserved via a spectral profile connection space, compatible also with more traditional colorimetric image encoding schemes. Spectral signatures are reconstructed pixel-by-pixel to a multiprimary projection system capable of delivering higher spectral accuracy versus target stimuli, a larger colorimetric gamut, reduced observer metamerism or a co-optimized response of all three. The system may also be engineered to deliver a prediction of object colors under alternate illuminants by combining reflectance estimation with a new user-defined observation illuminant, a process referred to as “illumination conversion.”

The primary Natural Vision still camera is a 16-band tunable filter-based system with a monochrome sensor. Calibration procedures include white balancing the spectral bands against a perfect reflecting diffuser and correcting for non-linear optoelectronic transfer functions and black signal bias. Despite tunable spectral accuracy from the filter wheel design, the camera is subject to notable issues with field uniformity and peripheral image accuracy. Further, mechanical lag during the collection of the 16 successive image channels is sufficient that motion blur and registration errors upon interaction with moving scene content would be unacceptable. Thus in a second system used for motion applications, a simultaneous multichannel capture design is implemented<sup>13</sup>. Two three-band HDTV CCD cameras are connected by way of an optical splitter and custom interference filtration in each camera path modifies the native spectral responses of the sensors to generate 6 specific spectral sensitivities, see Figure 1. Knee and gamma functions are turned off in each camera to yield 10-bit linear exposure signals over 4:4:4 HD-SDI connections. The signals are recorded in twin synchronized video streams to solid-state media.

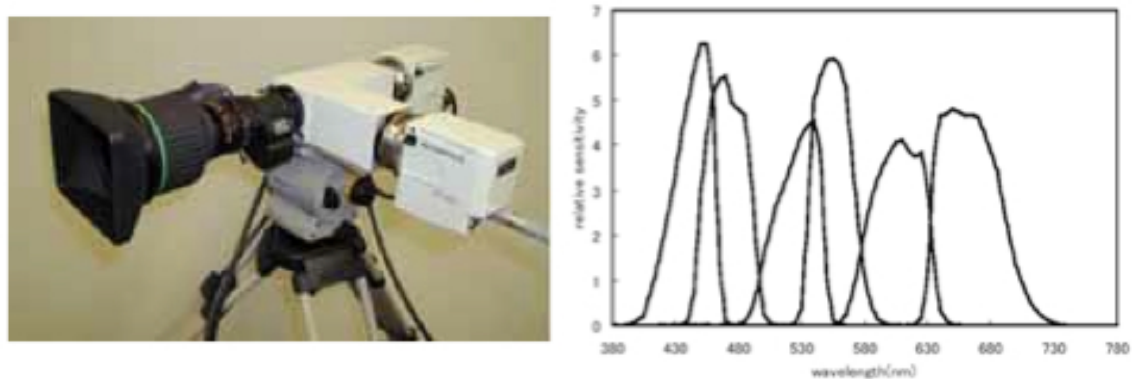


Figure 1. Natural Vision 6-channel HDTV camera; spectral sensitivity of measured channels also shown (reproduced from Yamaguchi, et al.<sup>16</sup>)

For initial evaluations of the six-channel camera, colorimetry predictions were employed to determine improvements over a single native three-channel HDTV camera. Using a forward model for the three and six channel camera signals, exposures for the 24 Macbeth Color Checker patches illuminated by daylight, incandescent and fluorescent sources were simulated and conversion matrices of appropriate dimension to CIE tristimulus values were constructed using least squares linear estimation. Nine matrices were built for each camera system employing capture simulation under each of the three taking illuminants further used to independently predict the standard colorimetry under the same three illuminants, with off-diagonal permutations intended as illuminant conversion transforms. In all nine scenarios, the six-channel system with a typical average  $\Delta E_{ab} < 1$  well outperformed the native three-channel camera with average  $\Delta E_{ab}$  between 2.0 and 4.0. Of some concern, however, is the spatial nonuniformity in the Natural Vision design. Angular dependencies in the interference filters and optical path contribute to color prediction differences in the corners of the frame as high as 4.0  $\Delta E_{ab}$  units when compared to a baseline frame-central reading.

Simple colorimetric prediction from the six-channel camera is impressive in the Natural Vision video system but is not sufficient to accommodate more serious spectral reproduction goals. For this, full spectral estimation is required. To capture information on spectral radiance as well as reflectance or transmittance, the ambient illumination spectra may be captured either through the cameras themselves or by way of external spectroradiometric measurement. Once collected, several spectral estimation techniques can be applied to the data in post-processing though the Natural Vision project team suggests the best success is found by using careful training target sets and Wiener estimation. Where training is impractical, a first-order Markov process provides fair accuracy for natural object spectra containing reasonably smooth spectral profiles. Unfortunately, many of these approaches to full spectral estimation cannot be implemented in real time for HD video signals.

For display, the Natural Vision project has built several prototype systems incorporating from  $K' = 4$  to 7 independent primaries and using front and rear projection or LED-illuminated LCD panels. The principle system employed in most of the experimentation, though, is a six-primary rear projection screen produced by differently filtering the native spectra of two superimposed DLP projector images. The premise of the design is foremost to expand colorimetric gamut beyond that described by the sRGB/ITU-R Rec. 709 or SMPTE-431 additive primary sets. Several other groups have proposed more saturated primaries such as those generated with lasers and narrow-band LEDs to enhance the gamut volume of a three-channel

system, but the Natural Vision team argues for more flexibility in color reproduction by expanding the gamut through additional control vertices in color space. In particular, the colorimetric gamuts of real surface colors summarized by Pointer<sup>14</sup> and the SOCS database<sup>15</sup> are more efficiently encompassed by the multi-primary design. Further, generating tristimulus matches to target colors with >3 primaries affords co-optimization in several supplemental areas thanks to excess degrees of freedom, including device energy consumption, observer metamerism and spectral reconstruction.

Independent of capture, driving the multiprimary display requires either  $K$ -to- $K'$  or  $N$ -to- $K'$  transforms (where  $K'$  is the number of multiprimary display channels, independent of captured or encoded channels,  $K$ , and  $N$  is target encoded spectral resolution), necessary to communicate color signals to the screen. In either case, implementation complexity and processing overhead must be evaluated in practical applications, especially for video. For traditional three-channel colorimetric encoding, the over-specified problem described for a multiprimary display affords flexibility in designing  $3$ -to- $K'$  processing to accomplish specific system goals such as power savings or rudimentary observer metamerism accommodation. Another such computational flow incorporating the six-channel HDTV camera and colorimetry prediction matrices described previously is summarized in Figure 2. Here, the camera signal is translated to an efficiently encoded all-positive colorimetric space (XYZ or large-gamut RGB) that comprises traditional 10-bit video packing. This calculation requires a 1-dimensional look-up table to account for camera opto-electronic transfer function and black bias followed by the  $6 \times 3$  colorimetry matrix. In the Natural Vision examples, these matrices can be customized to predict object colorimetry under either the capture illumination or some secondary illumination declared for illumination conversion. For display, a 3D LUT is implemented to pre-calculate six-channel outputs from three-channel input according to one of several proposed methodologies. This LUT is preceded by a 10-bit to 8-bit conversion LUT and followed by display transfer function LUT to generate device drive values. Video processing through the LUT may then progress in real time though colorimetric errors do manifest in the system as a function of digital quantization in the signals and low node counts in the 3D LUT lattice<sup>16,17</sup>. For alternate deliverables from spectrally defined target colors in  $N$  wavelengths, spectral approximations are engineered while concurrently minimizing standard observer colorimetric error. This approach has proven to further reduce observer metamerism in controlled experiments but, again, not at video framerates in the Natural Vision work<sup>18</sup>. Expanding a full spectral estimation in real-time video remains a challenge.

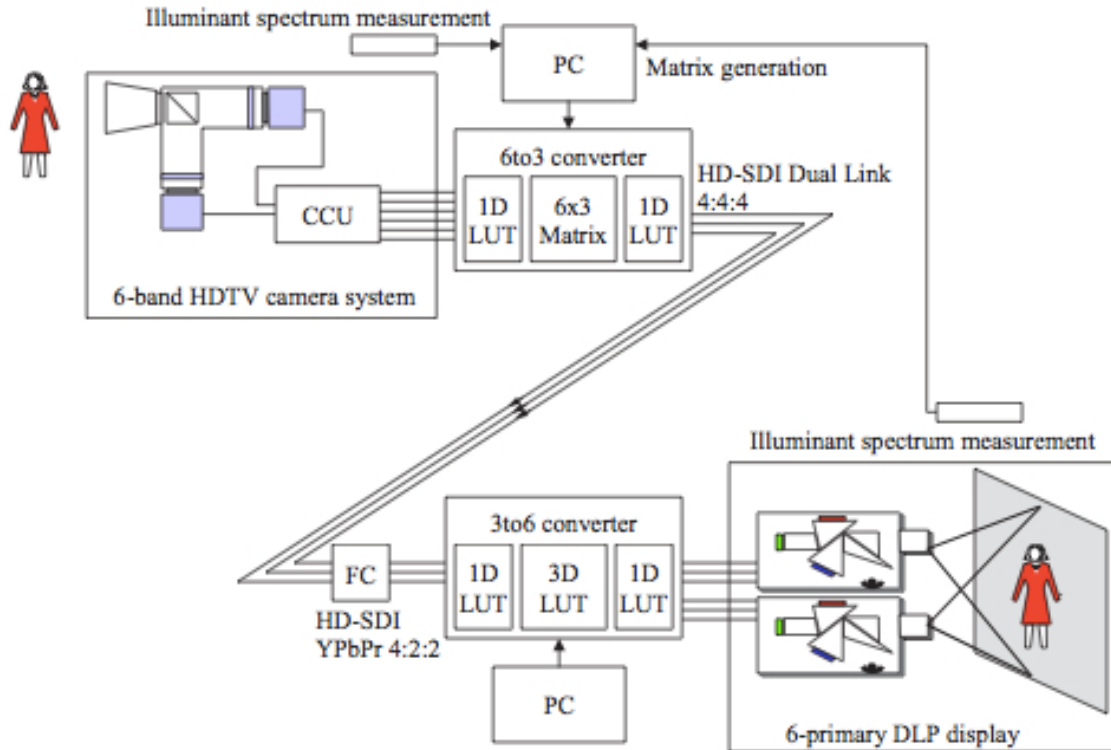


Figure 2. Real-time video processing for 6-channel HDTV camera and 6-channel display employing illuminant conversion matrices and colorimetric interchange (reproduced from Yamaguchi, et al.<sup>16</sup>)

The Natural Vision image encoding and transmission schemes are careful to offer flexibility of communication in either traditional colorimetric terms or high dimension spectral information, depending on application. Multispectral image data at each pixel and within each frame may be represented in terms of original camera signal, post-processed spectral estimation, rendered spectral reproduction or converted display drive signals. The onus for image processing may then be distributed amongst different system components as necessary to accommodate a particular imaging goal.

The proposed color management architecture is summarized in Figure 3 and is analogous to ICC-based systems though with emphasis on a physical model versus an appearance model<sup>18</sup>. The profile connection space may be colorimetry under a specified illuminant or spectral radiance or reflectance of scene or reproduction. Source and destination profiles carry necessary device-dependent metadata as well as captured environmental data to permit further spectral image processing of the raw multispectral capture and multiprimary display signals. These profiles also

specify algorithmic treatment for conversion from device data to the spectral profile connection space and may be updated as new methods and models are devised. The color-space conversion profile permits user-defined rendering objectives from the captured data. For example, image rendering options consistent with this system include:

1. traditional three-channel colorimetric reproduction of captured object
2. illumination conversion between capture space and observation space for specified objects
3. spectral reflectance/radiance reproduction of captured object
4. multi-observer colorimetric reproduction (reduced observer metamerism) of captured object
5. general source object spectral analysis

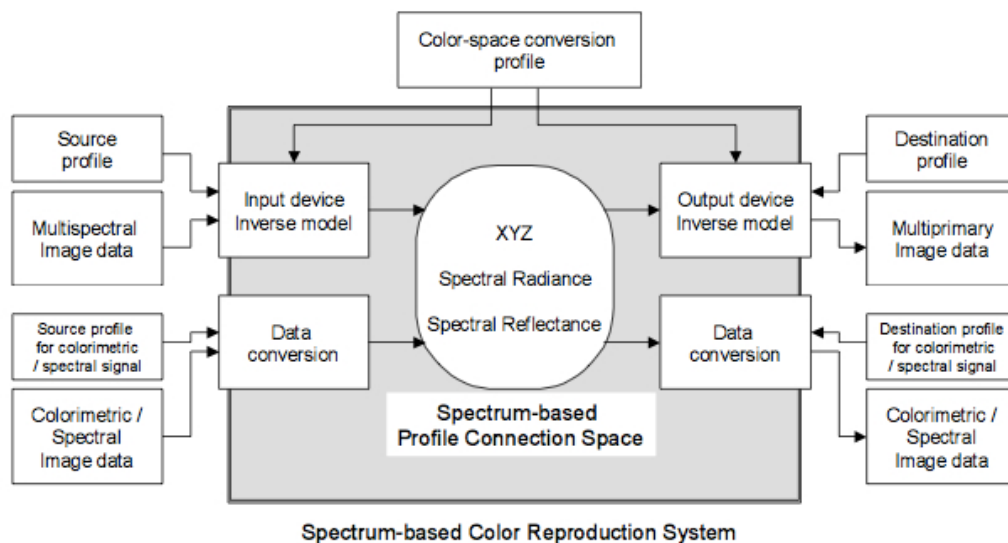


Figure 3. Natural Vision color management architecture (reproduced from Yamaguchi, et al.<sup>18</sup>)

The challenge of video is especially daunting as, even in three-channel paradigms, data rates are extremely high and most often compression strategies are necessary to fit hardware capabilities. When multi-channel signals are introduced, the issues are even greater. Figure 4 illustrates the real-time processing workflow implemented by the Natural Vision project using the six-channel HDTV camera rig and six-primary display in more detail. For actual signal packaging, JPEG2000 multichannel (JPEG2000-MCT) support for spectral basis function coefficients across both colorimetric and metameric black residual constituents provides a

suitable transmission and storage container (more detail on this approach will be offered in subsequent sections). This is further augmented by a Natural Vision file wrapper protocol that allows source and destination profiles as described in Figure 3 to be modified frame by frame if desired<sup>19</sup>.

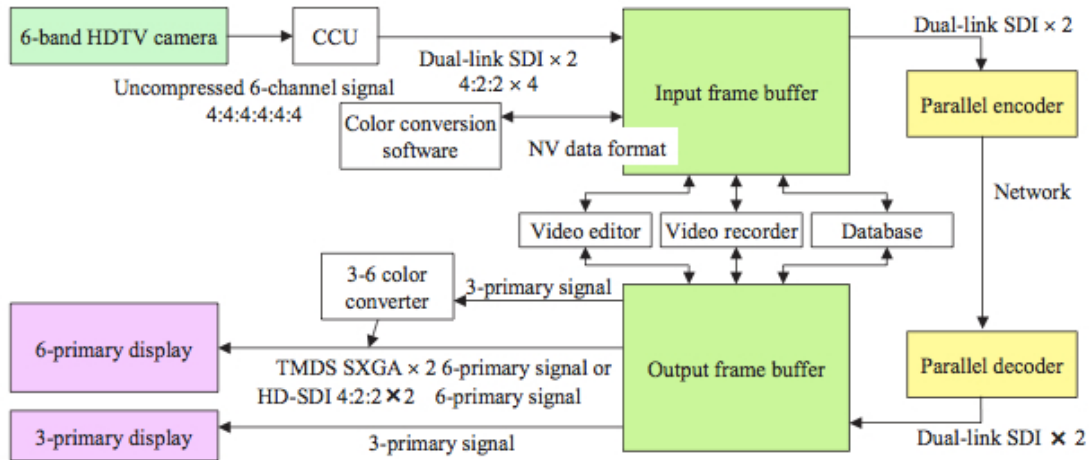


Figure 4. Natural Vision video processing workflow for real-time multiprimary capture and display (reproduced from Yamaguchi, et al.<sup>12</sup>)

While the Natural Vision project does an excellent job with re-creation of the physical color characteristics of captured targets, little work is put into color appearance modeling or creative manipulation of the spectral signal. Appearance and adaptation accommodation are a completely separate topic from the accurate spectral reconstruction of a physical stimuli under some specified illumination. Berns has summarized this dichotomy well indicating tristimulus values for corresponding colors interpreted under two different illumination conditions rarely match the tristimulus values for some single object in the same two environments<sup>74</sup>. In other words, an accurate spectral reconstruction is typically a goal independent of accurate appearance matching when viewing conditions are known to vary. For artistic applications, both paradigms require more critical understanding and control.

Much of the work incorporated in the Natural Vision project was completed between 2006 and 2007 and several additional multispectral video capture techniques have been devised in subsequent years. Cao, et al. have presented a camera system which employs a dispersing prism and occlusion mask to isolate a

limited spatial resolution sampling of scenes and expand a spectrum from each scene point onto a monochrome sensor<sup>20</sup>. Figure 5 summarizes the design. The occlusion mask segments incoming light rays from a scene before then passing them through a prism to split each sampled point into its constituent spectral distribution. Physical and optical parameters are closely controlled to avoid overlap of neighboring spectra on the image plane. The monochrome sensor is sufficiently sensitive to record energies across all visible wavelengths and the recorded digital signals can be related back to a spectral radiance as a function of indexed position in the sensor's pixel array. The camera shown in the figure can have its focal length altered so as to intersect more or less of the occlusion mask holes. With a longer focal length, fewer holes are intersected and the sampled scene is thus represented in a lesser spatial resolution. At the same time, though, each imaged hole generates an expanded dispersion of the spectrum onto the fixed resolution sensor and a greater spectral sampling per point is achievable. This trade-off of spectral and spatial resolution is a hallmark of the system in addition to the rapid processing of the spectral signatures per imaged 'pixel' (mask hole). Much as a single point spectrometer immediately measures a spectral signature for a single integrated sample, the Cao system takes advantage of high resolution, high framerate machine vision video cameras to produce a higher sampling of scene points in rapid succession. And it does so without the need for expensive optics, mechanical scanning systems, extensive reconstruction algorithms or spectral training as is typically used in abridged systems. Shortcomings of the design, however, include management of spectral and geometric distortions due to the prism and light losses and resultant low SNR from the camera and mask aperture effects. Another limitation is that the camera's depth-of-field must be set wide enough to keep the object and occlusion mask in focus so as to avoid spectral blur at the image plane. The mask itself must also be located close to the scene to avoid rays from multiple holes generating overlapped spectra on the sensor. A solution to this problem would be to add an objective lens in front of the mask so that an intermediate image is sampled rather than the original scene.

To effectively improve spatial resolution, Cao, et al., have modified the design of Figure 5 by inserting a beamsplitter in front of the mask and imaging half of the light from the scene to a full resolution RGB camera<sup>21</sup>. While the spectral signal is still sampled sparsely as above, a concatenation of spectral signature with the high-resolution RGB signals is accomplished by taking advantage of pixel color similarity and spatial proximity. A simple bilateral filter is extremely efficient for processing the image stream in real-time and can even be augmented with optical flow models across multiple video frames to improve keyframe spectral resolution.

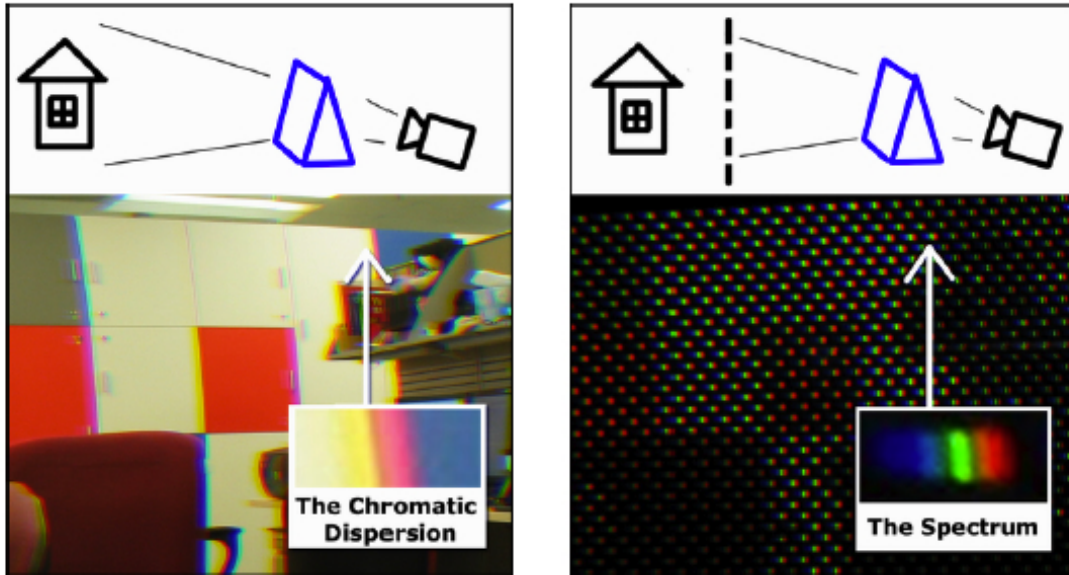


Figure 5. Prism-mask multispectral video capture capable of recording individual scene point stimuli to expanded spectral image plane signatures (reproduced from Cao, et al.<sup>20</sup>)

Other techniques with considerably more complex post-processing requirements and customized optics summarized by Cao include computed tomographic imaging spectrometry (CTIS) and coded aperture snapshot imager (CASSI). Each treat the spectral scene space as a 3D cube where 2 dimensions form the spatial projection and the 3<sup>rd</sup> dimension is a spectral axis. Each optical approach essentially projects 2D slices of the 3D scene cube onto the incorporated image sensor that must be then reconstructed into the full multispectral image via complex linear system solutions. Though sound in theory, these approaches suffer from limited spatial and spectral resolution despite their applicability to high framerate video capture and have only been demonstrated with very simple scenes.

### Capture Spectral Sensitivity Optimization

In three-channel image capture systems, control of spectral responsivity in the full system constitutes the paramount concern for controlling color rendition. If a camera is not designed to the human color matching function Luther condition, for example, it will easily manifest metamerism failures versus the CIE's standard observers. Customized deviations from the Luther condition are often carefully engineered in real systems to deliver acceptable artistic interpretations of captured scene color. Film and digital system manufacturers contribute significant resources to optimizing spectral responsivity within the limits of system noise and efficiency

constraints, manufacturing feasibility and available post-capture image processing. In multispectral image capture systems, channel responsivity is likewise critical to defining system accuracy and performance limitations. Increasingly sophisticated spectral estimation models may refine capabilities to a degree but the number and spectral nature of response channels in the system contributes the primary expectations for the system. In the limit of a uniformly subsampled spectral domain with channels of increasing spectral resolution and selectivity, spectral estimation becomes higher quality, though at the expense of system complexity and with potential degradation of image quality due to registration error, temporal subject blur and cascaded noise upon channel recombination.

Building an abridged multispectral capture system requires that actual spectral responsivity of included components is well understood. Currently, RIT's Munsell Color Science Laboratory (MCSL) employs a diffuse monochromator and radiometer test assembly to collect information on relative spectral sensitivity for existing camera systems. Exposures captured and signals recorded by the cameras at pre-selected monochromatic wavelengths are linearized to radiometric equivalents and normalized by the absolute radiance of the test stimuli at each wavelength. These adjusted signals at each wavelength are proportional to the system sensitivity and a full spectral response across  $N$  dimensions can be constructed.

A somewhat more practical methodology for determining actual system spectral responsivity is summarized by Hardeberg<sup>22</sup>. This assessment is based on a simplified model of the camera as it interacts with colored objects. The integrated response of the  $k$ th channel of the capture system,  $c_k$  (a re-labeled definition for  $W_k$  when spectral sensitivity is set equal to camera responsivity), for a given stimulus is a function of the spectral radiance of the illuminant associated with the stimulus,  $I(\lambda)$ , the reflectance of the stimulus,  $R(\lambda)$ , the spectral transmittance of optical features ahead of the detector in the system,  $o(\lambda)$ , the spectral transmission of the  $k$ th optical color filter,  $\phi(\lambda)_k$ , the native responsivity of the detector,  $a(\lambda)$ , and the internal system noise associated with the system,  $\varepsilon_k$ , Equation 2. The product of system optical components,  $o(\lambda) \phi(\lambda)_k a(\lambda)$ , can be pre-cascaded to deliver the  $k$ th channel spectral responsivity,  $\omega(\lambda)_k$ . In many cameras, the integrated response signal may undergo further non-linear processing before being reported, Equation 3. In these cases, collected signals,  $c'_k$ , will require mapping through  $\Gamma^{-1}$  to generate integrated linear capture values.

$$c_k = \int_{min}^{max} Il(\lambda) \cdot R(\lambda) \cdot o(\lambda) \cdot \phi(\lambda)_k \cdot a(\lambda) \partial\lambda + \varepsilon_k \quad (2)$$

$$c'_k = \Gamma c_k \quad (3)$$

Estimation of unknown camera spectral sensitivities can be produced by observing camera outputs from a series of J target stimuli ( $j=1\dots J$ ) with known spectral characteristics,  $s(\lambda)_j=Il(\lambda) R(\lambda)_j$ , and solving for  $\omega(\lambda)_k$  by rearrangement of Equation 4 across K total response channels with spectra defined at N equally sampled wavelengths. In this equation, the response matrix has dimensions JxK, the spectral stimulus matrix has dimensions NxJ prior to being transposed and the spectral responsivity matrix has dimensions NxK. Solutions may be obtained by Moore-Penrose psuedoinversion (designated mathematically as *pinv*) with all available data or principal eigenvector ranking where only the most significant stimuli set eigenvectors are included in the computation. Hardeberg offers further methodology for optimizing stimuli selection from a series of candidates by maximizing reflectance matrix singular value ratios in the assembled sets. This has practical importance for reducing the number of required measurements for adequately characterizing device spectral response. Advantages for full psuedoinversion versus the principal eigenvector ranking approaches in these reduced sets are also ultimately dependent on system noise sources such as quantization error.

$$c_{J,K} = s_{N,J}^T \omega_{N,K} + \varepsilon_K \quad (4)$$

Once native spectral sensitivities are well characterized in the design of a multispectral capture system, the next step involves determining specific spectral modifications appropriate to optimizing spectral estimation results for real stimuli. This is typically executed by adding some selected external filtration to the native device. Hardeberg summarizes several techniques for filter selection ranging from generating equal spaced filter (ESF) sampling at some desired bandpass characteristic over the visible spectrum to selecting spectral sampling which maximizes channel responsivity orthogonality in principal stimuli reflectance space<sup>23</sup>. In the case of the latter approach, training stimuli are evaluated via principal components analysis (PCA) to deliver a set of characteristic eigenvectors.

Candidate capture filters are then projected onto the  $I$  most significant eigenvectors and orthogonality in the  $I \times 1$  response vectors is maximized across  $K$  channels. Another approach involves exhaustive search wherein all possible permutations of needed filters for a  $K$  channel system are chosen from a starting collection of available filters. In this method, a candidate color stimuli set is identified and spectral estimation quality via rearrangement of Equation 4 or other candidate algorithms (to be discussed later) is maximized for all potential filter configurations. Hardeberg offers that ultimate estimation quality should be considered across several relevant spectral and colorimetric metrics, including spectral RMS and CIE color difference. Further, other researchers have found system noise considerations can negatively impact image quality when multiple channels are employed and so careful co-optimization of spectral and spatial quality should be considered also<sup>24</sup>.

In Hardeberg's work, it turns out that the exhaustive search optimized against either a spectral or colorimetric error minimization performs best for identifying appropriate filters for a  $K$  channel system, although at the expense of computational complexity. The approach used to maximize orthogonality shows promise, though only when given enough filters to choose from and a high enough value for  $K$ . In a compromised solution, the orthogonality constraint could be used to reduce candidates from a larger set of filters, followed by subsequent exhaustive search routines to maximize spectral estimation quality.

In work performed at MCSL by Berns, et al., spectral capture has been designed for 3 different camera systems comprising both full and abridged spectral resolution<sup>25</sup>. For full resolution capture, a monochrome sensor with a tunable liquid crystal filter delivers any combination of spectral responsivities at  $K$  total channels. For the first of the abridged systems, the monochrome sensor is used again but this time with a six-position sequential exposure filter wheel. In the second system, a Sinarback Bayer Color Filter Array (CFA) digital camera is used in combination with two alternating filters to deliver six channels of unique responsivity. For the CFA design, Berns, et al. have employed exhaustive search to determine the best possible combination of filters for reconstructing scene spectra. Selection criteria included a co-optimization of spectral estimation rms error, colorimetric error,  $\mu$ -factor (proximity of spectral sensitivity curves to standard color matching functions) and general signal-to-noise ratio. Results of modeling exposures for an Esser calibration target through 30,000 possible filter pairs are summarized in Figures 6 and 7. In various permutations of the system, different filter pairs from those showing especially good performance here have been implemented in MCSL research.

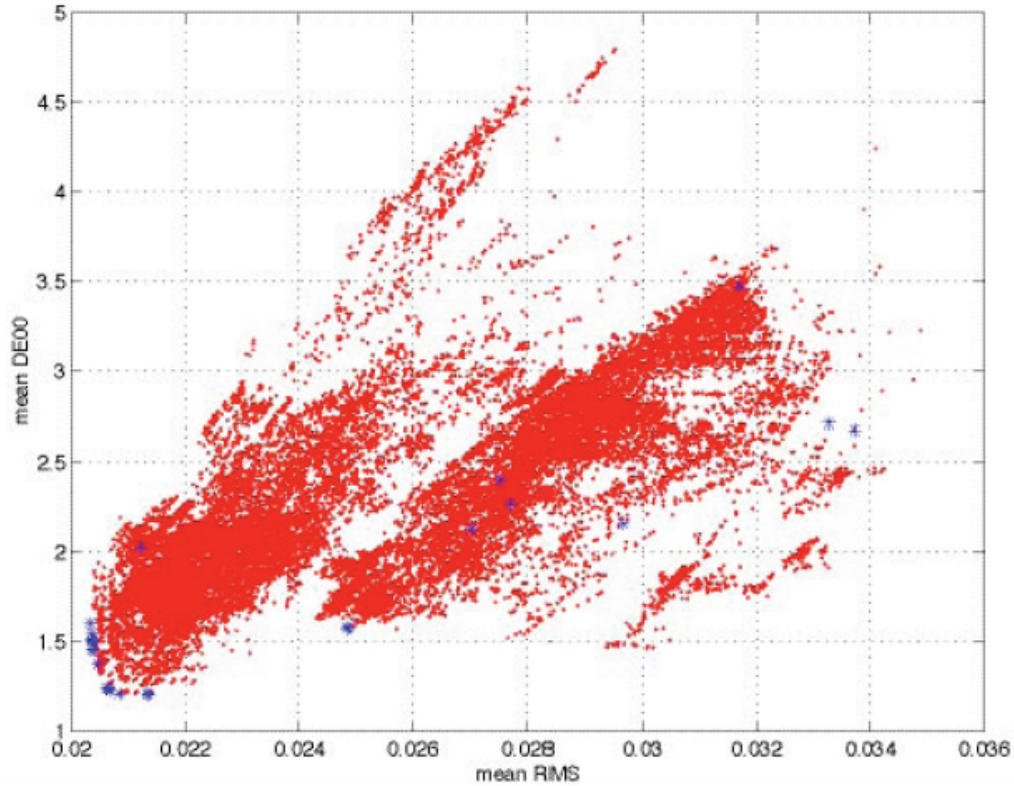


Figure 6. Mean color difference versus spectral rms error for 30,000 investigated filter pairs on Sinarback 54 dual exposure system, preferred candidates in blue (reproduced from Berns, et al.<sup>25</sup>)

Novati et al. have introduced an alternate statistical approach to filter selection for multiprimary capture known as Filter Vectors Analysis Method (FVAM)<sup>26</sup>. Here, a set of representative training color patches are selected and a collection of available optical filters for the multispectral capture system are identified. Vectors of linear exposure signal across all of the training colors for each filter are produced by simulation or direct measurement. A principal components analysis determines the most significant eigenvectors amongst these filter vectors and each actual filter is assessed to determine which most closely resembles the response characteristic of those first eigenvectors. A set of K total channels can be selected such that spectral or colorimetric estimation error is minimized with reasonable system complexity. Results achieved with this approach, though, are somewhat marginal relative to tactics already discussed.

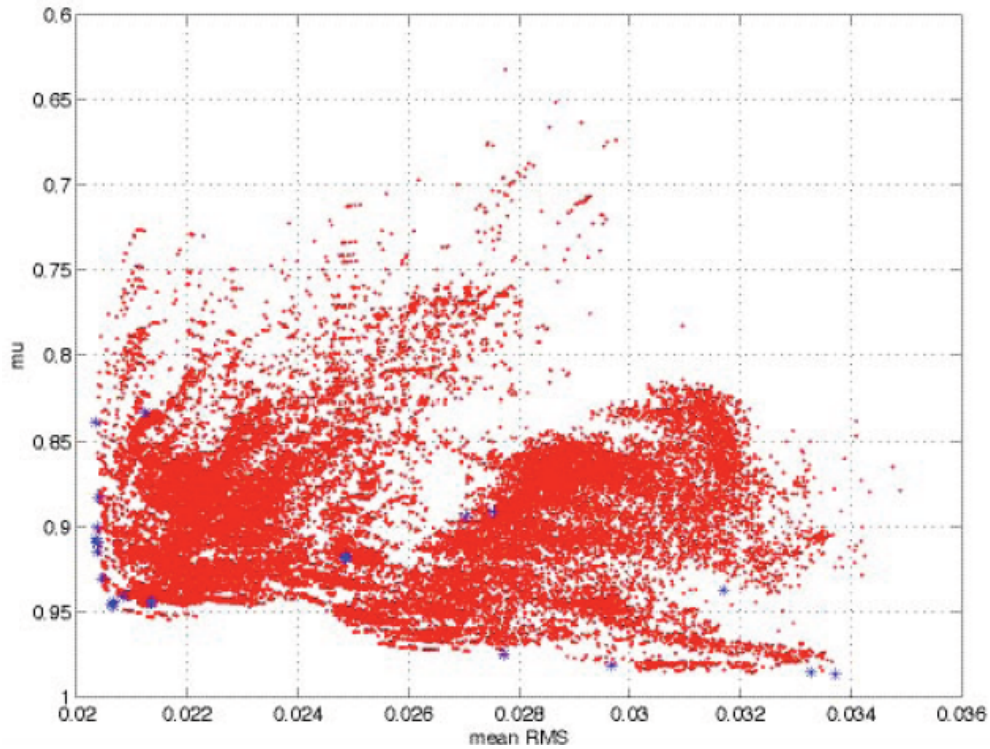


Figure 7.  $\mu$ -factor versus spectral rms error for 30,000 investigated filter pairs on Sinarback 54 dual exposure system, preferred candidates in blue (reproduced from Berns, et al.<sup>25</sup>)

## Training Set Selection

Additionally critical in maximizing spectral estimation quality for a multispectral capture system is selection of an appropriate training database used for device characterization. A number of researchers have identified viable candidate sets for multispectral work. Tajima, et al. have developed a 50,000 patch set representing photographic materials, graphic color printing output, paints, flowers, leaves, human skin tones and others known as the Standard Object Colour Spectra (SOCS) database<sup>27</sup>. Subsets of the collection are recommended for different imaging applications. Issues with the Tajima set include cultural bias in the included samples; especially for skin tones where nearly all measurements are made from the faces of Japanese women. The set is also influenced by differences in measurement device and geometry as well as sample preparation, though normalization and interpolation were applied where appropriate to limit undesirable data features.

Kohonen et al. have further summarized the spectral variability of a large number of existing databases, ranging from Munsell, Macbeth, Esser and NCS color patch collections to various studies addressing natural materials<sup>28</sup>. PCA is employed

within each set to characterize how many characteristic eigenvectors are necessary to reconstruct full database spectra to some reasonable mean and maximum colorimetric error. A higher number of required vectors indicates more spectral diversity in the particular data set, which may be beneficial in using the set to refine robust system design.

Within MCSL, there have been further attempts to customize fabricated training targets to specific spectral imaging applications. One such example is summarized by Mohammadi, et al.<sup>29</sup> where a collection of just nine high chroma and five neutral patches created using artist pigments provided a suitable training platform for predicting spectral reflectance of many of the more common spectral targets listed previously. This result was confirmation of previous work in spectral prediction quality utilizing cluster analysis<sup>30</sup>. In general, Mohammadi concludes spectral characteristics in the calibration training set are ultimately more important than patchset size, within the reasonable limits investigated. In art conservation as an example, limited available colorants certainly dictate strong results can be gathered from intelligently selected training patches.

From these large starting collections, it makes practical sense to attempt heuristic subsampling so as to yield high quality spectral training from a more reasonably sized set of patches, especially if characterization is to be attempted through actual imaging rather than system simulation. Pellegrini, et al. have studied a number of strategies for paring down the larger starting databases<sup>31</sup>. The first is Hue Analysis Method (HAM) wherein candidate spectra are considered under appropriate illumination and translated to CIELAB where the  $a^*b^*$  coordinates are explicitly considered. The hue circle in CIELAB is broken into  $n$  equal-angle segments and the particular samples closest to the centerline of each segment are selected, regardless of lightness or chroma. In a second approach called Camera Output Analysis Method (COAM), the output vectors,  $c$ , for a  $K$  channel capture system are simulated for every member of the candidate stimuli set and the results are subjected to PCA. The  $I$  most significant eigenvectors may be identified and the abridged training set is populated by patches whose camera output vectors best correlate with each eigenvector, according to angular distance, thereby enforcing maximum orthogonality in the chosen set. A variation on this theme may further be employed where primary patch selection based on the angular proximity of a candidate color output vector to a particular eigenvector is replaced by the principal component projection magnitude on that eigenvector. And in a third variation, both minimum and maximum principal component values are determined to further enforce significant sample spacing, but with a final sample set twice the size. A final approach explored by Pellegrini, et al. known as Linear Distance Maximization Method

(LDMM) ignores output proximity to the eigenvectors and simply attempts to maximize Euclidean distance in camera output vectors amongst the samples. This method is similar to work by Hardeberg outlined previously where sample reflectance vectors rather than camera output vectors for a constructed training set are selected based on optimizing singular value ratios in the assembled set<sup>22</sup>. Pellegri found through experimentation with the Macbeth CCDC patch set as starting population that the Hardeberg and LDMM methods deliver the best spectral training results while patchset size must be restricted to avoid over-fitting system noise. Roughly 31 of the 177 unique patches in the chart were sufficient for generating low error simulation models.

To co-optimize training and filter set selection approaches, Schettini, et al. have executed a full experiment addressing permutations of the FVAM and ESF filter selection techniques in combination with Hardeberg and LDMM training patch identification<sup>32</sup>. Utilizing a test bed containing a tunable filter with a 10nm bandpass and the Macbeth CCDC target, various patchset size configurations are summarized from real acquisition data (as opposed to simulation). Though definitive best practice is not generally reported in the results, the approach offers a guideline for future experiments and may be repeated with new prototype camera systems. As example of guidance offered, one reasonably conclusive finding is that spectral estimation based on real acquisition data tends to promote fewer capture channels are needed than when the same exercises are executed in simulation. This likely derives from noise influences in the models developed from real capture signals.

## **Spectral Estimation Algorithms**

As has been summarized, traditional three-channel electronic image capture systems are only capable of realistically interpreting metameric predictions of scene stimuli at each sampled pixel, and then only if their spectral responsivities are reasonable approximations of some standard color matching function set. For spectral imaging systems, a higher dimension response estimation is required. Reviews have thus far been provided for channel responsivity and training set optimization for multispectral imaging but mostly in the absence of detail around the spectral estimation algorithm employed. Generally, these algorithms fall into three classifications; direct, interpolated and learning-based. For the first two, training set selection does not apply as the spectral characteristic of a particular stimuli are directly interpreted from peak sensitivity and bandpass characteristics of each of the K channels in the acquisition system. Spectral signatures may be

presented in  $N=K$  dimensions of resolution or increased resolution may be interpolated via suitable spline or other curve-fitting techniques. In the third approach, estimation algorithms are derived and optimized from *a priori* information from select training spectra. For systems with lesser spectral sampling, this approach proves most practical and a number of solutions have been proposed.

One of the earliest examples of algorithm development for spectral estimation is provided by Pratt and Mancill who offer three forms of solution<sup>33</sup>. In the first, the discrete image capture integration model of Equation 4 provides the starting basis where  $\mathbf{s}_{N,J}$  may be isolated via psuedoinversion from known integrated capture signals and system spectral sensitivities. It is essentially the same premise as that offered by Hardeberg for responsivity estimation but with the alternate unknown quantity. Pratt and Mancill further describe a variation on the technique employing a suitable  $N \times N$  smoothing matrix,  $\mathbf{G}$ , which prevents aggressive oscillation in the inversion, see Equation 5. In their third variation, Wiener estimation is employed where the estimated spectrum of  $J$  patches,  $\hat{\mathbf{s}}$ , is assumed to be a sample of a vector random process with known mean and covariance matrix,  $\mathbf{K}_s$ , which is itself modeled by a first-order Markov process when actual training set characteristics are unknown.  $\mathbf{K}_n$  is further the covariance matrix representative of uncorrelated camera signal noise; the total expression is summarized as Equation 6. All three of the Pratt and Mancill variations may be executed with no *a priori* spectral stimulus knowledge, making them especially attractive for many practical imaging applications. They do, however, each require presumption of a system linear response in the image capture and a stable characterization of camera responsivities. Wiener estimation, further, may be improved if system covariance is characterized fully from some training set versus more generic Markov treatments.

$$\hat{\mathbf{s}}_{N,J} = \mathbf{G}^{-1} \boldsymbol{\omega}_{N,K} (\boldsymbol{\omega}_{N,K}^T \mathbf{G}^{-1} \boldsymbol{\omega}_{N,K})^{-1} \mathbf{c}_{J,K}^T \quad (5)$$

$$\hat{\mathbf{s}}_{N,J} = \mathbf{K}_s \boldsymbol{\omega}_{N,K} (\boldsymbol{\omega}_{N,K}^T \mathbf{K}_s \boldsymbol{\omega}_{N,K} + \mathbf{K}_n)^{-1} \mathbf{c}_{J,K}^T \quad (6)$$

For an improvement on the basic Wiener estimation model, Murakami, et al. have suggested expanding the assumption of simple Gaussian input probability functions to a nonlinear treatment based on actual stimuli probability distributions<sup>34</sup>. The method, known as Gaussian Mixture Distribution (GMD), minimizes mean square errors of spectral estimations when the input signals are treated as a random sequence of GMD. Successful improvements over straight

Wiener estimation are based, in part, on the inclusion of *a priori* training set probability distributions and cluster analysis to group stimuli according to fundamental spectral similarities.

One major practical issue with the Markov-based and *a priori* Wiener estimation algorithms is their overly simplistic treatment of noise, including the improbable presumption that system noise and captured signal are independent. Traditional electronic image capture models accommodate both true independent noise such as dark current and readout error and signal-dependent photonic shot noise. Urban, et al. have offered significantly improved spectral estimation for real capture signals via Wiener estimation accomplished with additional spatio-spectral and edge preserving Wiener variations<sup>35</sup>. These techniques offer especially useful results for high spatial frequency scene content.

Another popular technique for spectral estimation described by Vrehl and Trussell incorporates PCA to define spectral stimuli<sup>36</sup>. In this approach, spectral data are expanded into a scaled summation of orthonormal basis functions. Care is taken to identify basis functions from a comprehensive decomposition of a full set of intended target stimuli with spectral characteristics representative of the imaging situation. Eigenvalues further summarize the total variability contribution of each eigenvector in the set and allow the basis functions to be ranked by significance. The number of eigenvectors to be retained in subsequent calculations may be determined by evaluating the cumulative eigenvalue sum of the ranked vectors versus a threshold or by modeling reconstructed sample spectra from the eigenvectors and retaining the number necessary to achieve minimum colorimetric or spectral accuracy versus the originals. Once a collection of  $I$  significant eigenvectors,  $\mathbf{e}_{N,I}$  with spectral resolution,  $N$ , is computed (see Tzeng and Berns for an expanded treatment of the full PCA computations used with spectral data<sup>52</sup>), an input aim or measured spectral stimuli set,  $\mathbf{s}_{N,J}$  is decomposed via projection operators as in Equation 7 to its  $I$  principal components,  $\mathbf{b}_{i,j}$  ( $i=1$  to  $I$ ). If  $\mathbf{e}$  is not square then some appropriate asymmetrical inversion technique such as the Moore-Penrose psuedoinverse function must be applied. Reconstruction of the PCA-estimated stimuli,  $\check{\mathbf{s}}_{N,J}$  is then achieved according to Equation 8 and the difference between  $\mathbf{s}$  and  $\check{\mathbf{s}}$  represents the baseline or minimum system spectral error.

$$\mathbf{b}_{i,j} = \text{inv}(\mathbf{e}_{N,I})\mathbf{s}_{N,J} \quad (7)$$

$$\check{\mathbf{s}}_{N,J} = \mathbf{e}_{N,I} \cdot \mathbf{b}_{i,j} \quad (8)$$

Variations on this principal components decomposition have also been proposed where an appropriate mean of the spectral population is subtracted from each sample and the residual spectral curves are subjected to the orthonormal rotation. This method is suggested in systems where the spectral population's mean is not sufficiently reconstructed itself by the  $I$  selected eigenvectors derived from the full spectral PCA. In such cases,  $\mathbf{s}$ , in Equation 7 would be pre-processed by subtracting out  $\bar{s}$ , the population's spectral mean and  $\mathbf{e}$  would similarly represent eigenvectors of the residual spectra. In Equation 8, the population mean would be added as offset to properly predict  $\check{\mathbf{s}}$ .

Vrehl and Trussell offer an additional variation on the PCA method where principal components,  $\mathbf{b}$ , may be determined from integrated camera signals rather than direct decomposition of known spectral stimuli (such as in cases where an image of unknown spectral stimuli is captured). This approach requires knowledge of the system spectral responsivities in each of the  $K$  channels and effectively makes use of Equation 4 but with Equation 8's reconstructed spectra substituted in for  $\mathbf{s}_{N,J}$ , see Equation 9. Through appropriate rearrangement,  $\mathbf{b}$  may be isolated and independently determined for any imaged stimuli. The approach does, though, require previous identification of relevant eigenvectors,  $\mathbf{e}$ , for the defined stimuli set.

$$\mathbf{c}_{J,K} = (\mathbf{e}_{N,I} \cdot \mathbf{b}_{I,J})^T \boldsymbol{\omega}_{N,K} + \varepsilon_K \quad (9)$$

In the general PCA approach, if  $I$  is set to the spectral resolution of the original target stimuli,  $N$ , all variability will be accommodated in the orthonormal rotations and the original and reconstructed spectral signatures will match exactly. However, PCA is employed traditionally with a limited number of basis functions so as to promote efficiency in data communication and to eliminate some level of measurement noise or data redundancy.  $I$  would thus be kept less than the spectral resolution. In multiprimary and multispectral image capture and display systems there is also a mathematical convenience to setting  $I$  to the number of capture and/or display channels so long as the eigenvalue ranking suggests such a choice is statistically relevant. This, however, is not a strict requirement of spectral image processing designs. In order to avoid underdetermined solutions, though, the value of  $I$  should be kept equal to or less than the channel count,  $K$ .

A consequence of reduced dimensionality in the eigenvector set selected may be that some unintended error in spectral reconstruction is encountered. Further, this error may be differently manifested depending on exactly what data space is being deconstructed and what number of basis functions are retained. In turn, an alternate data space may offer additional conveniences to downstream processing.

Imai, et al. have addressed practical training-based PCA spectral estimation in multichannel capture<sup>53</sup>. By linearly relating multichannel camera outputs,  $\mathbf{c}$ , to principal components,  $\mathbf{b}$ , for a set of conditioning stimuli, a best-fit linear transform,  $\mathbf{L}$ , can be determined. Patches of known reflectance are decomposed in reflectance or other appropriate data space to optimize the linear prediction quality. Equation 10 summarizes the established linear relationship with  $\mathbf{L}$  possessing a dimensionality of  $I \times K$ . Solution of  $\mathbf{L}$  can be achieved using a psuedoinverse rearrangement of this expression. Subsequently, any real camera signal set,  $\mathbf{c}$ , derived from capture of a full gamut of subject colors can be multiplied by  $\mathbf{L}$  to generate pixel-by-pixel principal component scalars which are in turn used in Equation 8 to deliver the pixel's spectral estimation.

$$\mathbf{b}_{i,j} = \mathbf{L}_{i,k}(\mathbf{c}_{j,k})^T \quad (10)$$

Imai, et al. have found via the PCA approach that manipulating the spectral space deconstructed into principal components may improve overall spectral estimation accuracy. For example, reflectance factor is typically considered the most applicable space for digital capture signal correlations because the two spaces should vary linearly with one another. In other instances though, a Kubelka-Munk spectral absorption and scattering model may be better behaved when related to correspondingly transformed digital capture signals (so as to again enforce a plausible linearized model). This derives fundamentally from relating both the spectral space and the camera capture space to linear functions of colorant concentration for the proposed training set. In the Imai work, it is yet a third proposed spectral space based on a square root relationship to reflectance that actually delivers the best prediction results, again founded on relating the spectral space to colorant concentration in an empirical model.

Zhao and Berns compare two additional training-dependent spectral estimation algorithms based on simple psuedoinverse linear relationships and the Matrix-R method<sup>37</sup>. The former method resembles that already summarized in Equation 10, but encompassing a translation from integrated camera signals directly

to spectral signature rather than to principal component scalars, Equation 11. (In the following derivations, Zhao's original variable definitions will be used, a departure from and in place of some variables already thus far defined.) After assembling a suitable reflectance-space training set,  $\mathbf{N}$ , and determining resultant camera output signals,  $\mathbf{c}$ ,  $\mathbf{M}_s$  is computed by inversion of the expression, Equation 12, and may be substituted again into Equation 11 for any real stimuli's capture signal to generate an estimated spectrum,  $\check{\mathbf{N}}$ . The practical utility of this method derives from identifying strongly representative training spectra for the original determination of  $\mathbf{M}_s$ .

$$\mathbf{N}_{N,J} = \mathbf{M}_s(\mathbf{c}_{J,K})^T \quad (11)$$

$$\mathbf{M}_s = \mathbf{N}_{N,J} \times \text{pinv}(\mathbf{c}_{J,K})^T \quad (12)$$

Matrix-R represents a spectral estimation approach derived from the Wyszecki hypothesis of metameric black and the mathematical treatments of Cohen and Kappauf. In 1953, Wyszecki hypothesized that any color stimulus can be shown as the summation of two spectra, the fundamental stimulus,  $\mathbf{N}^*$  and the metameric black,  $\mathbf{B}$ . Tristimulus values for the metameric black are (0,0,0) by definition as it carries no colorimetric impact. The fundamental stimulus solves to the exact tristimulus values of the original spectra based on choice of illuminant and observer. Matrix-R theory represents the mathematical decomposition of any stimulus into these two spectra. The orthogonal projector,  $\mathbf{R}$ , has dimensionality  $N \times N$  and is derived from a tristimulus weighting matrix,  $\mathbf{A}$ , Equation 13.  $\mathbf{A}$  has dimensionality  $N \times 3$  and represents the illuminant  $\times$  observer weightings chosen for colorimetric calculation.

$$\mathbf{R}_{N,N} = \mathbf{A}_{N,3}(\mathbf{A}_{N,3}^T \mathbf{A}_{N,3})^{-1} \mathbf{A}_{N,3}^T \quad (13)$$

Equations 14 to 16 further summarize the orthogonal projections of a reflectance stimulus,  $\mathbf{N}$ , onto matrix  $\mathbf{R}$ , generating both the fundamental and metameric black stimuli,  $\mathbf{N}^*$  and  $\mathbf{B}$ . In these expressions,  $\mathbf{I}$  is an  $N \times N$  identity matrix. Combining Equations 13 and 14, the fundamental stimulus may also be computed as a function of stimuli tristimulus values,  $\mathbf{T}$ , see Equations 17 and 18.

$$\mathbf{N}^* = \mathbf{R}_{N,N}\mathbf{N} \quad (14)$$

$$\mathbf{B} = \mathbf{N} - \mathbf{N}^* \quad (15)$$

$$\mathbf{B} = (\mathbf{I} - \mathbf{R}_{N,N})\mathbf{N} \quad (16)$$

$$\mathbf{T} = \mathbf{A}_{N,3}^T \mathbf{N} \quad (17)$$

$$\mathbf{N}^* = \mathbf{A}_{N,3}(\mathbf{A}_{N,3}^T \mathbf{A}_{N,3})^{-1} \mathbf{T} \quad (18)$$

In applications where spectral radiance is considered rather than spectral reflectance,  $\mathbf{A}$  is simplified to color matching functions of a specified observer only and  $\mathbf{N}$  is replaced by the more generic radiant spectral stimuli notation we've used thus far,  $\mathbf{s}$ . Fundamental and metameric stimuli are likewise described as radiance functions.

To apply Matrix-R theory to a spectral estimation problem involving a capture system with  $K$  channels and known spectral response, Zhao and Berns have split the spectral prediction into two parts, one focused on generating the fundamental stimulus and the other on generating the metameric black. A series of training patches are measured to derive actual spectral reflectance values and Equation 12 is implemented via Moore-Penrose pseudoinversion to identify  $\mathbf{M}_s$ . Camera signals,  $\mathbf{c}$ , may be derived from either direct measurement or linear model as appropriate. Concurrently, the same training patch camera signals are further related to calculated tristimulus values for the set via Equation 19 where  $\mathbf{T}$  are computed from the measured patch reflectances and matrix  $\mathbf{A}$  according to Equation 17. In practice,  $\mathbf{M}_c$  is the unknown in this expression and is calculated by minimizing predicted color differences for the training set in a linear optimization.

$$\mathbf{T}_{3,J} = \mathbf{M}_c(\mathbf{c}_{J,K})^T \quad (19)$$

When both Equations 11 and 19 are used with some real stimuli's camera output vector and the trained values for  $\mathbf{M}_s$  and  $\mathbf{M}_c$ , estimated values for both reflectance,  $\check{\mathbf{N}}$ , and tristimulus,  $\check{\mathbf{T}}$ , for that stimuli may be generated. These estimates then provide input to the Matrix-R method according to Equations 20 and 21 where the tristimulus prediction is inserted into Equation 18 to generate the fundamental stimulus,  $\mathbf{N}^*$ , and the spectral reflectance prediction is inserted into Equation 16 to generate the metamerick black,  $\mathbf{B}$ .

$$\mathbf{N}_c^* = \mathbf{N}^* + \mathbf{B} \quad (20)$$

$$\check{\mathbf{N}}_c = \mathbf{A}_{N,3}(\mathbf{A}_{N,3}^T \mathbf{A}_{N,3})^{-1} \check{\mathbf{T}} + (\mathbf{I} - \mathbf{A}_{N,3}(\mathbf{A}_{N,3}^T \mathbf{A}_{N,3})^{-1} \mathbf{A}_{N,3}^T) \check{\mathbf{N}} \quad (21)$$

The main premise behind the Matrix-R method is combining spectral and colorimetric transforms to derive the best prediction in both spaces. In Zhao and Bern's work with standard color patch targets and artist paints, the technique did, in fact, show improvement over simple psuedoinverse estimation techniques (Equation 11 alone) for colorimetric predictions without detrimental impacts to spectral prediction. Figure 8 summarizes the full flow of calculations.

A few concerns regarding this method must be enumerated for more general spectral estimation applications. First, the orthogonal operator,  $\mathbf{R}$ , uses tristimulus weights as additive primaries for the projection space when actual system colorants might provide even better results. Second, any number of more sophisticated predictions of the metamerick black may replace the simple psuedoinverse approach used. Several have already been discussed in this review. Finally, matrix-R tends to tweak spectral prediction to the benefit of one particular illuminant and observer definition for colorimetric optimization. In their review, Zhao and Berns express some concern that this colorimetric tweak may, in some cases, worsen spectral estimation accuracy. For true reduction in metamerick limitations in a multispectral imaging system, a broader solution may be necessary.

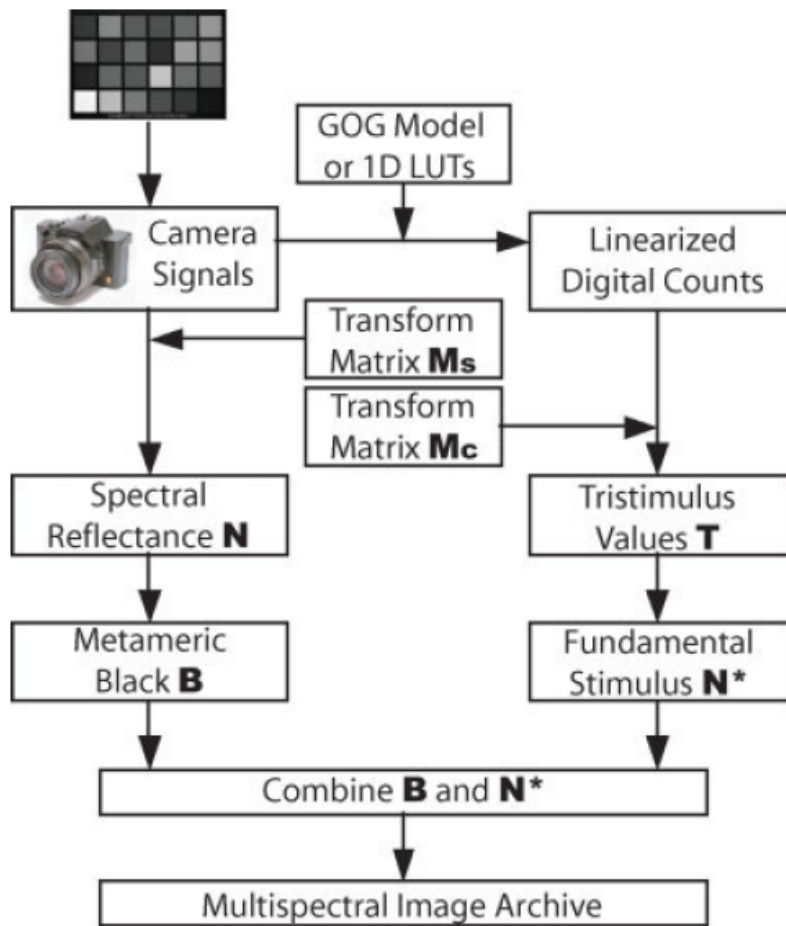


Figure 8. Functional flow diagram for Matrix-R spectral estimation (reproduced from Zhao, et al.<sup>37</sup>)

### RIT Prototype Multispectral Video Camera

With all of these hardware and image processing design options available, recent work at RIT yielded a functional six-channel video camera designed for abridged multispectral recording<sup>38</sup>. Twin Imaging Source DFK 31BF03 CCD cameras capable of 1024 x 768 sampling at 30 frames/sec are oriented as in Figure 9. The design enables imaging through a white light beamsplitter to simultaneously record six channels of integrated information. Though the cameras employ native Bayer CFAs, external filters for the transmission and reflection paths have been optimized to shape preferred spectral responsivities across the visible spectrum in all six channels. An exhaustive search of commonly available filter materials optically coupled to the native CFA sensitivities was performed via simulation. The goal was

minimization of observer metamerism via PCA training in the estimated spectra of the MacBeth CCDC color target illuminated by a combination of a 2856 K Planckian blackbody (effectively, CIE illuminant A), CIE D65, and the CIE F2 standard fluorescent illuminant. The filters chosen were Schott BG40 and VG09 glass, each 1mm thick. Spectral estimation is achieved utilizing the PCA approach of Equations 7 -10, further described by Vrehl and Trussel and Imai, et al. The six-channel spectral responsivities are shown in Figure 10a and an example spectral estimation of a MacBeth green patch made via the camera is shown in Figure 10b. It is worth noting that the translation from raw camera signal to predicted eigenvector principal component scalar that is fundamental to this particular methodology permits some reasonable amount of spectral estimation outside the sensitivity bounds of the camera (390 to 700nm in this example). This is for cases where the generated eigenvectors possess spectral power outside the camera’s sensitivity but may be expected to break down where there is greater spectral discrepancy versus the sensing limits. And as described previously, spectral continuity and a reduced number of significant eigenvectors from the PCA training and reconstructions sets are also critical to the quality of reconstruction expected. More variable target spectra (greater number of critical eigenvectors) or fewer sensing channels would impact estimation quality negatively versus the six-channel scenario described here. Native CFA responses optimized for traditional three-channel color reproduction applications can also be a restrictive element in yielding ultimate spectral estimation performance in systems like this and so investigations into custom materials and alternate optical designs remains active.

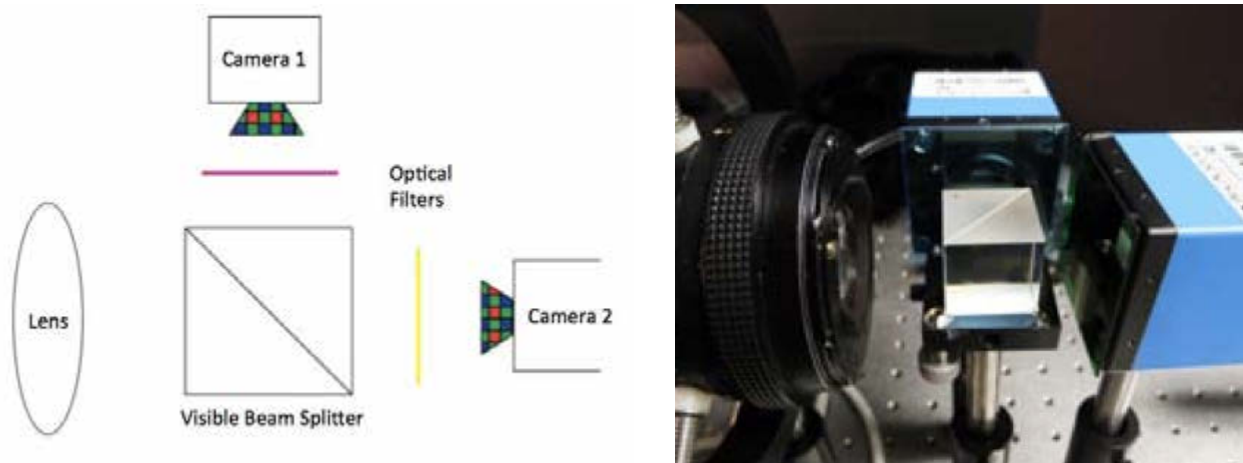


Figure 9. RIT multispectral camera schematic

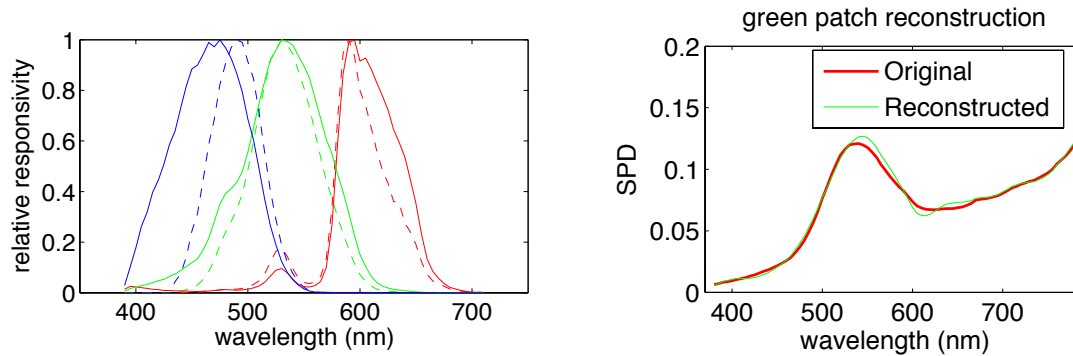


Figure 10. a) RIT camera spectral sensitivities b) spectral estimation of MacBeth green patch using camera

## Multispectral Displays

Traditional image display paradigms for both still and motion picture applications are rooted in a three-primary metameric match model relying exclusively on Grassmann’s laws of additivity. By integrating real radiometric spectra to suitable tristimulus scalars, basic RGB displays are capable of reasonable color reproduction across an adequate gamut of observable colors. Current trends in cinema display reflect a gamut expansion from the ITU-R Rec. 709 primary space of HDTV to the Digital Cinema Initiatives (DCI) “P3” primary set (ratified as SMPTE-431) and beyond to new laser-based technologies (ITU-R Rec. 2020). As previously discussed, gamut expansion in a three-channel display comes at the cost of spectral selectivity for the individual primaries and a potential challenge to generating reasonable overall display luminance as off-peak energy is eliminated from each primary’s output. And increased selectivity translates to greater observer metamerism and poorer spectral reproduction capabilities<sup>8</sup>. Thus a number of researchers including the Natural Vision project have turned to higher primary counts to attend to issues of both gamut volume and spectral reproduction accuracy.

Long and Fairchild have attempted six-channel spectral reproduction using external filtration in conjunction with a pair SMPTE-431 HDTV video projectors, optically superimposed as in Figure 11<sup>57</sup> (see Chapter 5 for detail). Steeply cutting bandpass filters can be used to narrow the native primary spectra and effectively enlarge colorimetric gamut, however, such spectral isolation leads to very poor spectral rms when reproducing real world surface colors such as those found in the Macbeth Color Checker. Beyond spectral shortcomings, the design also suffers from worsened observer metamerism versus the native three-channel device. Results suggest a larger number of broad and narrow spectral primaries may be preferable to simultaneously address spectral and colorimetric gamut expansion.

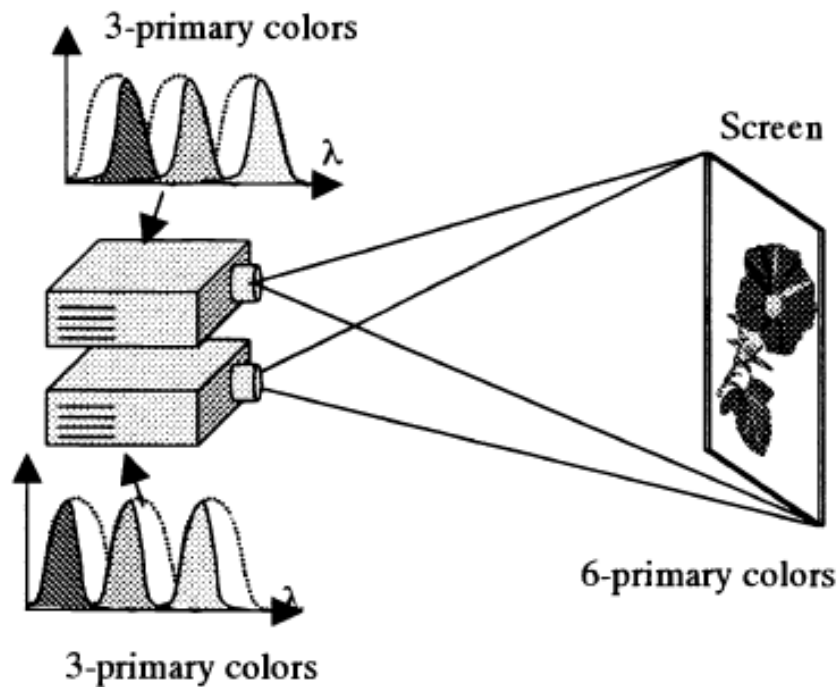


Figure 11. Dual overlaid projection paradigm of Ajito, et al. (figure reproduced from Ajito<sup>5</sup>) similarly used by Long & Fairchild

Ajito, et al. have similarly attempted manipulation of the native primary spectra of a D-ILA projector pair by internally adjusting the optical paths using high and low pass cut-off filters<sup>39</sup>. In their work, cut-off frequencies were optimized in all six channels to maximize CIELUV gamut volume. Despite a poor native contrast ratio and some peak luminance lost to the shaping filters, the system performed quite well in accommodating Pointer surface colors in a colorimetric sense. Continued component refinement could address both shortcomings. Unfortunately, though, little attention was paid to the larger issues of accurate spectral reconstruction and observer metamerism that are worsened when spectral peaks are narrowed so aggressively to maximize colorimetric gamut volume. Similar projection retrofitting efforts to maximize CIELAB and CIELUV color gamut with multiple DLP-based systems have also been investigated by Nystrom<sup>40</sup>. Hutchison has described alternate color filter wheel designs for single chip DLP devices, adding yellow and cyan primaries to expand gamut and device brightness<sup>41</sup>. Tomizawa, et al. have summarized emissive LCD display structures employing at least five sub-pixels to optimally accommodate the Pointer surface color gamut with secondary optimization of the screen luminance<sup>42</sup>. By restricting five-channel pixel architectural layout to the original RGB pixel dimensions in the backlit LCD system, white luminance may be enhanced simultaneously with absolute CIELUV gamut.

Ajito, et al. have further developed a multiprimary projection display by employing diffraction gratings instead of color filter arrays in an LCD modulation scheme<sup>43</sup>. Source white light is split into controlled diffraction bands across a neutral LCD panel where a collection of  $K'$  sub-pixels is used to produce a  $K'=N$  channel display, Figure 12. The design carries a number of optical complexities influencing final primary spectral distribution and saturation including chromatic aberration control, bandwidth management and LCD contrast ratio degradation. Utilizing the design in a practical configuration, a seven-channel display has been created with minimal colorimetric gamut expansion beyond typical NTSC video specifications, Figure 13. With improved optical design, the approach could be effective for generating distinctly controlled primary spectra at a high sampling across the visible domain, though modulator resolution must be improved for the sake of the viewer's visual integration as each full color pixel requires high sub-pixel counts.

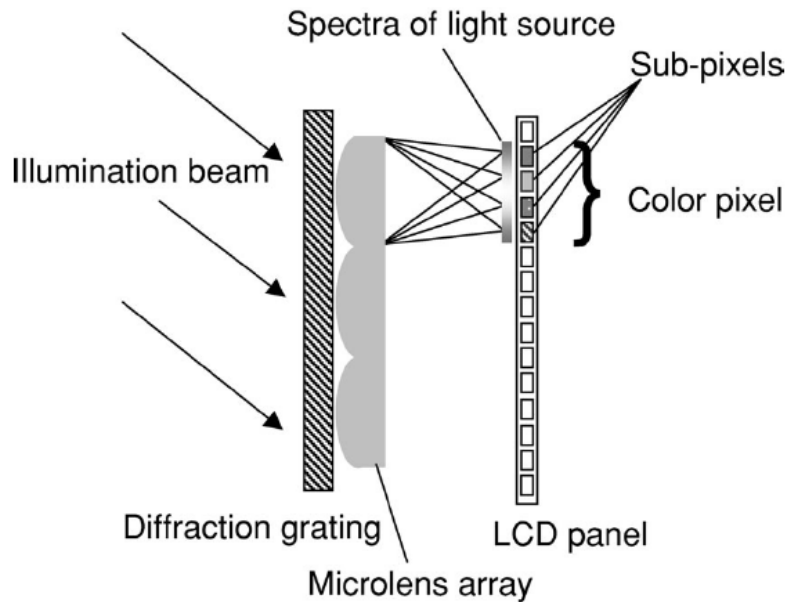


Figure 12. Diffraction-based multiprimary LCD projector (reproduced from Ajito, et al.<sup>43</sup>)

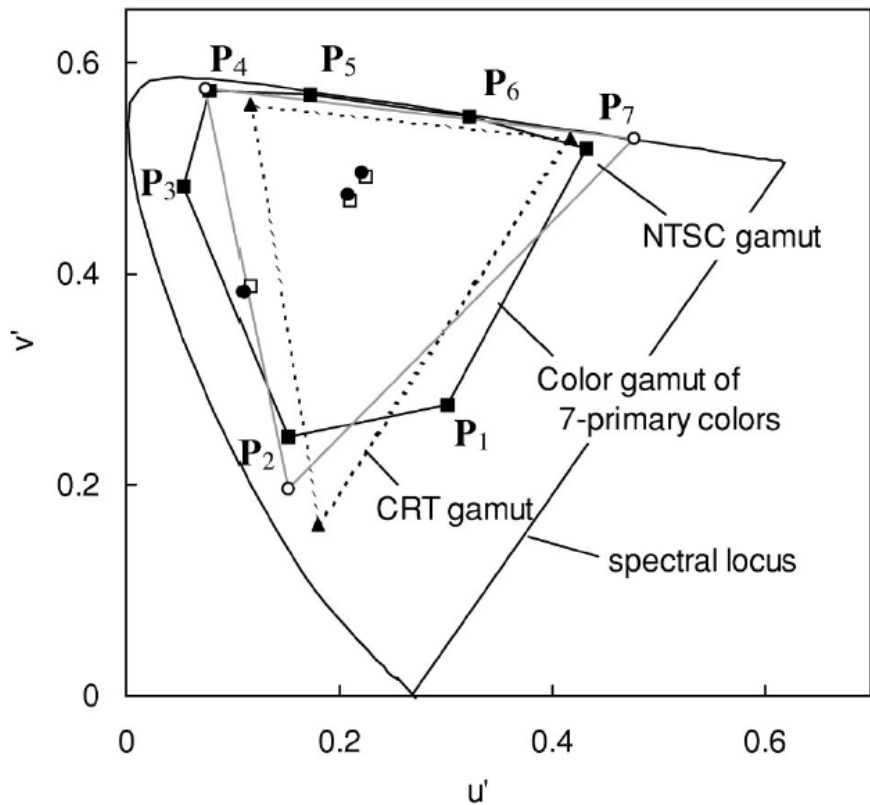


Figure 13. Ajito et al. seven-primary display gamut (reproduced from Ajito<sup>43</sup>)

### Driving Multispectral Displays

Building displays capable of reproducing spectral stimuli or expanded colorimetric targets represents only half of the design challenge. Once constructed, these devices require appropriate color processing algorithms for delivering meaningful benefit versus traditional three-channel systems. One of the more obvious challenges derives from the excess degrees of freedom associated with multiprimary displays used to image three-channel image signals, whether those signals be traditional device-dependent RGB values or independent XYZ colorimetry. Ajito, et al. have proposed a simple geometric solution based on matrix switching<sup>44</sup>. The approach takes advantage of CIEXYZ as a volumetric three-space in which a polyhedral color solid is constructed from all permutations of  $K'$  primaries, Figure 14. The display's individual primary vectors in XYZ space are denoted  $P_k$ .

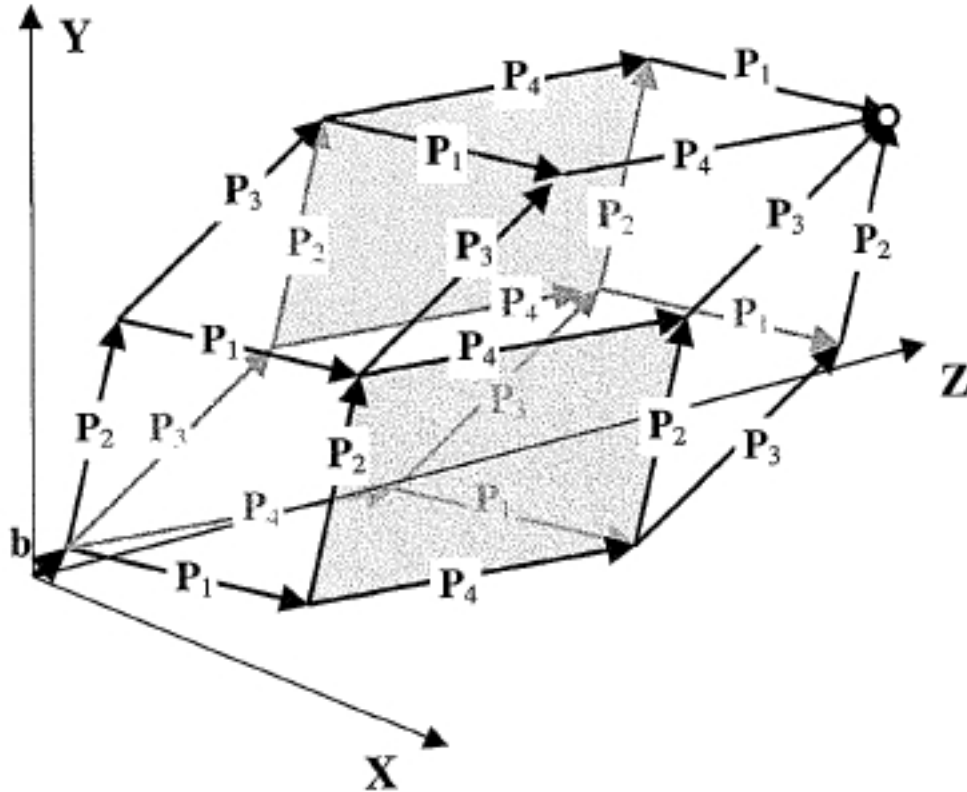


Figure 14. Example four-primary display color solid in XYZ three-space (reproduced from Ajito, et al.<sup>44</sup>)

A total of  $K'(K'-2)$  quadrangle pyramidal solids may be drawn to subdivide the polyhedron where the baseline black XYZ coordinate position,  $b_{XYZ}$ , is the vertex of each pyramid and parallelogram planes of each combination of two of the  $K'$  primaries are the bases. It should be noted that this scheme does not eliminate the excess degrees of freedom when a display with more than three primaries is used to deliver a three-channel colorimetry aim, but rather, pre-segments all of XYZ three-space to particular allowed combinations of the primaries as a function of colorimetric location. Identifying the appropriate pyramids containing an aim color XYZ set,  $\mathbf{W}_{XYZ}$ , becomes the principal computation since the pyramidal solids are all non-overlapping in the XYZ three-space. With each pyramid joint coordinate,  $q_l$ , generically defined as in Figure 15, Equation 22 specifies the fractional addressing of any aim  $\mathbf{W}_{XYZ}$ .

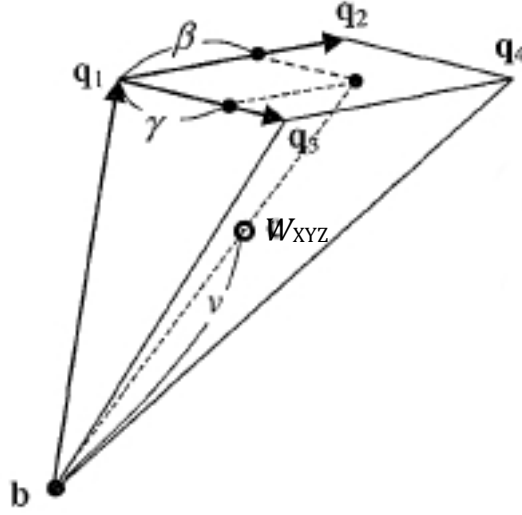


Figure 15. generic quadrangle pyramid from polyhedral color solid along with example interpolation (reproduced from Ajito, et al.<sup>44</sup>)

$$W_{XYZ} = \nu[(q_1 - b) + \beta(q_2 - q_1) + \gamma(q_3 - q_1)] + b_{XYZ} \quad (22)$$

Each of the fraction terms  $\nu$ ,  $\beta$  and  $\gamma$  must lie between 0 and 1 by definition and only one pyramid will satisfy this dynamic range constraint. Further, Ajito et al. have simplified the pyramid identification by converting tristimulus aims in three-space to planar chromaticity coordinates. Projection of the black-vertex polyhedra into the 2-dimensional chromaticity space yields a surface of non-overlapping, unique triangles. Using this strategy, all of visible chromaticity space can be pre-processed to define which of the  $K'(K'-2)$  subdivisions the aim color will occupy and the resulting 2-D index LUTs can be implemented computationally fast. Following, pyramid identification, linear estimation of the relative primary amounts needed to deliver aim colorimetry becomes a simple matrix computation involving the relevant primary vectors. Principle sources of inaccuracy in this scheme come from quantization error in the chromaticity LUT, additivity and scalability failures in the three-space volume model for real displays and measurement noise. Actual simulations of wide gamut XYZ target patches performed by Ajito using a six-primary multispectral display show excellent average and maximum color error.

As an alternative to matrix-switching, Motomura has suggested a similar three-space interpolation scheme based on equal-luminance plane mapping<sup>45</sup>. Rather than pyramidal polyhedra, aim color coordinates are projected into a triangle within the display's gamut whose vertices are located on the display neutral axis (all primaries driven equally) and on gamut ridgelines (vector boundaries of the three-space gamut volume). The full triangle also lays on the same luminance coordinate as the aim color coordinates. Identification of the triangular plane encompassing the aim color follows a relatively trivial (though computationally expensive) recipe and ultimate primary drive values are linearly interpolated from the particular full display drive matrices for the triangle vertices. As with the matrix-switching method, the gamut volume in colorimetry space is pre-parsed into finite regions. By enforcing the equi-luminance interpolation, smoothness of primary control gradations can be better imparted across smoothly varying input color series. In particular, aim color series which vary in CIELAB  $c^*$  but are otherwise constant in luminance and hue can be contained entirely within a single interpolation triangle and so yield particularly uniform gradations.

Because the excess degrees of freedom for matching single observer colorimetric aims with a multiprimary display are managed by subdividing the display's gamut based on the particular colorimetry vectors of each primary, the matrix switching and equal-luminance triangle methods are both prone to serious boundary errors for different types of stimuli ramps. In particular, two colorimetrically adjacent colors whose matrix switching solution described across a pyramid boundary yields a completely separate primary reconstruction subset will also typically result in distinctly different reconstructed spectra. Thus spectral dissimilarity may be large where colorimetric differences in the original pair were small. While this is not mathematically a problem for the standard observer, these discrepancies exacerbate metamerism failure for non-standard observers. In real multiprimary displays, the equal-luminance triangle method potentially mitigates some of these issues as interpolation cells are not as rigidly defined along display primary vectors as in the matrix switching method and as one vertex in the triangle is always defined on the display neutral axis (though results from Motomura do still suggest primary nodal transitions seen across aim color series). A concern with the equal-luminance triangular interpolation, though, is a more complex computation sequence for identifying vertices, potentially taxing the image processing workflows.

Konig, et al. have identified a methodology for minimizing the impact of transition errors in accommodating excess degrees of freedom in multiprimary display<sup>46</sup>. For the simple linear addition model of a multispectral display, Equation

23 shows the colorimetric reconstruction,  $\hat{W}_{XYZ}$ , as a function of linear primary radiometric scalars,  $\alpha$ .  $\alpha$  is a column vector of  $K'$  channels and  $\mathbf{P}_{3,K'}$  is a  $3 \times K'$  matrix of the CIE colorimetric vectors for each individual fully-driven primary.

$$\hat{W}_{XYZ} = b_{XYZ} + \mathbf{P}_{3,K'} \cdot \alpha \quad (23)$$

The simplest solution to the over-specified calculation of  $\alpha$  from an aim  $\hat{W}_{XYZ}$  involves the psuedoinversion,  $pinv(\mathbf{P}_{3,K'})$ , of the primary colorimetry matrix, however, this is only one possibility from an infinite combination of solutions if  $K' > 3$ . Konig, et al. have instead suggested inverting Equation 23 according to Equation 24 where each vector  $M_f$  is a  $K'$ -dimensional column and is orthogonal to the basis vector set represented in  $pinv(\mathbf{P}_{3,K'})$ . In device drive space,  $\alpha$ , these vectors represent a concept analogous to the Wyszecki metameric black outlined previously.

$$\alpha = pinv(\mathbf{P}_{3,K'}) \cdot (\hat{W}_{XYZ} - b_{XYZ}) + m_1 M_1 + \dots + m_{K'-3} M_{K'-3} \quad (24)$$

Fundamentally, the gamut of device drive values capable of reproducing  $\hat{W}_{XYZ}$  can be determined as a volume in the  $m_f$  vector space. Thus, unlike the matrix switching method which predefined colorimetry three-space via the specific primary vectors and effectively eliminated the available metameric solutions, the Konig method addresses the full reconstruction drive space available to each  $\hat{W}_{XYZ}$ . In the limit of no further color definition for the multispectral display, Konig suggests choosing the drive values for each  $\hat{W}_{XYZ}$  as the center of gravity of the  $m_f$  vector volume. It is here where gradual changes in the aim  $\hat{W}_{XYZ}$  will translate to only gradual changes in  $\alpha$  and thus only gradual changes in reconstructed spectra, minimizing metameric boundary failures and color contouring for non-standard observers, though again at the expense of high computational complexity.

In another approach to smooth device control value transitions as aim colorimetry signals are smoothly modulated, Kanazawa, et al. have suggested using spherical averaging to generate multiprimary signal determination<sup>47</sup>. This addresses weakness of each of the previous three outlined methods in color reproduction near the device gamut boundaries where a more limited set of device drive values operates for each aim color. In particular, the matrix-switching and equi-luminance approaches allow for only linearly smooth transitions as they derive

from simple linear interpolation between fixed points. As an aim color series is defined across interpolation sub-region boundaries, the components of the linear interpolation (the specific primary drive channels used) may also change abruptly. Kanazawa proposes instead to derive control signals from a spherical average where multidirectional influences provide less defined boundary transitions in device control values. In fact, the math is simplified where the spherical average itself comprises only unique control value sets found on the display's gamut boundary. Kanazawa shows how the method reduces abrupt changes in control signal levels for several smooth color gradients versus the previous methods.

Perhaps the most successful co-optimization of efficient computation and smooth transitioning in colorimetrically-defined chromatic series in real images on multiprimary displays is presented by Kang, et al.<sup>48</sup>. A linearized CIELAB space (effectively the more typical L\* a\* and b\* coordinate computations but with the one-third exponents removed) provides a superior additive space for addressing aim colorimetry. This transform is expressed in Equation 25 where the subscript w implies display white tristimulus values. XYZ or RGB-defined target colors can be converted via matrix transformation to the linear LAB space where they may be further converted to linear lightness, chroma and hue coordinates, again by the established CIE equations. Removal of the traditional perception space exponents yields a less efficiently encoded space, but one which is preferential for linear interpolation in a LUT implementation of radiometric quantities.

$$\begin{bmatrix} L \\ a \\ b \end{bmatrix} = \begin{bmatrix} 0 & 100/Y_w & 0 \\ 500/X_w & -500/Y_w & 0 \\ 0 & 200/Y_w & 200/Z_w \end{bmatrix} \begin{bmatrix} X \\ Y \\ Z \end{bmatrix} \quad (25)$$

To enforce trivial computation, the linear LAB gamut boundary for the specified multiprimary display is pre-computed and encoded within a LUT architecture. Figure 16 shows the linear LAB gamut definition for an example 4-primary display whose individual primary vectors in LAB space,  $\vec{P}_k$ , are summed in such an order so as to yield a fully concave boundary surface. Maximum lightness is defined where all of the primaries are fully driven,  $\alpha_k = 1.0$ . The effectively two-dimensional LUT is addressed by lightness and hue values in a cylindrical coordinate scheme. Outputs of the LUT at each node are the chroma and primary drive amounts, which are each uniquely defined, on the gamut boundary of the defined display (for a defined, hue and lightness, there is only one chroma and primary drive combination possible as seen in Figure 16).

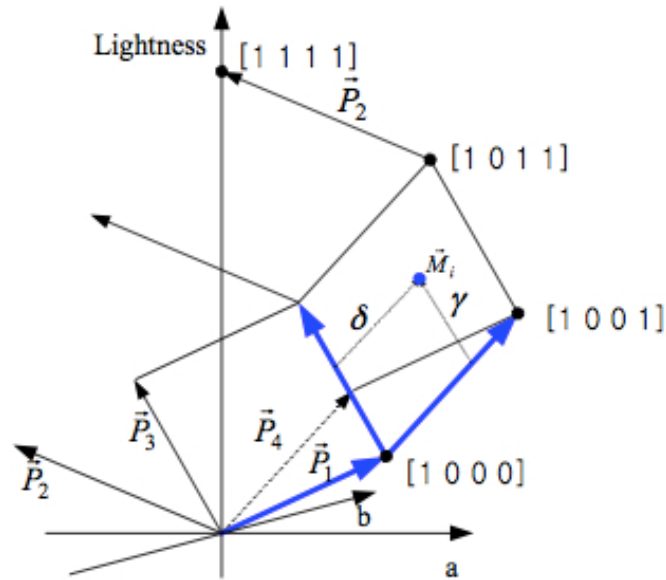


Figure 16. linear LAB gamut boundary for a 4-primary display (reproduced from Kang, et al.<sup>48</sup>)

To utilize the LUT, a target color is first converted from XYZ or RGB aim to the linear LAB space. The LUT nodes in hue and lightness immediately above and below the aim color are identified and a cylindrically linear interpolation of the chroma and display drive values,  $\alpha$ , at the target lightness and hue are computed. A chroma ratio between target color and gamut boundary establishes the final interpolation results for the displayed color. To minimize abrupt chromatic transitions, Kang et al. have further suggested interpolation employing hue angles beyond the LUT's native precision in order to pull interpolation results away from the gamut boundary. The full sequence of calculations for any color is summarized in Figure 17. In direct comparison to matrix switching and equal-luminance plane interpolation, the linear LAB approach delivers superior smooth transitions in lightness, hue and chroma series in real images and on real multiprimary displays. The method has the added benefit of being computationally efficient enough to handle HDTV video processing in real-time thanks to the trivial LUT implementation, though proper hue and lightness precision are critical in preventing quantization error in real displays.

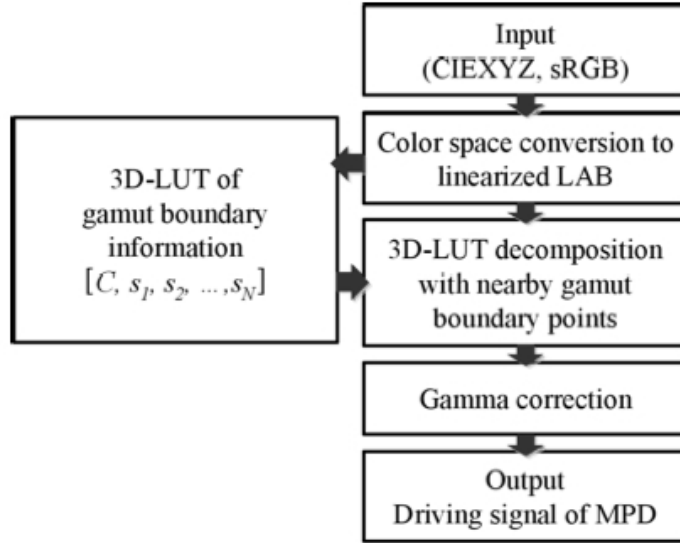


Figure 17. linear LAB gamut boundary for a 4-primary display;  $\alpha$  is shown as  $s$  in the diagram; also the LUT, though effectively 2D, is indicated here as 3D (reproduced from Kang, et al.<sup>48</sup>)

All of the methods thus far described for driving multiprimary displays have been limited to reproduction of tristimulus values for a single observer, based on intelligently accommodating the excess degrees of freedom present in the system when  $K' > 3$ . Murakami, et al. have proposed an alternative approach wherein both colorimetry and spectral reproduction of target stimuli can be co-optimized<sup>49</sup>. Specifically, spectral reproduction errors are minimized within the constraints of achieving an exact colorimetric match for a given set of color matching functions. Extending Equation 23 to the spectral domain, the reproduced spectra,  $\hat{s}$ , derived from the linear scalars,  $\alpha$ , and the matrix of individual primary spectra,  $\mathbf{u}_{N,K'}$ , is summarized in Equation 26 (assuming no offset bias for now). As the objective is to determine  $\alpha$  to match a given stimulus, the error of reproduction versus an aim spectra,  $s$ , can be quantified in Equation 27.

$$\hat{s} = \mathbf{u}_{N,K'} \cdot \alpha \quad (26)$$

$$E = \int (s - \hat{s})^2 \partial \lambda \quad (27)$$

Equation 27 may be expanded to the algebraically equivalent expression in Equation 28 where  $z$  and  $\mathbf{D}$  are defined in 29 and 30.

$$E = \int s \cdot s \partial\lambda + z^T \alpha + \frac{1}{2} \alpha^T \mathbf{D} \alpha \quad (28)$$

$$z_k = -2 \int s \cdot u_k \partial\lambda \quad (29)$$

$$D_{k,k'} = 2 \int u_k \cdot u_{k'} \partial\lambda \quad (30)$$

Equation 23 can be further re-written more generically for a 3-dimensional tristimulus determination,  $\hat{W}$ , as Equation 31 where  $\mathbf{Q}$ , a generic re-assignment of the CIEXYZ matrix  $\mathbf{P}$ , is the tristimulus matrix representing each of the  $K'$  primaries and defined versus a specific set of color matching functions (CIE standard observers or real observer data). This expression is key to establishing the colorimetric constraint on the spectral reconstruction.

$$\hat{W} = \mathbf{Q}_{3,K'} \cdot \alpha \quad (31)$$

The optimization of  $\alpha$  to faithfully reconstruct any real spectra,  $s$ , involves a constrained optimization routine such as Matlab's *fmincon* or other suitable gradient-based computation approaches using the objective function in Equation 28, the equality constraint in Equation 31, and the inequality constraint,  $0 \leq \alpha_k \leq 1.0$ . In a first approximation with no inequality constraint, Lagrange multipliers,  $\Lambda = (\Lambda_x, \Lambda_y, \Lambda_z)^T$ , and a 3x3 zero matrix,  $\mathbf{0}$ , are used to solve for  $\alpha$ , Equation 32. If all of the  $\alpha$  satisfy the gamut inequality by this method, no further iterative optimization is required and computation time may be saved.

$$\begin{pmatrix} \alpha \\ \lambda \end{pmatrix} = \begin{pmatrix} \mathbf{D} & \mathbf{Q}^T \\ \mathbf{Q} & \mathbf{0} \end{pmatrix}^{-1} \begin{pmatrix} z \\ \hat{W} \end{pmatrix} \quad (32)$$

Murakami, et al. have shown this proposed method delivers consistently superior spectral reconstruction of target stimuli,  $s$ , versus the colorimetry-based matrix switching method utilizing a seven-primary display system. Further, the method also provides superior protection against observer metamerism failures in both simulated colorimetric calculations with 20 Stiles and Burch observer sets and actual observer classification experiments. As a caution, though, optimization of the specific display primary spectra is key in establishing higher expectations for the absolute spectral matches between aim and reproduction. This sentiment, of course, fits into the larger investigation domain of this dissertation.

Starting with the Murakami algorithm, Uchiyama, et al. propose a computational workflow that is far less intensive than the gradient methods for determining  $\alpha$  when the LaGrange-based solution, Equation 32, exceeds display dynamic range in one or more of the primaries<sup>50</sup>. In these cases, the optimal solution must lie on the surface defined by the inequality constraint, meaning at least one of the  $\alpha_k$  has a value of 0 or 1. This definition limits the candidate solution sets for minimizing spectral error by Equation 27 in the subsequent optimization, affording a progressive analysis of all possible combinations. Considering degrees of freedom, some  $(1, \dots, K'-3)$  of the control values  $\alpha_k$  are fixed, yielding a total combination set size,  $C$ , defined in Equation 33. For each of the individual candidates in this set, the control values  $\alpha_k$  in each channel can be split between vectors of those which are fixed at 0 or 1,  $\alpha_f$ , and those which freely float between 0 and 1,  $\alpha_g$ . The corresponding primary spectra  $u_k$  are also split between the two classes and Equation 26 can be expanded to the form  $\hat{s} = \mathbf{u}_f \alpha_f + \mathbf{u}_g \alpha_g$ . A subsequent Lagrange expansion for both drive value types yields the expression in Equation 34. The subscripts  $f$  and  $g$  indicate the same matrix calculations as represented in Equation 32 but restricted to either the fixed or floating channel subsets, respectively. As a reminder,  $W$  represents tristimulus values for the aim color spectra and  $\hat{W}$  represents the tristimulus values of the reproduced spectra. This solution is executed for all the candidates in  $C$  and the overall minimum spectral error is determined to deliver the final control vector  $\alpha$ .

$$C = {}_K C_1 \cdot 2^1 + {}_K C_2 \cdot 2^2 + \dots + {}_K C_{K'-3} \cdot 2^{K'-3} \quad (33)$$

$$\begin{pmatrix} \alpha_g \\ \Lambda_g \end{pmatrix} = \begin{pmatrix} \mathbf{D}_g & \mathbf{Q}_g^T \\ \mathbf{Q}_g & \mathbf{0} \end{pmatrix}^{-1} \begin{pmatrix} 2\mathbf{u}_g^T (s - \mathbf{u}_f \alpha_f) \\ W - \hat{W}_f \end{pmatrix} \quad (34)$$

Uchiyama, et al. further summarize actual observer experiments where a highly metameric target image is selected for spectral capture via a 16-band multispectral camera and reproduction on a six-primary display. Participants are simultaneously presented the actual object and two variations of multiprimary reproduction, one generated via the Murakami/Uchiyama spectral co-optimization and one by either matrix switching or equal-luminance plane colorimetric interpolations. For the standard observer alone, all three presentations are found to match within  $0.26 \Delta E_{ab}$  for a reference color patch. Amongst the 11 observers, the spectral optimization reproduction was overwhelmingly preferred to the other methods as a match to the original stimuli, suggesting an enhanced accommodation of observer color matching function differences in the spectral approach. Computation times were also noted. Though the spectral approach still retained some disadvantage versus either colorimetric decomposition method in several examples, the Uchiyama modification was greatly improved versus the original Murakami gradient optimization, a result that is particularly important when considering any of the algorithms for video applications.

## **Observer Metamerism and Spectral Encoding**

In reconstructing target spectra with less than full spectral resolution display systems, compromises must be made in balancing spectral accuracy with reduced observer metamerism. One of the more significant goals of spectral reproduction is to yield a consistent viewing experience across multiple observers and so a multi-observer colorimetric treatment of the match does become attractive. Various approaches to this co-optimization have been addressed. Hill, for example, compares two different PCA encoding schemes for spectral communication between capture and display<sup>51</sup>. The first is the classic principal components decomposition of the target spectral stimuli described originally by Vrehl and Trussell and more fully by Tzeng et al.<sup>52</sup> and Imai et al.<sup>53</sup>. Target spectral data are expanded into a scaled summation of orthonormal basis functions. Care is taken to identify basis functions from a comprehensive analysis of a full set of intended training stimuli as has been described previously.

In the spirit of efficient spectral encoding for device-independent applications, though, Hill has suggested the second definition for the basis functions that concurrently optimizes the preserved signal for colorimetric accuracy across multiple observers and generates a trivial encoded signal for traditional three-primary displays. In this scheme, the first three basis functions  $e_1$ ,  $e_2$  and  $e_3$  are set to the inverse form of the 1931 2° color matching functions or a linear combination

thereof. In this manner,  $b_1$   $b_2$   $b_3$  calculated from Equation 7 with  $I=3$  are directly matrixable to XYZ tristimulus values which may be further converted to predictable drive values for a well behaved reproduction system.

The reconstructed spectrum predicted by Equation 8 from these three basis functions and  $b_1$   $b_2$  and  $b_3$  is an exact metameric match to the original spectrum for the standard observer. The residual error between original and reconstructed spectra is a metameric black for the same observer as defined by the Wyszecki hypothesis<sup>54</sup>. Hill next suggests that this residual spectral error itself be decomposed through PCA but in a manner that addresses individuals' color sensitivity differences. Specifically, an observer metamerism weighting function is defined which identifies the magnitude of color error at each wavelength associated with differences in individual color matching function among 24 tabulated observers from Judd, Stiles and Burch and including the 2° and 10° standard observers and the standard deviate observer<sup>55</sup>. Using a reflectance training data set from Vrehl<sup>56</sup> and various illuminants, the basis functions for computed metameric blacks further weighted by the observer metamerism function are determined via PCA. Full spectral reconstruction of target stimuli are accomplished by a two-step principal component scaling employing the metameric black basis functions and the standard observer basis functions. Hill confirms that this second approach yields superior colorimetric error results across multiple observers versus a straight Vrehl /Trussel spectral decomposition. What is missing in the analysis, though, is the influence of the spectral prediction of target stimuli from a multispectral camera, though Hill suggests the encoding comparisons thus far summarized remain consistent even as the camera model is varied.

## **Reducing Observer Metamerism in Multiprimary Display**

Acknowledging the difficulty of generating precise spectral matches to target stimuli using multiprimary displays, several researchers have instead focused exclusively on the goal of reducing observer metamerism in devising device drive values<sup>57</sup>. Hill has suggested a stochastic optimization based on his 24 observers that was shown to work well for both ideal display primaries of dimension  $K'$  and an actual six-primary display built as part of the Natural Vision project<sup>51</sup>. In this model, starting guesses for device radiometric scalars needed to drive the reconstruction of any target spectrum are achieved by a targeted PCA decomposition. First, employing Equation 7, the display primary spectra are set as the basis functions which are used to determine principal component vectors,  $b$ , for any aim spectra. By this logic,  $b$  and  $\alpha$  are now equivalent and the PCA reconstruction is restricted to

real display values. Next, for all 24 observers, the reconstructed spectrum from this starting guess (implementing Equation 8) is used to calculate colorimetric errors versus the aim spectra and the largest of the 24 is recorded. Iterative optimization of  $b$  is next employed to reduce the maximum color error for a target spectrum while simultaneously limiting the answer to real drive values.

Employing this same method for a generic number of observers, Konig and Hill, et al.<sup>58</sup> illustrate three practical limitations of the approach: 1) the display dynamic range may be limited in highlight reproduction if the scene and display white point don't match, 2) building in highlight range overhead to compensate may introduce quantization error in the control signals for the display and 3) the baseline black bias of the display limits the capability of the system to reproduce especially dark colors. Thus, system dynamic range and not just primary spectral characteristics are critical to generating strong spectral reconstructions. This becomes significant when design choices introduce optical configurations that will boost unnecessary system flare.

Another limitation of both Hill and Konig's approaches are that the image processing overhead necessary to compute drive values for each and every unique spectral pixel is excessive. Linear optimizations can be tuned to run quickly but they still have little chance of executing on HD resolution video streams at 30 or 60 frames per second. In a simplification for a six primary multispectral display, Ohsawa, et al.<sup>59</sup> have suggested building a matrix conversion to properly drive a metameric match for just two observers, the 1931 2° and 1964 10° standard observers. With matched degrees of freedom, the computation is trivial given no gamut restrictions, though the reduction of observer metamerism for all real observers is likely minimally improved over a three-channel display capable itself of metameric matches for a single observer. Still, the approach extends well the concepts of colorimetry-driven image interchange for multispectral video systems advocated by the Natural Vision project.

Perhaps a compromise between Hill's 24-observer optimization and the Ohsawa two-observer system can be found in the work of Sarkar, et al.<sup>60</sup> who successfully grouped 47 Stiles-Burch observers into just seven more general base CMF classifications by minimizing colorimetric prediction errors. The full candidate CMF sets were originated as 125 permutations derived from five distinct L, M and S cone fundamentals each (from cluster analysis on the Stiles-Burch set) and 61 variations calculated from the CIE 2006 age-dependency models for ages between 20 and 80 years old. It should be noted that Sarkar, et al. have offered serious reservation on the validity of the current CIE 2006 model to even well predict average measured observer CMFs within the Stiles-Burch data at selected age

ranges. Concerns are raised considering various physiological variability sources (age-dependent and otherwise) not well referenced in the models for any particular real observer<sup>61</sup>. As such, Sarkar argues CIE 2006 is more a source of potential category CMF sets than a strong predictor of any actual test subject. In related work, Alfvén and Fairchild and Fairchild and Heckaman have used Monte Carlo simulation based on physiological and psychophysical measurements of ocular media and cone responsivity functions to derive thousands of theoretical observer CMFs<sup>62,76</sup>. These have generally proven more predictive of inter-observer color matching experiment variability than any generalized visual system model. Again, though, this method does not account for the likely actual CMF of any real particular observer.

With a smaller set of color matching functions based in valid statistical reduction of larger populations, a more computationally robust display optimization can be formulated. Sarkar used the categorization approach to successfully identify the primary CMF descriptor of 30 real observers in a highly metameric matching experiment. Few observers fell outside the definition of the seven identified categories, suggesting the technique holds promise for actually declaring relevant deviate observers for multispectral system optimization.

In subsequent work, Fedutina, et al. improved upon the classification system and identified eight overall observer categories<sup>63</sup>. Where Sarkar, et al. utilized color difference in spectrally smooth Munsell Color Checker patches illuminated by CIE D65 in reducing the fundamental observer categories from 186 to 7, Fedutina employed more spectrally variable (and thus more metameric) color patches to aid in enhancing variability during classification. An observer calibrator apparatus was also constructed with narrow-band LED test primaries to classify any real observer into the eight identified CMF categories (a 9<sup>th</sup> choice comprising the CIE 10° observer was also included). Determination of category was based on the observer declaring quality of color match in a bipartite presentation using preselected test stimuli calculated to deliver metameric matches for each of the nine specific observer classes. The metameric match category cited most often as yielding the best visual match by the observer was ultimately assigned.

In further relevant work, Fedutina also showed that suprathreshold color difference perceptions vary somewhat predictably by observer category. Thus, traditional color difference formulae derived for CIE standard observers are not appropriate for reflecting difference perceptions for all observers. Though this is an expected result from understood principles of colorimetry and from previous work with color displays<sup>8</sup>, Fedutina offers a quantitative summary of the implications. These unique threshold determinations are especially important for small, though

still suprathreshold, color differences as observer variability influence becomes less pronounced as stimuli differences are colorimetrically exaggerated. In practical applications, subtle suprathreshold coloration differences perceived by certain color critical viewers may certainly not be respected as appearing similarly different for observers from other CMF categories. And this is a concern beyond the previously studied differences in absolute color difference thresholds (where differences are negligible for one observer class and above threshold for another). This carries serious implications for collaborative color grading work such as that employed in motion picture and video applications.

Evidenced in the results of Konig, Ohsawa and others and complicating the entire goal of spectral reproduction on multiprimary display further are issues of chromatic adaptation and color appearance. To this point, the objective of spectral reconstruction has been described as either an exact spectral match to original scene stimulus or an alternately minimized observer metamerism in the colorimetric reproduction of that stimulus. Determining that the design objective has been successfully met in any real system requires experimentation with human observers and a juxtaposed target with reproduced stimuli in a controlled viewing environment. Unfortunately, in real cinema applications, extreme differences in scene and display are common and are expected. On-set illumination typically possesses a white point distinctly different from that used in display as the most common indoor illuminants employ blackbody spectra at correlated color temperatures from 2800-3200K. Further, cinema reproduction environments usually comprise a dim or darkened room with a luminous white point far dimmer than the typical reflection values for the captured scene, both of which influence apparent reproduction contrast. Giorgianni extensively describes the compensating tone and color manipulations that must be made in order to build a television or cinema imaging system faithful to the color appearance of the captured scene, including accommodation of psychophysical phenomena and optical phenomena (flare)<sup>64</sup>. The question remains of how spectral reconstruction goals can be similarly augmented by proper accommodation of appearance phenomena for real system applications.

## **Multispectral Image Encoding**

One of the major design considerations of any multispectral imaging system is the physical image encoding scheme and the fundamental profile connection space used to link input and output devices of differing capability (dynamic range, gamut, number of image bands, etc.). Work summarized thus far has described

various capture technologies from  $K = 6$  to 31 bands encompassing various unique spectral responsivities,  $\omega_k$ , and abridged multispectral display systems of  $K' = 4$  to 7 channels, also with unique spectral radiance characteristics,  $u_k$ . With such discrepancy in  $K/K'$  and channel spectral profiles for candidate systems, it is clear that direct connection between input and output is only possible utilizing capture post-processing connected with the camera or reproduction pre-processing connected with the display (or possibly both). This represents a serious departure from the image chains used in traditional ITU-R Rec. 709/sRGB video. And in either case, computing power must be sufficient to cope with high spatial resolution images at realistic framerates. In current infrastructures, this effectively eliminates a full spectrum profile connection space for real-time video work, though such solutions remain plausible for offline processing or still image applications.

Uchiyama, et al. offer a comparison of three proposed profile connection spaces for translating spectral information from scene to screen<sup>65</sup>. The first two are based on a PCA treatment of the captured and estimated spectra, Equations 7 and 8. First is the Hill approach<sup>51</sup> where the initial three basis functions are linear combinations of the CIE standard observer CMF and additional basis functions are used for metameric black residual errors to maximize spectral accuracy for a given set of stimuli. Second is an alternate basis function definition embodied in the Karhunen-Loeve Transform (KLT) which also attempts to minimize color difference between the actual and estimated spectra for specific observer classes. Though PCA can provide strong spectral reconstruction, it is fundamentally limited in more generic image chain applications. For example, basis functions for PCA approaches are driven heavily by specific training sets and there is not an agreed upon universal set which effectively describes all potential stimuli under all potential illuminants. PCA coefficients,  $b$ , may also be plagued by dynamic range issues, negative values and quantization errors, all detrimental to effective communication of the captured image to the intermediate encoding space, especially if it is restricted in bit-depth. Further, transforms from camera to display become necessary if common basis function sets are not employed for both ends of the imaging chain. Spectral resolution and accuracy may be lost effectively in these conversions.

Uchiyama's third proposed solution, however, offers some promise as a more universal encoding and interchange space for spectral information. The issue of accommodating capture systems with varying channel counts,  $K$ , is solved by introducing a virtual multispectral camera (VMSC). The VMSC is most effectively a theoretical device with some number of equally spaced and equally shaped spectral responsivities distributed throughout the visible spectrum. Rather than capturing the original image stimuli, the VMSC instead operates on the resultant spectral

estimation,  $\acute{s}$ ,  $\check{s}$ , etc., by suitable processing of the real integrated channel responses of any real K-channel system (Equation 6 for example). By “taking a picture of the picture,” the VMSC may translate full spectral information from the arbitrary capture space to a pre-defined generic one. Uchiyama shows how an eight-channel VMSC offers excellent re-estimation of the original spectral estimation of real multiband cameras with respect to overall colorimetric error. The spectral RMSE is also strong, though not quite as good as an eight-channel version of Hill’s PCA method. Still with proper definition of spectral response, the VMSC will not be plagued by excessive dynamic range or negative coefficient values in the real encoding space. Further study on the ideal VMSC band count and spectral profile made in consideration of specific display characteristics may offer additional improvements.

An additional consideration for selection of a proper spectral encoding scheme involves image compression. The eight-channel VMSC space just described would require a nearly 3:1 subsequent compression scheme to utilize existing image transmission protocols. Erring towards a more accurate encoding scheme such as full resolution spectral profiles per pixel would require even more. A benefit of the spectral characteristic of most natural stimuli, though, is relative smoothness. This same premise is the basis of the Wiener estimation methodology for spectral estimation. Ma, et al. have proposed a lossless compression scheme for multispectral images where spectral band coefficients are linearly predicted from values in the preceding bands (encoding is typically ordered from low wavelength to high wavelength across the defined spectral domain)<sup>66</sup>. Ma argues that spectral bands are even more highly correlated than spatial or temporal features in normal image sequences and maximum compression ratios are enabled by addressing this dimension in a moving multispectral image sequence. For each encoded band at a given pixel location, residual error between prediction and original is represented with a Golomb-Rice coding to deliver bitrates and compression ratios for multispectral test images that are notably improved over JPEG-LS and JPEG2000.

While lossless encoding is necessary for the most critical spectral imaging applications it may not provide enough bandwidth savings for many real applications, especially multispectral video. Shinoda, et al. present an additional investigation of multispectral image compression schemes accommodating lossless as well as lossy bitrates<sup>67</sup>. In particular, they show how KLT algorithms for reducing data redundancy across spectral bands employed within JPEG2000 Part2’s multicomponent spatial transforms (JPEG2000-MCT) deliver superior spectral reconstruction peak-signal-to-noise-ratio (PSNR) results for K=6 to 121 image bands. Optimization of this approach has evolved from considerable work in the

remote sensing community though further options from the video world are available in multichannel compression codecs such as MPEG4 Studio Profile and H.264/AVC. Shinoda argues that a predominant decision in choosing appropriate multispectral compression follows from the image analysis needs of the particular application space. For example, some algorithmic treatments are adept at preserving full N-resolution spectral information at each pixel while others excel in eliminating redundancy in K-channel series obtained from specific imaging devices (thus suitable for the VMSC methods outlined previously). And others focus on tristimulus quality in either XYZ or sRGB spaces needed for visualization of colorimetrically accurate images. As such, a choice of compression and image encoding is somewhat dependent on whether the objective of the spectral imaging system is precise spectral reproduction, minimization of observer metamerism, colorimetrically accurate illuminant conversion or any of the other possibilities reflected in the literature.

For imaging schemes where a tristimulus signal carries relative importance, Shinoda offers a hybrid approach to multispectral image encoding. An image defined by the channel response vector,  $g$  (equivalent to Equation 2's  $c_k$ ), is split into an sRGB component and a residual spectral error component which are separately compressed as summarized by the workflow of Figure 18.

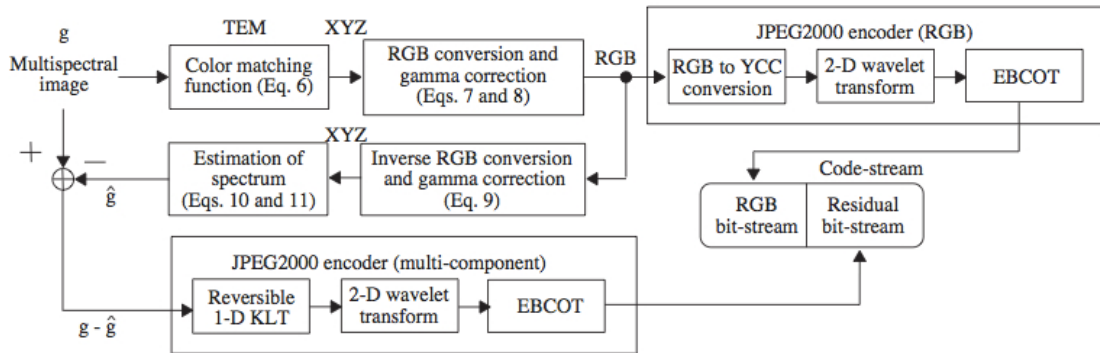


Figure 18. multispectral encoding scheme accommodating both tristimulus and spectral channel signals (reproduced from Shinoda, et al.<sup>67</sup>)

Via Wiener estimation, trained pseudoinversion, PCA or any of the other spectral estimation algorithms thus far presented, the camera vector,  $g$ , may be converted to an N-dimension spectrum per pixel. Following this, a standard conversion to CIE XYZ colorimetry and sRGB is employed to provide a colorimetrically accurate three-channel image. Though ill-defined, Wiener

estimation is subsequently used to reverse the process and re-predict the original camera vector from the tristimulus set,  $\hat{g}$ . Some error,  $g-\hat{g}$ , is expected from these steps and can itself be encoded as a residual N-channel spectral signature. JPEG2000 2-D wavelet compression is employed on a chroma subsampled version of the sRGB image (in  $YCbCr$  space) to handle spatial reductions while the residual undergoes KLT optimization before being spatially processed itself by multicomponent JPEG2000. While the total algorithm can be tuned to be lossless for the full image sequence, a compromised lossy solution can also be employed where lost data is isolated to the colorimetric components, spectral components or both, depending on requirements. In particular, the proposed algorithm is more effective at preserving high SRGB PSNR than the straight JPEG2000-MCT approach applied to the  $g$  vectors at low bitrates and yields quite reasonable spectral PSNR comparisons where slightly higher bitrates are afforded. There is also potential to expand the colorimetric treatment to multiple observer classifications to account for some observer metamerism.

## Metrics for Evaluating Spectral Match

A final subject that warrants attention in a literature review of multispectral imaging technologies is spectral evaluation metrics. The choice of analysis metrics is critical for all aspects of system design, from component optimization to performance assessment. Imai, et al. have summarized four major classes of metric common to evaluations of multispectral imaging systems: color difference equations, spectral curve differences, metamerism indices and weighted rms errors. Each class brings significance to a different aspect of the spectral imaging problem and no single metric is fully descriptive of a system's full capabilities.

Color difference equations derive from the work of the CIE and are computed in several relevant forms. The simplest equations in common use are Euclidean three-space vector lengths in either CIELUV or CIELAB color spaces. These have more recently been tweaked to better reflect extensive psychophysical experiments and to include application-dependent variables in color difference resulting in the CIE94 and CIE2000 variations, each a derivative of CIELAB. Inputs to color difference equations imply a specific color matching function set be chosen. Though the CIE 2° and 10° observers are popular choices traditionally, individual observer CMFs or a weighted average of a population of observers may be used to improve relevance. CIE TC1-36 has offered conversion matrices to compute  $\overline{xy\bar{z}}(\lambda)$  CMFs from  $\overline{lms}(\lambda)$  cone fundamentals. Color difference formulae traditionally only represent the expected perception of the single specified observer.

Spectral curve differences are used to quantify magnitudes of difference in physical stimuli amount, either radiometric (radiance, irradiance, etc.) or relative (reflectance or transmittance). In assessing spectral match, these metrics are most appropriate for summarizing the actual radiometric quality. They are typically not designed to incorporate the significant perception behaviors of the human visual system. As such, much time can be wasted optimizing systems based on these metrics in regimes where human visual thresholds are much more forgiving. Pertinent metrics include spectral root mean square error, Equation 35, and the Hernandez-Andres goodness of fit coefficient, Equation 36. Another popular form is the simple maximum spectral error (across the wavelength domain defined by N),  $\max|s_\lambda - \hat{s}_\lambda|$ . The logic for using this is that curve matches with a low maximum error will always also have a low rmse but the opposite may not necessarily be true.

$$\text{rmse} = \sqrt{\frac{\sum_{\lambda=1}^N (s_\lambda - \hat{s}_\lambda)^2}{N}} \quad (35)$$

$$\text{gfc} = \frac{|\sum_{\lambda=1}^N (s_\lambda \cdot \hat{s}_\lambda)|}{\sqrt{|\sum_{\lambda=1}^N (s_\lambda)^2|} \cdot \sqrt{|\sum_{\lambda=1}^N (\hat{s}_\lambda)^2|}} \quad (36)$$

Metamerism indices are used to quantify color differences represented by two stimuli across differences in observers or illuminants. The CIE’s “special index of metamerism” is a standard color difference for two spectral stimuli under a test observer/illuminant definition when a perfect metameric match is computed under a reference condition. This type of index is potentially more relevant in cases of illuminant metamerism than observer metamerism when the work of Fedutina<sup>63</sup> is considered since it is unknown if suprathreshold color difference scalability is common for all observer classes. Further, the metric requires predefined reference conditions and an inference that the match is indeed perfect for at least one condition. This isn’t always a relevant assumption in the midst of a system optimization. The CIE “general index of metamerism” represents a scaled absolute difference between two spectra with consideration given to perception weighting. Viggiano’s  $M_v$  ratio is another example using CIELAB, Equations 37 and 38. This type of metric is a particularly strong combination of spectral differences and vision-relevant differences and may adequately combine the best of all spectral match evaluation goals.

$$M_v = \sum_{\lambda=1}^N w_{\lambda}(s_{\lambda} - \hat{s}_{\lambda}) \quad (37)$$

$$w_{\lambda} = \sqrt{\left(\frac{\partial L^*}{\partial s_{\lambda}}\right)^2 + \left(\frac{\partial a^*}{\partial s_{\lambda}}\right)^2 + \left(\frac{\partial b^*}{\partial s_{\lambda}}\right)^2} \quad (38)$$

Other weighted spectral curve differences are also proposed based on a modification of simple spectral rmse, Equation 39. Candidate weighting strategies include  $w_{inv,\lambda}$  where the weighting factor is the inverse of the reference spectrum at each wavelength,  $s_{\lambda}$ . This approach helps to accommodate color appearance phenomena where perceived spectral differences are more pronounced in darker colors than in lighter ones. Another approach which does not account for lightness scaling but does better account for particular wavelengths of maximum cone sensitivity is  $w_{R,\lambda}$  where the weighting spectrum is the diagonal of matrix R from Equation 13. Each of these approaches reflects a somewhat compromised co-optimization of spectral and colorimetric accuracy.

$$wrmse = \sqrt{\frac{\sum_{\lambda=1}^N w_{type,\lambda}(s_{\lambda} - \hat{s}_{\lambda})^2}{N}} \quad (39)$$

## Further Literature Review

The remainder of this dissertation is focused exclusively on experimental results associated with work done in address of the fundamental engineering and color science questions posed in Chapter 2. In several instances, a supplemental introduction and expansion of supporting literature will be used within following chapters to maintain a cohesive introduction for the topics addressed. This is done intentionally to permit these chapters to operate as independent research units for any reader who wishes to review all material explicit to a full accounting of the associated topic. At the same time, the preceding literature review serves as comprehensive background information on the larger thread of multispectral video systems and observer metamerism in general. It is intended that both modalities are ultimately useful to the reader and are thus deliberately included in this dissertation.

# Chapter 4

---

## Literature Influences on Work

As presented in Chapter 2, this dissertation work was executed across six primary objectives which can be fundamentally grouped into two larger experiment phases, 1) multiprimary projection optimization and design and 2) investigation and confirmation of observer metamerism psychophysics. The following summarizes guidance provided by the literature in shaping specific research goals for each phase.

### Experiment #1 – Multiprimary Projector Design

Objectives for the completed dissertation comprise the analysis of abridged multispectral displays for the purposes of optimizing spectral accuracy and reducing observer metamerism in a full video workflow versus traditional three-channel systems. Simulations and metrics were devised to inform design decisions made in the constructed multiprimary display prototype. Specifically, assessment of improvements in color consistency for multiple observers guided management of primary count, spectral composition and gamut control decisions.

Refining the spectral reproduction gamut of a limited primary display device is critical in executing a successful spectral video system. The literature summarizes several different design strategies worthy of further investigation for generating precise spectral reconstruction of aim targets. In the simplest approach, the visible spectrum is split into  $K'$  equally spaced channel emission profiles individually controllable in the engineered device. Primary spectra shapes are well behaved and allow for reasonable reconstruction of smooth continuous object/illuminant spectra. This presumes to be the primary strategy applied by the Natural Vision project in their system construction. A notable restriction for this model though is its inability to account for more spectrally variant object or illumination characteristics. With only 6 or 7 primaries, the peculiarities of fluorescent-illuminated colorants, for example, are misrepresented. A second approach that can solve some of these problems involves selecting a target training set and optimizing device primary capabilities to that set. This training strategy is different from that employed for a capture system in that rather than attempting to optimize an estimation transform, decisions here are intended to optimize a gamut. But in accommodating one particular set of target colors, it may become difficult to generate perfect spectral match to an ancillary set. Further, an abridged spectral

approach demands compromises be made relative to absolute spectral accuracy goals even within the training set. Examples of this result for a reproduction goal as simple as the 24 patches of the Macbeth Color Checker under CIE D65 illumination are reported in Chapter 5. A third approach serves to simply encompass a larger colorimetric gamut with increased dimensionality, utilizing either increased primary saturation, new primaries beyond the traditional RGB or both. This approach certainly enhances capability in representing the colorimetry of all conceivable illuminated objects but at the potential expense of heightened spectral mismatch to aim and observer metamerism failure.

Complicating the preceding design choices are the restrictive native spectral capabilities of available RGB display equipment. As the defining technical specification du jour for color in RGB video displays becomes the absolute area of the  $u',v'$  chromaticity triangle, individual primaries necessarily become more saturated and more monochromatic. As such, it becomes very difficult to modify these primaries into a set that adequately reproduces the full visible spectrum for rendering reconstruction of real objects under real illuminants. And as already stated, even the best attempts to construct six or more primaries from devices with such narrow native characteristics may actually serve to exacerbate observer metamerism failure rather than solve it as intended (again, see Chapter 5 for a review). A native primary can generally only be made more narrowly distributed via external filtration tuning.

Precise spectral matches in abridged multiprimary display architectures are inherently compromised if the channel count is too low or if the target spectral gamut is too highly dimensional. An alternate approach that fundamentally accomplishes most of the goals associated with spectral color accuracy is minimized observer metamerism. If observer CMFs can be classified into a smaller set of statistically similar performance, it may be possible to optimize more accurate colorimetric matches for the group with a precision equivalent to that afforded by an exact spectral match of aim and reproduction. Much of the literature from Hill and others suggests this is a preferable objective given the large anticipated variability of real spectral stimuli in typical imaging scenarios.

### *Categorizing Spectral Match / Metamerism Metrics*

As already stated, the principal objective of a multispectral display system is to generate an image signal which represents high color accuracy versus the scene, either radiometrically or colorimetrically. This may be defined in terms of a color difference for a standard observer, a color difference for multiple observers

(metamerism) or an explicit spectral match. Viable options for metrics from the literature include color difference formulae, absolute spectral curve differences and metamerism indices (utilizing various defined observer CMF sets). Colorimetric metrics are also explicitly referenced against various vision models proposed by previous researchers. This full set of possibilities provides a strong collection of alternatives useful for assessing an ultimate multiprimary display design.

To assist with final metric selection, candidates are assessed in a generic spectral simulation system to determine relevance. Attention is given to metrics that convey enough signal variability to warrant use in differentiating the actual proposed multiprimary display systems. Metrics must also appropriately scale relevant color difference qualities and not generate false or misleading conclusions. As such, interpretation of visual experiments aids in refining metrics and models for observer metamerism and spectral reproduction accuracy.

### *Identifying Candidate Projectors*

In the dissertation work, two display configurations are considered. In the first, traditional three-channel RGB devices are used with external filtration to craft an optimized primary set. In the second design, images from K' white light projectors are superimposed with adjusting filtration to craft optimized system primaries. This latter approach affords more control over primary spectra shape though adds complexity for optical alignment, image plane uniformity and radiometric scaling. But as the goal of the full spectral video system is to either reconstruct target spectra precisely or minimize observer metamerism, both approaches provide merit for this study. Practical attention was specifically given to identifying available equipment rather than delaying with an exhaustive search for the ideal starting device. Selections were made intelligently considering the two primary engineering limitations of native spectral performance and optical path complexity.

Once equipment was identified, a full characterization of tone transfer function, dark bias, screen uniformity, spatial independence, bit-depth limitation and stability was required to construct a viable control model. Native primaries were also measured for inclusion in spectrum optimization simulations. Each of these factors radically influence display quality.

### *Determining Optimized Primaries*

Rigorous system simulation was executed with deference to three experiment criteria, 1) number and spectral profile of channels, 2) training set influence and 3) spectral reproduction objective. Starting with traditional RGB projection devices allowed for a practical primary count of 6 or 9; while the architecture employing  $K'$  superimposed primaries afforded other permutations. In the latter case, primary spectral shape was treated parametrically (Gaussian, bandpass, etc.) rather than as wavelength-by-wavelength tunable. This simplified optimization routines and restricted synthesized results to a practical and buildable solution.

For system training set options, the literature offers two general approaches for acquiring suitable representative samples. In the first, spectra are identified from a number of sources that exemplify typical imaging subjects for the proposed application. Candidates are chosen either from available databases or actual measurements. The distribution of samples must be deemed qualitatively representative of key classification areas such as flesh tones, textiles, artistic colorants, objects in nature, etc. The ultimate distribution of samples is often arrived upon subjectively and care must be taken to avoid unwanted bias in the distribution of object and illumination types. The second type of training set selection seeks to maximize spectral differentiation in the proposed imaging system. Principal components analysis of various forms is implemented to maximize signal variability and minimize spectral redundancy in the candidate samples. The approach tends to be more quantitative than the first though has not necessarily delivered much stronger performance in previous work, perhaps because collecting candidate spectra to evaluate by this manner is still somewhat qualitative.

For spectral video applications, there is added complexity in that scene illumination will not be factored out of the estimations in real applications. Thus to the varied collections of candidate object reflectance spectra must be added a reasonable set of illumination sources to influence the system training. Results of this research indicate how feasibly multispectral displays can operate when emulating disparate light sources such as spectrally irregular fluorescent and smooth, continuous incandescent.

A final issue of training set selection involves real versus virtual objects. While optimization simulations are privy to any collected spectrum for inclusion in analysis, testing of the constructed prototypes relies on actual color samples for observer comparison. Much work has been done by Gretag Macbeth and other manufacturers of test charts to generate useful uniform color patches suitable for

color analysis. These proved a solid basis for practical system evaluation in this work as construction of custom color sets representative of typical scene objects and illumination in cinema applications would have been somewhat tedious.

## **Experiment #2 – Observer Metamerism**

The second experiment represents an investigation of observer metamerism with the actual multispectral display prototype. By addressing theories of multiprimary optimization in the context of observer metamerism models, a better understanding of the requirements for absolute spectral reconstruction accuracy versus limited metamerism accommodation is yielded. Having observers compare color matches between the constructed multiprimary display and traditional three-channel systems confirmed much of the metric development and vision models from the literature that were applied to this particular problem.

### *Optimizing Observer Metamerism Amongst Various Display Types*

A comparison of the optimized multispectral display to more traditional three-channel displays based in LCOS and laser modulation schemes via visual experimentation offers insight to the magnitude of observer metamerism and variability manifest in each design. Initially, full spectral color targets were identified and matches utilizing each technology type were optimized. Two rendering schemes, focused on traditional color management paradigms, formed the basis for the observer experiments. In the first pass, target object color was reproduced on the displays employing a colorimetric match for a single standard observer, the 1931 2° color matching functions. This represents the traditional metameric match color management employed across the motion picture industry today. For the abridged multispectral display, additional constraints were necessary to manage the excess degrees of freedom available. In the second pass, each display type was re-optimized to deliver a superior observer metamerism performance based on simulation metrics previously derived and the viewing experiment was repeated to determine improvements in viewer consistency. The observer experiments serve additional purpose to aid in refining CMF binning and observer metamerism models. Current work by both the CIE TC1-36 committee and Sarkar, et al. attempt to categorize observer color matching functions into manageable subsets suitable for gross population predictions and the current display work does serve to elucidate the applicability of the different approaches.

## **Salience to Current Cinema Trends**

For practical cinema applications, the ultimate questions addressed in the executed experiments focus on the magnitude of observer metamerism in traditional three-primary standard and emerging wide-gamut imaging systems based on laser illumination. As the industry promotes larger colorimetric gamut, previous research suggests the consistency of viewing experience amongst a population of observers will suffer. Optimized multiprimary reproduction focused on spectral reproduction accuracy or metamerism reduction may ultimately prove a better answer to enhancing the color experience in future systems. The recommendations garnered from experience with the prototype multiprimary system permit improved color reproduction consistency for all observers and ensure that creative image quality decisions are faithfully rendered to a full audience.

## Chapter 5

---

### The Two-projector Proof-of-Concept

#### Abstract

A proof-of-concept prototype multiprimary display was designed as an exploratory exercise to identify benefits and shortcomings of a simplified and inexpensive six-primary system. In this effort, two consumer-grade LCD digital projectors were used to construct an abridged multispectral display from SMPTE-431 digital cinema-compatible equipment. Native primary spectra from each device were modified by way of external optical filtration to generate six unique spectral bands superimposable for final color rendering. By careful characterization of the projectors and optimization of primary drive amounts, rudimentary spectral reconstruction of simple color patch targets was achieved with the produced system.

#### Native Display Models

Traditionally, additive electronic displays are well represented by a gain-offset-gamma (GOG) or gain-offset-gamma-offset (GOGO) model as summarized by Day, et al., to relate device drive value in each channel (analog voltage or digital drive value for example) to a radiometric scalar of the maximum channel output spectrum<sup>68</sup>. An example of the luminance output,  $L$ , of an analog display as a function of drive voltage,  $V$ , is given in Equation 40 where  $G$  is electronic gain,  $\varepsilon$  is an adjustable black bias,  $L_k$  is device black offset and  $\gamma$  is the power function exponent commonly associated with the nonlinear or *gamma* characteristic of the display.

$$L = G(V + \varepsilon)^\gamma + L_k \quad (40)$$

For each primary channel in a typical display (usually red, green and blue),  $L$  in Equation 40 can be translated to the relative radiometric scalar proportional to the normalized output of the primary. Equation 41 summarizes the spectral derivation of these scalars in the absence of a black offset for an RGB device where  $R$ ,  $G$  and  $B$  are the scalars and  $SPD_{i,max}$  is the spectral power distribution of the maximum output achievable in the calibrated state for each primary. From this

definition, the scalars occupy a domain between 0 and 1. Equation 42 further generalizes the mixture for the case of a non-trivial black offset.

$$SPD(\lambda)_{mix} = R \cdot SPD(\lambda)_{r,max} + G \cdot SPD(\lambda)_{g,max} + B \cdot SPD(\lambda)_{b,max} \quad (41)$$

$$SPD(\lambda)_{mix} = SPD(\lambda)_r + SPD(\lambda)_g + SPD(\lambda)_b + SPD(\lambda)_k \quad (42)$$

Where a display does not render radiometric output consistent with the strict parametric definitions of Equation 40, an empirical *look-up-table (LUT)* can be constructed by sampling *XYZ* colorimetric outputs in each individually driven color channel across a full range of drive values  $d_i$ , Equations 43 and 44. These LUTs are commonly referred to as *electro-optic transfer functions (EOTFs)*.

$$\begin{aligned} R &= lut(d_r) \\ G &= lut(d_g) \\ B &= lut(d_b) \end{aligned} \quad (43)$$

$$\begin{aligned} R(d_r) &= X_{d_r} / X_{r,max} \\ G(d_g) &= Y_{d_g} / Y_{g,max} \\ B(d_b) &= Z_{d_b} / Z_{b,max} \end{aligned} \quad (44)$$

Via primary translation to CIE tristimulus amounts, Equation 45, these scalars can further predict generated colorimetry in a metameric reproduction model. In cinema applications, the 1931 2° standard observer is typically used when characterizing these devices and in specifying standard expected performance. Currently all SMPTE, EBU and ITU display definitions follow this convention.

$$\begin{bmatrix} X \\ Y \\ Z \end{bmatrix}_{mix} = \begin{bmatrix} X_{r,max} - X_k & X_{g,max} - X_k & X_{b,max} - X_k & X_k \\ Y_{r,max} - Y_k & Y_{g,max} - Y_k & Y_{b,max} - Y_k & Y_k \\ Z_{r,max} - Z_k & Z_{g,max} - Z_k & Z_{b,max} - Z_k & Z_k \end{bmatrix} \begin{bmatrix} R \\ G \\ B \\ I \end{bmatrix}_{0-1} \quad (45)$$

## Multiprimary Design Objectives

Owing to natural variations in ocular media transmission, photoreceptor spectral sensitivities and post-retinal mechanisms, any sampled population of human observers will embody a disparate set of color matching functions. Further, even single observers will experience alteration of their color matching functions with age and field of view<sup>11</sup>. As such, a metameric reproduction of some aim stimuli for the 1931 observer does not guarantee a similar match for any real observer<sup>69</sup>. For emissive displays, the only sure way to avoid all observer metamerism failure is to produce an accurate spectral reconstruction of the target object stimuli<sup>58,59</sup>. Much of the historical work progressing multiprimary display development has focused on general gamut expansion with ancillary benefit to the observer metamerism problem<sup>43,39,9</sup>. However, Hill has specifically shown how multispectral display signals may be algorithmically optimized to limit observer metamerism when there are device limitations to fully accurate spectral reconstruction<sup>51</sup>.

A rigorous multispectral reproduction system would require a narrow band primary for each desired wavelength within the intended full-width spectrum. This type of system is largely impractical for typical motion image capture, processing and reproduction workflows owing to hardware complexity, processing overhead and storage bandwidth. An alternative abridged spectral reproduction system is deemed more sensible for this proof-of-concept. Analogous abridged multispectral reproduction systems have proven successful in generating reasonable spectrum reconstruction in the fields of digital image capture and multi-ink inkjet printing<sup>2,70,53</sup>. In these applications a co-optimization of spectral accuracy and reduced illuminant and/or observer metamerism performance is often employed. Abridged filter-based approaches have also been used extensively in low-end spectrometers and colorimeters. Yamaguchi, et al. have demonstrated an end-to-end multispectral capture and display system employing a 16-channel digital camera and 6-channel projection display, complete with models for data management and transmission in an ICC-analogous workflow<sup>18</sup>. Several attempts have also been made to adapt the techniques to real-time video workflows for motion imaging applications<sup>17</sup>.

The current work serves to explore primary spectra optimization for a six-band display system employing available consumer LCD HDTV projectors having native primary spectra consistent with the SMPTE-431 theatrical exhibition standard. Figure 19 summarizes the  $u',v'$  chromaticity gamuts for display systems conforming to the current worldwide HDTV standard, ITU-R Rec. 709, the digital cinema theatrical standard, SMPTE-431 (DCI 'P3'), and the proposed unified wide gamut standard for cinema and television, ITU-R Rec. 2020. It is noteworthy that none of these standard express any spectral definition for the three primary channels so long as chromaticity expectations are met. All three systems also promote a balanced white point consistent with colorimetry for CIE illuminant D65.

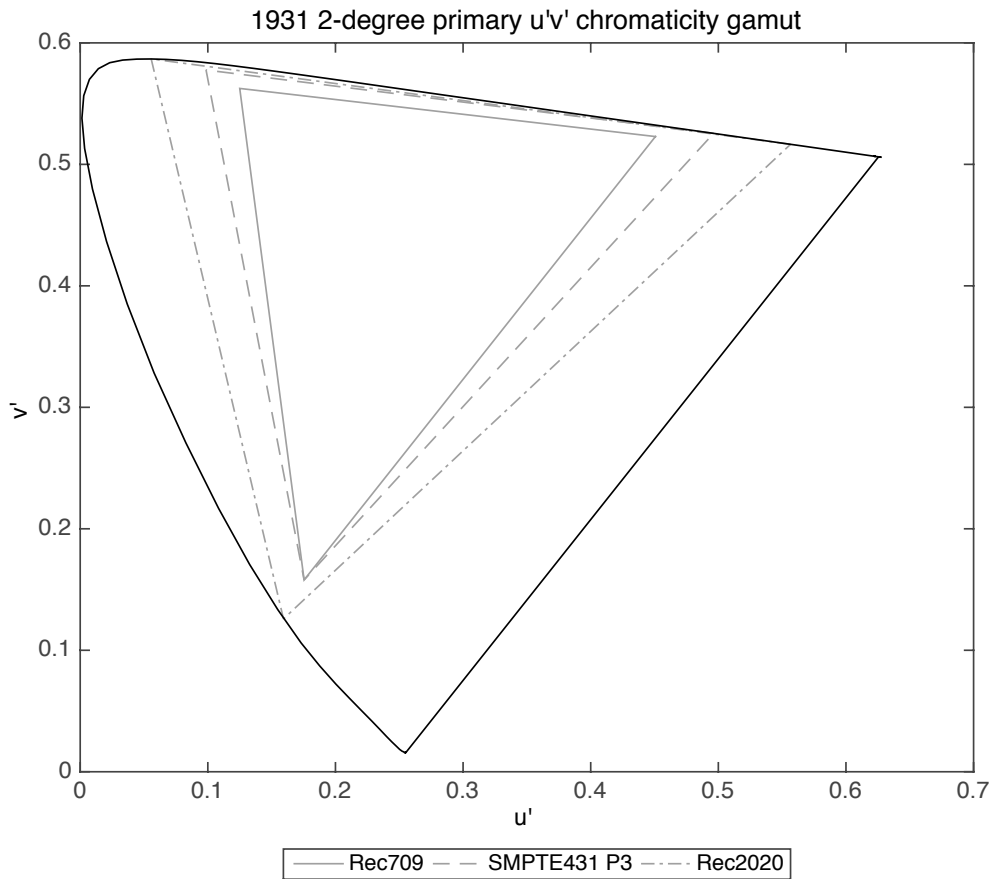


Figure 19. Standard colorimetric gamuts for RGB-based television and cinema systems

Using two projectors and external optical filtration, the spectral peaks of the primaries should prove separable enough to yield six independent color channels, appropriate for generating some semblance of a spectral match to reasonably well-behaved aim stimuli.

Once the constituent projectors ‘A’ and ‘B’ have been appropriately characterized, a basic spectral reconstruction model can be built for the six-channel system via Equation 46 (which recognizes baseline black signatures for each device as well). Taking advantage of presumed primary stability in a well-behaved additive system, Equation 46 can be further expanded to Equation 47 where the characteristic primary spectra,  $SPD(\lambda)_{i,max}$ , are, again, the absolute radiometric measures of the maximally driven primary in each projector and for each channel. Relative radiometric primary amounts in the full summation are generalized by the scaling constants,  $k$  (1x6 vector for the proposed system), which are analogous quantities to *RGB* radiometric scalars in the Day et al. model and  $\alpha$  introduced in Chapter 3, defined generically for multi-channel systems with more than three controllable primaries.

$$SPD(\lambda)_{mix} = SPD(\lambda)_{r,A} + SPD(\lambda)_{r,B} + SPD(\lambda)_{g,A} + SPD(\lambda)_{g,B} + SPD(\lambda)_{b,A} + SPD(\lambda)_{b,B} + SPD(\lambda)_{k,A} + SPD(\lambda)_{k,B} \quad (46)$$

$$SPD(\lambda)_{mix} = \begin{bmatrix} \mathbf{k} & 1 & 1 \end{bmatrix} \begin{bmatrix} SPD(\lambda)_{r,max,A} \\ SPD(\lambda)_{r,max,B} \\ SPD(\lambda)_{g,max,A} \\ SPD(\lambda)_{g,max,B} \\ SPD(\lambda)_{b,max,A} \\ SPD(\lambda)_{b,max,B} \\ SPD(\lambda)_{k,A} \\ SPD(\lambda)_{k,B} \end{bmatrix} \quad (47)$$

Typically, aim spectra will be presented as a radiometric goal for the multiprimary display system and as such, an optimization approach can be used to determine theoretical scalars,  $k$ , needed to reproduce any target (recognizing that there are dynamic range limitations on the amplitude of each term within  $k$ ). Unlike

typical reflectance space spectral reconstruction modeling performed by Wyble, et al. on inkjet systems<sup>70</sup>, emissive spectral reproduction demands consideration of absolute radiometric output, especially when accounting for the superposition of the two distinct projector optical paths. Because the drive lamps are independent, a relative shift in the absolute white luminance of one projector versus the other during typical use can lead to degraded spectral output quality through the full model. Further, a spectral aim set that demands more flux than the total system is capable of from any single channel likewise restricts the optimized performance.

$k$  scalars from Equation 47 may be derived for any aim spectra set utilizing appropriate constrained optimization. For best results, a spectral/colorimetric co-optimization is desirable. The spectral reconstruction system proposed in this work offers six distinct primary spectra and is thus capable of infinite combinations of output for achieving standard observer colorimetric matches to the aim spectra. Several potential techniques are available for this task including 2-stage co-optimization wherein an initial spectral optimization provides  $k$  inputs to a colorimetric refinement or matrix-switching approaches focused on optimizing colorimetric processing efficiency for real-time video sequences at the expense of spectral accuracy<sup>44</sup>. Further, full Lagrange multiplier-based spectral/colorimetric co-optimizations that potentially bypass the computational overhead of nonlinear optimization are also proposed in previous work<sup>49</sup>.

## **Building the System**

To generate six superimposed channels of color for spectral reconstruction, twin Panasonic PTAX200U LCD projectors capable of 1920x1080 resolution were used. Each projector employs an optical block with three independent LCD modulators and internal optical filtration and prismatic splitting/re-combining to isolate the RGB signal paths. Each projector was driven natively in 8-bits using standard dual-head graphics hardware from a host computer. Prior to use and measurement, the projectors were allowed a 30-minute warm-up time. For tests in which both projector outputs were superimposed, a vertical stack rig was used to overlap both images and provide reasonable alignment. A schematic is provided in Figure 20.

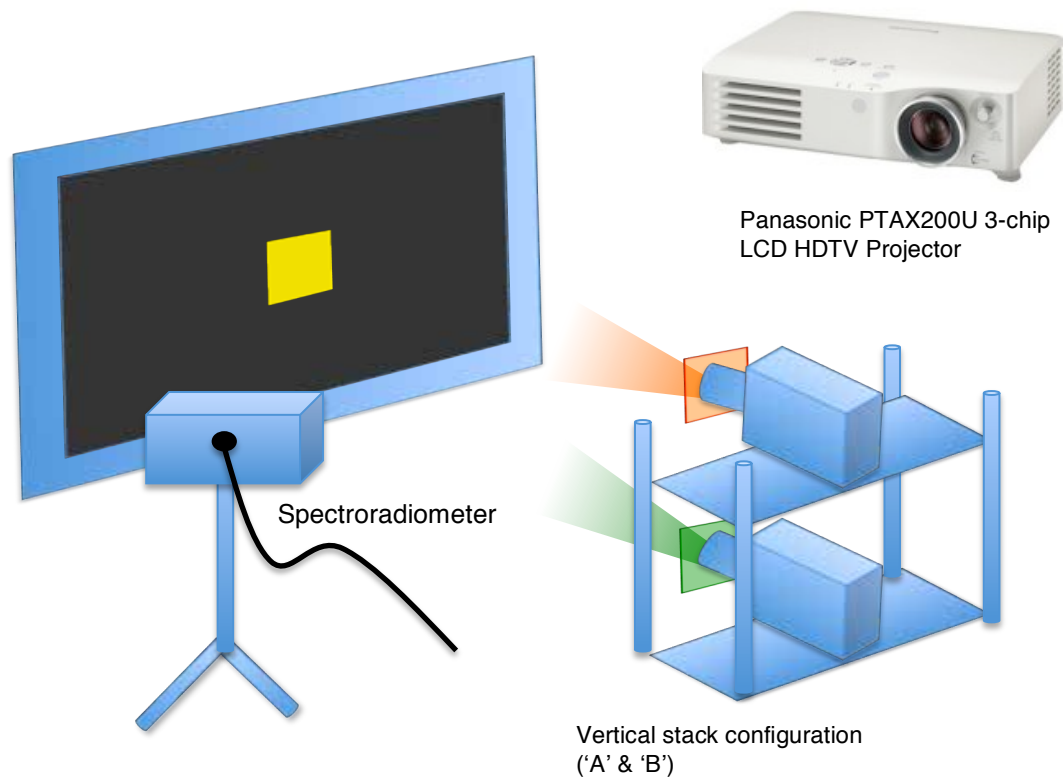


Figure 20. Schematic of RIT 6-primary proof-of-concept multiprimary display

Spectra and colorimetry from projected patches on each device were obtained via a Photo Research PR655 spectroradiometer. Color patches were generated for neutral, red, green and blue ramps as well as for two series of 5x5x5 factorial color channel combinations, one across the full 8-bit domain and one concentrated at lower drive values of 20 and less. The patches were sized to 400 pixels square oriented in the screen's center; surrounding pixels were set to black.

## Results and Discussion

Prior to repurposing in the multiprimary display prototype, the Panasonic equipment was fully characterized for tonescale reproduction, color gamut, colorimetric stability, radiometric additivity, spatial uniformity/independence and temporal stability. Spectral measurements were also collected of the native primary output.

## Baseline Display Characterization

Neutral scale additivity in luminance across the full display dynamic range of Projector A is provided in Figure 21. The device delivers excellent radiometric additivity for the sum of the individually measured primaries as compared to the neutral ramp. In fact, it appears it is only the fully driven white where differences are greater than 1.0%. Projector B showed similar results.

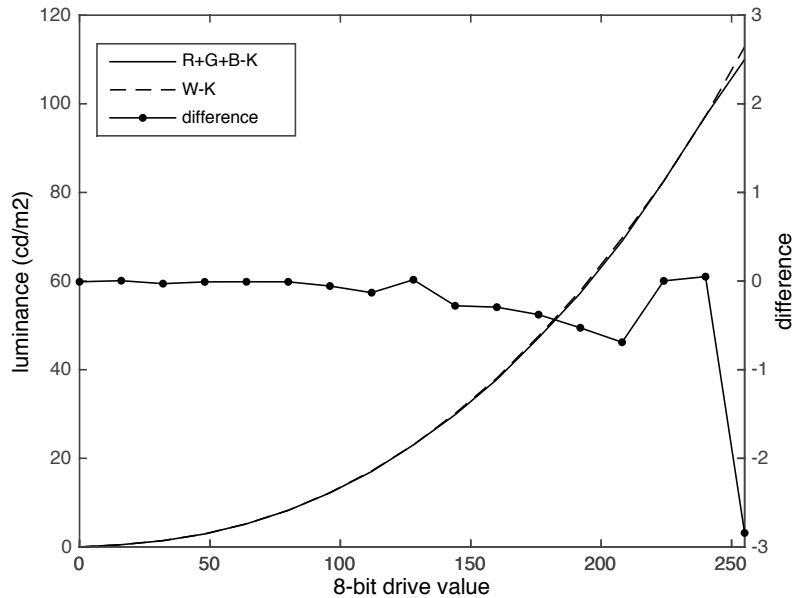


Figure 21. Full grayscale additivity test results for Projector A, showing summed luminance of RGB primary ramps versus luminance of neutral scale ramp (offset black luminance subtracted out)

To evaluate display scalability, black-corrected chromaticity coordinates for each of the primary ramps for Projector A are shown in Figure 22. The overall gamut of Projector A is consistent with the digital cinema SMPTE-431 standard and Projector B is, again, similar.

Using the full collection of patch measurements and the Day et al. optimization scheme, the primary colorimetry matrix for each projector and display radiometric scalar EOTF LUTs were computed for inclusion in the rigorous spectral models. Projector A's data is shown in Figure 23 and Equation 48.

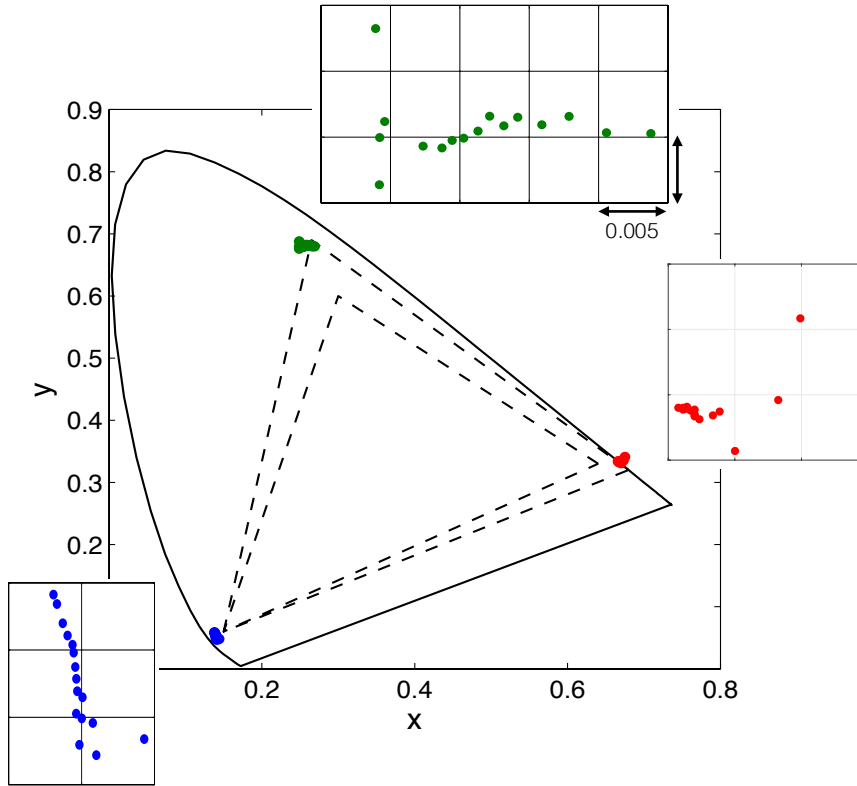


Figure 22. Primary ramp scalability test results for Projector A in 1931 x,y chromaticity, offset black level subtracted out; smaller triangle shown is ITU Rec. 709 (sRGB) primary gamut; larger is digital cinema SMPTE-431 gamut; grid division in call-out figures is 0.005 chromaticity units

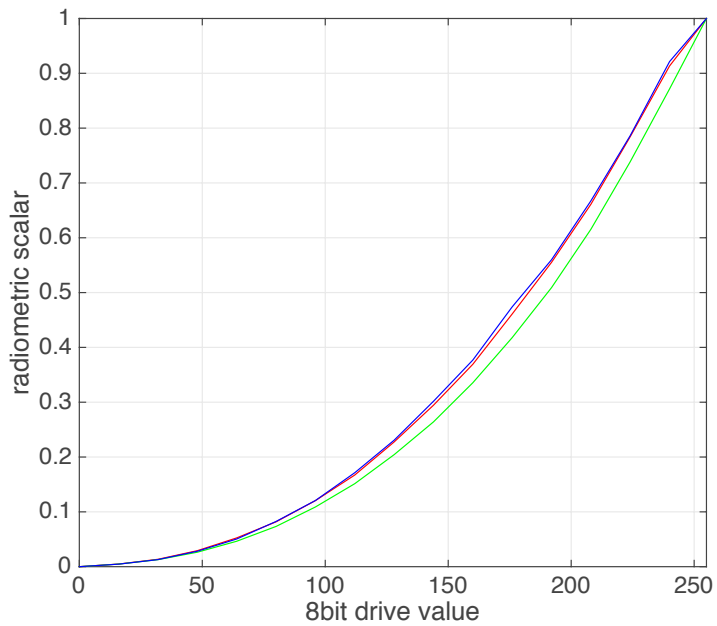


Figure 23. Projector A EOTF

$$\begin{bmatrix} X \\ Y \\ Z \end{bmatrix} = \begin{bmatrix} 0.435 & 0.254 & 0.158 & 0.001 \\ 0.217 & 0.665 & 0.065 & 0.001 \\ 0 & 0.053 & 0.928 & 0.002 \end{bmatrix} \begin{bmatrix} R \\ G \\ B \\ 1 \end{bmatrix} \quad (48)$$

Spatial uniformity in the projectors was determined by driving white patches against a black background in symmetrical positions throughout the full screen area. Maximum luminance fall-off from screen center to corner was 20.6%. For higher end theatrical projection, SMPTE demands screen luminance falls to no more than 75% of the center luminance in any portion of the image area. Further, white point chromaticity is permitted to drift from the center reading by as much as 0.015. Thus while presenting some level of concern for more serious color simulation, the projectors lie within acceptable tolerances for even high-end theatrical viewing. However for a superimposed multispectral projection system, these variations must be compensated as luminance and chromaticity non-uniformities will render localized variation in the mixing model needed to produce aim spectral color reproduction.

Spatial independence was analyzed for the projectors to assess how color patches generated in the middle of the image area might vary in measurement when presented against differently colored backgrounds. Darker patches proved most influenced by the variation in background color, suggesting the majority of the differences can be attributed to optical flare. The overall magnitude of these errors is visually significant, further complicating the utility of the projectors for serious color simulation work. Overall, results of these tests are far inferior to those measured on high-end emissive LCD panels by Day et al.<sup>68</sup>, not surprising considering the increased optical complexity and elevated light management challenges of a 3-chip projection architecture.

### *Verification and Long-term Stability*

Characterizing the radiometric performance of the LCD projectors in a single stable experimental exercise is only useful for interpreting color reproduction models for the devices in a finite window of time beyond the characterization. Extending the utility of models over longer operational periods is only possible if the projectors themselves are consistent in performance. An extensive verification experiment was executed for each projector over a four-month period. The maximum output luminance and white chromaticity of the projectors were measured periodically over a span encompassing 211 lamp hours for Projector A

and 82 lamp hours for Projector B. Figures 24 and 25 summarize the results gathered. Projector A loses 18% of its peak output after 50 hours and 38% after 200 hours. Projector B shows similar trending though results were not collected over as long a lamp life. In terms of white point chromaticity stability, both projectors likewise exhibited a drift with Projector A trending slightly green-cyan and Projector B trending yellow.

To assess the consistency of the optimized color reproduction models derived for each projector at each point in the four-month study, a set of 11 color patches were driven to each device and measured during the sampling sessions. Mean and maximum  $\Delta E_{00}$  values for the actual measurements versus the radiometric model predictions were tallied for each trial. Figure 26 shows the trend of mean  $\Delta E_{00}$  for each projector over time. Versus the baseline starting error of approximately 0.6, projector A drifted to greater than 2.0 average color difference by 200 hours.

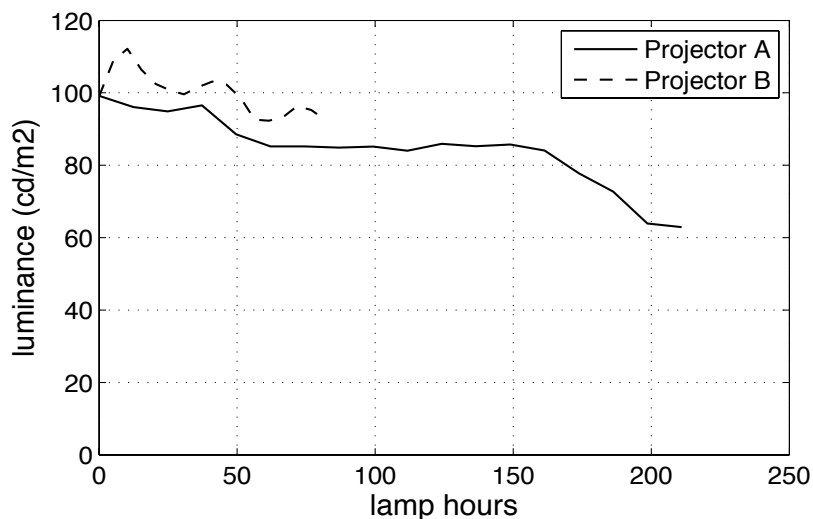


Figure 24. Full-on white luminance stability

### Primary Characterization

Principal components analysis was employed to determine the major eigenvectors in the primary spectra for each color channel and for each projector independently. The first eigenvectors in each channel, normalized to a peak of 1.0, are shown in Figure 27. For Projector A, these eigenvectors account for 99.96%, 99.93% and 99.90% of the total spectral variability in red, green and blue. For Projector B, the eigenvalues are 99.97%, 99.94% and 99.93%. Though primaries

found in many LCD-based displays can be quite variable across the full system dynamic range, the stability of the Panasonic primaries here is excellent.

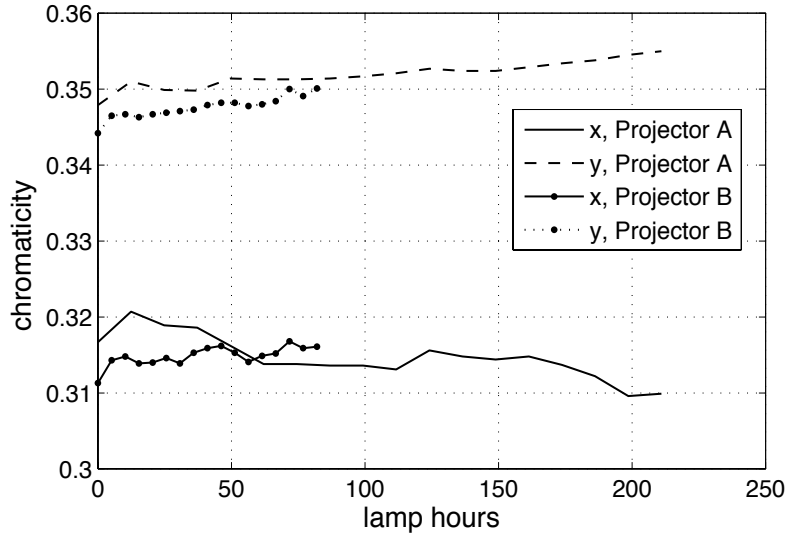


Figure 25. Full-on white chromaticity stability

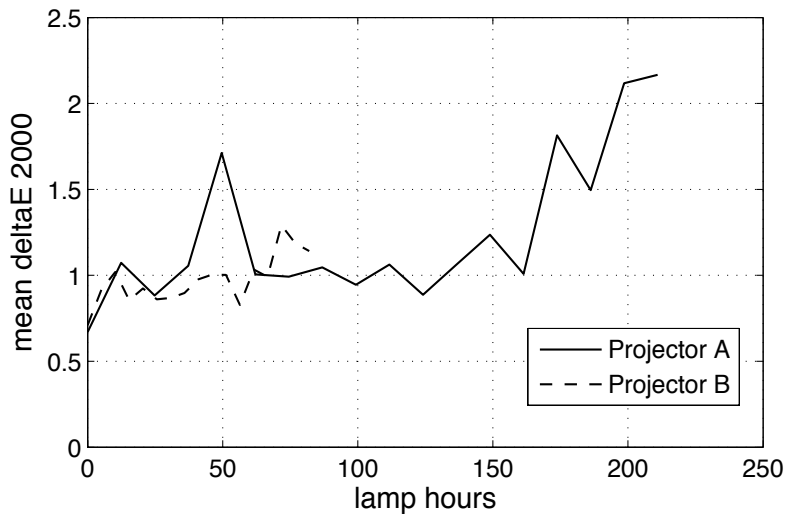


Figure 26. Optimized model prediction stability

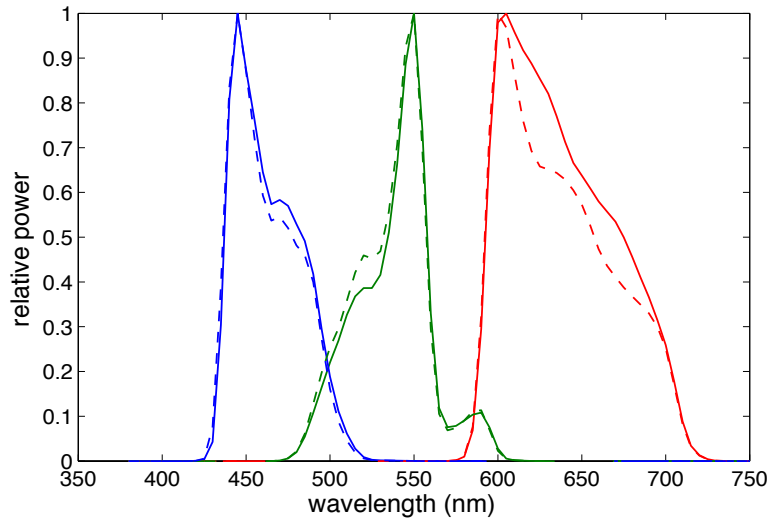


Figure 27. First eigenvectors from RGB primary series for Projectors A (solid) and B (dashed), normalized to 1.0 peak

## Filter Selection Models

Ideal filters for modifying native spectra in this application will employ a narrow notch or steep bandpass characteristic in at least one strategic spectral location that would impact the normalized peak position of 1 or 2 of the original primary spectra without distorting the other channel(s). The intent would be to exaggerate spectral diversity for the system. While a parametric definition for candidate filters could allow for an intelligently constrained optimization of filter properties, the goal of the proof-of-concept multiprimary design was to construct the system at minimal cost. Thus, exhaustive search of available filter materials from vendors such as Schott, Semrock and others was used to guide the design process. Candidate filters for the proposed system were evaluated through a full spectral reconstruction model. The first criterion assessed was total luminance loss expected by inclusion of the filters. In Figure 28, the absolute radiometric summation of the maximum driven primaries are shown for the native system. Also summarized are the predicted absolute spectra and individual attenuated spectra for a system comprising Schott UG5 1mm glass over Projector A and Schott GG455 1mm glass over Projector B. Finally shown are the aim white spectra representing the white MacBeth Color Checker target patch illuminated by a CIE D65 illuminant and the spectral reconstruction match for this system, achieved following a minimization of spectral rms error (defined by Equation 35 but further normalized against maximum spectral power across the visible domain to yield a relative error metric) using Equation 47.  $k$  scalar amounts derived from the reconstruction

optimization are shown in the legend of this subplot. For this combination the relative spectral rms error is 0.36 and the  $\Delta E_{00}$  (D65-illuminated MacBeth white patch, 1931 2° observer) is 8.5.

Neither the spectral nor the colorimetric performance reported in Figure 28 for reconstruction of the MacBeth white is impressive. At the very least, the six-channel system is more than capable of yielding a perfect colorimetric match for the 1931 observer. Figure 29 summarizes the results of matching the D65-illuminated MacBeth Color Checker white patch with a goal of minimizing  $\Delta E_{00}$  and using the previously determined  $k$  scalars from the spectral rms minimization as starting guess in a constrained optimization. Radiometric scalars were restricted to a physically realizable maximum value of 1.0 but allowed to vary as much as needed from the spectrally optimized starting point to achieve the colorimetric match. As expected, the color difference error is easily nulled altogether with superfluous degrees of freedom but at the expense of the relative spectral rms error which has risen from 0.36 to 0.40. The visual match of the two spectra remains poor for not only the white but for a repeat of this secondary optimization for all 24 MacBeth patches, Figure 30. Table 2 summarizes the quality of spectral reconstruction for the MacBeth patches for this modeled system as well as a number of other notable projector filter combinations investigated in the exhaustive search. As evidence of the limitations in effective manipulation of the original projector spectra, many of the combinations perform only marginally better than the native system without any added filtration (first row, Table 2).

### **Actual Filter Characterizations**

A real system incorporating a Schott GG455 glass filter over Projector A and a UG5 filter over Projector B was constructed to assess actual system performance. Expected results for the dual projection system were simulated from real device primary measurements and are shown in Table 3. Variations here summarize expected spectral and colorimetric matches for four different spectra/colorimetry co-optimization constraints – specifically, the original spectrally-optimized  $k$  scalars are held to within 10%, 20%, 30% or no constraint for predicting the optimal co-optimization  $k$  values. As the constraint is tightened, perfect colorimetric matches for all patches are not possible and the mean and maximum color difference predictions versus aim increase from 0. Results for the actual filter model with no constraints compare favorably with the results of Table 2. For the 10% constraint, however, the rms advantage gained (12% improvement in mean rms error) comes at the cost of an average  $\Delta E_{00}$  of 2.4. Figure 31 provides a summary of the spectral matches achieved under this particular condition for all 24 MacBeth patches.

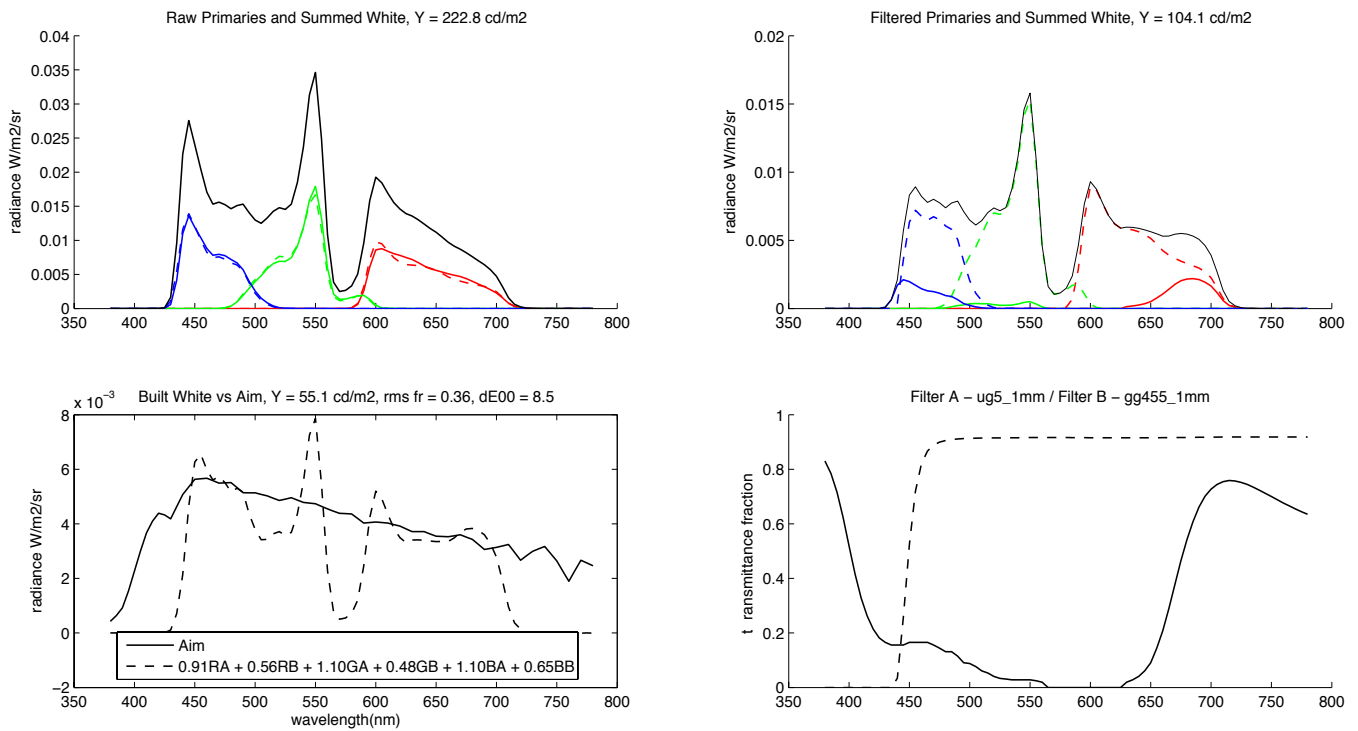


Figure 28. Model of Schott UG5, 1mm and GG455, 1mm glass in multiprimary projection system – (upper left) PCA modeled maximum spectra for each projector; (upper right) predicted primary spectra attenuated by inclusion of filters; (lower left) modeled spectral reconstruction of MacBeth white under D65; (lower right) Schott filter transmission spectra

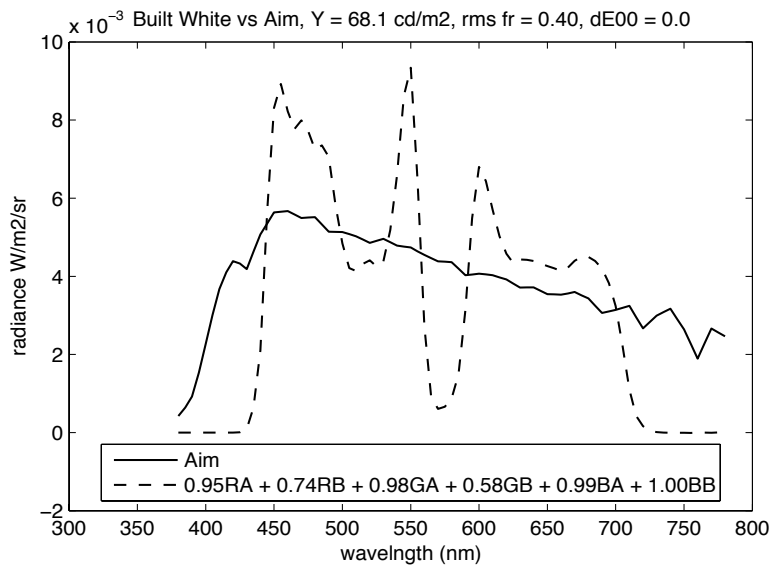


Figure 29. Model of Schott UG5, 1mm and GG455, 1mm glass in multiprimary projection system – predicted reproduction of MacBeth white patch under D65 from colorimetric optimization

Table 2. D65-illuminated MacBeth CC spectral reconstruction for various filter combinations from Schott and Semrock on native projectors, derived from manufacturer's filter data and PCA-characterized projector primaries

Filter A	Filter B	Spectral RMS optimization only (24 patches)				RMS/ $\Delta E_{00}$ co-optimization	
		mean rms	max rms	mean $\Delta E_{00}$	max $\Delta E_{00}$	mean rms	max rms
none	none	0.14	0.34	6.0	10.0	0.15	0.36
BG1(1mm)	GG10(1mm)	0.12	0.31	4.6	7.1	0.14	0.35
BG24(1mm)	GG10(1mm)	0.11	0.31	5.0	8.2	0.13	0.35
BG28(1mm)	OG570(1mm)	0.13	0.32	4.9	9.8	0.14	0.34
BG7(1mm)	BG36(1mm)	0.14	0.34	5.9	12.3	0.18	0.51
BG7(1mm)	OG570(1mm)	0.13	0.32	5.0	8.8	0.14	0.33
DI01_488_532_6	none	0.14	0.33	4.9	8.2	0.17	0.38
FF01_510_42	none	0.13	0.32	4.5	7.4	0.15	0.35
UG5(1mm)	GG455(1mm)	0.12	0.32	5.0	8.8	0.14	0.38
GG475(1mm)	FF660	0.12	0.33	5.1	7.3	0.15	0.36

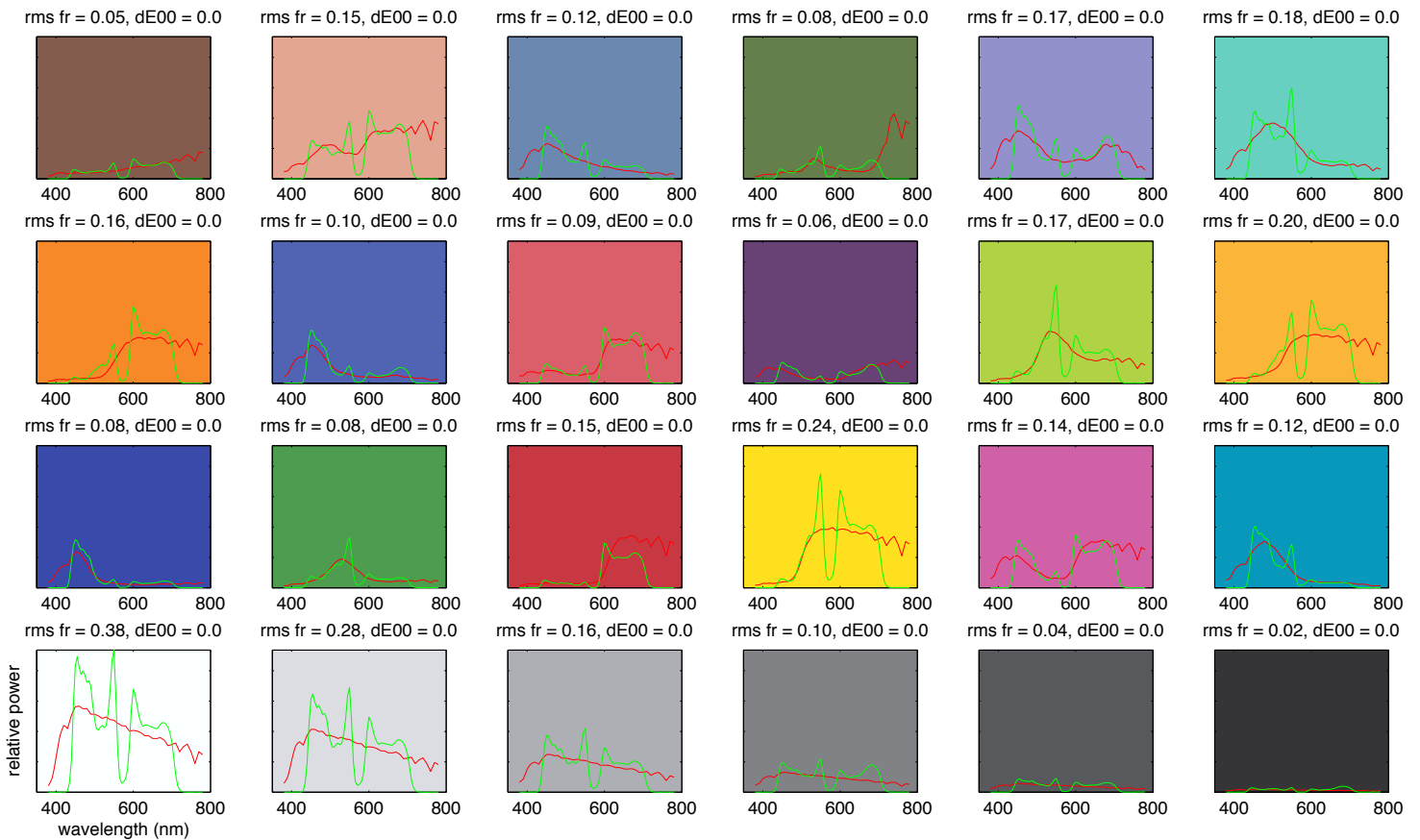


Figure 30. UG5/GG455 modeled MacBeth spectral/colorimetric co-optimized reconstruction, minimizing  $\Delta E_{00}$

Table 3. Predicted spectral reconstruction model performance for GG455/UG5 projection system implementing spectral rms and  $\Delta E_{00}$  co-optimization

mean rms	max rms	mean $\Delta E_{00}$	max $\Delta E_{00}$	k constraint
0.135	0.372	0.0	0.0	none
0.131	0.350	0.2	1.8	30%
0.126	0.333	0.7	2.6	20%
0.119	0.324	2.4	4.9	10%

### Observer Metamerism

Spectral matches evaluated via an rms error metric and from simple visual inspection of the reproduced signatures in Figures 28 and 29 prove the two-projector multiprimary display is inadequate for representing even simplistic scene stimuli. Ultimately, success in generating spectral matches of target stimuli using the dual projection system could be better judged by characterizing observer metamerism.

Fairchild, et al. have documented a methodology used to evaluate observer metamerism in additive electronic displays employing the CIE 2006 color matching function models for observers of varying ages and subtending various angular fields of view<sup>8</sup>. Primary drive amounts needed to enforce a metameric match between aim spectra and the multiprimary reproduction are calculated using a chosen CIE 2006 color matching function. Once matched for that particular observer, the resultant modeled spectra of each system are assessed for subsequent colorimetric match assuming the 1931 2° standard observer and resulting color difference values are tallied.

For the present work, spectral/colorimetric co-optimization is performed based on CIE 2006 color matching function sets incorporating observer ages of 20, 32, 40, 60 and 80 all at a 2° field of view. Results reported here are for the “no constraint” co-optimization method to provide the best possible observer metamerism results for each scenario.

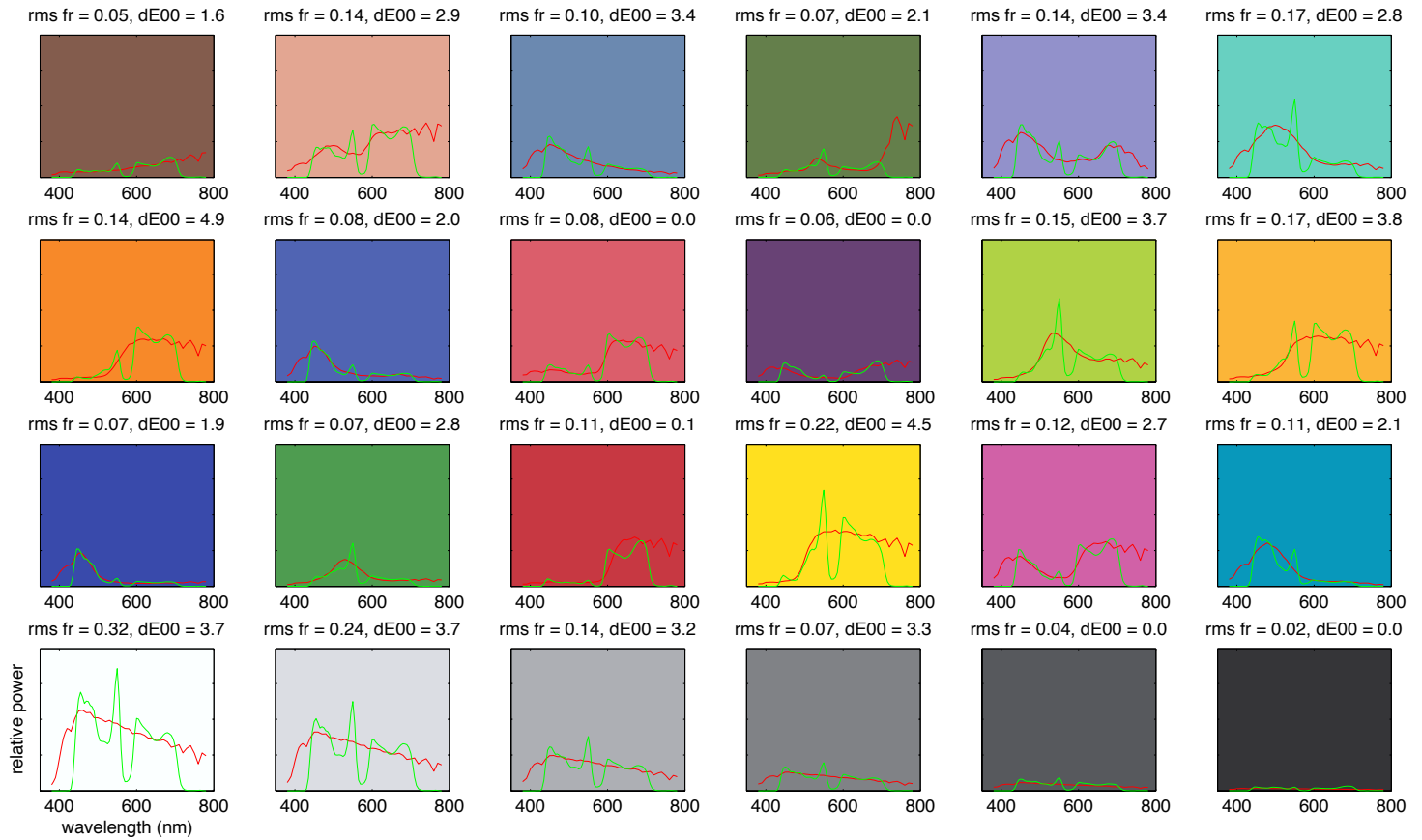


Figure 31. UG5/GG455 actual system reconstruction model, minimizing  $\Delta E_{00}$  with 10%  $k$  constraints from initial spectral rms minimization

The GG455/UG5 dual projector system described thus far is compared for observer metamerism performance versus a model incorporating only a single projector. Mean  $\Delta E_{00}$  (1931 2°) for the 24 patches as a function of metameric-match age for each system are compared in Figure 32. Clearly, the six-channel dual projection system fails to deliver any benefit for observer metamerism versus the native performance of projector A alone. This likely stems from the fact that though six channels are provided in the dual projection system, each primary spectral peak is notably narrower than that found in the native single projector and thus large first derivative variations in spectral reconstruction plague the colorimetric sensitivity of the observer metamerism approach.

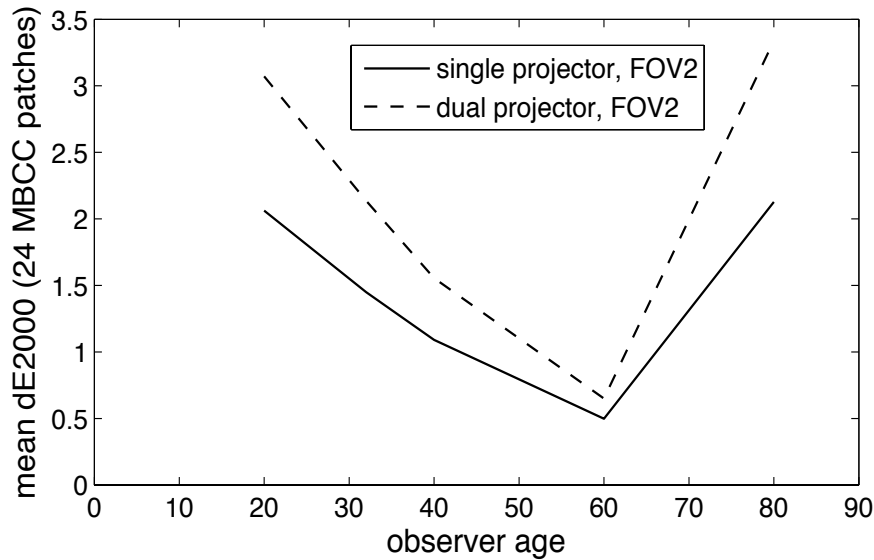


Figure 32. Color difference summary for 1931 2° observer after generating metameric matches in projection to D65-illuminated MacBeth Color Checker patches for CIE2006 observers of ages 20, 32, 40, 60 and 80 at 2° fov, single projector vs GG455/UG5 system

With the less than ideal results determined for the actual GG455/UG5 projection system, attention is turned to alternate primary spectra that may perform better. A candidate set of Gaussian primaries was investigated to see if mathematically simplified spectra could yield improved matches in six channels versus the narrow native primary reconstruction of the Panasonic projectors. The spectral rms error optimization model was invoked to generate ideal spectral matches to a subset of the MacBeth patches: light skin, red, green, blue, cyan, magenta, yellow and white. Independent variables in the optimization were the six Gaussian peak wavelengths,  $\mu_i$ , and the six standard deviations (peak widths),  $\sigma_i$ . Table 4 summarizes parameters for the optimized primaries and Figure 33 shows the individual and summed spectra. Generating a full spectral/colorimetric co-optimization of the D65-illuminated MacBeth patches via these primaries, the mean and maximum rms spectral fraction values were lowered significantly to 0.02 and 0.05 respectively. The maximum co-optimized  $\Delta E_{00}$  value was 0.02 as colorimetric optimization alterations to  $k$  were restricted to 10% deviation from original spectral optimizations with no issue in achieving near perfect metameric matches across all the patches. Spectral matches for all 24 patches are shown in Figure 35. For the observer metamerism models, the results are similarly impressive. Figure 28 shows benefits gained in various observer ages versus the single three-primary projector.

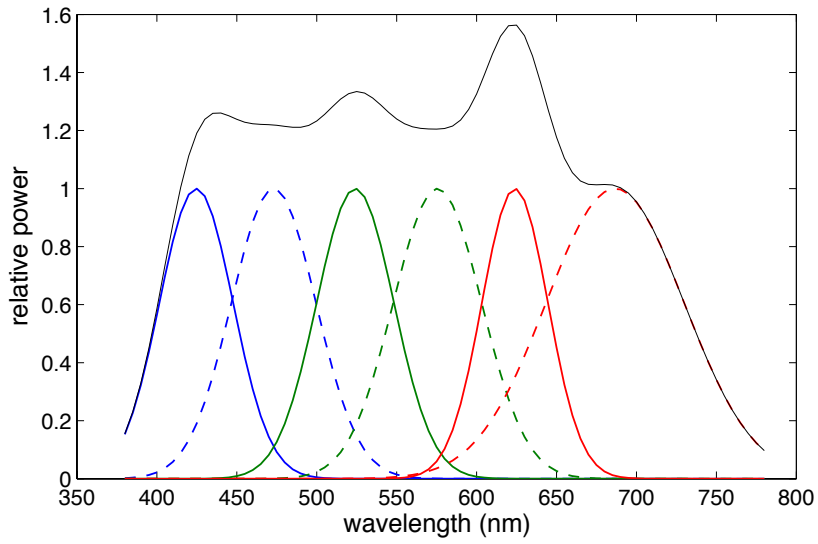


Figure 33. Optimized Gaussian primaries

Table 4. Optimized Gaussian Primary Parameters

	<b>B 1</b>	<b>B 2</b>	<b>G 1</b>	<b>G 2</b>	<b>R 1</b>	<b>R 2</b>
$\mu$	425	473	524	576	624	687
$\sigma$	23.1	26.4	24.2	27.7	20.6	43.2

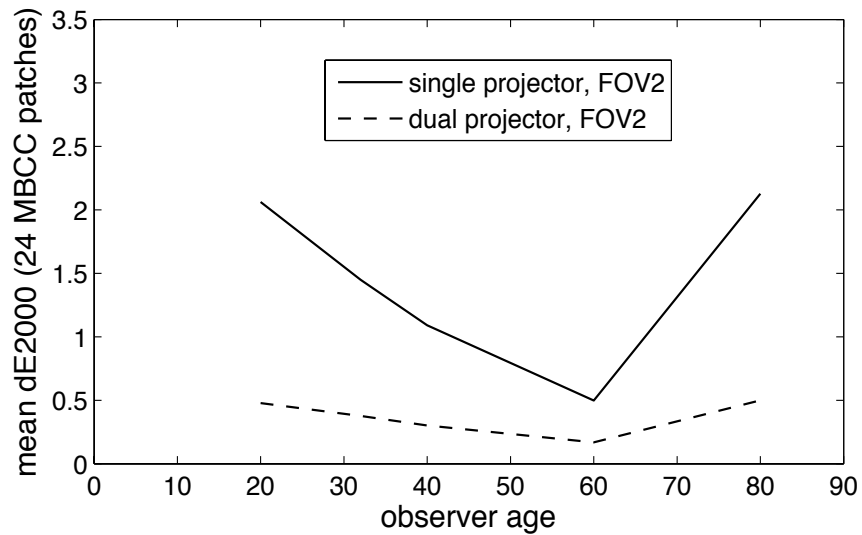


Figure 34. Observer metamerism summary; single projection model versus ideal Gaussian dual projection model

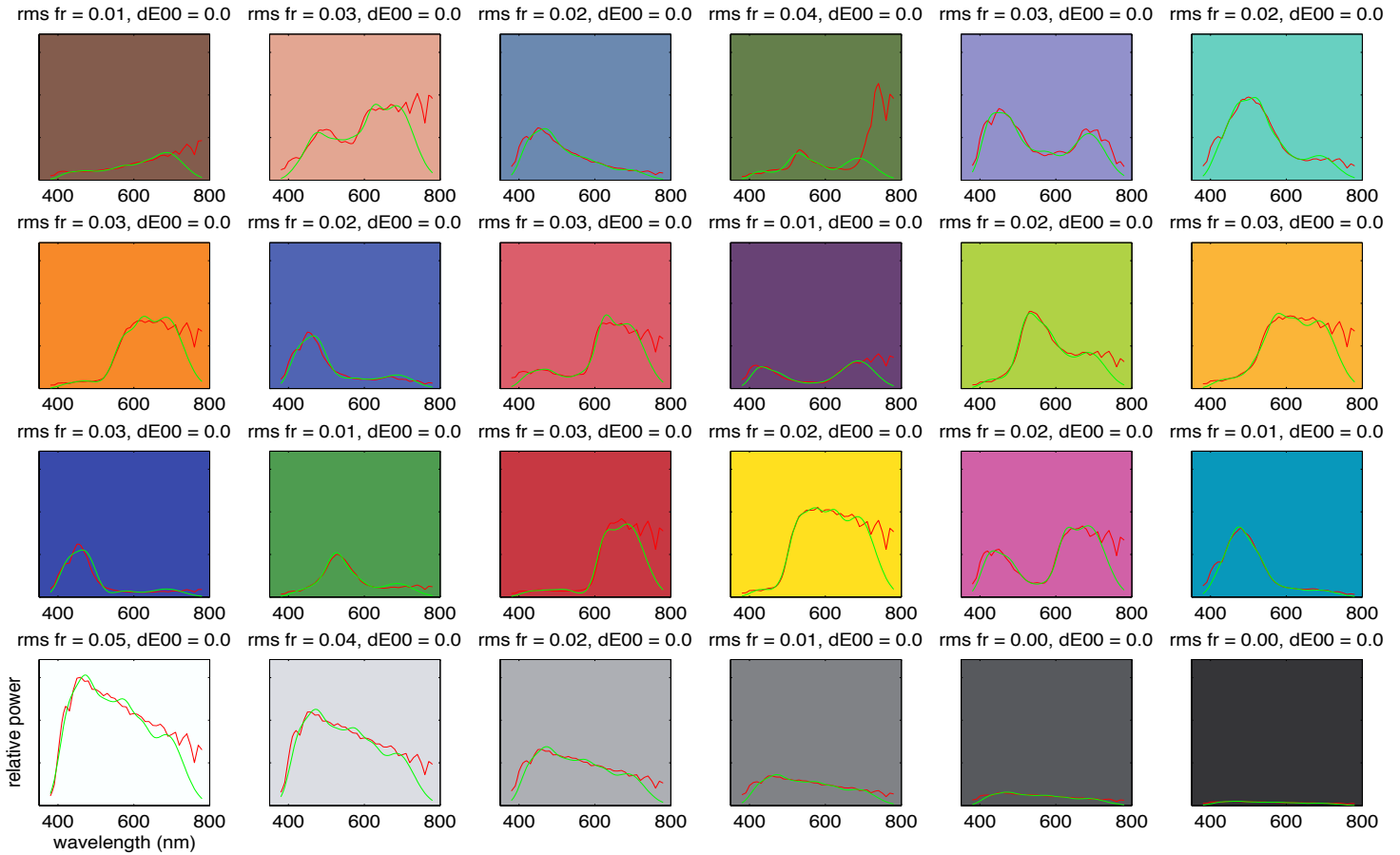


Figure 35. Ideal Gaussian primary six-channel spectral reconstructions after spectral and colorimetric co-optimization

## Conclusion

Abridged multispectral projection shows promise for reducing observer metamerism and expanding spectral gamut reproduction; however, the current generation of native wide-gamut LCD, DLP and laser projection technologies provides limited flexibility based on techniques utilizing external optical filtration. Improved performance is realized when narrow band native primary spectra can be removed and idealized primary spectra inserted instead.

Beyond primary spectra optimization, additional engineering concerns around display uniformity, spatial independence and long-term colorimetric drift must also be addressed to make these techniques viable.

## Chapter 6

---

### Modeling Observer Variability and Metamerism in Electronic Color Displays

#### Abstract

Employing near-monochromatic spectral primaries in electronic color displays poses a risk to the consistency of visual experience amongst a group of disparate, but otherwise normal, color observers. Several models of spectral color vision have surfaced in recent research and are helping investigators better understand the implications for color experience variability. This chapter serves to summarize various color difference indices that may be useful in predicting the magnitude of observer response inconsistencies and applies them to simulations of current electronic displays as examples of potential concerns these new high-gamut technologies might raise. In particular, various laser-based displays are shown to perform with significantly increased observer variability versus traditional ITU-R Rec. 709 and SMPTE-431 RGB-primary displays utilized in the cinema industry. Further, observer metamerism can be reduced significantly with proper optimization of a multichannel projection system comprising seven explicitly designed primary spectra.

#### Color Vision Models

In architecting digital color management strategies for still photography, computer graphics or motion picture imaging systems, the principal model for color vision employed comes from the International Commission on Illumination (CIE) 1931 2° standard observer<sup>64</sup>. This single trichromatic model summarizes a mathematical representation of the spectral sensitivity of the three integrated channels of human color vision isolated to the 2° field of view of the fovea. These color response curves were derived from bipartite field color matching experiments executed by Guild and Wright in the 1920s, involving 17 observers and validated by the CIE as representative of the worldwide population of normal color observers<sup>55</sup>. The published standard observer spectral responses represent an intentional transformation of the actual average data collected from these experiments to a form based on non-realizable primaries yielding  $\bar{x}_\lambda$ ,  $\bar{y}_\lambda$  and  $\bar{z}_\lambda$  color matching functions (CMF), summarized in Figure 36. The transformation is architected such that each spectral curve contains all positive values (a necessity for colorimeter hardware developed concurrent to the standard) and such that the 1924 photometric response curve,  $V_\lambda$ , could be matched by the  $\bar{y}_\lambda$  function.

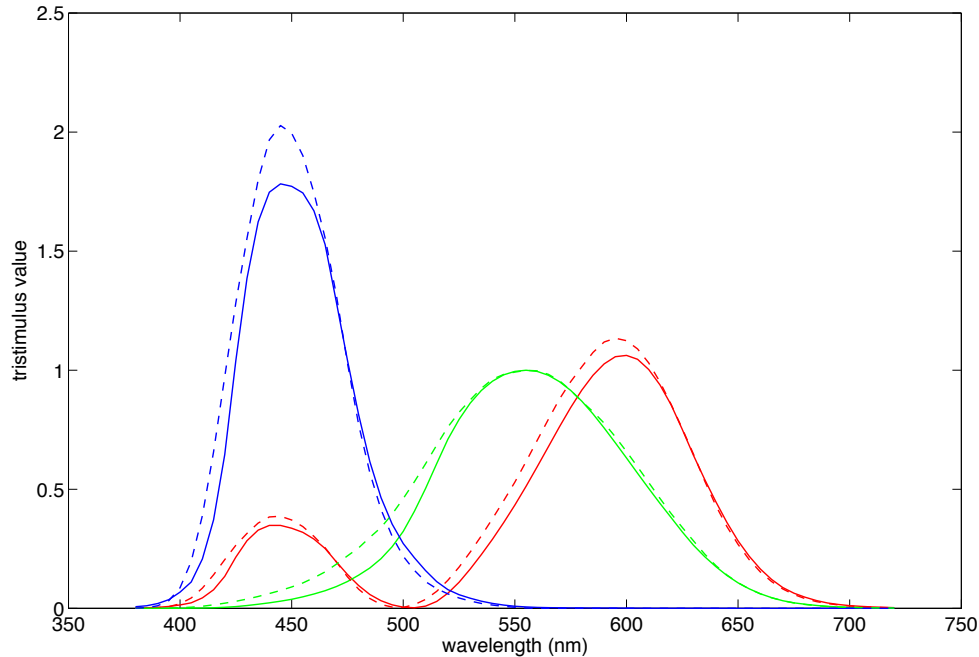


Figure 36. CIE 1931 2° (solid) and 1964 10° (dashed) standard observer color matching functions

In 1964, the CIE sanctioned the addition of a wider field standard observer to be used in colorimetry of larger field-of-view stimuli<sup>55</sup>. The data were collected in 1959 in separate experiments at high illumination levels with 49 observers by Stiles and Burch<sup>71</sup> and at low illumination levels with 27 observers by Speranskaya<sup>72</sup> with each experiment subtending a 10° visual field. Designated as  $\bar{x}_{10\lambda}$ ,  $\bar{y}_{10\lambda}$  and  $\bar{z}_{10\lambda}$  and shown also in Figure 36, these response curves have a firmer statistical grounding than the 1931 set. However, the 10° observer has no mathematical connection to modern photometry or the universally-used  $V_\lambda$  response and most imaging industries have continued to employ system design based on the older narrower field observer.

Concerns for both the 1931 and 1964 CIE standard observers surround their derivation from limited demographic populations and their declaration of average behavior for all color normal observers. In the 1980s, the CIE attempted to address inadequacies in models of observer variability and observer metamerism by introducing the Standard Deviate Observer<sup>73</sup>. These color matching functions were computed from differences amongst the original 1959 Stiles and Burch data and permitted confidence limits to be calculated for any colorimetric calculation. Unfortunately, subsequent research with this observer set has found it to grossly under predict real observer variability<sup>74</sup>.

More recent research has generated greatly improved understanding of the anatomical and optical disparities amongst color normal human observers. The CIE 2006 model (from the work of CIE TC1-36) summarizes a prediction of peak-normalized fundamental cone sensitivities and corresponding CMFs as dependent on observer age and field of view<sup>11</sup>. The general form of predicted  $\bar{l}_\lambda$ ,  $\bar{m}_\lambda$  and  $\bar{s}_\lambda$  cone fundamentals is summarized in Equation 49. Specifically, cone absorptivities,  $\alpha_\lambda$ , and maximum macular density,  $D_{\tau,max,macula}$ , are treated as field-size dependent, based on anatomical studies associated with each. Ocular media densities,  $D_{\tau,ocul}$ , do not vary with field of view but are known to vary with observer age. The cone fundamentals can be further transformed to CMFs via matrices recommended by CIE TC1-36 and used in calculating colorimetry and color difference values for compared stimuli. Specifically, CIE TC1-36 defines an LMS-to-XYZ 3x3 linear matrix for converting the peak-normalized 32 year-old observer in the 2° cone fundamental model to best match the area-normalized 1931 CIE standard observer, but with explicit constraints. These include the resulting best match CMF a) be non-negative, b) possess a  $\bar{y}_\lambda$  prediction equivalent to the TC 1-36 re-definition of the 2° luminous efficiency function,  $V_{LM,\lambda}$ , c) yield equal integrated tristimulus values under the equal-energy illuminant, d) possess a  $\bar{z}_\lambda$  prediction directly and solely proportional to  $s_\lambda$ , e) have a minimum spectral chromaticity coordinate in the predicted  $x$  channel match the same for the 1931 standard  $\bar{x}_\lambda$  and f) deliver a minimization of Euclidean sum of squares between the predicted spectral chromaticity coordinates and the 1931 chromaticity coordinates across the domain 390-830nm. A second matrix is used to transform the 32 year-old/10° cone fundamentals to the 1964 standard observer. CIE TC1-82 is currently refining methodology to convert cone fundamentals from any age and field-of-view definition to an appropriate CMF. In the present work, however, the absolute variability of observer response is a key attribute analyzed. In an attempt to not diminish or exaggerate this variability from established cone fundamental models for which there are no corresponding CMF data, only the 2° LMS-to-XYZ matrix is considered for all transformations (and thus area normalization and all-positive response in the CMFs is also not preserved). Figure 37 summarizes a sampled collection of modeled observer CMFs spanning ages 20 to 80 and fields of view from 1° to 10°. Several researchers have pointed out that the CIE's model is imperfect in predicting the spectral behaviors of any single real observer but that the models generally encompass the ranges expected in a normal population. In future work, an alternate matrix transformation strategy may be employed for the CIE 2006 CMF models where the starting  $\bar{l}_\lambda$ ,  $\bar{m}_\lambda$  and  $\bar{s}_\lambda$  series as a function of age and field size are area-normalized prior to transformation. This would better reflect a chromatic adaptation treatment in the generated cone fundamentals than the current peak normalization approach.

$$\begin{aligned}
\bar{l}_\lambda &= \alpha_{i,l,\lambda} \cdot 10^{-D_{\tau,max,macula}} \cdot D_{macula\ relative,\lambda} \cdot 10^{-D_{\tau,ocul,\lambda}} \\
\bar{m}_\lambda &= \alpha_{i,m,\lambda} \cdot 10^{-D_{\tau,max,macula}} \cdot D_{macula\ relative,\lambda} \cdot 10^{-D_{\tau,ocul,\lambda}} \\
\bar{s}_\lambda &= \alpha_{i,s,\lambda} \cdot 10^{-D_{\tau,max,macula}} \cdot D_{macula\ relative,\lambda} \cdot 10^{-D_{\tau,ocul,\lambda}}
\end{aligned} \tag{49}$$

In computational models, Sarkar, et al.<sup>60,61</sup> have statistically grouped 47 of the Stiles and Burch observers into seven general base CMF sets by minimizing colorimetric prediction errors. The full candidate CMF sets were originated from 125 permutations derived from five distinct  $\bar{l}_\lambda$ ,  $\bar{m}_\lambda$  and  $\bar{s}_\lambda$  cone fundamentals each. The five discrete fundamentals per cone type originated from cluster analysis on the Stiles and Burch data set together with 61 variations calculated from the CIE 2006 models for observer ages between 20 and 80. Sarkar used the categorization approach to successfully identify the primary color matching function descriptor of 30 real observers in a highly metameric matching experiment. Fedutina, et al.<sup>63</sup> further confirmed viability of the generalized Sarkar observers but refined the fundamental set to eight candidates using more metameric classification stimuli. Figure 38 summarizes the final CMFs which were again each produced via transformation of cone functions using a single optimized LMS-to-XYZ matrix for all candidates. As in the CIE 2006 CMFs, these sets do not achieve area-normalized behavior and so do not all possess equal tristimulus values under the equal energy illuminant as is a constraint of the 1931 standard observer. An observer calibrator apparatus was also constructed with narrow-band LED test primaries to classify any real observer into one of the fundamental CMF categories<sup>75</sup>.

Alfvin and Fairchild<sup>69</sup> as well as Fairchild and Heckaman<sup>76</sup> have utilized Monte Carlo models to generate color matching functions for likely observers based on real quantified anatomical variability in spectral lens transmission, macula density and  $\bar{l}_\lambda$ ,  $\bar{m}_\lambda$  and  $\bar{s}_\lambda$  cone sensitivities. In the Heckaman examples, age-dependent transmission characteristics of the crystalline lens as described by Pokorny, et al.<sup>77,78</sup> and Xu, et al.<sup>79</sup> are taken and used to randomly generate transmission characteristics against US census data. Next, the macula density function described by Bone, et al.<sup>80</sup> is similarly normally varied in peak density to conform to standard deviation values suggested by Berendschott and van Norren<sup>81</sup>. Finally, the cone fundamentals of Stockman, et al.<sup>82,83</sup> are varied according to genetic models suggested by Neitz and Neitz<sup>84</sup> and selections of cone response with distributions in L- and M-type peak absorptions are made comprising the final modeled physiology. A heuristic Monte Carlo collection of 1,000 fictitious observers

is generated and made available to compute probable distributions of observer variability and metamerism for real colorimetric match scenarios. Heckaman has generated CMFs via this method using a single LMS-to-XYZ matrix from peak-normalized cone fundamentals to center responses against the 2° 1931 observer or alternatively using a second matrix to center all CMFs about the 10° 1964 observer (neither approach yielding area-normalized, all-positive curves for each observer). The 2° set of 1,000 CMFs considered in the present work are shown in Figure 39.

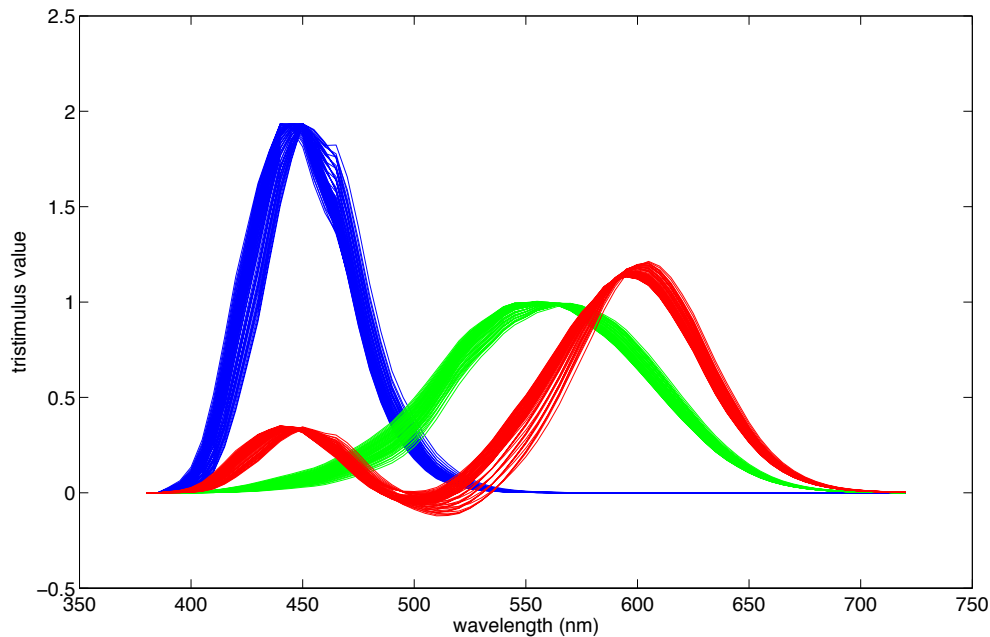


Figure 37. CIE 2006 color matching functions for observers ranging from 20 to 80 years of age and across 1° to 10° field of view

While none of these techniques is able to characterize precise color matching functions of any single actual observer, they each present an extent of response potentials useful in analyzing metameric failures in reproduced imagery on displays. Or, in the case of Sarkar and Fedutina, they offer potential for compartmentalizing real observers into broader populations of reasonably similar color sensitivity, permitting discrete display customization in color critical applications. An example would be observer-dependent calibration of electronic displays for mixed-media color comparators used in print publishing.

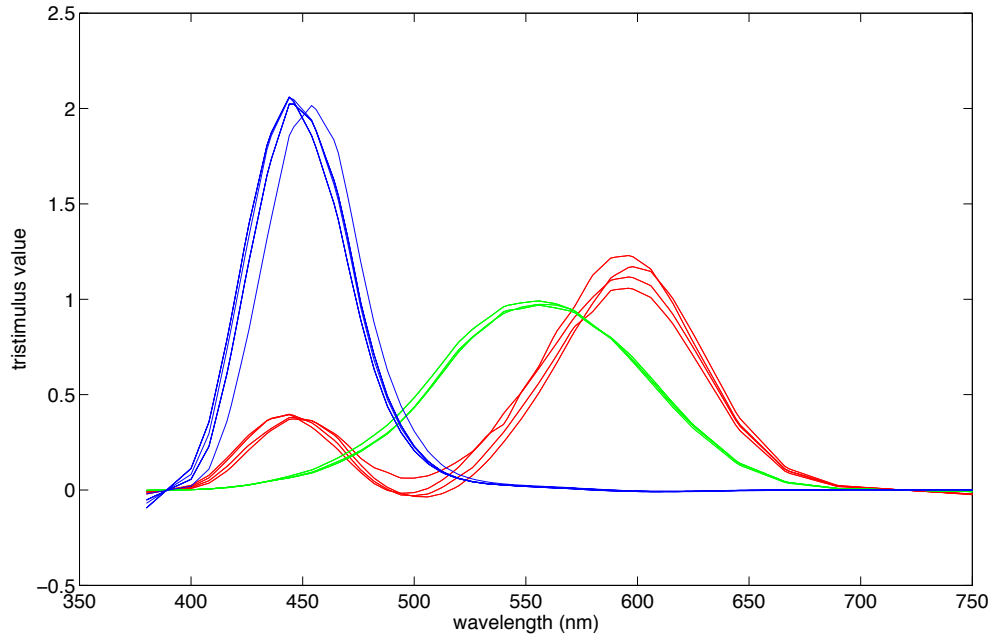


Figure 38. Sarkar/Fedutina color matching functions

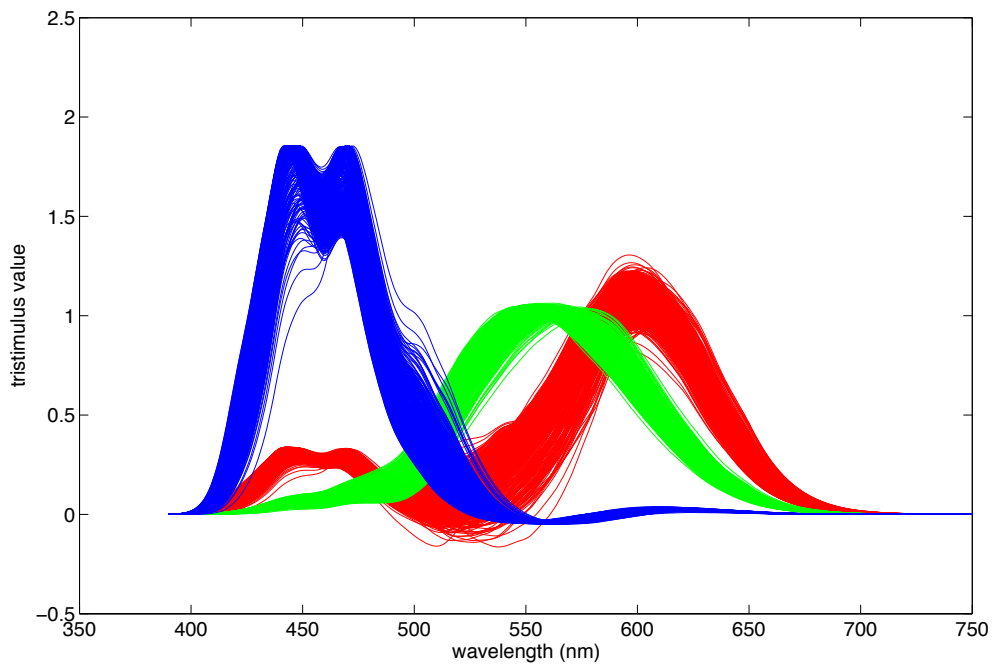


Figure 39. Fairchild and Heckaman 2° color matching functions

Another example pertinent to motion picture workflows would be display calibration for mastering color-corrected content across multiple distribution platforms (film, ITU-R Rec. 709 HDTV displays, SMPTE-431 digital cinema projectors, ITU-R Rec. 2020 monochromatic primary displays, etc.). What is most important in considering future digital color management paradigms is that advanced display technologies will necessarily challenge the utility of a single standard observer model to represent best practice color mastering. Creative professionals with one particular color response function may be generating aesthetic choices interpreted in very different ways by a full population of observers viewing content on narrow-spectra wide-gamut color displays.

### **Observer Metamerism Indices**

Quantifying observer metamerism for critical analysis demands attention to two different attributes of disparate CMF populations, color mismatch magnitude and observer variability. The former addresses traditional issues of color calibration where a device is tuned to deliver a color response against aim as defined by standard colorimetry employing intentionally chosen CMFs. The CIE has published three color difference formulae used widely in contemporary color industries,  $\Delta E_{ab}$ ,  $\Delta E_{94}$  and  $\Delta E_{00}$ , which are each derived from the 1976 CIELAB color space. The 1994 and 2000 permutations address failures of perceptual uniformity in CIELAB and the Euclidean  $\Delta E_{ab}$  vector length calculation. Still, the premise of the CIELAB space and its validity as base index for metamerism quantification remains sound. The CIELAB coordinate system acts as an elementary color appearance space, defined in orthogonal axes of lightness perception, approximate red-green hue/chroma perception and approximate blue-yellow hue/chroma. The  $a^*b^*$  plane can be further considered a circular coordinate system with appearance attribute hue represented as angle and chroma as distance from origin. Accepted appearance phenomena represented in the CIELAB encoding include a CMF-relevant chromatic adaptation, a reference white lightness adaptation and exponential radiometric scaling associated with visual perception uniformity. CIELAB itself is derived via input of XYZ tristimulus coordinates. By varying the CMF chosen to compute XYZ, CIELAB can serve as a reasonable appearance model for a specific theoretical observer and thus color difference indices calculated can be presumed appearance-relevant for that same observer. This practice is common, for example, in interchanging the 1931 and 1964 standard observers into CIELAB calculations as warranted by different applications. Ohsawa, et al.<sup>59</sup> have inferred such interchange is useful for interrogating observer statistics in cases where field size isn't even a practical factor. The models of CIE 2006, Sarkar/Fedutina and Heckaman all

support general demographic analyses with their observer CMFs. In evaluating distributions amongst observer CMFs within a population, this tactic becomes critical for providing a uniform translation of color error when spectral responsivity is intentionally varied.

Turning to observer variability, gross observer response inconsistencies are less an issue of absolute magnitude of color difference percept and more an issue of the variance of color differences experienced by a group of defined observers. The two are de-coupled in the example where overall color difference from reference for each of a set of disparate observers is large but the shared experience amongst the observers relative to one another is similar. The opposite scenario is also possible though to a lesser significance where each observer may experience a small perception of color difference from reference but the population of observers perceive significantly different experience in hue, chroma or lightness error from one another. Several indices of observer response variability can be described by treating color difference not as a directionless quantity in CIELAB coordinates but by instead breaking error vectors into their constituent axial components in the three-dimensional space. Using  $\Delta L^*$ ,  $\Delta a^*$  and  $\Delta b^*$  designations (where the origin of the color space represents a perfect colorimetric match) permits the creation of an error ellipsoid in CIELAB whose volume is proportional to the magnitude of observer variability in assessing a test and reference stimuli. Again, each observer contributes unique CMF in computing the full set of  $\Delta L^*a^*b^*$  vectors, but the magnitude and direction of error from reference are deemed relatable by treatment of CIELAB as a uniform color appearance space for small magnitude differences.

In the present research, the following indices are used to quantify observer metamerism magnitude and variability. Stimuli pairs may derive from any established reference spectrum and a corresponding reproduction spectrum.

$$OM_x = \max(\overline{\Delta E_{y,P,i}}) \quad (50)$$

$$OM_{x,max} = \max(\Delta E_{y,P,i}) \quad (51)$$

where  $OM_x$  refers to observer metamerism magnitude based on CMF sets from  $x =$  Sarkar/Fedutina (S), CIE 2006/TC1-36 (C) or Heckaman (H). Color difference values between a reference stimuli and test sample are computed for  $y = \Delta E_{ab}$  (ab),  $\Delta E_{94}$  (94) or  $\Delta E_{00}$  (00) for each patch in a patchset, P, for each observer, i, in the CMF set. The observer metamerism magnitude is the maximum individual observer average patchset color difference across all the patches in P. In this manner, the

observer metamerism represents the on-average poorest color matching observer from the population of CMFs for the patchset. A slight variation of this index,  $OM_{x,max}$  is based on measurement of the worst color difference patch across all observers in the given CMF set. This is thus the worst color match achieved across a full set of stimuli in the patchset considering all candidate observers. To minimize either of these indices suggests a move towards improving the color match between two stimuli for all observers in a population and thus a minimization of observer metamerism magnitude.

Observer variability indices are summarized by Equations 52 and 53.

$$OM_{x,var} = \overline{Vol(\Delta(L^*a^*b^*)_P)} \quad (52)$$

$$OM_{x,varmax} = \max(Vol(\Delta(L^*a^*b^*)_P)) \quad (53)$$

where  $OM_{x,var}$  refers to observer metamerism variability, the mean CIELAB ellipsoid volume constructed from CMF-based error vectors in  $L^*$ ,  $a^*$  and  $b^*$  from each patch in a patchset  $P$ . The index is again dependent on the CMF set chosen as above. For the present work, covariance analysis is used to construct the ellipsoid volumes from individual observer CIELAB error vectors with a 90% statistical significance.  $OM_{x,varmax}$  is the maximum ellipsoid volume from all patches in the patchset and is thus the particular stimuli pair with the broadest observer variability.

These observer metamerism and variability indices provide a complement to the approach of Fairchild, et al. introduced in Chapter 5 during assessment of the proof-of-concept multiprimary display<sup>8</sup>. As a review of that method, primary drive amounts needed to enforce a metameric match between aim spectra and the generated reproduction on the tested display are calculated using a chosen CIE 2006 color matching function at a given age and field-of-view. Once matched for that particular observer, the resultant modeled spectra of each system are assessed for subsequent colorimetric match assuming the 1931 2° standard CMF as observer and resulting color difference values are tallied. This methodology maintains benefits of using a single CMF color space for all determined color difference indices and also allows RGB color rendering of differences for visualization. The method, however, does not permit summary of the color difference experienced by any particular disparate observer within the context of their own CMF and so the previous indices summarized are preferred in the subsequent analyses.

Other traditional indices of color difference for a pair of stimuli invoke methods summarized in Chapter 3, including objective assessment of the spectroradiometric power distribution of the samples. As spectral signatures for the compared colors become more similar, all attributes of perceived color difference, regardless of observer CMF, will shrink to zero. Two spectra may be compared by assessing the root mean square of spectral differences (RMS Error) across a defined range of wavelengths or by assessing the maximum spectral error at any wavelength between the two samples. Many researchers prefer the latter because it is plausible for the RMSE to be small while a single wavelength may experience a large and consequential error but the opposite is seldom true. In the present research, all errors are scaled as fraction of the reference stimuli maximum radiometric power prior to the RMSE or maximum error computation. This permits analysis in relative spectral power output for comparing significance amongst stimuli of variable absolute spectral power. It also permits comparison of spectra in a more perceptually uniform context.

Finally, any stimuli pair may also be compared by accepted color difference formulae for a standard observer. The present research utilizes the 1931 standard observer, common to imaging system color evaluations. As appropriate,  $\Delta E_{ab}$ ,  $\Delta E_{94}$  or  $\Delta E_{00}$  are considered.

The various indices previously defined offer candidate response treatments for quantifying color error and color response variability amongst a group of observers interacting with colors reproduced on different additive electronic displays. However, such an analysis requires a sensible color reproduction objective for each evaluated display to be defined. In the present research, cross-media metamerism is evaluated by forcing a best match of spectral or colorimetric display output to a series of conventionally illuminated reflective test patch aims. The patch sets considered include:

- 1) MacBeth Color Checker (24 samples)
- 2) MacBeth Color Checker DC (240 samples)
- 3) US Patent No. 5,582,961 “Kodak/AMPAS” test spectra (190 samples)
- 4) Munsell sample spectra (1269 samples)
- 5) select high metamerism color set (65 samples)

Luminous spectral stimuli are produced via model of these patch sets under CIE D65, CIE Illuminant A, a measured hydrargyrum medium-arc iodide (HMI) motion picture studio lamp and CIE fluorescent illuminant F2. Though comparison of different displays in metameric match to one another is common practice in motion picture workflows, an analysis encompassing metameric match to real surface colors offers broader interpretation of experiment results. Specifically, color and spectra-matching of real scene stimuli on the display screen bridges the workflow between image acquisition and reproduction, setting expectation for exhibition color reproduction control that exceeds current trichromatic convention and permits evolution to future spectral color correction models.

### **Observer Metamerism Simulations**

To simulate observer metamerism in additive displays, six different systems were chosen and their primary spectra collected:

- 1) Sony 14L2 PVM-class professional CRT
- 2) NEC3000 3-DLP SMPTE-431 professional digital cinema projector
- 3) Panasonic PTAX200U 3-LCD SMPTE-431 HDTV consumer projector
- 4) Prototype ITU-R Rec. 2020-compatible laser cinema projector
- 5) chromaticity-gamut-optimized eight-primary laser projector
- 6) metamerism-optimized seven-channel projector

The  $u'v'$  chromaticity-space gamut of each display is shown in Figures 40-45 along with normalized plots of measured spectra for each of the system color channels. Also included for gamut perspective are the chromaticity coordinates of the Kodak/AMPAS color patch set illuminated by CIE D65 and the boundaries of standard display gamuts defined by ITU-R Rec. 709 and Rec. 2020 and SMPTE-431's Digital Cinema P3 gamut. Figure 46 further contrasts the scene gamut occupied by the Kodak/AMPAS target stimuli under all four tested illumination sources and Figure 47 shows the gamuts of the other patchsets illuminated by D65. Systems 1-3 were chosen as representative of current motion picture industry three-channel primary standards, including current HDTV video and current digital cinema exhibition. Systems 2 and 3 are particularly interesting as they offer different spectral interpretations of the same chromaticity display standard. ITU-R Rec. 2020 represents a next-generation laser display standard with wavelengths of 467, 532 and 630nm. The gamut optimized laser projector was modeled based on

maximizing the polygon area of the display's u'v' chromaticity gamut versus the CIE spectral locus, using eight channels. Wavelengths thus determined were 395, 485, 505, 520, 540, 610, 650 and 700nm. Chromaticity-plane color gamut is often touted in professional electronic display marketing materials and so this hypothetical multiprimary system with absolute maximum performance was conceived for comparison to the actual display systems. The metamerism-optimized display represents the color characteristics of a seven-projector prototype multi-primary display built at RIT to confirm associated models of observer variability. This display was designed explicitly to generate a reduced observer metamerism according to Sarkar/Fedutina CMF models and to further the prior work of Koenig et al.<sup>58</sup> It's design follows from learning gained subsequent to the construction of Chapter 5's proof-of-concept two-projector system and summary of it's explicit engineering can be found in Chapter 7.

For initial assessment, the chosen displays were color managed to match the various reference stimuli under the various illuminants according to 1931 standard observer color difference indices. Because systems 5 and 6 are over-specified in this objective (owing to eight and seven adjustable primaries, respectively), these displays were co-optimized to constrain an exact metameric match to the stimuli as determined by the 1931 standard CMF set while subsequently minimizing  $OM_x$ . This optimization was not run for the 1269 Munsell color patches owing to extreme calculation times in the simulations. For some color patches on these two displays, color stimuli were outside the reproducible gamut of the device and so observer metamerism minimization alone was employed. For similar out-of-gamut failures on the three-channel displays, a minimization of the 1931 standard observer color difference was used rather than an observer metamerism optimization so as to faithfully maintain original color management intent for an RGB system. A summary of observer metamerism indices for each display modeled to reproduce the color of each candidate patchset under each illuminant is presented in Tables 5-8. In each of these assessments, the Sarkar/Fedutina CMF set is used to generate the computed metamerism index values. A maximum 1931 2° color difference ( $\Delta E_{00}$ ) of 0.0 for a given patchset in these tables is evidence that all patches were within the given display's gamut and rendered colorimetrically perfect to the standard observer according to the simulation intent employed. Again, where these color difference maxima are greater than 0.0, not all patches within the set were in gamut and an alternate optimization was executed for those patches.

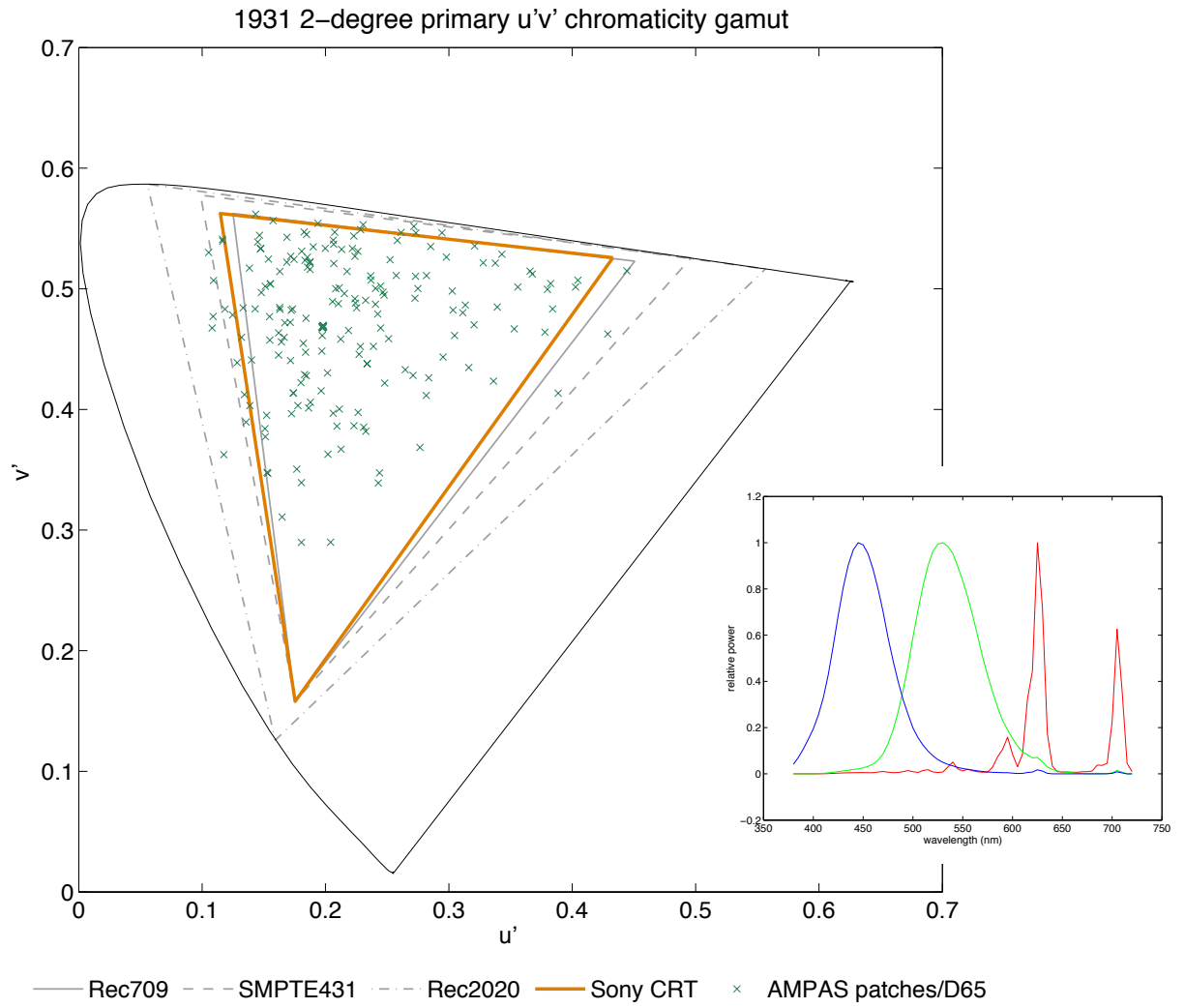


Figure 40. Sony PVM 14L2 CRT chromaticity gamut and peak-normalized primary spectra; color points representing Kodak/AMPAS color patches illuminated by CIE D65 also included

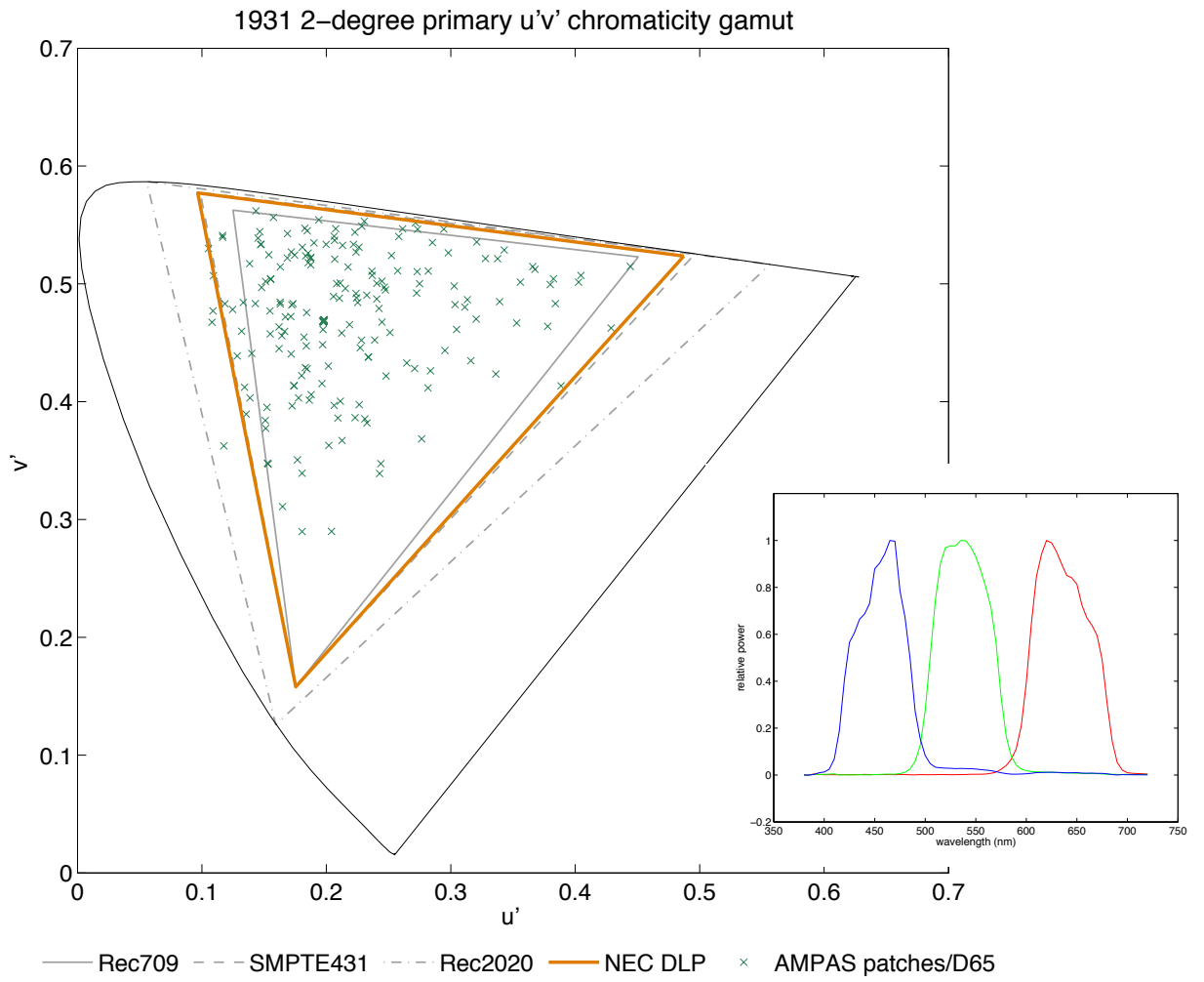


Figure 41. NEC 3000 digital cinema projector chromaticity gamut and peak-normalized primary spectra; color points representing Kodak/AMPAS color patches illuminated by CIE D65 also included

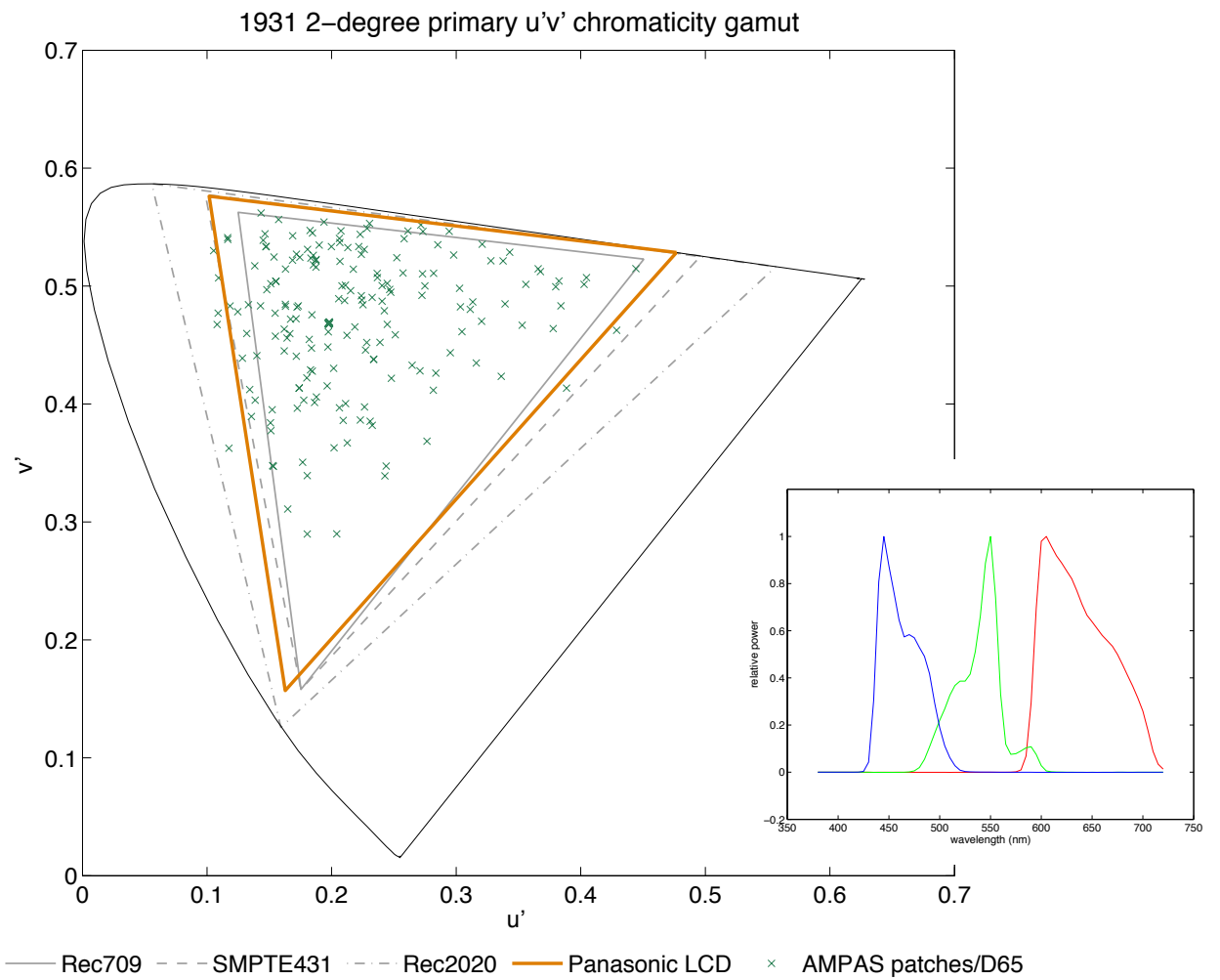


Figure 42. Panasonic PTAX200U LCD cinema projector chromaticity gamut and peak-normalized primary spectra; color points representing Kodak/AMPAS color patches illuminated by CIE D65 also included

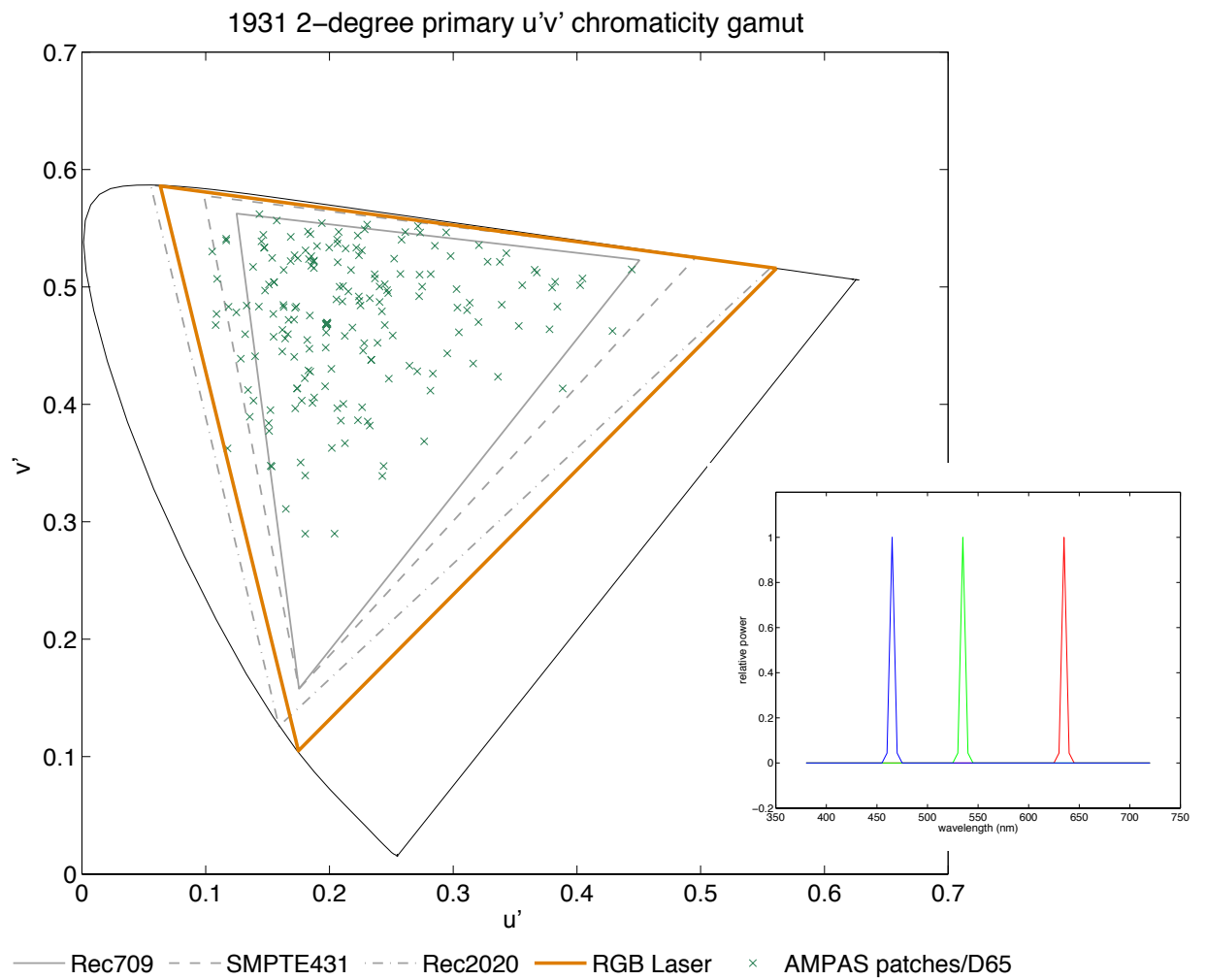


Figure 43. Example ITU-R Rec. 2020 RGB laser projector chromaticity gamut and peak-normalized primary spectra; color points representing Kodak/AMPAS color patches illuminated by CIE D65 also included

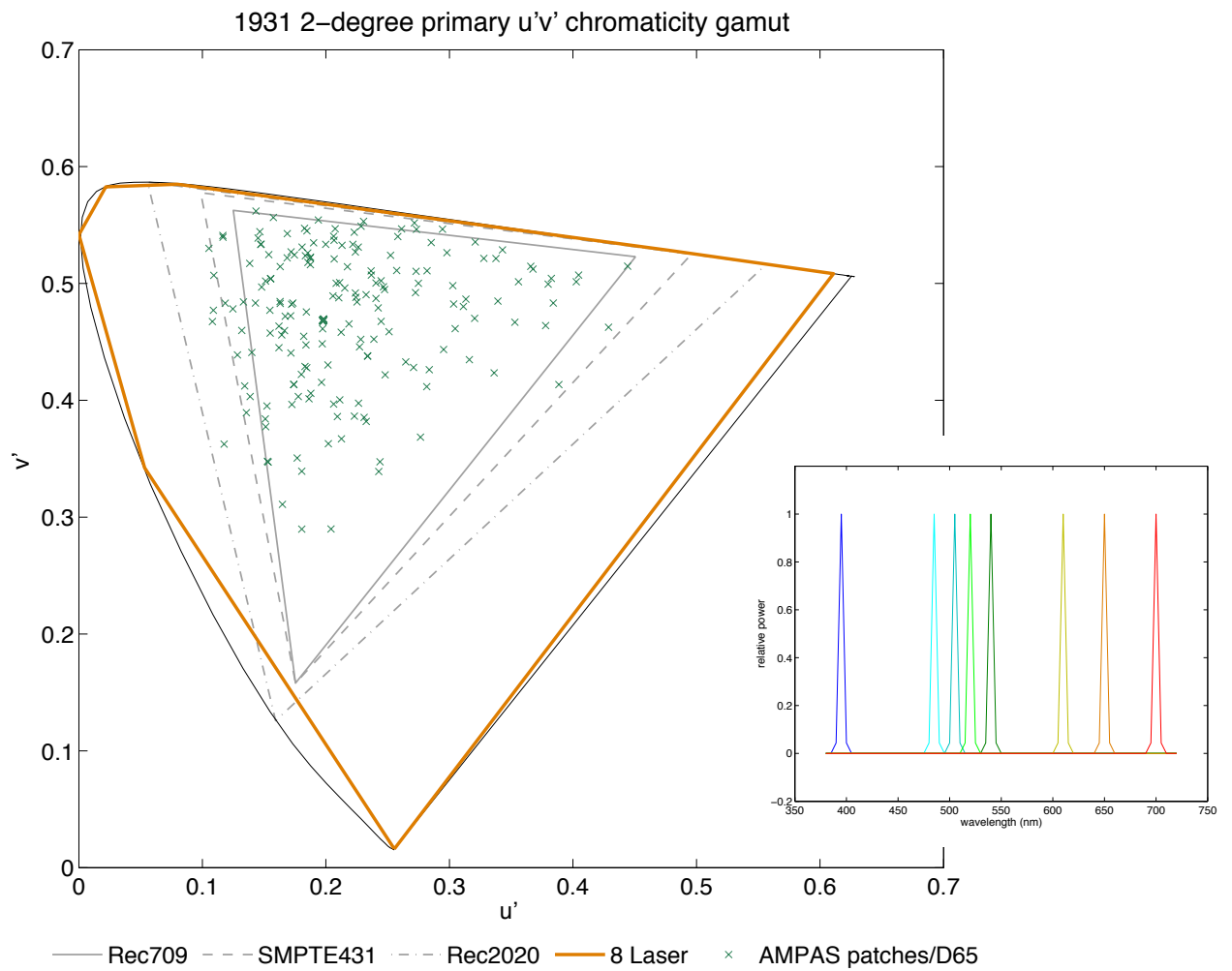


Figure 44. Maximized chromaticity area 8-primary laser projector chromaticity gamut and peak-normalized primary spectra; color points representing Kodak/AMPAS color patches illuminated by CIE D65 also included

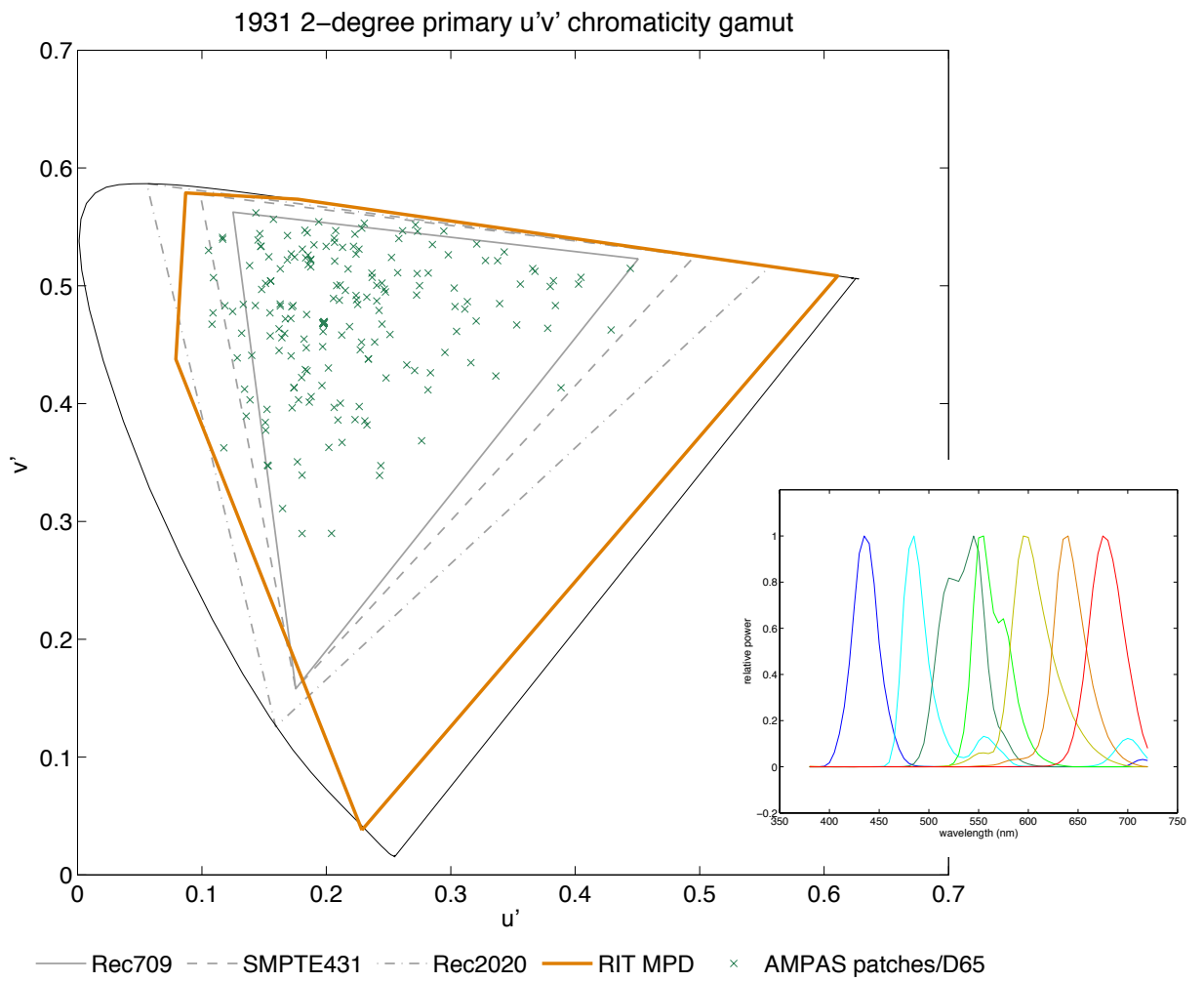


Figure 45. RIT seven-channel projector chromaticity gamut and peak-normalized primary spectra; color points representing Kodak/AMPAS color patches illuminated by CIE D65 also included

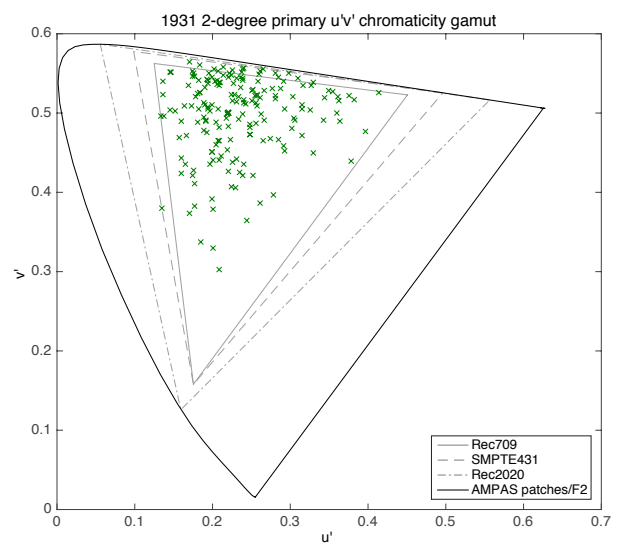
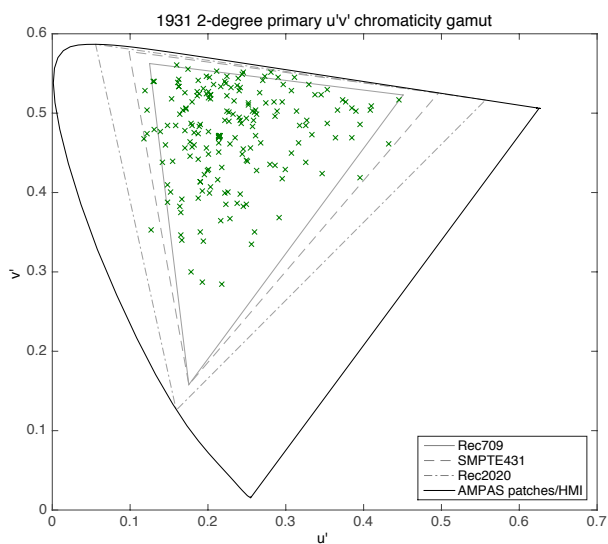
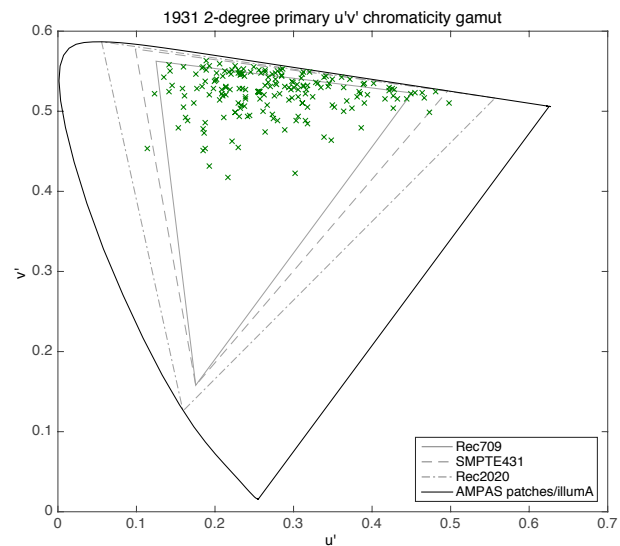
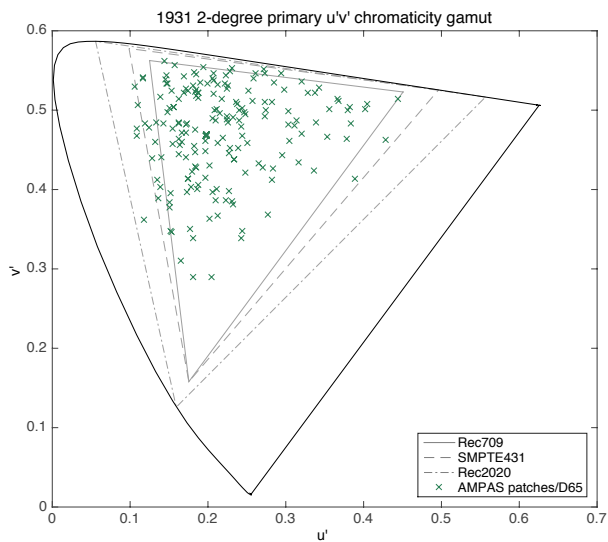


Figure 46.  $u'v'$  chromaticity gamut for Kodak/AMPAS color patch set illuminated by CIE D65 (upper left), CIE illuminant A (upper right), HMI studio light (lower left) and CIE illuminant F2 (lower right)

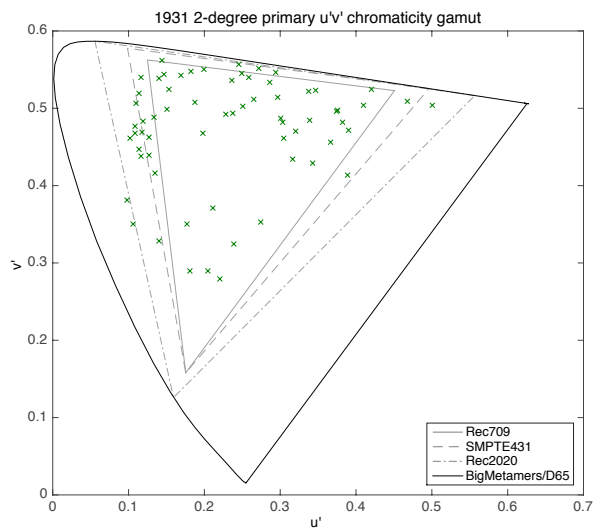
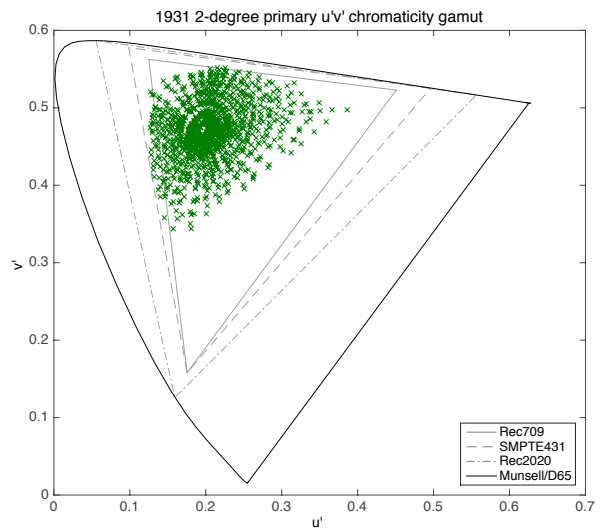
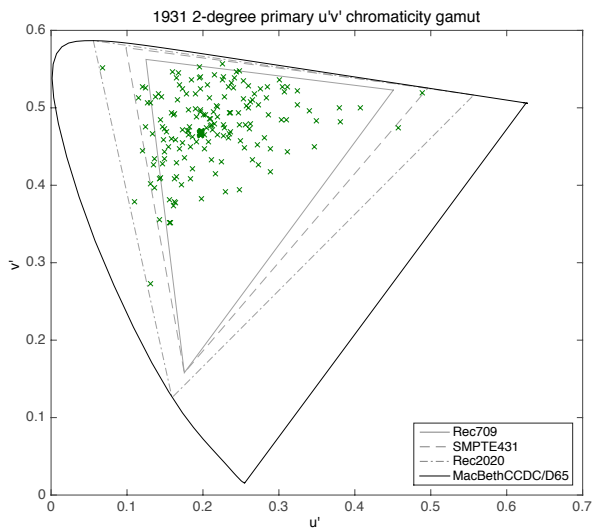
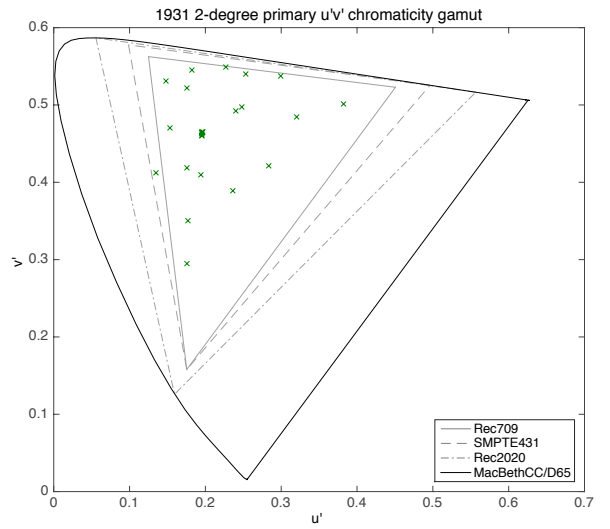
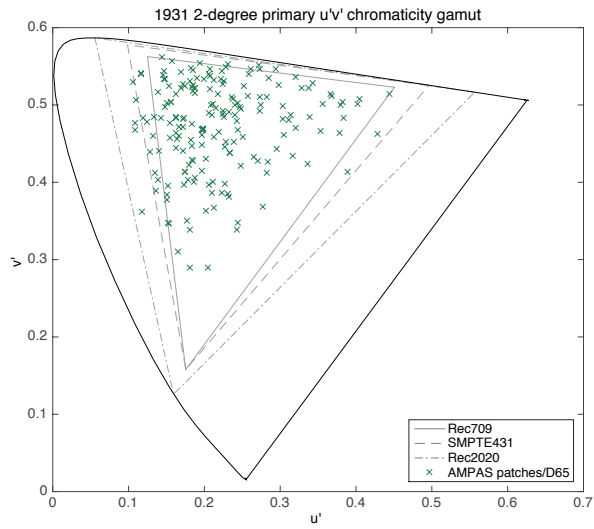


Figure 47. u'v' chromaticity gamut for all 5 tested color patch sets under CIE D65

An investigation of results for the D65-illuminated stimuli reveals very consistent performance across the five patchsets for the six modeled displays. In each case, metamerism magnitude,  $OM_s$  (based here on simple  $\Delta E_{ab}$ ), is best for the RIT multiprimary display and worst for the eight-laser system by a ratio of at least 10:1. The Rec. 709 CRT and SMPTE-431 DLP projectors represent the current display technologies used for cinema applications and so set the baseline for comparison to the other devices. In general, the professional grade digital cinema projector from NEC bests the consumer-grade Panasonic device (Figures 41 and 42 reveal how each delivers near exact SMPTE-431 chromaticity gamut with notably different primary spectra) and the CRT performs reasonably close to both. Each of these legacy systems though is deficient versus the RIT prototype by a factor of 2x to 3x. Models of the Rec. 2020 laser gamut projector yield a significant drop in color match versus the legacy equipment, though the performance is still not as poor as the eight-laser system. Diving deeper into the maximum color error amongst the eight Sarkar/Fedutina observers and amongst all the patches in each set,  $OM_{s,max}$ , very similar trends in both rank order and magnitude of performance are noted, though the consumer SMPTE-431 projector does fare better relative to the professional system than it did for average observer metamerism. The most telling trend for these results is the poor performance achieved by increasingly monochromatic primary sets. As such, enlarged chromaticity-area gamut is traded in these systems for a reduced observer metamerism.

Observer set variability, as modeled by color error ellipsoid volumes tracks well with the trends in overall color difference magnitude. Again, the RIT MPD performs best and the eight-laser system worst. The variability index also proves much more sensitive to display change as there are roughly seven orders of magnitude in mean metamerism variability and maximum metamerism variability between the two. The CRT and DLP displays perform two orders of magnitude poorer than the RIT display and the Rec. 2020 laser drops another two orders of magnitude from there. Figure 48(a-f) shows the CIELAB error ellipsoids for the 24 MacBeth Color Checker patches illuminated by D65 for each of the simulated displays. Plots are presented with common scaling of axes to permit proper examination of the comparative variability. An interesting attribute of these figures is the lack of symmetry about the  $\Delta L^*a^*b^*$  origin; metameric matches generated for the 1931 2° observer yield hue, saturation and lightness bias for the Sarkar/Fedutina observers. Replicate ellipsoid volume plots for other patchsets and illuminants are not included as they scale well with the tabulated observer variability indices and generally yield the same conclusions as those shown for the D65 MacBeth series.

Table 5: Sarkar/Fedutina observer metamerism indices for various displays relative to test patch sets illuminated by CIE D65 (1931 2° colorimetry match)

<u>CIE D65</u>	$OM_s$	$OM_{s,max}$	$OM_{s,var}$	$OM_{s,varmax}$	mean RMSE	mean peak err	max $\Delta E_{00}(31)$
<b><u>AMPAS190</u></b>							
Sony CRT	2.77	17.13	4.6E-03	1.8E-01	0.44	1.92	6.43
NEC DLP	2.48	14.40	1.8E-03	1.3E-01	0.25	0.55	4.83
Panasonic DLP	2.71	10.20	2.4E-03	5.3E-02	0.27	0.77	3.35
Rec2020 Laser	5.50	11.47	3.8E-01	4.7E+00	2.07	9.41	0.00
8-laser	10.78	26.83	2.5E+02	1.9E+03	1.95	10.22	0.00
RIT MPD	0.79	6.35	1.0E-05	3.6E-04	0.28	0.63	0.00
<b><u>MacBeth24</u></b>							
Sony CRT	2.15	8.77	2.6E-03	4.7E-02	0.44	1.95	0.44
NEC DLP	1.83	8.52	2.8E-04	2.7E-03	0.25	0.52	0.00
Panasonic DLP	2.49	5.20	1.0E-03	5.5E-03	0.27	0.76	0.00
Rec2020 Laser	5.50	10.44	2.6E-01	1.3E+00	2.18	9.66	0.00
8-laser	11.61	27.31	3.1E+02	2.0E+03	2.08	11.01	0.00
RIT MPD	0.78	2.43	6.2E-06	7.5E-05	0.31	0.66	0.00
<b><u>MacBeth DC</u></b>							
Sony CRT	2.55	32.39	2.6E-02	2.4E+00	0.49	2.15	14.64
NEC DLP	2.28	25.36	8.2E-03	6.4E-01	0.30	0.60	11.21
Panasonic DLP	2.60	25.00	1.6E-03	1.3E-01	0.31	0.88	11.32
Rec2020 Laser	5.57	14.38	4.0E-01	2.7E+00	2.41	10.21	1.66
8-laser	11.53	27.89	2.8E+02	1.2E+03	2.35	12.34	0.00
RIT MPD	0.81	9.77	3.5E-04	8.1E-02	0.38	0.77	7.39
<b><u>Big Metamers</u></b>							
Sony CRT	5.57	24.47	5.1E-02	1.1E+00	0.40	1.65	8.60
NEC DLP	4.69	21.71	1.8E-02	2.2E-01	0.23	0.53	7.18
Panasonic DLP	4.26	16.83	8.3E-03	2.6E-01	0.25	0.71	5.90
Rec2020 Laser	5.38	16.02	3.3E-01	2.8E+00	1.57	7.40	2.22
8-laser	8.21	26.83	1.2E+02	1.9E+03	1.46	7.57	0.00
RIT MPD	0.71	2.84	1.7E-05	3.7E-04	0.20	0.51	2.91
<b><u>Munsell</u></b>							
Sony CRT	1.95	11.10	2.3E-03	1.8E-01	0.49	2.19	1.22
NEC DLP	1.94	10.61	8.5E-04	7.1E-02	0.30	0.62	0.00
Panasonic DLP	2.43	8.36	9.5E-04	1.2E-02	0.32	0.87	0.00
Rec2020 Laser	5.60	10.87	3.2E-01	2.6E+00	2.47	10.49	0.00
8-laser	--	--	--	--	--	--	--
RIT MPD	--	--	--	--	--	--	--

Table 6: Sarkar/Fedutina observer metamerism indices for various displays relative to test patch sets illuminated by CIE Illuminant A (1931 2° colorimetry match)

<u>CIE IllumA</u>	$OM_s$	$OM_{s,max}$	$OM_{s,var}$	$OM_{s,varmax}$	mean RMSE	mean peak err	max $\Delta E_{00}(31)$
<b><u>AMPAS190</u></b>							
Sony CRT	4.35	42.56	4.3E-03	1.7E-01	0.58	2.62	17.97
NEC DLP	2.37	9.64	1.6E-03	6.2E-02	0.25	0.55	5.50
Panasonic DLP	2.20	8.48	2.3E-03	2.2E-01	0.27	0.70	4.18
Rec2020 Laser	5.38	12.63	1.9E-01	1.5E+00	1.77	7.79	0.00
8-laser	5.48	12.10	7.0E+00	1.1E+02	1.58	7.70	0.00
RIT MPD	0.46	1.81	4.8E-07	4.1E-05	0.21	0.49	0.00
<b><u>MacBeth24</u></b>							
Sony CRT	4.67	25.96	3.1E-03	2.1E-02	0.62	2.81	11.20
NEC DLP	2.28	7.12	8.5E-04	9.5E-03	0.26	0.54	0.00
Panasonic DLP	2.07	6.44	4.8E-04	6.2E-03	0.27	0.67	0.00
Rec2020 Laser	5.45	9.62	1.9E-01	1.5E+00	1.85	7.88	0.00
8-laser	6.01	12.12	8.9E+00	5.3E+01	1.68	8.01	0.00
RIT MPD	0.45	1.88	4.4E-06	1.0E-04	0.22	0.51	0.00
<b><u>MacBeth DC</u></b>							
Sony CRT	3.70	41.37	1.1E-02	1.2E+00	0.62	2.83	17.46
NEC DLP	2.48	12.28	5.4E-03	4.8E-01	0.28	0.58	4.84
Panasonic DLP	2.14	11.40	2.2E-03	1.2E-01	0.29	0.70	6.32
Rec2020 Laser	5.48	10.98	3.6E-01	2.2E+00	1.93	8.12	0.00
8-laser	5.89	11.40	5.6E+00	6.7E+01	1.70	7.78	0.00
RIT MPD	0.37	2.77	8.7E-07	1.6E-04	0.21	0.49	2.08
<b><u>Big Metamers</u></b>							
Sony CRT	7.89	44.91	3.2E-02	7.3E-01	0.49	2.11	17.97
NEC DLP	3.87	17.98	1.7E-02	4.2E-01	0.22	0.54	6.27
Panasonic DLP	3.57	15.49	1.3E-02	3.9E-01	0.25	0.73	6.08
Rec2020 Laser	4.87	12.63	9.6E-02	1.5E+00	1.39	6.57	1.30
8-laser	4.16	12.10	2.9E+00	6.0E+01	1.33	6.79	0.00
RIT MPD	0.69	9.03	1.0E-03	6.4E-02	0.17	0.45	0.00
<b><u>Munsell</u></b>							
Sony CRT	3.00	28.53	1.8E-03	1.0E-01	0.64	2.92	11.91
NEC DLP	2.25	8.28	5.7E-04	3.3E-02	0.29	0.59	0.65
Panasonic DLP	1.93	8.61	2.8E-04	2.0E-02	0.29	0.70	0.00
Rec2020 Laser	5.44	9.92	2.6E-01	1.8E+00	1.99	8.32	0.00
8-laser	--	--	--	--	--	--	--
RIT MPD	--	--	--	--	--	--	--

Table 7: Sarkar/Fedutina observer metamerism indices for various displays relative to test patch sets illuminated by HMI motion picture studio light (1931 2° colorimetry match)

<u>HMI</u>	$OM_s$	$OM_{s,max}$	$OM_{s,var}$	$OM_{s,varmax}$	mean RMSE	mean peak err	max $\Delta E_{00}(31)$
<b><u>AMPAS190</u></b>							
Sony CRT	3.10	14.81	5.8E-03	2.2E-01	0.42	1.79	6.76
NEC DLP	2.83	9.53	7.8E-03	1.1E-01	0.25	0.54	2.75
Panasonic DLP	3.70	9.01	3.7E-02	6.1E-01	0.25	0.67	2.06
Rec2020 Laser	6.46	11.93	1.6E+00	1.5E+01	1.77	7.92	0.00
8-laser	11.04	26.01	2.9E+02	1.8E+03	1.59	8.34	0.00
RIT MPD	0.33	2.21	1.5E-07	4.4E-06	0.18	0.45	0.00
<b><u>MacBeth24</u></b>							
Sony CRT	2.82	7.25	4.7E-03	3.5E-02	0.42	1.82	0.33
NEC DLP	2.68	5.87	4.6E-03	2.1E-02	0.26	0.55	0.00
Panasonic DLP	3.74	7.33	3.1E-02	1.9E-01	0.25	0.67	0.00
Rec2020 Laser	6.62	10.65	1.5E+00	1.0E+01	1.86	8.13	0.00
8-laser	11.92	25.91	3.4E+02	1.9E+03	1.69	8.99	0.00
RIT MPD	0.32	1.19	4.6E-08	6.9E-07	0.17	0.44	0.00
<b><u>MacBeth DC</u></b>							
Sony CRT	3.35	24.19	8.4E-03	5.4E-01	0.45	1.92	11.25
NEC DLP	2.92	18.53	7.2E-03	7.3E-02	0.28	0.59	8.02
Panasonic DLP	3.72	18.09	2.2E-02	1.5E-01	0.27	0.71	8.07
Rec2020 Laser	6.58	12.96	2.1E+00	1.1E+01	1.92	7.90	0.00
8-laser	11.78	25.25	3.3E+02	1.6E+03	1.75	9.02	0.00
RIT MPD	0.36	5.43	9.5E-05	2.2E-02	0.18	0.46	4.03
<b><u>Big Metamers</u></b>							
Sony CRT	4.59	19.08	2.1E-02	3.4E-01	0.39	1.56	8.33
NEC DLP	4.01	16.29	1.4E-02	2.9E-01	0.22	0.53	5.47
Panasonic DLP	3.94	12.79	5.0E-02	1.8E+00	0.23	0.65	4.15
Rec2020 Laser	5.76	13.96	8.3E-01	1.2E+01	1.45	6.84	1.03
8-laser	8.47	26.10	1.1E+02	1.8E+03	1.32	6.95	0.00
RIT MPD	0.41	1.86	3.2E-06	1.2E-04	0.17	0.48	2.51
<b><u>Munsell</u></b>							
Sony CRT	2.94	9.13	3.7E-03	1.7E-01	0.46	2.00	1.86
NEC DLP	2.68	7.76	6.3E-03	6.5E-02	0.30	0.61	0.00
Panasonic DLP	3.71	7.71	2.2E-02	2.3E-01	0.28	0.73	0.00
Rec2020 Laser	6.71	10.72	1.6E+00	9.9E+00	2.01	8.27	0.00
8-laser	--	--	--	--	--	--	--
RIT MPD	--	--	--	--	--	--	--

Table 8: Sarkar/Fedutina observer metamerism indices for various displays relative to test patch sets illuminated by CIE F2 fluorescent (1931 2° colorimetry match)

<u>F2</u>	$OM_s$	$OM_{s,max}$	$OM_{s,var}$	$OM_{s,varmax}$	mean RMSE	mean peak err	max $\Delta E_{00}(31)$
<b><u>AMPAS190</u></b>							
Sony CRT	5.61	26.90	1.0E-01	2.1E+00	0.49	2.15	11.47
NEC DLP	4.63	10.67	7.1E-02	4.9E-01	0.34	0.65	2.25
Panasonic DLP	5.13	9.83	1.7E-01	1.1E+00	0.29	0.71	1.66
Rec2020 Laser	7.63	13.04	4.5E+00	3.0E+01	1.76	7.71	0.00
8-laser	10.69	21.48	3.0E+02	2.3E+03	1.47	7.51	0.00
RIT MPD	0.21	0.93	9.9E-08	6.1E-06	0.13	0.36	0.00
<b><u>MacBeth24</u></b>							
Sony CRT	5.66	15.19	1.1E-01	8.0E-01	0.51	2.24	5.50
NEC DLP	4.90	8.79	6.6E-02	4.2E-01	0.35	0.68	0.00
Panasonic DLP	5.53	8.58	1.7E-01	1.1E+00	0.30	0.74	0.00
Rec2020 Laser	7.97	12.15	4.7E+00	3.6E+01	1.86	8.01	0.00
8-laser	11.47	21.05	3.2E+02	1.8E+03	1.57	7.95	0.00
RIT MPD	0.21	0.67	2.0E-07	4.6E-06	0.14	0.38	0.00
<b><u>MacBeth DC</u></b>							
Sony CRT	5.92	30.59	1.0E-01	2.3E+00	0.50	2.16	10.98
NEC DLP	4.91	11.05	9.5E-02	5.3E-01	0.36	0.69	2.90
Panasonic DLP	5.35	10.33	2.1E-01	1.1E+00	0.31	0.74	3.00
Rec2020 Laser	7.98	13.57	7.1E+00	3.9E+01	1.78	7.46	0.00
8-laser	11.11	20.26	4.0E+02	1.9E+03	1.46	7.00	0.00
RIT MPD	0.23	3.11	3.3E-06	7.7E-04	0.14	0.39	0.00
<b><u>Big Metamers</u></b>							
Sony CRT	5.12	31.75	1.7E-01	3.2E+00	0.45	1.93	12.61
NEC DLP	3.99	11.46	5.7E-02	7.5E-01	0.28	0.59	3.76
Panasonic DLP	3.95	10.70	1.1E-01	2.0E+00	0.25	0.67	3.35
Rec2020 Laser	6.02	14.12	1.4E+00	1.3E+01	1.60	7.53	0.00
8-laser	8.58	21.63	6.4E+01	6.9E+02	1.39	7.28	0.00
RIT MPD	0.31	4.96	5.6E-06	3.6E-04	0.14	0.37	0.00
<b><u>Munsell</u></b>							
Sony CRT	5.82	17.02	7.6E-02	1.5E+00	0.52	2.23	6.99
NEC DLP	4.96	10.36	7.5E-02	4.5E-01	0.37	0.71	0.00
Panasonic DLP	5.49	9.73	1.6E-01	9.7E-01	0.32	0.76	0.00
Rec2020 Laser	8.09	12.92	5.1E+00	3.1E+01	1.83	7.52	0.00
8-laser	--	--	--	--	--	--	--
RIT MPD	--	--	--	--	--	--	--

The most compelling conclusion from RMSE and maximum spectral error ratios generated here is that none of these systems do a particularly good job at matching reference stimuli spectrally. The strongest average patch match from the best display still yields an RMSE of 25% of maximum spectral output across all visible wavelengths. The laser displays, not surprisingly, are significantly worse as would be expected from attempted matches of continuous spectra with discrete monochromatic primaries. Still, the strong metamerism results achieved for some of these displays suggests absolute spectral match might be an unnecessary objective for observer consistency in abridged multispectral system optimization.

Finally, maximum  $\Delta E_{00}$  color matches for the 1931 2° observer show where not all of these displays are capable of rendering colorimetric matches for all of the patches in the stimuli set. The smaller gamut displays, CRT and DLP in particular, are consistently unable to produce exact matches according to traditional digital color management strategies.

Table 9 is an extension of Table 5 for D65-illuminated MacBeth patches and summarizes observer metamerism indices for the CIE 2006 and Heckaman CMF models. In general, the displays all perform in rank and relative magnitude similar to the Sarkar/Fedutina results though absolute numerical performance is worse for the CIE 2006 observers and then worse again for Heckaman's observers. As each represents an intentionally extreme array of potential observer response functions versus the Sarkar/Fedutina statistical CMF categories, these results are not surprising. Turning to observer variability ellipsoids, CIE 2006 actually predicts less disparity than Sarkar/Fedutina though Heckaman again represents exaggerated differences considering his full observer set. With these seemingly consistent indicators, what remains is to scale each model absolutely against real metamerism experiments in Chapter 8 to validate which correlates best with the degree of observer variability noted across a population of actual observers.

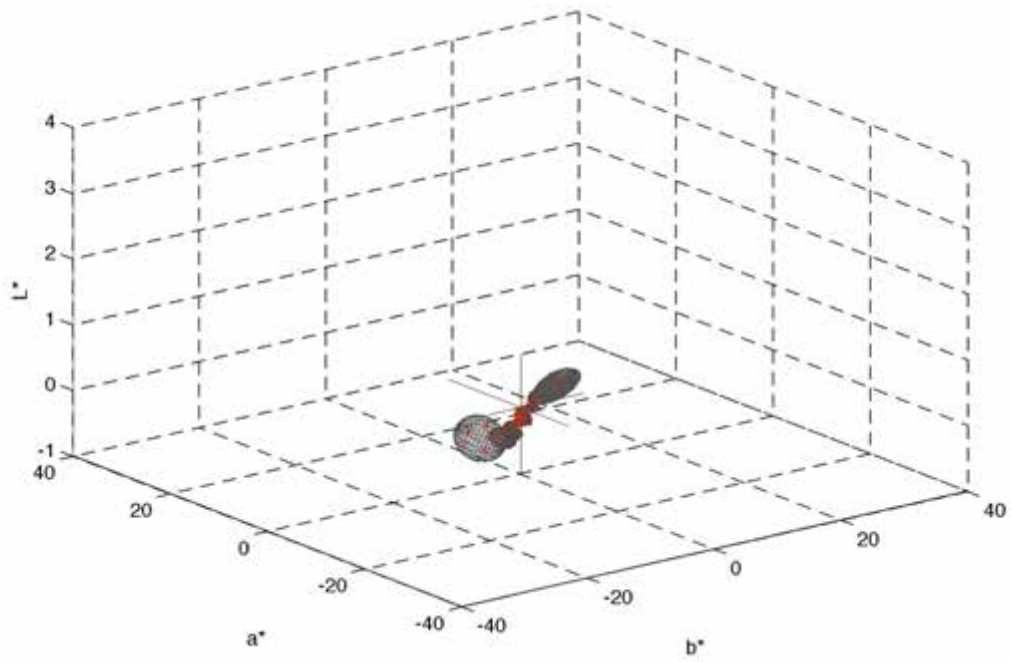


Figure 48(a): Sony CRT observer variability ellipsoids based on reproduced 1931 2° colorimetry match to MacBeth 24 patches illuminated by CIE D65

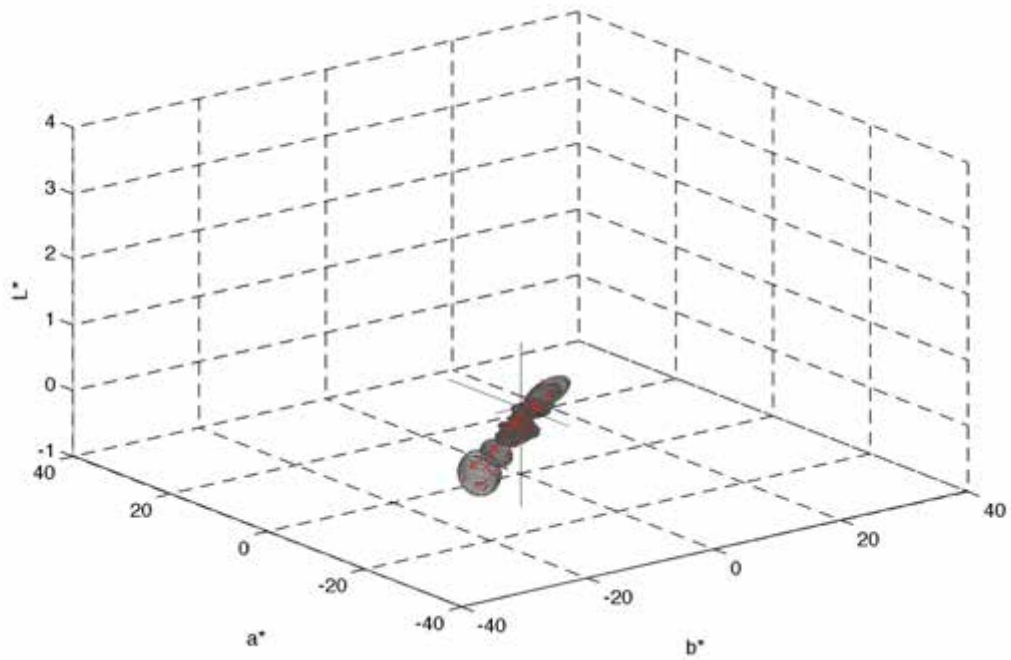


Figure 48(b): NEC DLP observer variability ellipsoids based on reproduced 1931 2° colorimetry match to MacBeth 24 patches illuminated by CIE D65

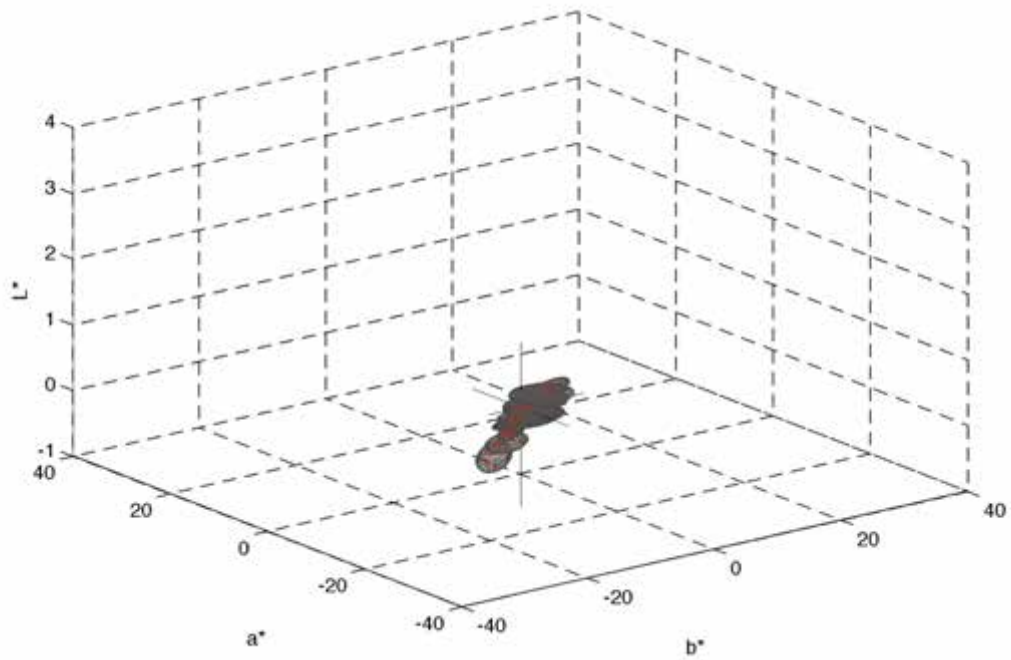


Figure 48(c): Panasonic DLP observer variability ellipsoids based on reproduced 1931 2° colorimetry match to MacBeth 24 patches illuminated by CIE D65

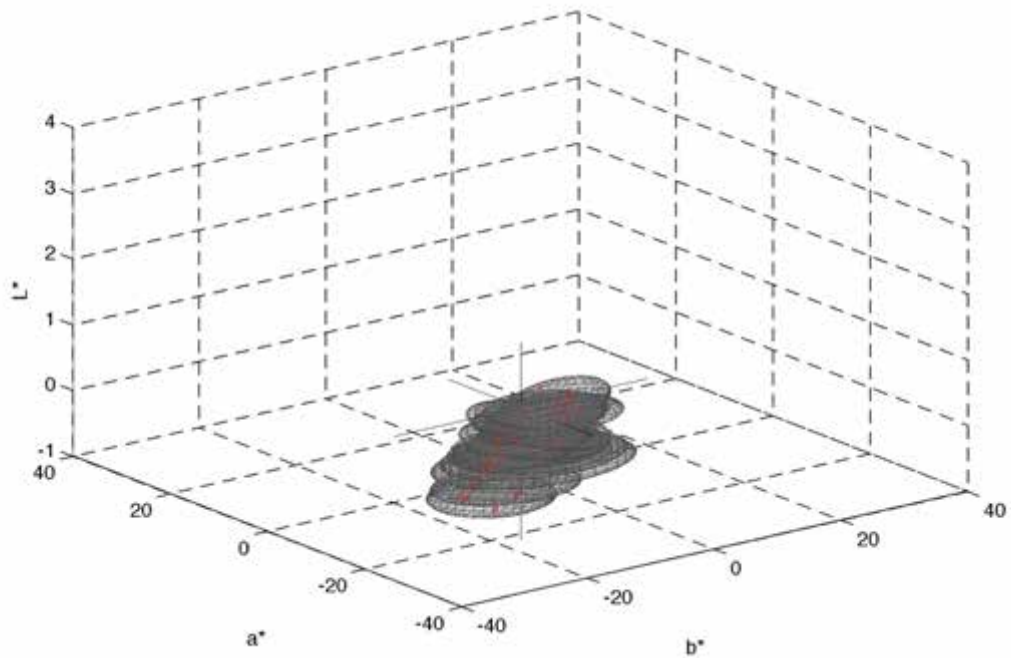


Figure 48(d): Example ITU-R Rec. 2020 laser projector observer variability ellipsoids based on reproduced 1931 2° colorimetry match to MacBeth 24 patches illuminated by CIE D65

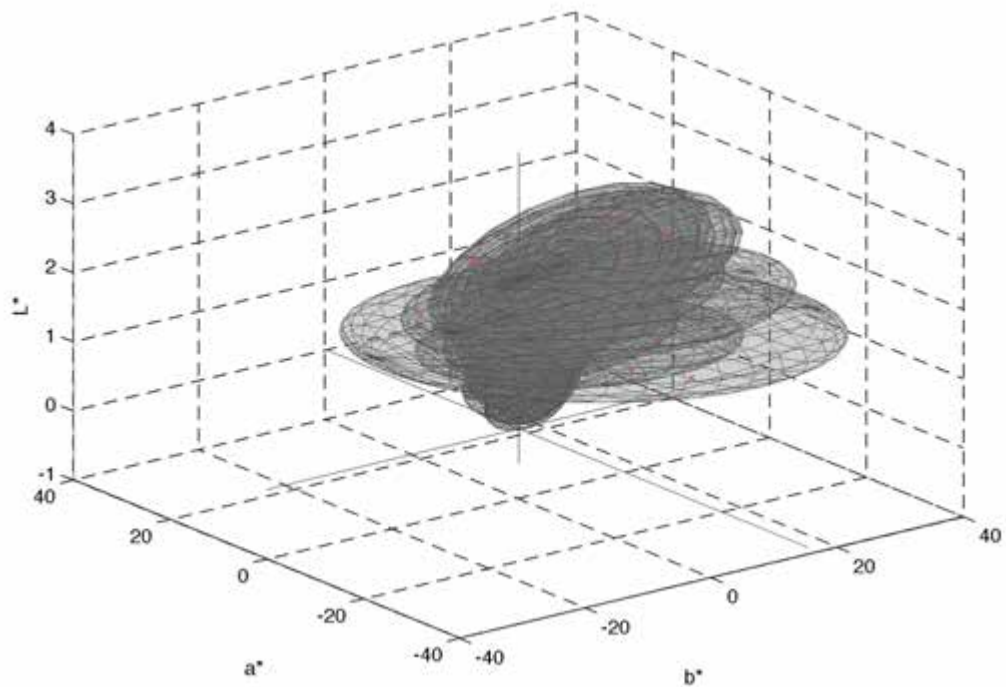


Figure 48(e): Chromaticity-area-optimized 8-channel laser projector observer variability ellipsoids based on reproduced 1931 2° colorimetry match to MacBeth 24 patches illuminated by CIE D65

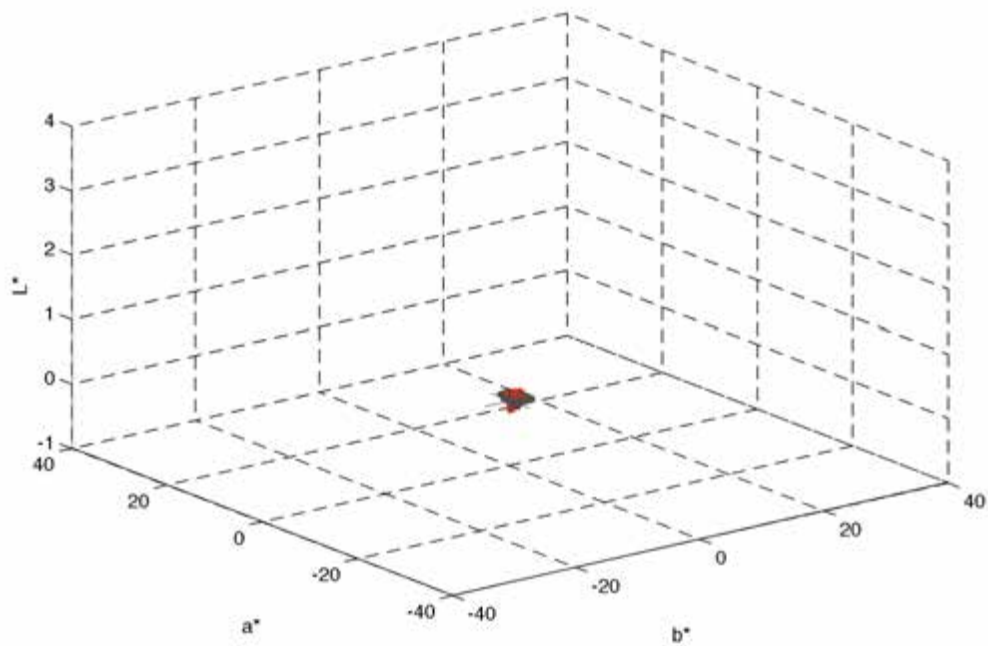


Figure 48(f): RIT seven-channel projector observer variability ellipsoids based on reproduced 1931 2° colorimetry match to MacBeth 24 patches illuminated by CIE D65

Table 9: CIE 2006 and Heckaman, et al. observer metamerism indices for various displays relative to MacBeth 24 test patches illuminated by CIE D65 (1931 2° colorimetry match)

<u>CIE D65</u>	$OM_c$	$OM_{c,max}$	$OM_{c,var}$	$OM_h$	$OM_{h,max}$	$OM_{h,var}$	<b>max</b> $\Delta E_{00}(31)$
<b>MacBeth24</b>							
Sony CRT	2.81	9.47	4.5E-04	11.31	41.61	2.9E-02	0.44
NEC DLP	2.95	8.46	9.6E-05	11.00	41.93	2.4E-02	0.00
Panasonic DLP	3.31	5.74	4.0E-04	9.75	30.41	4.4E-03	0.00
Rec2020 Laser	12.84	20.61	1.9E-01	33.38	58.46	5.7E+00	0.00
8-laser	19.87	50.49	7.1E+00	43.29	75.42	2.3E+02	0.00
RIT MPD	2.67	6.35	3.1E-06	6.25	15.21	6.9E-04	0.00

Data trends from models of CIE Illuminant A, HMI and fluorescent F2 sources reveal only a few notable differences from the D65 data. First, illuminant A offers a significant gamut challenge to the Rec. 709 CRT and it thus performs quite poorly under this source across all patchsets and all indices. Also under illuminant A, the eight-laser system fares a bit better than under D65, generating observer metamerism and observer variability levels more similar to the Rec. 2020 laser, still though, worst among the candidate technologies. The RIT display improves its performance in tungsten light versus the D65 models by factors near 2-to-1 and under HMI and fluorescent illumination by nearly 3-to-1 and 4-to-1, respectively. This advantages it consistently over the other investigated technologies. For the remaining displays, HMI and fluorescent lighting change their performance little versus under D65.

Particularly intriguing in these results overall is the disparity in observer metamerism and observer variability in the eight-laser system versus either a simpler Rec. 2020 three-channel laser display or the RIT optimized seven-channel display. Given its advantage of the greatest number of primary spectra, the greatest degrees-of-freedom for controlling metamerism (albeit with restriction to satisfy color matches for the 1931 observer) and the absolute largest overall chromaticity gamut area, this system well underperformed across the Sarkar/Fedutina observers. It's understandable that the RIT display had advantage over this system since the primary spectra used to construct it were explicitly optimized to minimize observer metamerism against the eight Sarkar/Fedutina observers and specifically

in consideration of the patchsets and illuminants represented in this test. But the eight-laser system represents an example gamut goal of multiple display manufacturers and technologists in the motion picture industry. It is capable of generating visible content across nearly the entire gamut of human color vision. The eight wavelengths were selected to produce the maximum geometric overlap with the 1931 chromaticity diagram yet yielded observer variability drastically higher than all of the smaller-gamut systems. The mathematical justification for this result likely stems from alignment of the eight laser wavelengths with regimes of maximum CMF disparity amongst the eight observer categories.

To analyze this result further, an alternate eight-laser system was theorized and simulated. Given the benefit in observer metamerism for the three-laser Rec. 2020 system over the eight-laser display, three of the eight monochromatic primaries (485, 540 and 650nm) were replaced by the Rec. 2020 wavelengths closest in chromaticity space, the idea being to take advantage of five additional degrees of freedom above the Rec. 2020 set. The resultant chromaticity gamut area was reduced only slightly from the ideal, but metamerism results were significantly improved. Figure 49 shows the new u'v' gamut. Table 10 further summarizes the metamerism indices for the D65-illuminated MacBeth Color Checker. Though still not as good as the exemplary RIT MPD, the new eight-laser system yields much stronger metamerism and variability than either of the other laser systems and in fact exceeds the performance of the CRT and DLP displays. This solidifies the extreme sensitivity of observer metamerism and variability to tuned monochromatic primaries. Even small adjustments can generate large performance differences if the wavelengths chosen exacerbate physiological and psychophysical differences in response.

Table 10: Sarkar/Fedutina observer metamerism indices for alternate laser displays relative to MacBeth 24 test patches illuminated by CIE D65 (1931 2° colorimetry match)

<u>CIE D65</u>	$OM_s$	$OM_{s,max}$	$OM_{s,var}$	$OM_{s,varmax}$	mean RMSE	mean peak err	max $\Delta E_{00}(31)$
<b>MacBeth24</b>							
Rec2020 Laser	5.50	10.44	2.6E-01	1.3E+00	2.18	9.66	0.00
8-laser	11.61	27.31	3.1E+02	2.0E+03	2.08	11.01	0.00
8-laser + 2020	2.09	3.26	3.2E-03	2.8E-02	1.94	2.58	0.00
RIT MPD	0.78	2.43	6.2E-06	7.5E-05	0.31	0.66	0.00

A final assessment was run to determine how the displays could perform if optimized for Sarkar/Fedutina observer metamerism magnitude,  $OM_s$ , rather than being forced to make metameric matches for the 1931  $2^\circ$  observer. Tables 11-14 summarizes results for the patches (excluding Munsell to save computational time) illuminated by each of the four test sources. For all displays, the metamerism magnitude is notably improved, especially for the chromaticity-area maximized eight-laser system which proves to have been handicapped by its requirement to match the standard observer's response for each patch previously. In this new paradigm, it achieves results superior to the three-channel Rec. 2020 laser in every scenario. Figure 50 further summarizes variability ellipsoids for the eight-channel laser and seven-channel RIT display, validating the RIT system still affords multiple orders of magnitude advantage. For both devices, ellipsoid errors are more symmetrically distributed about the CIELAB origin. The penalty for this strategy, though, lies with the standard observer color difference index that is now appreciably higher for all of the displays. This result further confirms that the  $2^\circ$  CMF are not statistically similar to any of the Sarkar/Fedutina observer categories in the context of this particular analysis. Given Sarkar/Fedutina observers are derived from Stiles and Burch data focused on  $10^\circ$  field experiments, this may not be entirely surprising.

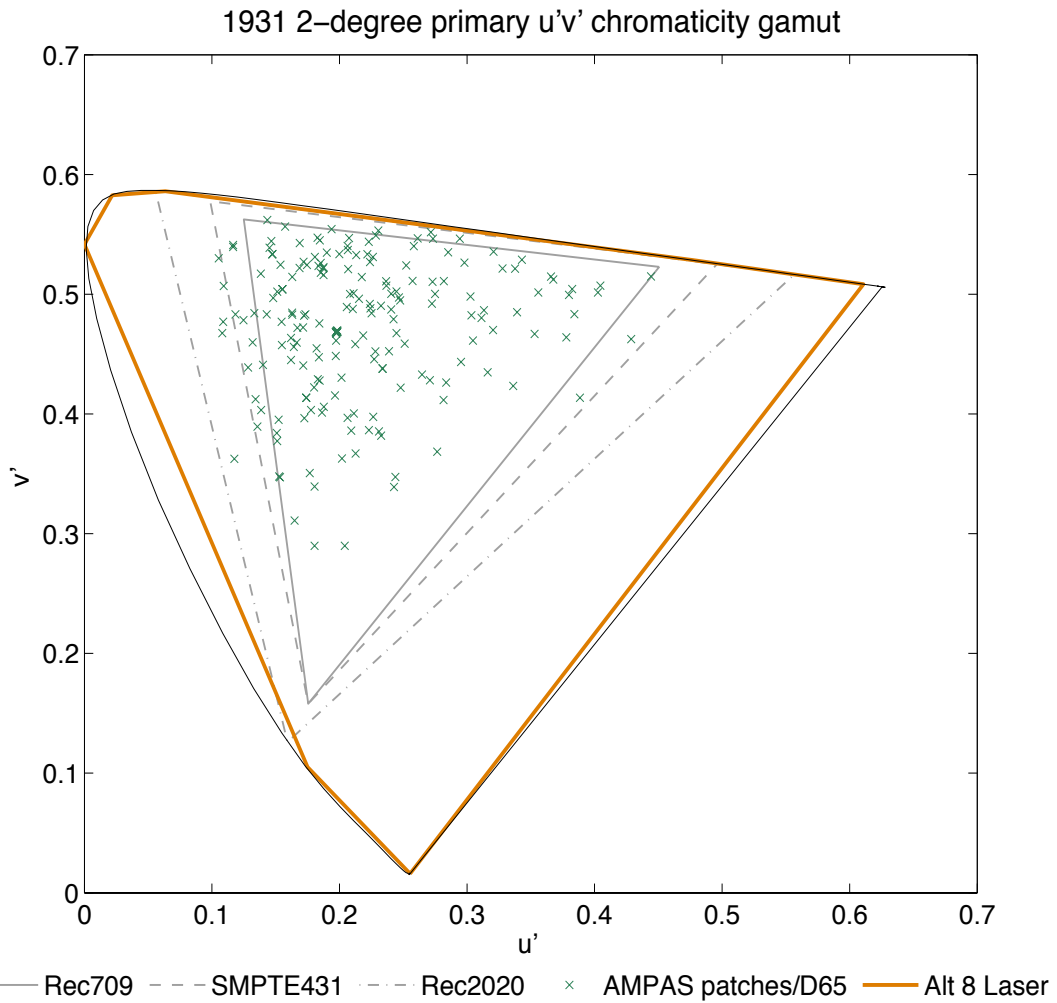


Figure 49. Alternate 8-primary laser projector chromaticity gamut; color points representing Kodak/AMPAS color patches illuminated by CIE D65 also included

Table 11: Sarkar/Fedutina observer metamerism indices for various displays relative to test patch sets illuminated by CIE D65 (optimized observer metamerism)

<u>CIE D65</u>	$OM_s$	$OM_{s,max}$	$OM_{s,var}$	$OM_{s,varmax}$	mean RMSE	mean peak err	max $\Delta E_{00}(31)$
<b><u>AMPAS190</u></b>							
Sony CRT	1.74	16.20	4.8E-03	1.7E-01	0.45	1.97	8.53
NEC DLP	1.61	11.81	1.9E-03	1.2E-01	0.26	0.55	8.31
Panasonic DLP	2.01	7.96	2.6E-03	5.7E-02	0.28	0.78	6.04
Rec2020 Laser	4.84	7.52	3.8E-01	5.3E+00	2.10	9.49	3.70
8-laser	4.18	18.98	4.0E+01	1.7E+03	2.78	14.30	21.94
RIT MPD	0.15	0.95	2.3E-06	1.1E-04	0.25	0.60	3.27
<b><u>MacBeth24</u></b>							
Sony CRT	1.13	5.61	2.8E-03	4.9E-02	0.45	2.00	4.08
NEC DLP	1.37	2.44	3.0E-04	3.2E-03	0.26	0.52	3.93
Panasonic DLP	1.88	3.14	1.1E-03	6.1E-03	0.27	0.77	2.31
Rec2020 Laser	5.06	7.56	2.5E-01	1.2E+00	2.20	9.70	3.40
8-laser	4.69	18.50	8.0E+01	1.6E+03	3.03	15.96	19.95
RIT MPD	0.14	0.91	2.6E-06	4.9E-05	0.27	0.64	3.34
<b><u>MacBeth DC</u></b>							
Sony CRT	1.64	31.34	2.7E-02	2.9E+00	0.50	2.21	20.07
NEC DLP	1.65	23.85	8.7E-03	6.6E-01	0.30	0.60	15.24
Panasonic DLP	1.98	23.28	1.6E-03	8.3E-02	0.32	0.89	15.74
Rec2020 Laser	4.92	7.59	4.1E-01	3.0E+00	2.44	10.30	6.51
8-laser	3.99	17.81	8.1E+00	1.9E+02	3.18	16.78	24.47
RIT MPD	0.18	9.77	3.4E-04	8.1E-02	0.31	0.74	7.39
<b><u>Big Metamers</u></b>							
Sony CRT	4.51	23.12	4.7E-02	1.0E+00	0.42	1.70	11.79
NEC DLP	2.95	18.88	1.8E-02	2.0E-01	0.24	0.53	11.05
Panasonic DLP	2.87	14.33	9.2E-03	2.9E-01	0.26	0.76	9.28
Rec2020 Laser	4.26	8.24	3.2E-01	3.3E+00	1.61	7.60	8.01
8-laser	3.96	19.82	8.5E+01	1.6E+03	2.09	11.28	15.91
RIT MPD	0.27	2.75	7.8E-06	2.4E-04	0.18	0.47	2.91

Table 12: Sarkar/Fedutina observer metamerism indices for various displays relative to test patch sets illuminated by CIE IllumA (optimized observer metamerism)

<u>CIE IllumA</u>	$OM_s$	$OM_{s,max}$	$OM_{s,var}$	$OM_{s,varmax}$	mean RMSE	mean peak err	max $\Delta E_{00}(31)$
<b><u>AMPAS190</u></b>							
Sony CRT	3.80	41.53	5.4E-03	2.4E-01	0.60	2.71	21.30
NEC DLP	1.35	8.60	1.6E-03	7.4E-02	0.26	0.56	6.08
Panasonic DLP	1.47	7.84	2.3E-03	2.2E-01	0.27	0.71	4.49
Rec2020 Laser	4.14	6.22	2.1E-01	1.6E+00	1.80	7.94	4.24
8-laser	1.97	4.46	8.3E-02	2.6E+00	1.89	9.68	10.44
RIT MPD	0.08	0.42	4.3E-08	4.6E-06	0.15	0.38	1.50
<b><u>MacBeth24</u></b>							
Sony CRT	4.22	25.19	3.9E-03	2.7E-02	0.63	2.90	12.96
NEC DLP	1.18	2.08	7.7E-04	9.0E-03	0.26	0.56	2.68
Panasonic DLP	1.31	2.35	5.2E-04	6.5E-03	0.27	0.67	2.22
Rec2020 Laser	4.24	6.34	2.1E-01	1.6E+00	1.88	7.96	4.83
8-laser	2.12	4.33	1.7E-01	2.7E+00	2.03	10.42	11.80
RIT MPD	0.07	0.43	3.3E-07	7.9E-06	0.17	0.40	1.61
<b><u>MacBeth DC</u></b>							
Sony CRT	2.70	40.77	1.2E-02	1.3E+00	0.64	2.92	20.34
NEC DLP	1.43	10.14	6.0E-03	5.8E-01	0.29	0.60	7.18
Panasonic DLP	1.37	10.06	2.3E-03	1.2E-01	0.29	0.71	7.19
Rec2020 Laser	4.20	6.40	3.9E-01	2.4E+00	1.97	8.28	4.62
8-laser	2.07	4.67	5.2E-02	1.3E+00	2.03	10.40	11.57
RIT MPD	0.07	2.77	2.1E-07	3.8E-05	0.15	0.37	2.08
<b><u>Big Metamers</u></b>							
Sony CRT	7.53	44.03	3.2E-02	5.9E-01	0.51	2.20	21.30
NEC DLP	2.26	14.86	1.7E-02	3.8E-01	0.22	0.55	10.09
Panasonic DLP	2.48	12.77	1.3E-02	3.8E-01	0.26	0.76	9.15
Rec2020 Laser	3.74	5.61	1.2E-01	1.7E+00	1.43	6.80	5.06
8-laser	1.66	4.46	1.2E-01	2.6E+00	1.59	8.46	7.88
RIT MPD	0.17	1.73	3.8E-06	2.2E-04	0.14	0.36	1.50

Table 13: Sarkar/Fedutina observer metamerism indices for various displays relative to test patch sets illuminated by HMI (optimized observer metamerism)

<u>HMI</u>	$OM_s$	$OM_{s,max}$	$OM_{s,var}$	$OM_{s,varmax}$	mean RMSE	mean peak err	max $\Delta E_{00}(31)$
<b><u>AMPAS190</u></b>							
Sony CRT	1.82	13.56	7.3E-03	3.0E-01	0.43	1.86	8.16
NEC DLP	2.03	6.77	8.5E-03	1.3E-01	0.26	0.54	5.34
Panasonic DLP	2.75	7.49	3.6E-02	6.1E-01	0.25	0.67	4.17
Rec2020 Laser	5.64	8.96	1.6E+00	1.5E+01	1.77	7.88	4.44
8-laser	4.35	18.98	4.7E+01	2.2E+03	2.40	12.38	20.95
RIT MPD	0.14	1.22	1.6E-07	8.7E-06	0.16	0.40	2.08
<b><u>MacBeth24</u></b>							
Sony CRT	1.43	2.42	5.6E-03	4.0E-02	0.44	1.90	3.05
NEC DLP	2.05	3.19	4.8E-03	2.3E-02	0.26	0.55	2.42
Panasonic DLP	2.82	4.46	3.1E-02	2.0E-01	0.25	0.66	4.69
Rec2020 Laser	5.92	9.02	1.5E+00	9.9E+00	1.86	8.05	4.73
8-laser	4.85	18.00	9.8E+01	2.0E+03	2.56	13.70	20.01
RIT MPD	0.12	0.37	4.1E-08	9.4E-07	0.16	0.41	1.49
<b><u>MacBeth DC</u></b>							
Sony CRT	1.73	23.24	9.5E-03	6.0E-01	0.46	1.99	15.19
NEC DLP	2.07	17.18	8.0E-03	7.4E-02	0.29	0.59	11.31
Panasonic DLP	2.81	16.70	2.4E-02	1.5E-01	0.27	0.70	11.24
Rec2020 Laser	5.74	9.03	2.1E+00	1.2E+01	1.92	7.84	4.97
8-laser	4.15	17.02	9.0E+00	2.2E+02	2.49	12.87	24.28
RIT MPD	0.15	5.43	9.5E-05	2.2E-02	0.17	0.41	4.03
<b><u>Big Metamers</u></b>							
Sony CRT	3.42	18.07	2.3E-02	4.1E-01	0.40	1.62	9.27
NEC DLP	2.39	13.00	1.5E-02	3.0E-01	0.23	0.53	8.78
Panasonic DLP	2.78	9.96	5.0E-02	1.7E+00	0.24	0.68	7.38
Rec2020 Laser	4.75	8.56	8.4E-01	1.2E+01	1.47	6.96	5.98
8-laser	4.10	18.97	1.2E+02	2.2E+03	1.95	10.55	15.73
RIT MPD	0.22	1.86	3.7E-06	1.2E-04	0.15	0.41	2.51

Table 14: Sarkar/Fedutina observer metamerism indices for various displays relative to test patch sets illuminated by CIE Illum F2 (optimized observer metamerism)

<u>CIE Illum F2</u>	$OM_s$	$OM_{s,max}$	$OM_{s,var}$	$OM_{s,varmax}$	mean RMSE	mean peak err	max $\Delta E_{00}(31)$
<b><u>AMPAS190</u></b>							
Sony CRT	2.94	25.56	1.2E-01	2.7E+00	0.51	2.26	13.47
NEC DLP	2.53	3.91	8.1E-02	5.8E-01	0.34	0.66	5.08
Panasonic DLP	3.08	5.06	1.9E-01	1.1E+00	0.29	0.71	6.25
Rec2020 Laser	5.99	9.26	4.8E+00	3.2E+01	1.76	7.60	6.97
8-laser	4.16	15.10	1.1E+01	6.7E+02	2.10	10.63	18.17
RIT MPD	0.10	0.78	1.8E-08	1.2E-06	0.13	0.36	1.05
<b><u>MacBeth24</u></b>							
Sony CRT	3.00	13.52	1.4E-01	1.0E+00	0.53	2.35	7.23
NEC DLP	2.64	3.87	7.6E-02	5.1E-01	0.36	0.69	5.38
Panasonic DLP	3.24	5.02	2.0E-01	1.3E+00	0.31	0.73	6.82
Rec2020 Laser	6.31	9.58	5.0E+00	3.9E+01	1.85	7.84	7.60
8-laser	4.55	12.04	1.5E+01	2.5E+02	2.20	10.99	17.96
RIT MPD	0.09	0.39	6.9E-08	1.6E-06	0.14	0.38	0.99
<b><u>MacBeth DC</u></b>							
Sony CRT	2.67	29.14	1.2E-01	3.0E+00	0.52	2.26	12.12
NEC DLP	2.57	6.48	1.1E-01	6.4E-01	0.36	0.69	5.66
Panasonic DLP	3.14	6.32	2.4E-01	1.3E+00	0.31	0.74	6.90
Rec2020 Laser	6.15	9.67	7.7E+00	4.3E+01	1.77	7.28	7.71
8-laser	4.22	13.68	4.4E+00	1.8E+02	1.97	9.47	20.37
RIT MPD	0.09	2.15	5.5E-07	1.3E-04	0.13	0.39	1.33
<b><u>Big Metamers</u></b>							
Sony CRT	3.68	30.44	2.1E-01	4.1E+00	0.47	2.02	14.16
NEC DLP	2.27	7.71	6.1E-02	8.2E-01	0.28	0.59	5.40
Panasonic DLP	2.65	5.46	1.2E-01	2.0E+00	0.25	0.67	4.49
Rec2020 Laser	4.97	8.18	1.5E+00	1.4E+01	1.60	7.51	5.02
8-laser	3.76	15.10	2.5E+01	6.7E+02	2.01	10.62	13.64
RIT MPD	0.14	0.94	2.1E-07	7.8E-06	0.14	0.37	1.19

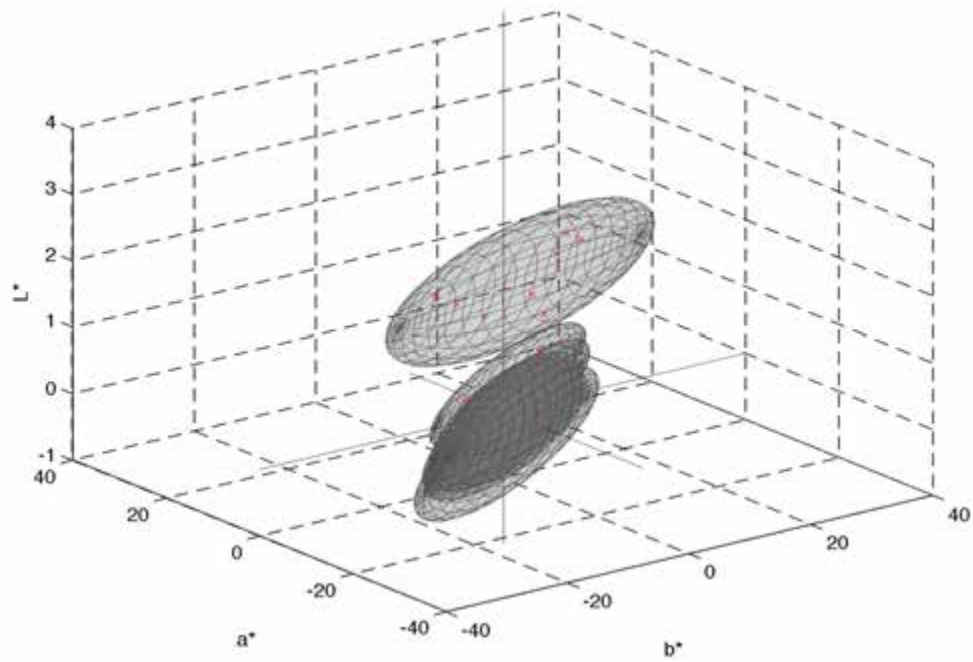


Figure 50(a): Chromaticity-area-optimized 8-channel laser projector observer variability ellipsoids based on minimized observer metamerism for MacBeth 24 patches illuminated by CIE D65

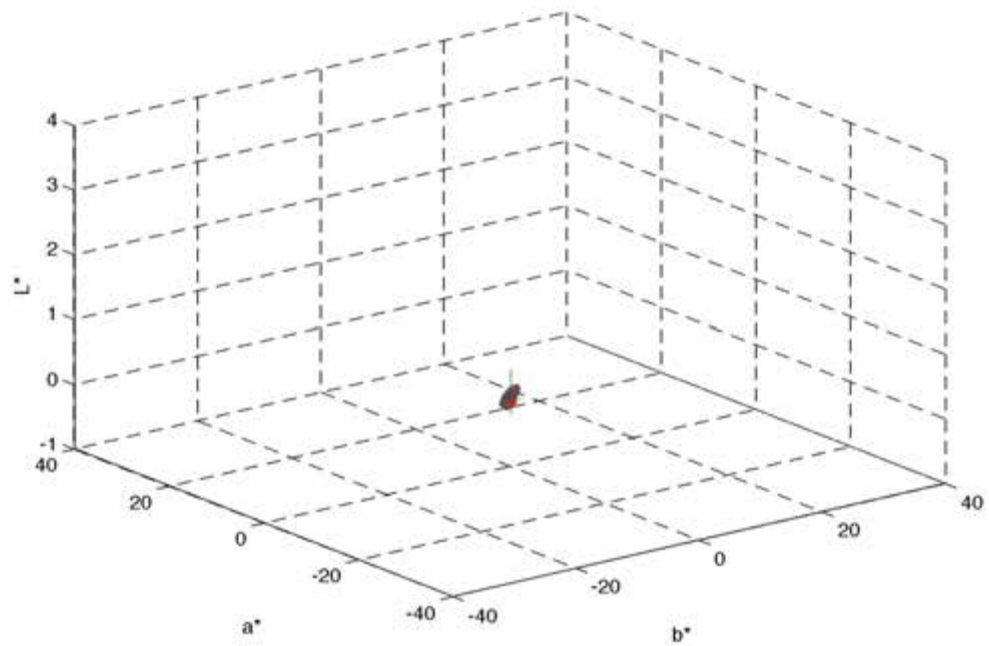


Figure 50(b): RIT seven-channel projector observer variability ellipsoids based on minimized observer metamerism for MacBeth 24 patches illuminated by CIE D65

## Conclusions

In designing color primaries for accurate color reproduction, spectral characteristics do carry significant importance. A move towards monochromatic color designs such as are found in laser displays adds significant chromaticity gamut area for users but at the expense of observer metamerism and variability. Investigation of real displays designed around three current color standards for motion picture work reveals that the latest specification, ITU-R Rec. 2020, offers strong potential for viewer disparity when compared with older broad-spectrum standards like ITU-R Rec. 709 and SMPTE-431. Expanding to more than three laser primaries can help but only if those wavelengths are themselves optimized to the objective of improved observer consistency. Attempting, instead, to simply generate the largest color gamut possible from multiple laser wavelengths may actually exacerbate metamerism failure. Finally, it is possible to craft customized primary spectra with the intent of minimizing observer metamerism. The prototype seven-channel projection system at RIT has been constructed with modeled results significantly improved over any legacy three-color display. The next chapters will detail the design of the RIT system and discuss findings of forced-choice color difference experiments executed with it.

# Chapter 7

---

## The Seven-channel RIT Multiprimary Display

### Abstract

Building on learning gained from the two-projector multiprimary display of Chapter 5, a more rigorous seven-channel prototype multiprimary display has been simulated and built to minimize observer metamerism and observer variability according to custom indices derived from emerging models for human color vision introduced in Chapter 6. The constructed display has further been implemented in observer experiments to validate practical performance and confirm the vision and metamerism models. Summary of those results will be discussed in Chapter 8.

### Trends in the Cinema Space

Dye-based film systems and phosphor-based CRT displays are generally forgiving in the metamerism illusion across disparate observers. Broad spectral representation in each colorant limits the chance for quantal integration differences within the cones amongst a diverse population. But emerging displays are decidedly more narrow-band in their spectral composition, an intentional design feature which influences reproducible color gamut. Chapter 6's results confirm that spectrally selective primary sets necessary for expanding color gamut exacerbate observer variability<sup>85</sup>. In related work, the Society of Motion Picture and Television Engineers is exploring alternatives to standard observer colorimetry for calibrating newer video mastering displays employing these same physics. This stems from user experience where visual white point calibrations made between flat-panel displays and reference CRT displays are inconsistent with calibrations made alternatively by standard colorimeters employing a single observer CMF<sup>86,87</sup>.

The designed RIT multiprimary imaging system offers options for co-optimization of increased palette and reduced observer variability. The optimization of such a system, though, must be deliberate, assessed against meaningful objective criteria for color reproduction, metamerism reduction and spectral gamut. Here, summary of efforts to build and test the prototype system are provided. The intended purpose of the RIT multispectral display is to confirm current understanding of variability amongst real observers and to provide evidence for potential in metamerism reduction versus emerging cinema display technologies.

## Design Methodology

The starting objective for design of the RIT multi-primary display (MPD) was to deliver meaningfully reduced observer variability versus traditional three-channel RGB systems. The MPD display was modeled as a two-part optical projection system comprising a wide-band illumination source and individual transmission filters defining distinct color channels. All channels utilized a common light source so as to permit consistency in either time-multiplexed or space-multiplexed prototype configurations. Candidate filter spectra were originally simulated via parametric optimization as opposed to being restricted to a heuristic selection from a set of available commercial color filters. The final design was implemented using materials then that performed most closely to the resultant computational models. In this manner, deficiencies in available filter sets could be quantified versus optimized results. To keep the mathematics simple in the constrained computational optimization, a generalized Gaussian transmission profile,  $T(\lambda)$ , was modeled for each potential primary filter, Equation 54. The peak transmission fraction of all candidates was normalized to 1.0 and no accounting for system white balance was otherwise enforced. Subsequent assessments of the MPD prototype were performed via absolute radiometric models and thus no color management against traditional normalized white was required.

$$T(\lambda) = \frac{1}{\sigma\sqrt{2\pi}} \exp\left[-\frac{(\lambda - \mu)^2}{2\sigma^2}\right] \quad (54)$$

Within the design, candidate transmission filters were illuminated using one of two measured source spectra common in cinema applications and generally available for prototype construction, one a typical large-venue xenon arc lamp and the other a consumer-grade mercury arc UHP lamp, see Figure 51 for spectra. Thus the modeled MPD primaries in each channel represent the absolute spectral concatenation of the illumination source and the transmission profile of the simulated Gaussian filter. Across  $K'$  total primaries for the display system, the transmission profiles were varied in both peak transmission wavelength,  $\mu$ , and profile-width,  $\sigma$ , in order to achieve cost function minimization. The majority of simulations were executed with Matlab's *fmincon* optimization tool. Additional permutations investigated for the system design included the number of primaries ( $K' = 3$  through 8), the starting guess for Gaussian parameters and the spectral domain permitted for iteration of each primary's characteristics (each primary

having its peak wavelength constrained to a window of wavelengths versus permitting any monotonic array of peak wavelengths for the K' primaries between constrained spectral endpoints of 400 and 700nm).

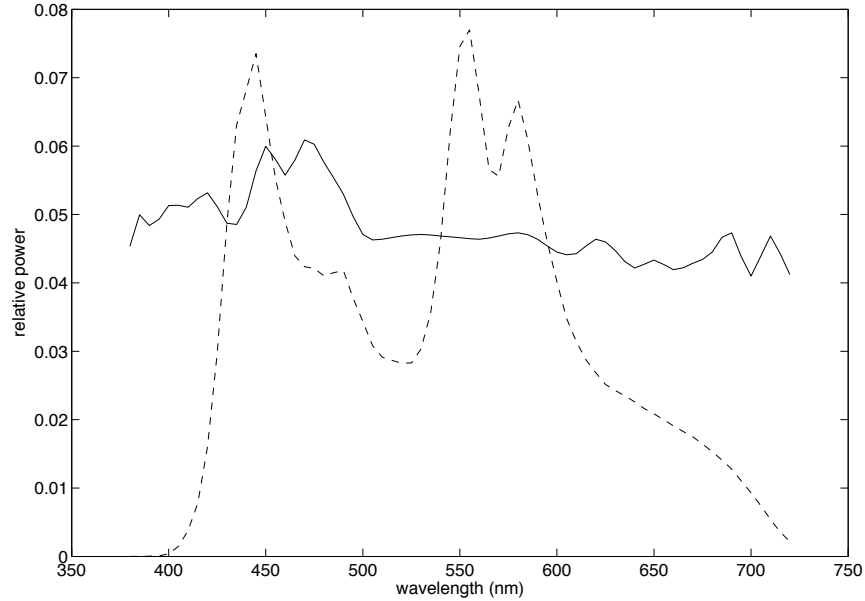


Figure 51. Projector illuminant candidates for the RIT MPD: xenon (solid) and mercury arc UHP (dashed)

The cost function objective for the primary parameter optimizations was minimized observer metamerism in the MPD display's reproduction of a set of *a priori* reference spectra. Specifically, a training/verification strategy was employed where only one candidate collection of spectra was chosen for inclusion in the optimization routine. Additional unique spectra were then used with the optimization results to verify model quality. A collection of six different candidate reflective spectra sets were investigated and compared for training the MPD design, see Table 15. The two MacBeth Color Checkers represent popular color calibration tools used for image capture and which are widely available for practical experimentation. The Kodak/AMPAS set is a collection of 190 spectra determined by Kodak to deliver superior statistical representation of typical surface colors encountered in traditional photography. It is also the spectra set currently recommended by the Academy of Motion Picture Arts and Sciences for color management research. The high metamerism colors were similarly derived from Kodak research as a subset of surface colors with particularly high metamerism failure in traditional photographic applications. Munsell spectra were measured

from a sample matte Munsell Book of Colors. Finally, the Standard Object Colour Spectra (SOCS) database is a compilation of many other spectra sets and includes skin tones, textiles, flowers, leaves, paints, photographic materials and printing inks/pigments. It's chromaticity gamut under D65 illumination is shown in Figure 52. All other patchset gamuts were shown previously in Chapter 6. There are certainly other high quality candidate color stimuli which were not included in this effort but may be investigated in future work<sup>28</sup>.

Table 15. Reflectance patchsets considered in MPD design optimization

- |   |
|---|
| 1) MacBeth Color Checker (24 samples)                               |
| 2) MacBeth Color Checker DC (240 samples)                           |
| 3) US Patent No. 5,582,961 "Kodak/AMPAS" test spectra (190 samples) |
| 4) Munsell sample spectra (1269 samples)                            |
| 5) select high metamerism color set (65 samples)                    |
| 6) SOCS <sup>15</sup> spectral database (53,350 samples)            |

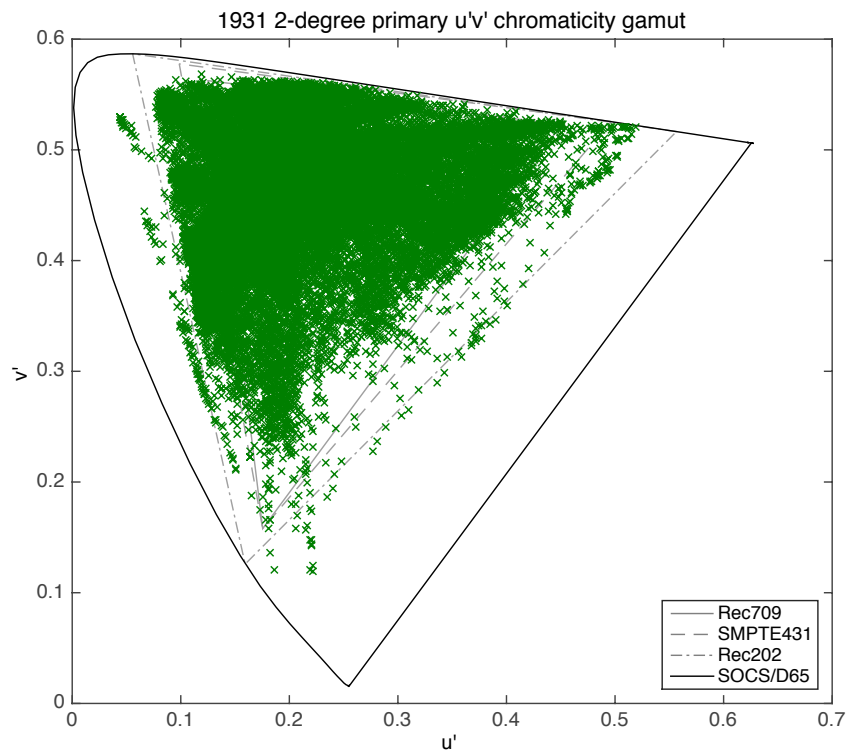


Figure 52.  $u'v'$  chromaticity gamut for SOCS color patch set illuminated by CIE D65

To further define the absolute reference stimuli used for training, the reflection spectra from each of the above sets was illuminated via one of four common indoor or outdoor cinema lighting sources, see Table 16. Again with all reflection spectra and all illuminants, training was performed with one permutation followed by performance verification with each of the other permutations.

Table 16. Scene illuminants considered in MPD design optimization

1) CIE Illuminant D65
2) CIE fluorescent, F2
3) CIE Illuminant A
4) Measured Hydrargyrum Medium-arc Iodide lamp (HMI)

Various indices discussed in Chapter 6 were used to quantify observer metamerism magnitude and observer variability for both cost function minimization and subsequent performance verification. The objective for the optimizations was to identify the most robust training spectra, illuminant and optimization parameters to develop an idealized MPD design with the most effective number of primaries across the larger set of validation stimuli. The primary spectra modeling progressed in two stages. In a first screening simulation, the  $K \times P$  radiometric scaling matrix,  $\mathbf{R}$ , necessary to generate spectral matches to the  $\lambda \times P$  training stimuli matrix,  $\mathbf{S}_{train}$ , was computed via psuedoinverse linear algebra using Equation 56. During optimization,  $\lambda \times K'$  primary spectra,  $\mathbf{PS}$ , were produced via iteration of the Gaussian transmission parameters,  $\mu$  and  $\sigma$ , and using a concatenation of the resultant filter spectra in each channel with the projector illuminant spectra,  $I$ , Equation 55. Equation 57 was then used to predict the reconstructed spectral stimuli. The optimization was allowed to progress until a minimization of  $OM_x$  or  $OM_{x,var}$  was achieved for the original  $\mathbf{S}_{train}$  versus the reconstructed  $\hat{\mathbf{S}}_{train}$ . Once primary spectra for each training scenario were determined, Equations 56 and 57 were used to assess the  $\mathbf{R}$  and  $\hat{\mathbf{S}}$  matrices for the verification stimuli,  $\mathbf{S}_{ver}$ . Observer metamerism metrics were again computed between  $\hat{\mathbf{S}}_{ver}$  and  $\mathbf{S}_{ver}$ . For the second stage of simulation,  $\mathbf{PS}$  spectra were retained from the screening models for each permutation. However, the  $\mathbf{R}$  matrices in this variation were computed not via psuedoinversion of the spectral data but rather via a fully constrained nonlinear optimization, permitting much better spectral reconstructions to be produced though at the cost of computing speed.

$$\mathbf{PS} = \mathit{diag}(\mathbf{I}) \cdot \mathbf{T} \quad (55)$$

$$\mathbf{R} = \mathit{pinv}(\mathbf{PS}) \cdot \mathbf{S}_{\mathit{patchset}} \quad (56)$$

$$\mathbf{PS} \cdot \mathbf{R} = \hat{\mathbf{S}}_{\mathit{patchset}} \quad (57)$$

## Optimization Results

Each of the first five patchsets from Table 15 were used independently to train the optimization of primary Gaussian parameters, followed by performance validation from each of the remaining sets and the SOCS set (which was itself not used as a trainer in the optimizing routines due to computational restrictions). To provide a clean baseline comparison, the patchsets were first illuminated by only a CIE D65 source to generate reference training stimuli and the Gaussian transmission filters iterated by the optimization routine were concatenated with only the xenon arc projector source to define **PS** (a dynamic range of 10,000:1 was also used to set the MPD black). A starting guess of  $K'=6$  primaries with initial peaks,  $\mu$ , distributed uniformly across the visible domain and with starting profile-widths,  $\sigma$ , of 25nm was chosen. The optimization of the 12 Gaussian terms was performed via Equations 56 and 57 to minimize  $OM_s$  ( $y = \Delta E_{ab}$ ) for the training spectra. Models from Ref [85] and Chapter 6 suggest optimizations incorporating  $OM_c$  or  $OM_h$  from the CIE2006 and Heckaman, et al. CMF models should deliver reasonably similar results and so the Sarkar set was predominant for the bulk of the design work. Constrained nonlinear optimization was used to restrict the peak filter transmission wavelengths to binned domains, each 50nm wide and distributed uniformly between 400 and 700nm. Transmission profile-widths were also constrained to a maximum upper bound. Table 17 summarizes the resultant Gaussian parameters for each of the six channels optimized in the five distinct training scenarios. The primaries synthesized from varying the training patchset are significantly different across each permutation of the above methodology, offering a fairly strong signal in the modeling. Figure 53 shows the observer metamerism and variability indices for the verified reproduction simulations for all of the patchsets as a function of each candidate training set.

Table 17. 6-channel Gaussian filter parameters optimized for each training patchset (D65 patch illumination, xenon source, minimization of  $OM_s$ )

<u>Training Patchset</u>	<u>Optimized Primary Gaussian Parameters <math>\mu/\sigma</math> (nm)</u>											
	1		2		3		4		5		6	
<b>MacBeth 24</b>	431	12.7	459	20.1	516	25.1	560	24.9	605	24.3	651	20.8
<b>MacBeth DC</b>	437	16.7	478	13.8	517	19.4	557	21.8	601	18.0	661	29.1
<b>Kodak/AMPAS</b>	436	14.8	472	12.9	518	19.5	559	22.4	606	18.5	650	17.3
<b>Munsell</b>	434	15.5	473	13.7	509	18.4	552	24.7	603	25.7	674	32.9
<b>Big Metamers</b>	436	14.0	470	14.2	522	21.1	570	22.7	621	17.2	670	14.6

The Kodak/AMPAS test spectra generate the most robust training results when all other patchsets are verified using its optimized primary spectra. This can be validated for both  $OM_s$  and  $OM_{s,var}$  indices and looking at all six of the verification patchsets. To prove the model is behaving as expected, Figure 53 shows that most verification patchsets perform best for average observer metamerism  $OM_s$  when trained by themselves while the AMPAS training is consistently second best for each. The lone exception is the Big Metamers set which introduces particularly difficult spectral reproduction objectives to the model. Here, the Kodak/AMPAS training set delivers better results than the self-trained scenario. For the large SOCS verification set, the Kodak/AMPAS trainer is clearly best in all three indices, followed by the Big Metamers and MacBeth DC trainers. Among the five candidate training sets, the Munsell and Macbeth DC patches perform most inconsistently across the full population of reference stimuli. Focusing on just verification results, it's interesting to note that each of the MacBeth patchsets and the Munsell spectra are all relatively insensitive to training permutations, suggesting they may be poor candidates for screening additional model variations going forward.

The first major variation from the above baseline scenario involves use of a constrained nonlinear optimization methodology for generating the radiometric scaling matrix,  $\mathbf{R}$ , during prediction of  $\hat{\mathbf{S}}_{ver}$  from each psuedoinverse-trained  $\mathbf{PS}$ . Implementing this rigorous reconstruction, all trained primary variations prove much better at delivering reduced observer metamerism and variability across the verification patchsets, see Table 18. The AMPAS set still performs well but is

effectively comparable to the other training permutations for  $OM_s$ . Delving deeper into  $OM_{s,max}$  values across all permutations, however, the AMPAS set maintains reasonable superiority along with the MacBeth DC set. Nonlinear optimization of  $\mathbf{R}$  generates excellent spectral reproductions of the verification patches regardless of optimized MPD primary set but at the cost of greatly increased computation time. In fact, Munsell and SOCS verifications were omitted from this analysis due to excessive processing requirements for the 1,300 and 50,000 patches in each, respectively.

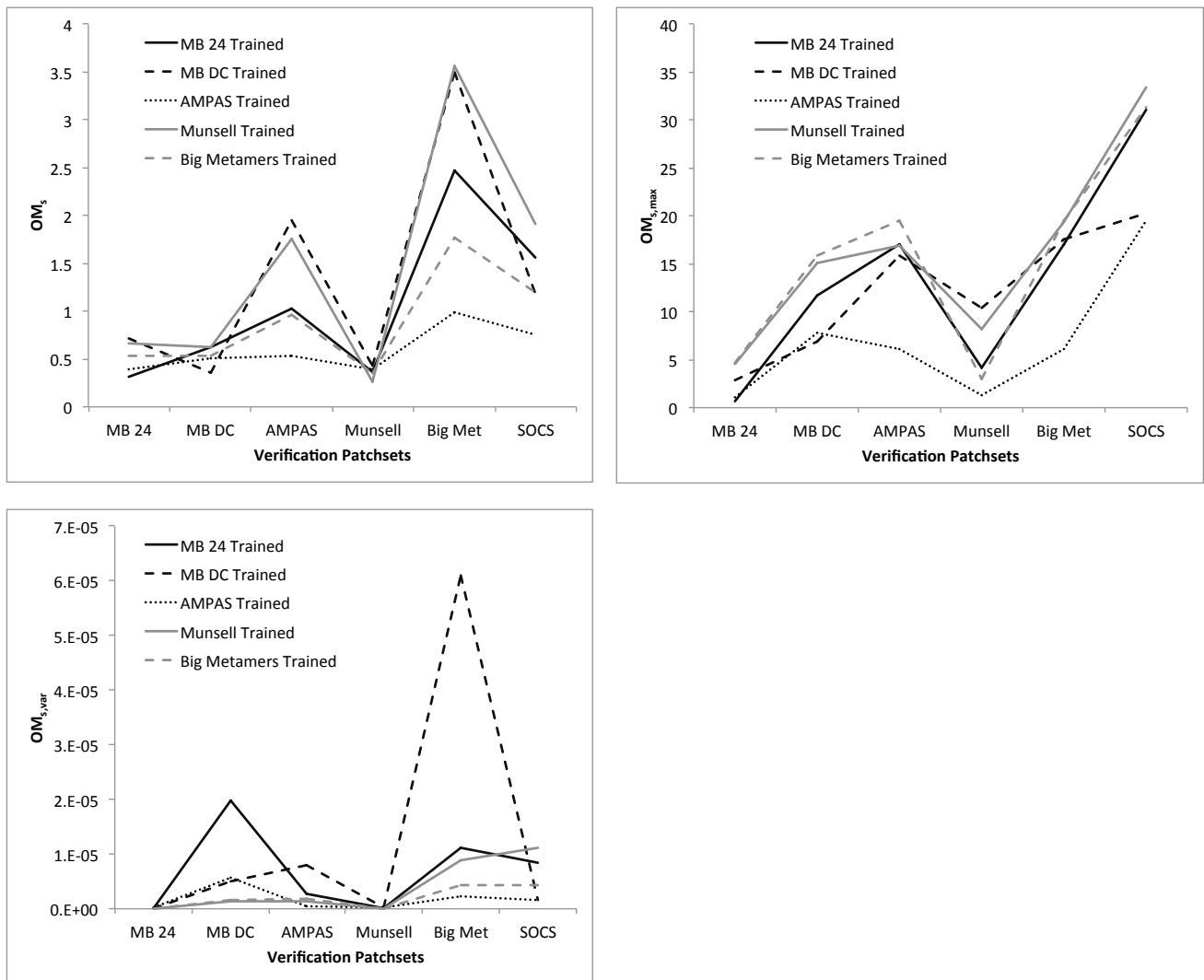
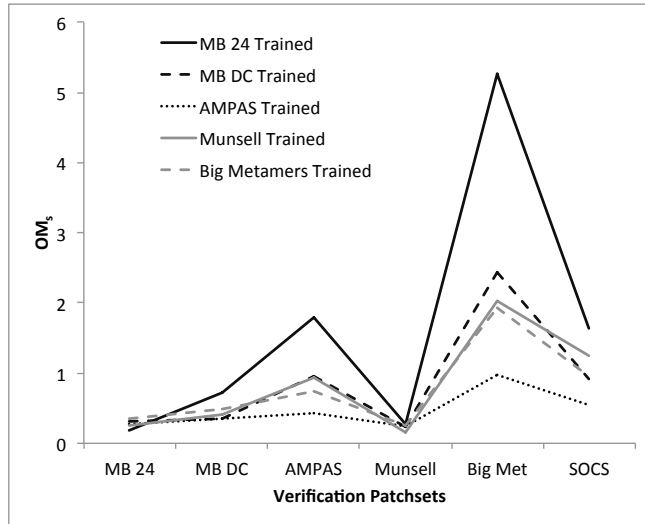


Figure 53. Pseudoinverse-optimized six-channel MPD metamerism verifications derived from five candidate training spectra (D65 patch illumination, xenon source, minimization of  $OM_s$ );  $OM_s$  (upper left),  $OM_{s,max}$  (upper right) &  $OM_{s,var}$  (lower left)

Table 18. Nonlinear-optimized six-channel MPD metamerism verifications derived from five candidate training spectra (D65 patch illumination, xenon source, minimization of  $OM_s$ )

<u>Training Patchset</u>	<u>Observer Metamerism, <math>OM_s</math></u>				<u>Max Observer Metamerism, <math>OM_{s,max}</math></u>			
	MB 24	MB DC	AMPAS	Big Met	MB 24	MB DC	AMPAS	Big Met
<b>MacBeth 24</b>	0.14	0.16	0.15	0.32	0.43	4.24	1.36	3.46
<b>MacBeth DC</b>	0.08	0.08	0.10	0.12	0.15	0.18	1.23	0.63
<b>Kodak/AMPAS</b>	0.12	0.13	0.13	0.19	0.30	0.64	0.87	0.79
<b>Munsell</b>	0.07	0.07	0.08	0.13	0.25	2.17	0.70	1.48
<b>Big Metamers</b>	0.30	0.35	0.32	0.41	0.71	1.03	0.89	2.42

Varying starting guesses for the  $\mu$  and  $\sigma$  Gaussian parameters in each channel makes very little difference in results as long as the peak wavelengths are well distributed throughout the 400-700nm domain. A small improvement is seen, though, when the iterating peak wavelengths are permitted to vary subject to a monotonic vectorization versus each primary being binned in a restricted spectral span. The latter technique was hypothesized to be beneficial to enforcing full spectrum coverage across all visible wavelengths in the design though proved somewhat restrictive to the observer metamerism objective function. Figure 54 shows the training quality when the six transmission peaks are permitted to iterate in a monotonic series to any wavelengths between 400 and 700nm. Only the MacBeth Color Checker training is hampered versus the original compartmentalization strategy. For a sense of scale, the average  $OM_s$  across all six verification sets produced via the Kodak/AMPAS training drops from 0.59 when primary peaks are binned to 0.47 when non-binned. Also shown are the resultant peak wavelengths and profile-widths for the Kodak/AMPAS training permutation, comparing the original binned result to the non-binned result. The spectra do change somewhat significantly with non-binned primaries #5 and #6 optimizing to positions that would have been prohibited in the binned permutation.



Primary	Binned	Non-binned
<b>1</b>	$\mu = 436$ $\sigma = 14.8$	426 10.4
<b>2</b>	472 12.9	456 17.7
<b>3</b>	518 19.5	509 19.6
<b>4</b>	559 22.4	551 23.1
<b>5</b>	606 18.5	599 19.4
<b>6</b>	650 17.3	643 18.3

Figure 54. Pseudoinverse-optimized six-channel MPD metamerism performance derived from five candidate training spectra with primary peaks permitted to optimize to any wavelength between 400 and 700nm (D65 patch illumination, xenon source, minimization of  $OM_s$ ); resultant Gaussian parameters for the binned and non-binned optimizations

Relative to the number of primaries necessary to produce optimum metamerism reduction,  $K' = 7$  and  $8$  were shown to generate some performance benefits versus systems with six or fewer total primaries. Figure 55 summarizes trends in observer metamerism and variability as a function of primary count for the Kodak/AMPAS verification set when trained by itself. While  $OM_s$  and  $OM_{s,var}$  see diminishing incremental improvements above five primaries,  $OM_{s,max}$  experiences a notable jump with an eighth primary added.

Simulations to this point have restricted the reference stimuli to D65 illumination. To understand implications for other common light sources in photographic applications, the baseline analysis was repeated with each of the other three sources used for training. The only major differences versus the baseline results of Figure 53 were inclusion of eight primaries in the optimized design and verification spectra inclusive of all six patchsets under all four illuminants.  $OM_s$  results for the Kodak/AMPAS and SOCS verification sets when trained using the Kodak/AMPAS patches under each of the four illuminants in Table 16, respectively, are summarized in Figure 56. Additionally, training was attempted with a Kodak/AMPAS set illuminated by all four illuminants simultaneously (thus comprising 760 unique stimuli). Verification scenarios are shown for these two patchsets under each Table 16 illuminant individually along the x-axes. A few notable trends in the MPD designs are evident. First, for each verification illuminant, the best training comes from a matched training illuminant. The HMI-

illuminated verification set is best when HMI is similarly used for training, for example. Overall, the HMI training yields the best results in verification when averaged across all verification illuminants. The CIE F2 illuminant, on the other hand, is the poorest trainer of the set. Interestingly, the D65 trainer is also quite poor for generating HMI and F2-based verifications. For training F2-illuminated verifications, only the F2 trainer is adequate as each of the other three training illuminants are quite poor. The F2 spectra is significantly less continuous across the visible spectrum versus the other three, which may explain this performance, see Figure 57. Finally, the compromised trainer, inclusive of all four illuminants and the Kodak/AMPAS patches, does a solid job for all four verification scenarios for both of these patchsets.

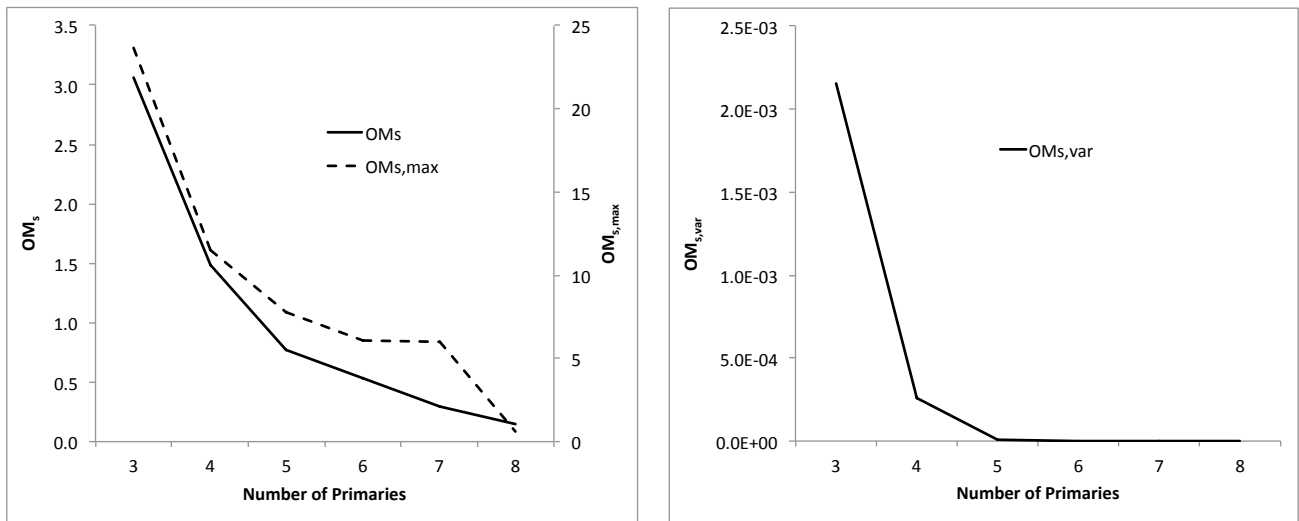


Figure 55. Pseudoinverse-optimized MPD metamerism performance as a function of modeled primary count (training via Kodak/AMPAS set, D65 patch illumination, xenon source, minimization of  $OM_s$ )

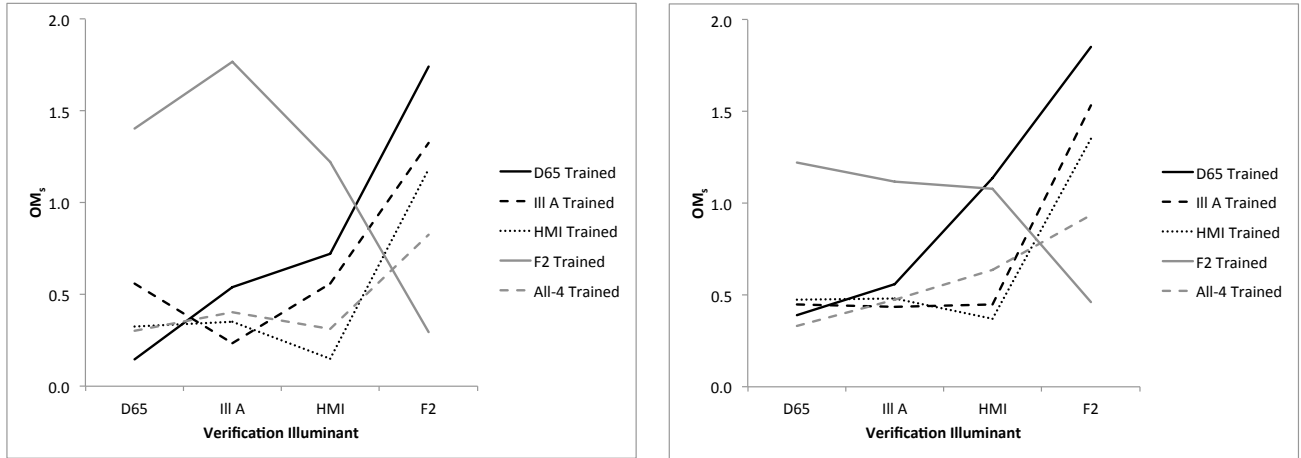


Figure 56. Pseudoinverse-optimized eight-channel MPD metamerism verifications as a function of training illuminant (training via Kodak/AMPAS set, xenon source, minimization of  $OM_s$ ); Kodak/AMPAS verification results (left) vs SOCS verification results (right)

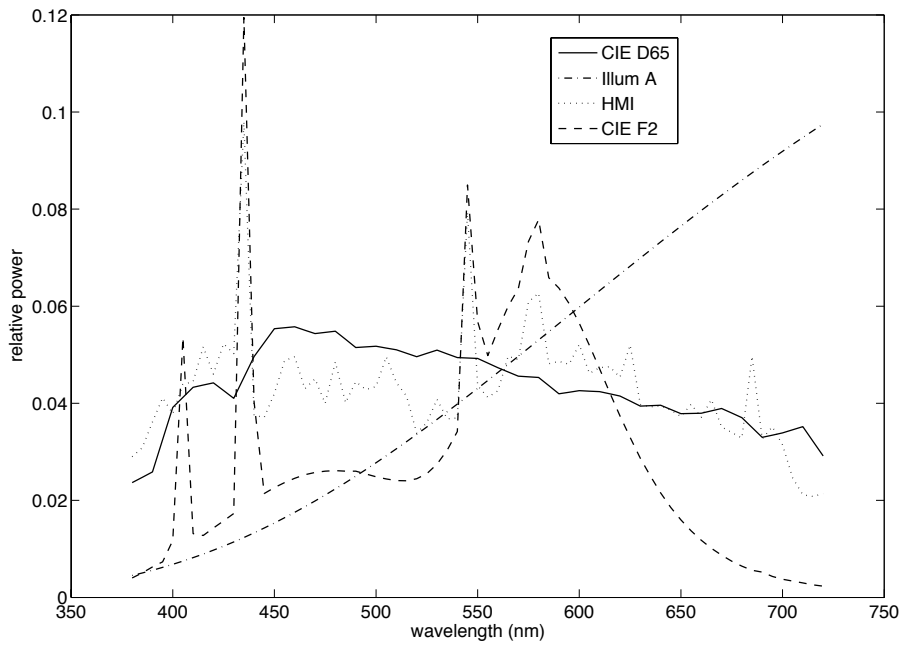


Figure 57. MPD training illuminant spectra

## Seven-projector MPD Prototype

The RIT MPD prototype was simulated based on results from the previous optimization studies, focusing specifically on the key learning gained from investigating the various training permutations. The initial modeling incorporated eight primaries iterated to minimize  $OM_s$  based on pseudoinversion training inclusive of the Kodak/AMPAS patchset and the “All-4” illumination spectra. Primary peak wavelengths were non-binned. One practical modification versus the previous models came in the form of the projector illumination source implemented. Consumer-grade Optoma DX339 projectors were identified to construct this prototype system, each using a UHP lamp rather than a xenon source with the spectra shown in Figure 51. Further, the contrast of these projectors was roughly 2,000:1 rather than the 10,000:1 xenon system previously modeled. The Optoma DX339 projector is a time-multiplexed, single-chip DLP system that uses a spinning filter wheel with six color segments engineered by Texas Instruments to generate reproduction of RGB video signals. For incorporation into the RIT MPD, the filter wheels were removed permitting a monochromatic modulation of the lamp spectra within the full resolution of the DLP chip (1024x768). To avoid impact from any internal color processing, signals sent to the projector were restricted to neutral scale values in 8-bit with all three color channels equivalent (user menu settings were ‘Default’ Brightness and ‘Graphics’ Gamma setting).

Figure 58 summarizes the best simulated Gaussian primaries for a  $K' = 8$  design cascaded with the source spectrum of the consumer UHP lamp. The resulting primary transmission filters are relatively narrow-band and so the change in projector illumination source from xenon to UHP for the actual prototype design yielded only minor observer metamerism performance penalties. As example for the Kodak/AMPAS verification set,  $OM_s$  actually improved very slightly with verification illuminants of D65 and Ill A while yielding a result nearly 100% poorer for the F2 verification. For the SOCS set,  $OM_s$  was 20% poorer for D65, Illum A and HMI and 100% poorer for F2.

Ultimately, Gaussian transmission filters which perfectly match the optimization results of Figure 58 do not exist and a compromised set built from commercially available materials was chosen instead. In Figure 58 are shown modeled primaries utilizing color filters closest in performance to the Gaussian predictions. These selections followed an exhaustive search of materials available from major manufacturers. The penalty for choosing from only currently available filters is significant. Verification simulations for the real filters yielded  $OM_s$  values approximately 8x worse than the ideal case across all of the previously tabulated patchsets and illuminants. Average  $OM_{s,max}$  suffered a penalty of approximately 3x

and average  $OM_{s,var}$  was twice the Gaussian model optimum. Clearly, a commissioned set of filters produced for subsequent prototypes would serve to radically improve the expected performance of the constructed system. At the same time, these metamerism assessments are reflective of the pseudoinverse color reproduction strategy of Equations 56 and 57 only. Additional experimentation with the RIT MPD takes advantage of further refinements to stimuli matches such as nonlinear optimization of radiometric scalars,  $\mathbf{R}$ , to generate standard colorimetric matches to example reference stimuli, see Ref [85].

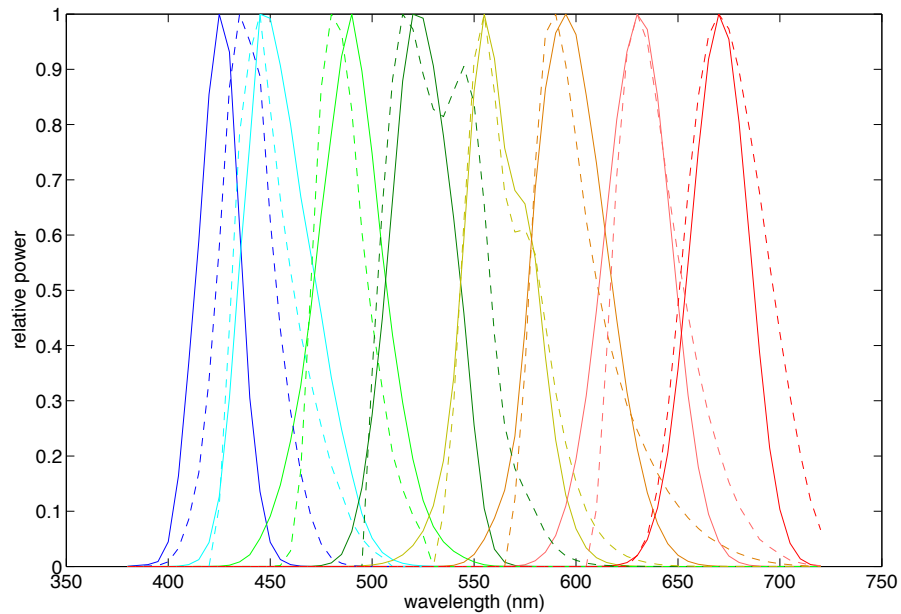


Figure 58. Optimized UHP-concatenated eight-channel primaries from Gaussian model (solid) versus primaries simulated from commercially available color filters (dashed) for RIT MPD

The prototype RIT MPD was constructed from individual Optoma projectors all modified to remove their color filter wheels and retrofitted with the individually chosen external filters. Optical paths were overlaid to a single screen, permitting reconstruction of additive multispectral images. Each projector was treated as a single, independent color channel driven via independent NVIDIA GeForce GT120 graphics cards from a modified Mac Pro. Because the combined black level of the MPD was the sum of individual projector black levels attenuated by the external filtration, EOTF curves were not normalized to a 0-1 radiometric scalar domain but rather measured on the black end against absolute contrast ratio of the maximum white output in each channel. Custom software was written to perform optical alignments and drive full resolution multispectral images to all color channels.

Installation and subsequent characterization of the 8-channel system yielded some measurable spectral differences from the Figure 58 models. Most was due to variability in UHP lamp spectra amongst the eight projectors, though some units also suffered from significant temporal spectral and radiometric drift. Not only did the eight projectors have measurable differences in absolute luminance output from each respective lamp, but the measured power from each varied by as much as 10-15% each time the full system was powered up. Upon implementation of temperature control equipment, an alternate configuration comprising only seven of the original eight primaries was ultimately deemed best for laboratory experiments (a particularly variable projector from the original eight was intentionally removed from the system). Modeled metamerism performance in this configuration proved effectively equivalent to the eight-channel simulation; a representative measure of the spectra for this system is shown in Figure 59 (though it should be noted that these spectral shapes were prone to visible variability over longer operating runs which will be discussed further in Chapter 8). Filter sets chosen in the construction of the system are summarized in Table 19. Colorimetric stability of the seven channels through the full dynamic range of the projector outputs is shown in Figure 60. The projector electro-optic transfer functions were also extensively characterized with no external filtration applied to permit radiometric modeling of the base lamp output, Figure 61. Both absolute and peak-normalized curves from one representative session are shown to exhibit the level of differing performance amongst the individual units.

Table 19. External filtration used with seven-projector RIT MPD

Channel 1	Channel 2	Channel 3	Channel 4	Channel 5	Channel 6	Channel 7
Schott BG42 (3mm)	Schott BG40 (2mm)	Schott KG5 (3mm)	Schott BG7 (3mm)	Schott BG38 (3mm)	Schott BG25 (1mm)	Schott BG3 (3mm)
Schott OG550 (1mm)	Schott RG630 (1mm)	Schott RG655 (2mm)	Schott OG515 (1mm)	Schott OG590 (1mm)	Schott GG475 (3mm)	Schott GG395 (2mm)

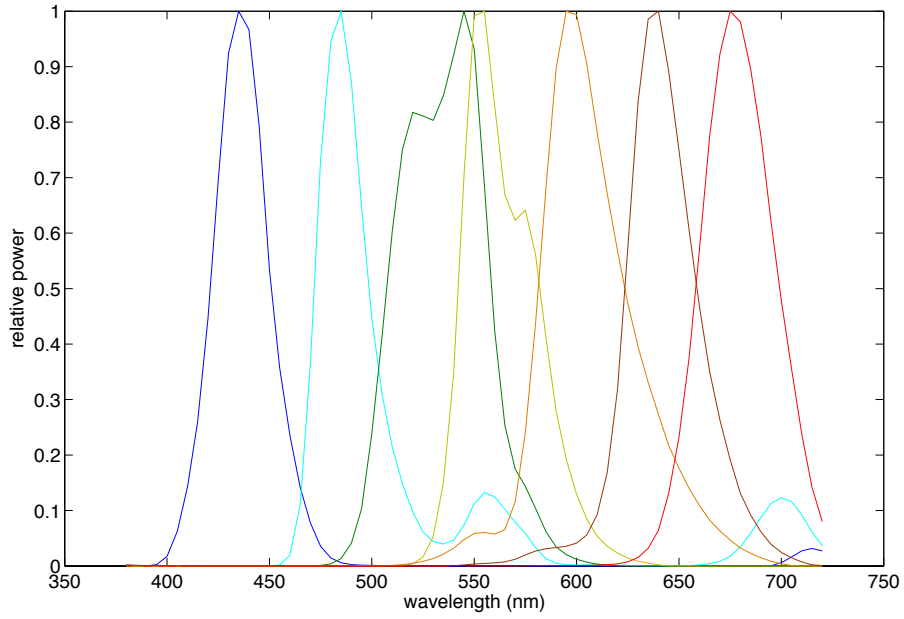


Figure 59. Measured primaries for constructed seven-projector RIT MPD

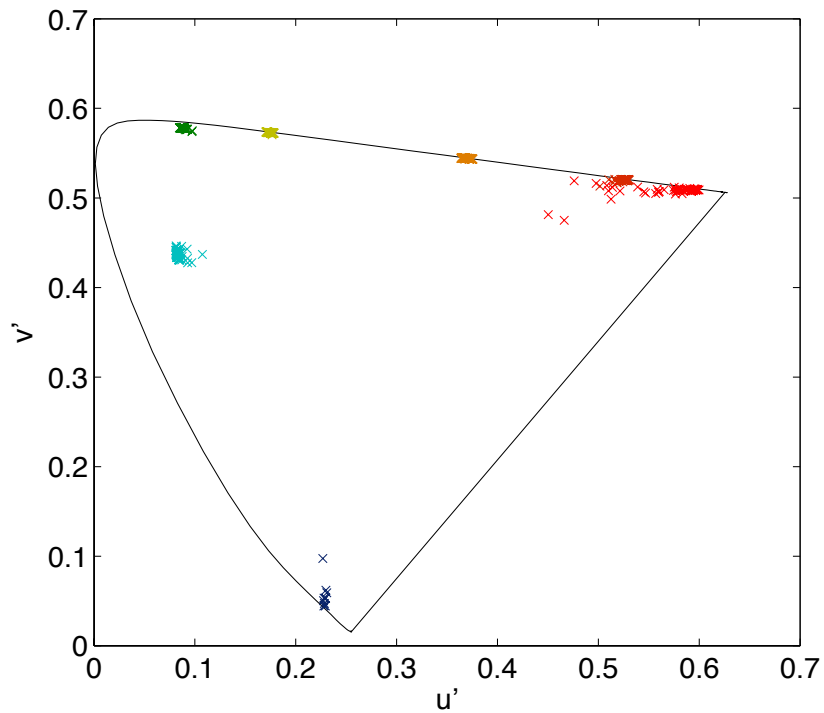


Figure 60. Colorimetric stability of the seven-projector RIT MPD primary channels over the 8-bit dynamic range; larger chromaticity variability is from darker measurements

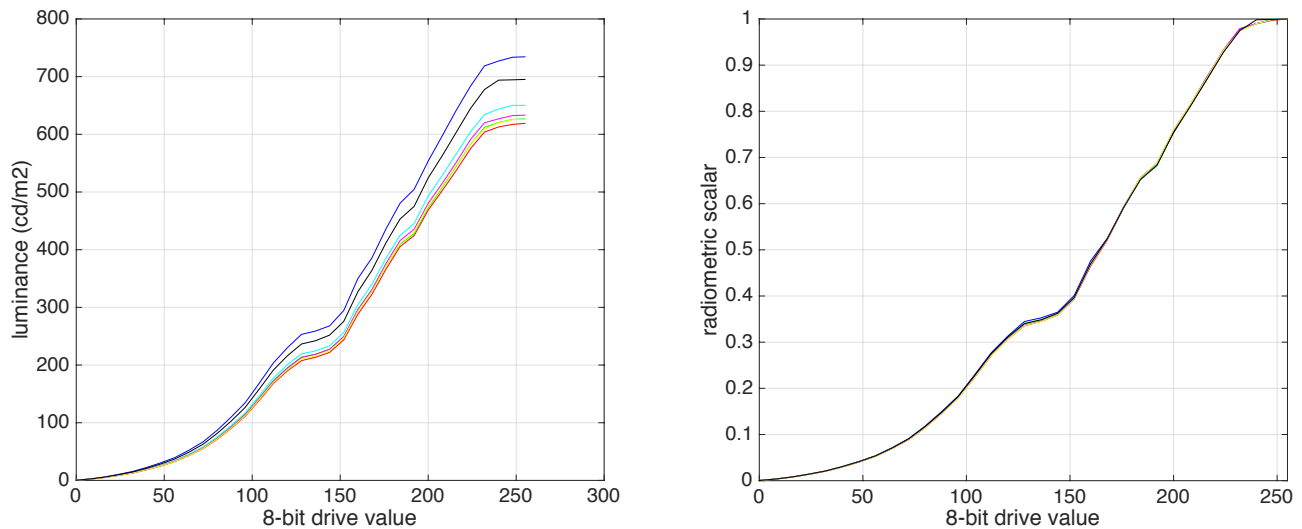


Figure 61. Representative measured EOTF LUTs for each channel of the seven-projector RIT MPD, absolute luminance (left) versus normalized to maximum output in each individual channel (right)

Subsequent spectral reconstructions of target stimuli using the seven-projector MPD were reasonably successful but temporal stability necessary for effective observer experiments remained a challenge. Figure 62 shows the drift in radiometric output from 6 of the 7 projectors tested over a short 15-minute trial, chosen as the time domain expected for subsequent observer experiments using the system. The maximum spectral power across the spectrum for each channel at time = 0 (following a 30-minute warm-up period for the full system) was used to normalize subsequent radiometric measurements at those same peak wavelengths. Interestingly, all six projectors show a loss of energy output with time but at very different magnitudes. Channel 3 experiences a more severe unexplained drop in output approximately 10 minutes into the measurements. Next, two different aim color patches, a MacBeth Color Checker magenta and green, were modeled assuming D65 illumination and reproduced on the system. Spectra were measured for each reproduction over the same 15-minute span with results shown in Figure 63. Again, this instability in spectral output using the seven-projector system is deeply concerning when considering needs for repeatability in observer experiments. The major issue lies in the different projectors failing at radically different rates; this would carry notable color drift consequences for the reproduced stimuli.

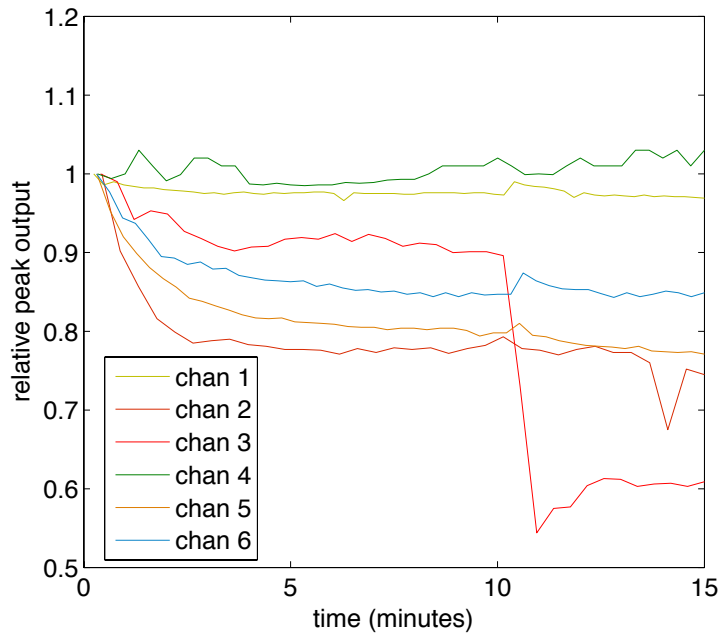


Figure 62. Normalized peak spectral output for 6 of the 7 channels of the seven-projector RIT MPD over a 15-minute stability test

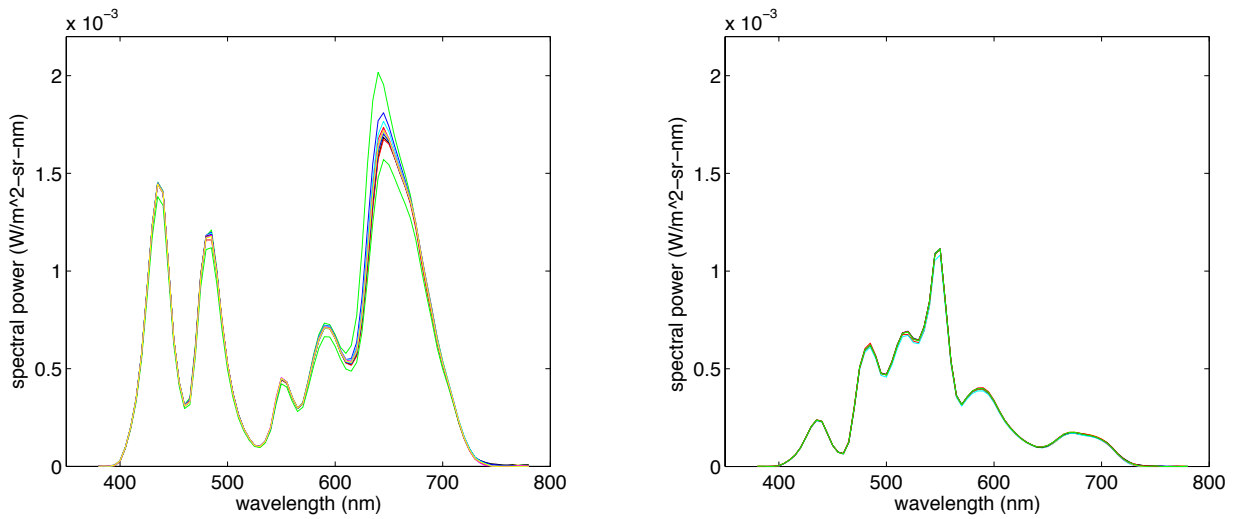


Figure 63. Spectral reconstruction stability for seven-projector RIT MPD over 15-minute trial; uniform interval spectral measurements of a reproduced MacBeth magenta patch (left) and green patch (right)

The gamut of the MPD in  $u'v'$  coordinates versus standard color spaces ITU-R Rec. 709, ITU-R-Rec. 2020 and SMPTE-431 is shown in Figure 64. Gamut area advantages versus even the monochromatic UHDTV performance specifications of Rec. 2020 are evident. Ref [85] and Chapter 6 offer significant analysis of the RIT MPD's modeled improvements in observer metamerism and variability versus several representative RGB displays. Of course, these improvements assume temporal stability in the system.

## **The One-projector Solution**

Ultimately, the temporal instability of the seven independent projectors comprising this first MPD prototype dictated this system would not be reliable for critical observer experiments. Even if daily radiometric calibrations were performed each time the system was powered on, the inter-projector drift in spectral and radiometric output after just 15 minutes of driving an intended reproduction to the screen was untenable. Thus, a second form factor was built with a single projector and seven optically isolated primary channels recombined in an integrating chamber for delivering a single area of uniform spectral intensity to an observer. This unit presents advantages in spectral and radiometric stability over extensive time periods and through multiple system power cycles but sacrifices capability to render actual images from multispectral content. The spectra of the primaries in this color patch generator are effectively identical to those shown in Figures 59 and 64. Channel EOTF performance is also fundamentally consistent with Figure 61, though summary measurements of the system used in observer metamerism experiments will be presented in Chapter 8. An exhaustive calibration routine was built for this one-projector MPD to account for fluctuations in channel spectra and EOTF characteristics as a function of power-cycling the equipment. Figure 65 shows optical configuration images for the 1-projector MPD.

## **Conclusions**

Emission spectra for the different color channels of a multiprimary display can be optimized to reduce observer metamerism and variability. An investigation of training permutations focusing on different metamerism indices, reference spectral stimuli (illuminants and reflective patches), primary counts, color filter bandpass constraints and projection illuminants delivered a prototype MPD design which was ultimately constructed for use in visual experiments.

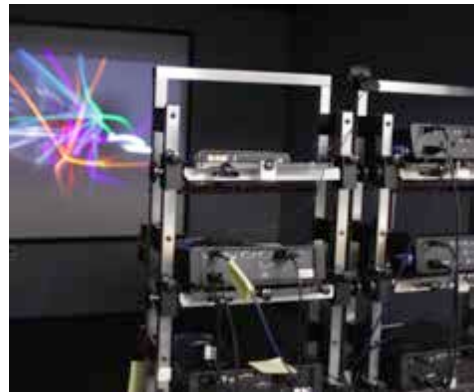
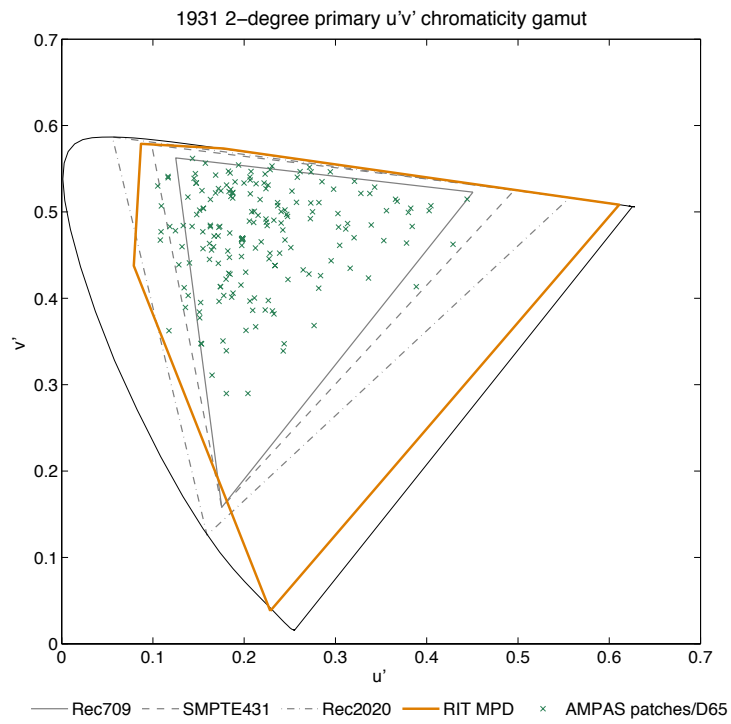


Figure 64. RIT seven-projector chromaticity gamut - color points representing Kodak/AMPAS color patches illuminated by CIE D65 shown for reference; also included are images of the physical form factor of the prototype MPD



Figure 65. one-projector RIT MPD design images showing organization of seven-channel filters, monochromatic Optoma DX339 illumination source, focusing optics and integrating sphere for generating uniform spectral color stimuli for observer experiments

Chapter 8 will summarize experiments to confirm the advantage of the seven-channel system versus contemporary displays (including laser systems) in minimizing observer variability when generating matches to reference spectra. These experiments have been designed to validate the utility of both the color vision models employed and the metamerism and variability indices suggested in this work.



## Chapter 8

---

### **Validating Observer Metamerism Models and the Multiprimary Display Design**

#### **Abstract**

It is intended that the vision models and metamerism indices of Chapter 6 and the optimized display system of Chapter 7 can be used in conjunction to show how variability of observer response to cross-media comparisons encompassing drastically disparate spectral stimuli is controllable. Many researchers have confirmed the magnitude of observer metamerism in color matching in both uniform colors and imagery in such scenarios but few have shown explicit color management with an aim of minimized difference in observer perception variability. The following results show that not only can observer metamerism influences be quantitatively predicted and confirmed psychophysically, but that intentionally engineered multiprimary displays can offer increased color gamut with drastically improved consistency of experience.

#### **Review of the Problem Statement**

Color matching functions (CMFs) defined for a single statistical standard observer are insufficient for describing spectral responsivity variability amongst a population of color normal observers. Several recent studies have shown where color management employed under the direction of the 1931 or 1964 standard observer alone yields unacceptable results for color critical applications such as reference display calibration and cinema color grading<sup>86,87</sup>. Models focused on more inclusive CMF definitions respectful of physiological variations suggest a wide distribution of CMFs is necessary to accurately reflect realities of color vision<sup>11,63,76</sup>. Further, color matching tasks performed by real and simulated observers have been shown to vary significantly as a function of the spectral signature of test stimuli<sup>8</sup>. In the cinema industry in particular, great attention is being paid to the potential for decreased quality of experience (QoE) as a function of emerging color trends in display technology. Next generation cinema and television systems promise to deliver a wider color gamut through implementation of laser, LED and quantum dot illumination under the mandate of ITU-R Rec. 2020 color specifications. These effectively monochromatic color primaries have been shown to greatly increase variability of color perception and color matching<sup>85</sup>. In an industry where tremendous investment is put into controlling color reproduction characteristics of

wardrobe, makeup and set decoration across a myriad of image capture and display technologies, the potential for exaggerated differences of perception amongst audience members is a direct assault on the care taken by directors, cinematographers and colorists to dictate every element of the communicated imagery.

A solution to the resultant increase of observer variability that accompanies a push for larger color gamut and more selective spectral primaries may lie in multispectral color management and multiprimary display systems. In Chapter 7, the design of a seven-channel multiprimary display (MPD) engineered to intentionally minimize observer metamerism and to narrow observer variability of perception while simultaneously delivering increased color gamut was outlined. Here, color matching experiments configured to validate the color models implemented and the display systems built will be described.

### **Other Experiences with Highly Metameric Color Matching**

Asano, et al. have sought to characterize the magnitude of observer metamerism present in color matching tasks associated with both uniform expanses of color and real images<sup>88</sup>. In their work, a commercial LCD display was pitted against a pico laser projector to assess how much variation would result from intentional color corrections made by real observers. Reference stimuli were shown on the laser projector and again on an LCD display in a paired comparison. Observers were asked to manipulate the mean CIE L\*a\*b\* of the LCD image until it best matched the fixed laser projector image. From their results, they found inter-observer variability for the matches was significant versus any intra-observer noise. Further, with three different images used, they noted the mean population match as interpreted by a 1964 standard observer summary color difference metric between displays was different in each case. Their conclusion was that field size changes to each individual's CMF were at play as the deviations between imagery with lesser and more spatial complexity could be reasonably simulated by intentional changes in CIE2006 field size predictions. Smaller field sizes correlated with the results from the more spatially complex samples. As visualization of the magnitude of difference in matches, Figure 66 shows the sRGB rendered LCD images matched to the baseline laser projector images by five extreme observers and the predicted 1964 observer for both the uniform color stimuli and high spatial complexity image.

As complement to the work of Asano, et al., the current experiments serve to validate that observer color matches across disparate display technologies can on average be predicted and that failures of observer metamerism and variability in

cross-media applications can be minimized with an intentionally designed display system. Results are intended to confirm the vision models and metamerism indices derived in Chapter 6, including the CMF sets of CIE2006, Sarkar and Heckaman and the color difference and variability indices of Equations 50-53.

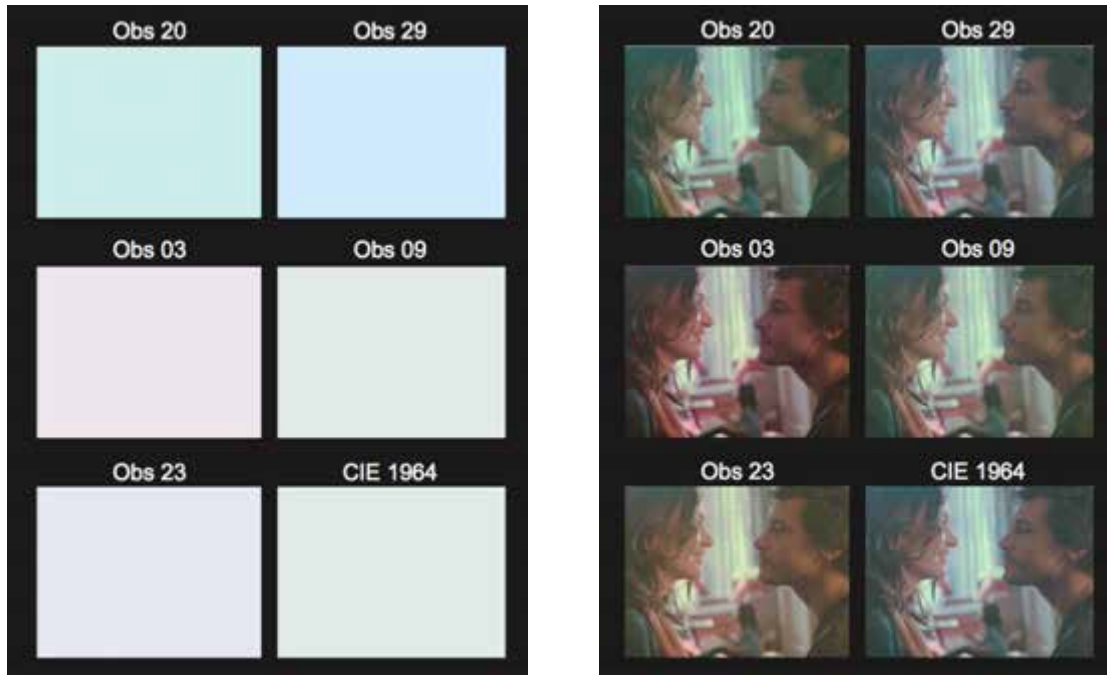


Figure 66. Example observer color matching variability (reproduced from Asano, et al.<sup>88</sup>) showing rendered sRGB reproductions for a uniform color patch (left) and a high spatial complexity image (right)

## Experiment Equipment

Observers participating in this experiment were asked to assess color matches from uniform stimuli generated in a simultaneous paired comparison. Three different emissive color systems were compared for observer preference in confirmation of the developed observer metamerism models. The first was the one-projector RIT MPD introduced in Chapter 7, comprising seven spectral channels optimized to deliver minimized observer metamerism,  $OM_s$ , against the Kodak/AMPAS training patches illuminated by four practical cinema light sources. A neutral illumination spectrum from one retrofitted Optoma DX339 is focused onto the specified grid of transmissive color filters using 8-bit native modulation and a spatial segregation scheme. The separately modulated channels are then recombined through focusing optics and an integrating sphere in order to present a uniform color patch to the observer. This system is not capable of projecting

multispectral image content. The displayed spectra fluctuated slightly over the course of all experiment sessions conducted due to some instability in the consumer-grade UHP lamp but a representative measurement is shown in Figure 67. Also shown are representative peak-normalized EOTF curves from the seven primaries for the system. Even though a single lamp powered the system, spatial non-uniformity across the image field yielded slight variation amongst these response functions for all of the channels. Images summarizing the optical configuration are seen in Figure 68. Exhaustive calibration was executed at the start of each experiment session to account for slight spectral and radiometric drift in the equipment.

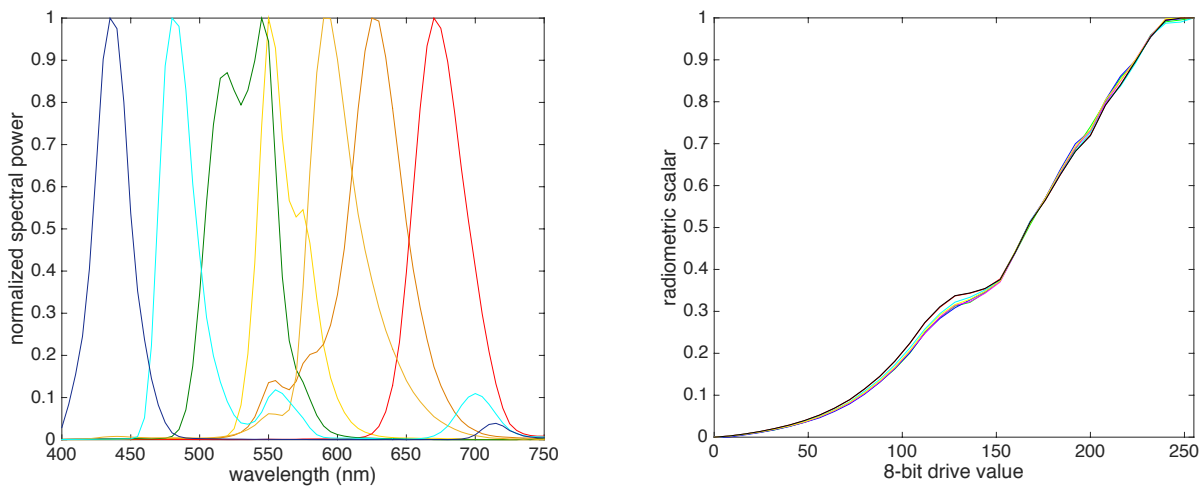


Figure 67. one-projector RIT MPD representative spectral output and EOTF

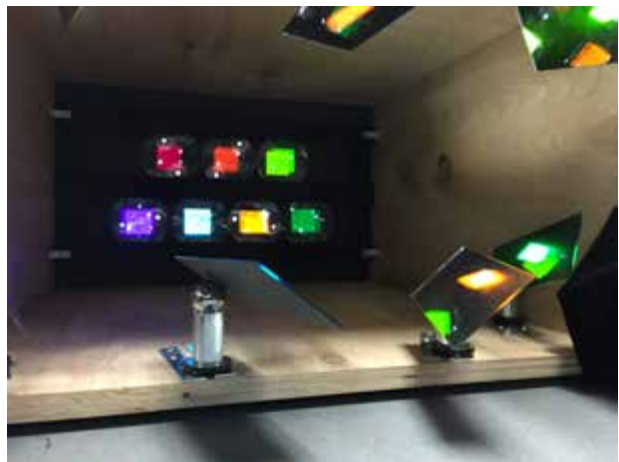


Figure 68. one-projector RIT MPD illumination optics

The second system was the Panasonic PTAX200U LCD projector capable of 1920x1080 resolution employing an optical block with three independent LCD modulators, internal color filters and a splitting/re-combining prism to isolate the RGB signal paths. This projector is driven natively in 8-bits and focused onto a diffuser screen so as to produce a uniform color patch to the observers. This is the same projector characterized in Chapter 6 and delivers a native SMPTE-431 P3 gamut. It is thus appropriately representative of contemporary standard digital cinema color reproduction. Spectra and EOTF, again, varied slightly over the course of experimentation but representative samples are presented in Figure 69.

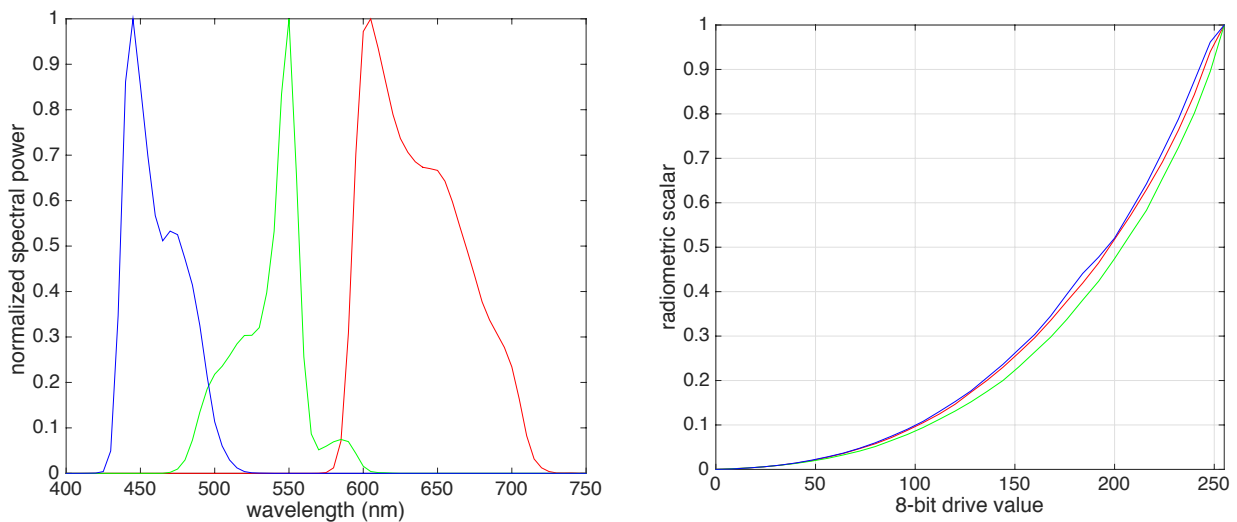


Figure 69. Panasonic PTAX200U representative spectral output and EOTF

The final color system comprised a Necsel Matrix 250 laser illumination engine and Necsel Intelligent Controller used to modulate laser output intensity. The RGB laser emissions conform to center wavelengths of 465, 525 and 638nm, very close to specifications for ITU-R Rec. 2020 wide-gamut primaries (467, 532 and 630nm). Output spectra were confirmed using a PhotoResearch 655 spectroradiometer with 8nm bandwidth and 5nm sampling. Radiometric control was implemented using pulse-width modulation (PWM) at 50Hz, near threshold for human flicker fusion. To minimize flicker further, each 20msec PWM period was split into 200 duty cycle spans that were alternately indexed with 'on' state commands according to input drive percentages in 0.5% increments. White balance was controlled to the three independent channels via an individual amperage setting. Figure 70 summarizes representative spectra and EOTF responses for the

system. Influences of variable laser 'on' state rise and fall times are evidenced in the non-linearity of the three channel EOTFs as a function of duty cycle. The laser outputs were directed into an integrating sphere to present uniform color stimuli to the observer. Cooling fans directed onto the system also served to vibrate the laser sub-assembly slightly, thus eliminating any visual speckle from coherent diffraction. Some fringe aberrations were visible through the integrating sphere exit port and observers were asked to ignore those in making color assessments. Images of the optical assembly are shown in Figure 71.

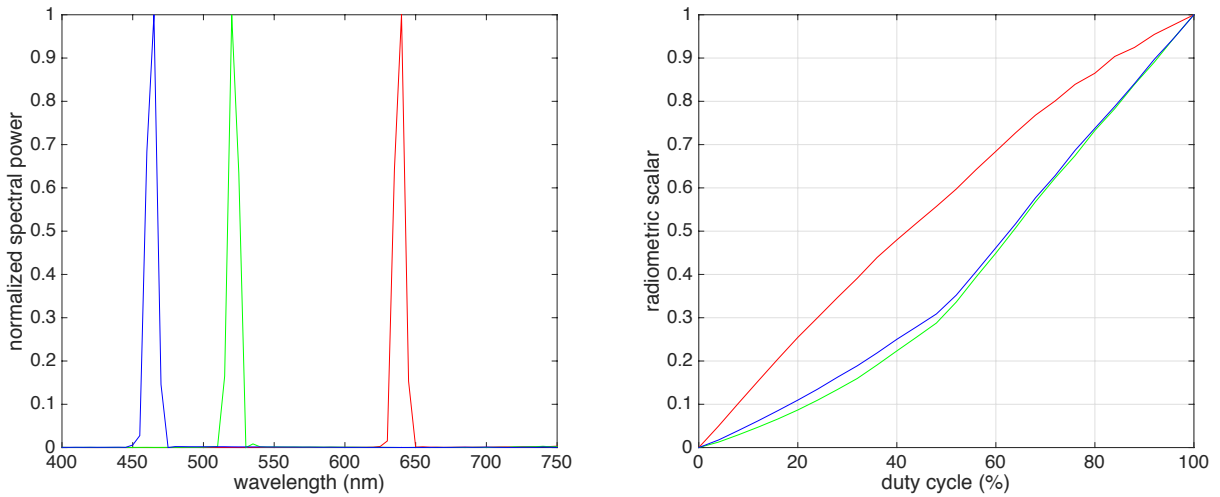


Figure 70. Necsel Matrix 250 Laser representative spectral output and EOTF

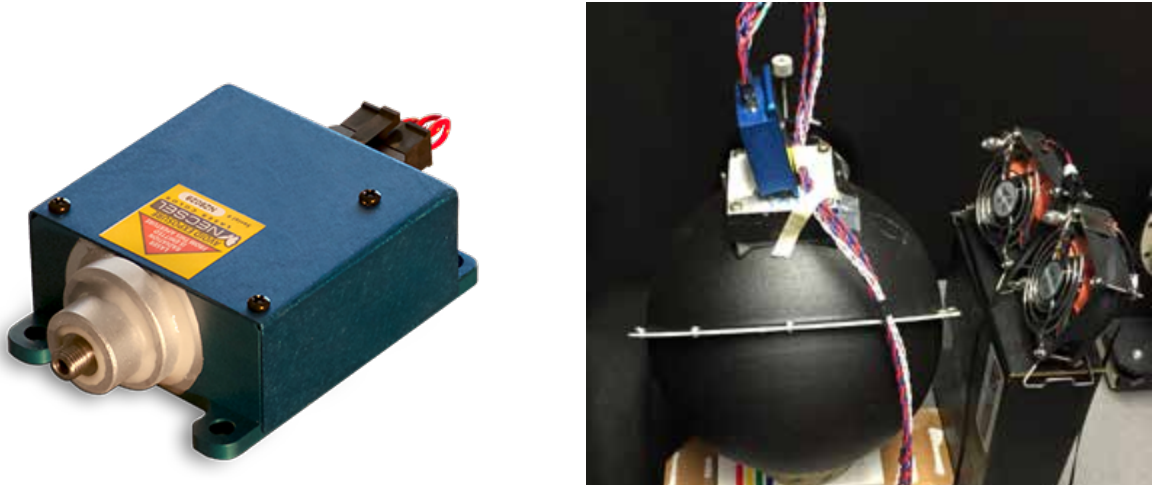


Figure 71. Necsel Matrix 250 Laser and optical assembly

Reference stimuli for color matching were generated using Color-aid artist papers and a JUST LED light booth set to CIE D65 output. The spectral emission from each of the available papers were measured and then a subset was chosen based on delivering a representative gamut of observer metamerism capabilities across all three display systems. Care was also taken to not deliver any color stimuli out of gamut for the three-color reproduction systems. The nature of LED illumination in the light booth allowed for significant spectral variability in the reference stimuli. Representative spectra of 25 sample colors used in the experiments is shown in Figure 72. Figure 73 shows the experiment setup as experienced by the observer. The reference color patch is visible through a round port on the front of the light booth (left) and the exit ports of the compared display integrating spheres are isolated to the right. It should be noted that the form factor of the MPD demanded it always be the left of the two reproduced color systems while the three-channel systems occupied the right port. For each experiment session, the room lights were turned off and the observer was aware only of the three color stimuli in front of them. Each sample patch subtended an approximate  $2^\circ$  visual field.

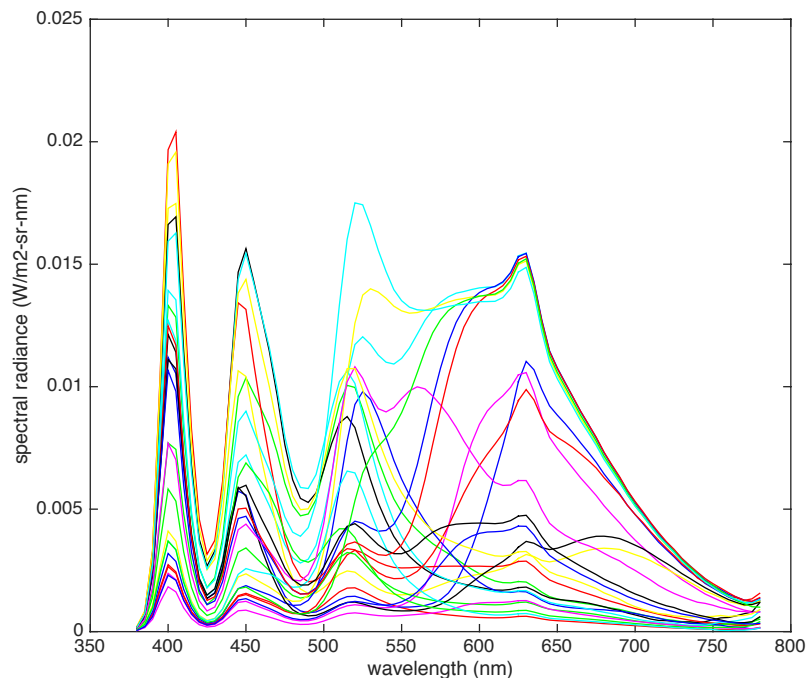


Figure 72. Color-aid paper / JUST lightbooth reference spectra

## Equipment Calibration

A total of 88 observers took part in color matching experiments over the course of several weeks. Each of the four optical assemblies used drifted with daily power-cycling and so an exhaustive calibration scheme was executed at the beginning of every observation session. The JUST light booth was turned on and allowed to warm up for 20 minutes before the spectra of each reference Color-aid paper intended for that day's experiment was measured. A Teflon diffuser was also measured within the booth to quantify radiometric output and to provide a reference white for all color difference formulae for that session. All spectral measurements were taken from the vantage of the seated observer with the PR-655 spectroradiometer.



Figure 73. Two-alternative forced-choice experiment setup with aim stimuli produced using Color-aid papers in lightbooth on the left and reproduction systems presented through integrating sphere exit ports for two displays at a time on the right.

Primary spectra for each of the display systems were measured so that reconstruction models could be customized to exact system performance on a given day. Of the different systems, the one-projector RIT MPD tended to drift the most spectrally due to instability in the UHP lamp. Figure 74 shows sample measurements taken over the course of six months of operation with the major

variability noted between 500 and 580nm where the mercury arc UHP lamp has a distinct spectral transition from low to high power (see Figure 51). With each spectra measurement, a white and a black calibration were also performed. Absolute radiometric scalars necessary to gain the peak-normalized spectra to match the black-corrected white output were needed to establish radiometric translation in all channels consistent with the reference stimuli reproduction models. EOTF responses were also re-measured periodically as these were used to generate drive values responsible for specific spectral output as well as to refine spectral matches in subsequent calibration steps.

With the daily characterization of each system complete, spectral models were used to generate aim drive values for each display with intention to match the reference Color-aid stimuli under constraint of each experiment's objectives. Ideal values were computed in simulation utilizing constrained nonlinear optimization per patch and sent to each display for measurement affirmation. An iterative adjustment loop was then executed to refine drive values until color difference indices measured against aim were as consistent as possible. These refined values were then saved for use during the observer experiments. The full process was completed every day experimental data was collected.

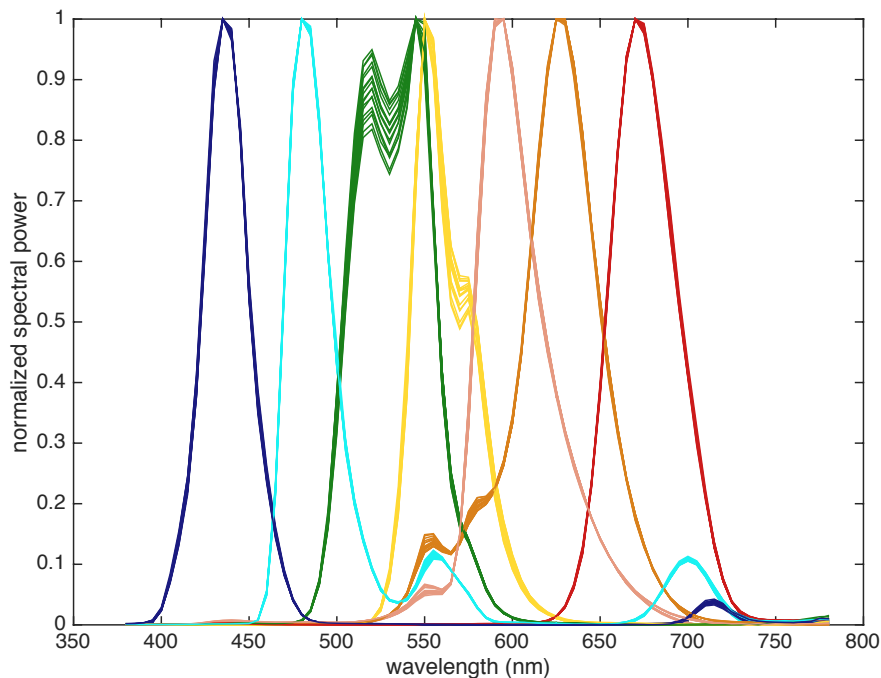


Figure 74. Spectral variability of 1-projector MPD over 6 months of use

## Experimental Procedure

Validation of the RIT seven-channel MPD design for reducing observer metamerism was executed using a two-alternative forced-choice experiment in four optimization configurations. In Experiment 1, the one-projector RIT MPD was compared to the Panasonic SMPTE-431 P3 display system. Both systems were calibrated to deliver an excellent metameric match to the 25 Color-aid paper reference spectra using the 1931 2° standard observer. This scenario mimics typical color management strategies employed in professional cinema equipment calibrations. The Panasonic system theoretically yields a single ideal match within the limitations of quantization error in the 8-bit drive system as well as system noise. The one-projector MPD, on the other hand, is over-specified and thus a nonlinear co-optimization was executed where observer metamerism,  $OM_s$ , was minimized using the seven primary channels under constraint of a perfect standard observer colorimetric match. The color differences achieved are summarized in the middle row of Figure 75. 28 observers participated across four different days of testing and the tabulated data shows the calibrated performance accomplished across each session. Most samples deliver  $\Delta E_{94}$  well below 1.0 in each system with reasonable consistency across the experiment duration and with the two displays evenly matched. The top row of Figure 75 shows the observer metamerism performance realized in each system using standard observer color management. Here, the three-channel system is inferior to the MPD for all but a very few of the patches as is consistent with results summarized in Chapter 6.

During the course of the experiment, participating observers were seated directly across from the middle of the three stimuli. Room lights were turned off and a short period of dark adaptation was permitted while experiment instructions were delivered. One at a time, the Color-aid reference papers were placed in the light booth and presented to each participant as the aim color to be compared to each of the other two stimuli visible. The Panasonic and MPD systems were then controlled to display their optimized attempt for a color match to the shown aim. The observer was asked to enter their choice for which of the two was a better color match to aim using keyboard input. Observers were instructed to ignore any optical aberrations or imperfections in the colored circles. They were also instructed to simply select which of the two test stimuli was a better match to the reference in their opinion and they were encouraged not to be concerned about any trending in their selections. Observers had a short time to rest between each selection as Color-aid papers had to be manually replaced in the light booth.

Experiment 2 used the same two displays and 25 Color-aid reference spectra; however, the optimization scenario enforced on the two systems was a minimization of  $OM_s$  versus reference irrespective of consequences to standard observer colorimetric match. Figure 76 shows the achieved calibration performance for the two display systems across 4 different observation sessions. Versus Figure 75, the one-projector MPD yields far superior observer metamerism with many patches yielding values less than 0.5. The Panasonic display, on the other hand, has improved very little versus the optimization of Experiment 1, showing values of 1.0 - 1.5 and higher. Both systems suffer penalties to standard observer color difference with a number of patches approaching a  $\Delta E_{94}$  of 4.0 on each.

Experiments 3 and 4 repeat the scenarios of Experiment 1 and 2 but with the Panasonic display replaced by the Necsel laser system. Statistics for optimized performance can be found in Figures 77 and 78. In Experiment 3, only 13 of the original 25 Color-aid patches were used and the participants completed observations across three days. Because there are no color gamut issues, each system achieved standard color errors versus aim typically well below 0.5 and were generally well matched. For observer metamerism, however, the laser system was well deficient with magnitudes for  $OM_s$  near 5.0 for most. This is, again, consistent with findings from Chapter 6. For Experiment 4, a hybrid presentation of display stimuli was implemented across two days of testing. Six of Experiment 3's Color-aid patches were selected and shown to the observers with the identical respective standard observer optimization of Experiment 3. The same six patches were then repeated but with each display re-optimized to minimized observer metamerism. This served to confirm findings from Experiment 3 and permit direct comparison to the observer metamerism minimization using a consistent group of observers. Calibration performance in Figure 78 reflects this approach with patches 1-6 yielding statistics very similar to their counterparts in Experiment 3 and patches 7-12 (the repeats with minimized observer metamerism) generating superior  $OM_s$  and degraded standard observer matches.

Finally, Table 20 summarizes demographic data for the observers in each of the four experiments. Prior to participation, each was screened for normally functioning color vision using Ishihara color blindness plates, #1-13. Though there are other more rigorous color vision screenings such as the Farnsworth-Munsell 100-hue test, results afforded by these were considered outside the scope of the present work; there was no intention to attempt correlation between performance on such tests and the color matching selections of the present experiments. The objective statement for this work emphasizes the identification of color matching variability amongst *color normal* observers and it is the intent that a single binomial

screening methodology is sufficient for identifying appropriate participants. For the sake of this work, *color normal* implies an observer able to successfully read the first 13 plates of the Ishihara set. Only one male observer was rejected for a red-green deficiency during observer screening. For context, 60 unique observers, 24 female and 36 male, completed the 88 observation trials. The rate of color blindness in the male candidate population was thus 1 out of 37, reasonably aligned with demographic expectations.

Table 20. Experiment participants

	<b>Experiment 1</b> Panasonic P3 min $\Delta E$ (1931)	<b>Experiment 2</b> Panasonic P3 min $OM_s$	<b>Experiment 3</b> 2020 Lasers min $\Delta E$ (1931)	<b>Experiment 4</b> 2020 Lasers min $OM_s$
<b>Male / Female</b>	17 / 11	14 / 11	16 / 8	5 / 6
<b>Age 17-24</b>	19	19	16	7
<b>Age 25-39</b>	3	3	2	1
<b>Age 40-60</b>	6	3	6	3

## Results

In all four experiment variations, the rendered observer metamerism as defined from the Sarkar CMF set for displayed patches on the RIT one-projector MPD versus the compared three-channel system was superior for all but a small number of displayed stimuli. And in those few cases, the two systems were effectively the same. If the models are statistically sound, it would be logical for any single observer with unknown individual CMF to still preferentially select the MPD in forced choice comparison across all viewed patches in a test session. Histograms for number of observers versus individual percentage preference to the MPD in Figures 75-78 verify that the multiprimary display is indeed the more likely chosen stimulus match to a Color-aid reference in any particular observation. Qualitatively, the larger the discrepancy between the MPD and three-channel  $OM_s$  average, the more the histogram trends to the right or 100% preference to the MPD. For example in Experiments 1 and 2 where the Panasonic spectra were less metameric than the laser spectra of Experiments 3 and 4, there are a few observers who did preferentially select the SMPTE-431 device (histogram values less than 50%). In Experiment 3 where a minimization to the 1931 standard observer color difference was attempted for the laser, two observers showed 50% or less preference to the MPD, suggesting they might themselves be characterized very near the 1931 CMFs.

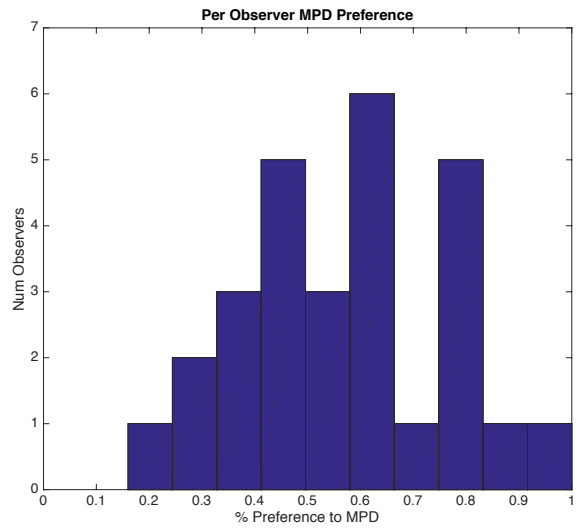
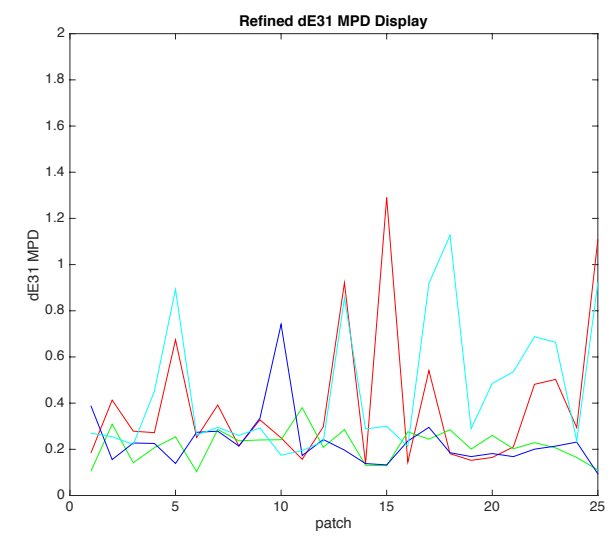
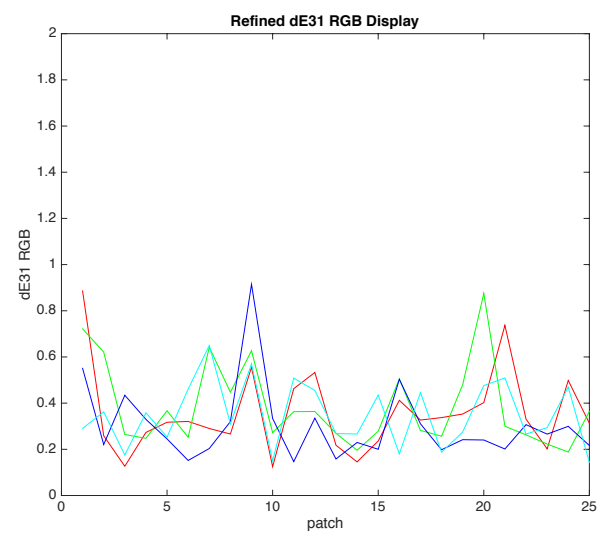
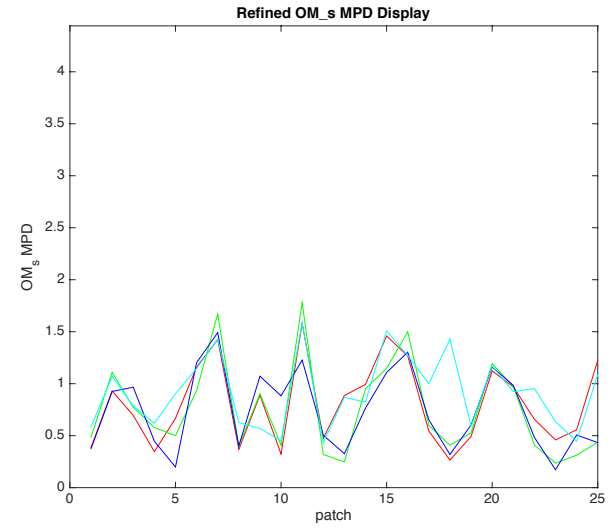
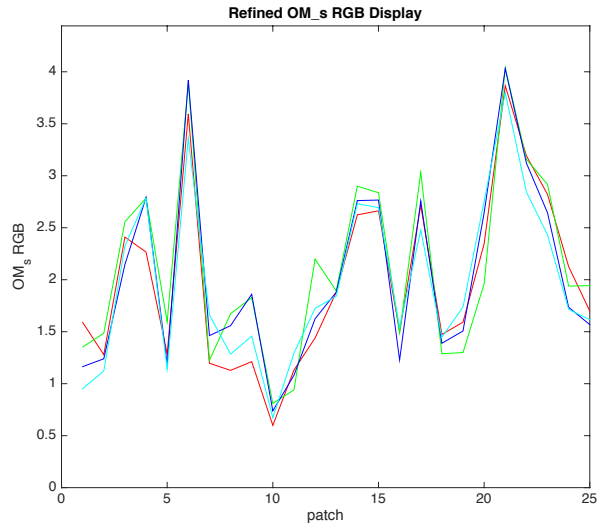


Figure 75. Measurements of 25 test stimuli for Experiment 1 across 4 test sessions - minimization of  $\Delta E$  versus Color-aid reference stimuli on Panasonic P3 projector and RIT MPD

$OM_s$  for Panasonic versus RIT MPD (top row);  $\Delta E_{94}$  for Panasonic versus RIT MPD (middle row); histogram of observer preference to selection of RIT MPD in paired comparisons (bottom row)

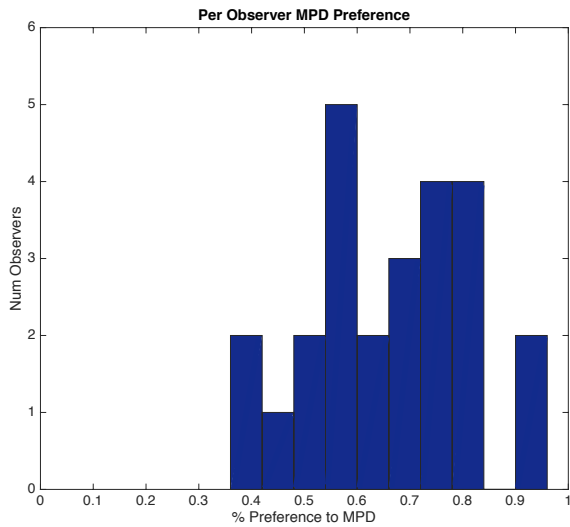
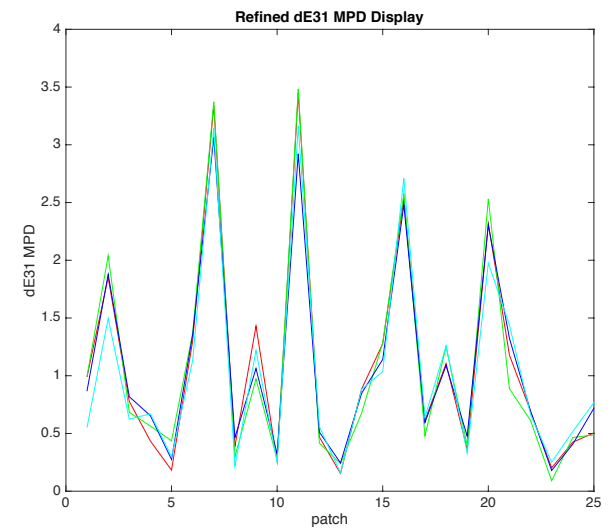
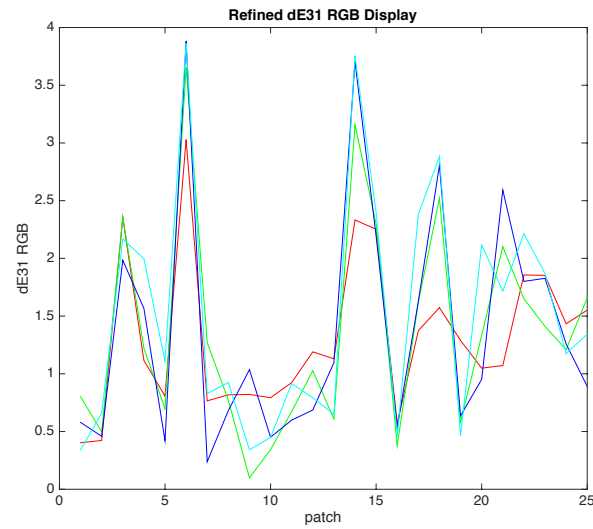
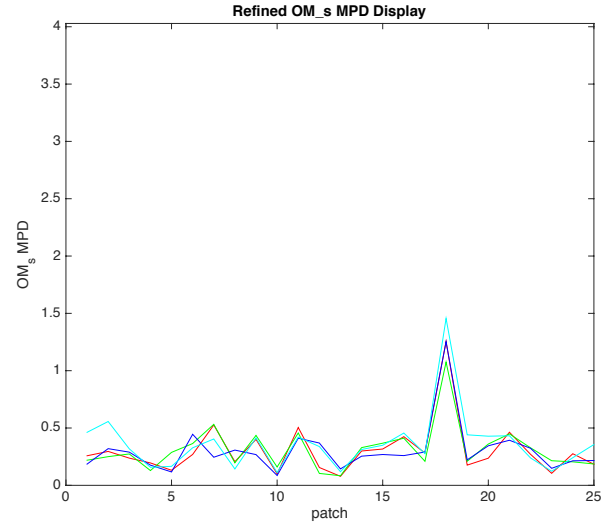
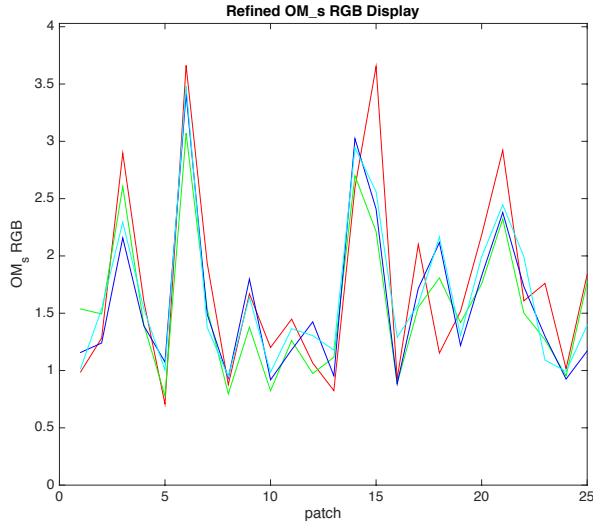


Figure 76. Measurements of 25 test stimuli for Experiment 2 across 4 test sessions - minimization of  $OM_s$  versus Color-aid reference stimuli on Panasonic P3 projector and RIT MPD

$OM_s$  for Panasonic versus RIT MPD (top row);  $\Delta E_{94}$  for Panasonic versus RIT MPD (middle row); histogram of observer preference to selection of RIT MPD in paired comparisons (bottom row)

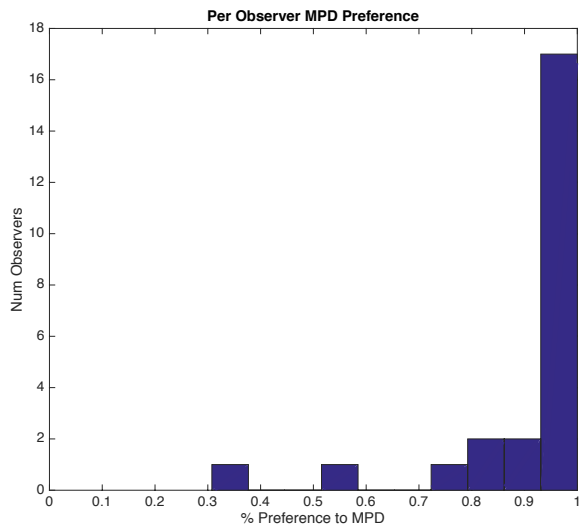
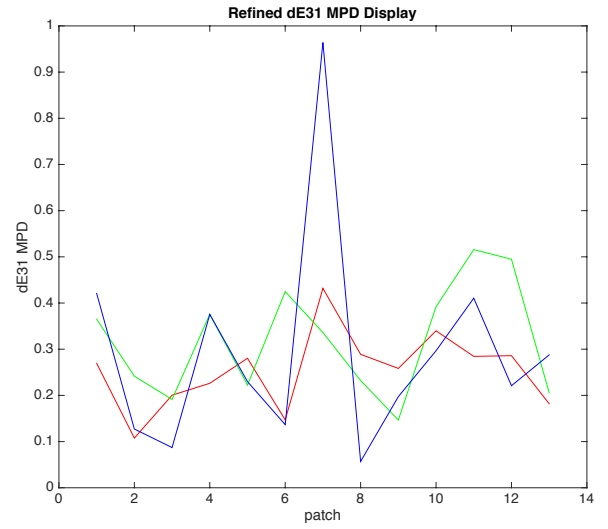
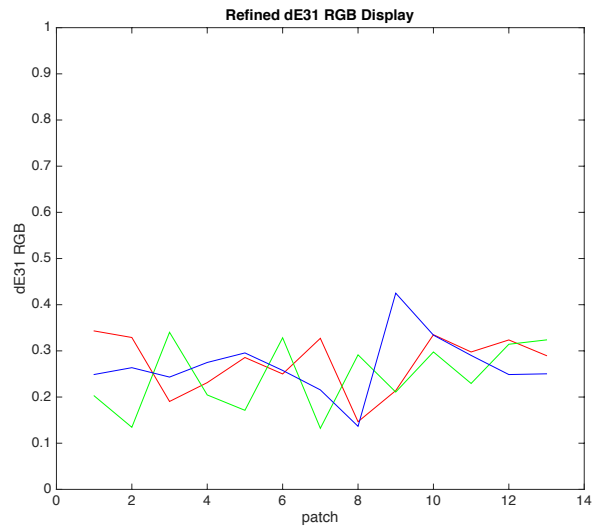
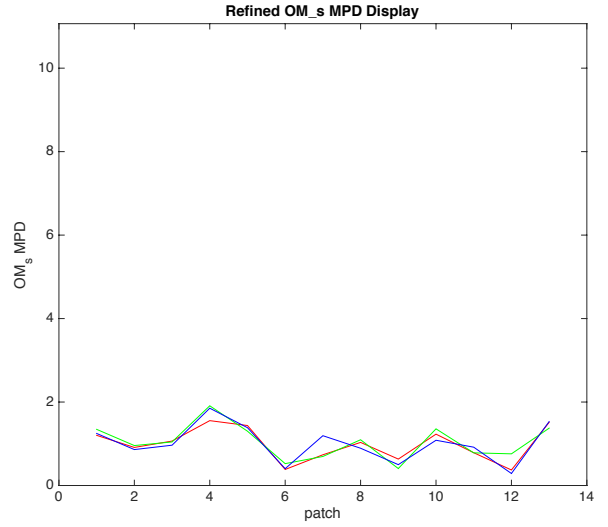
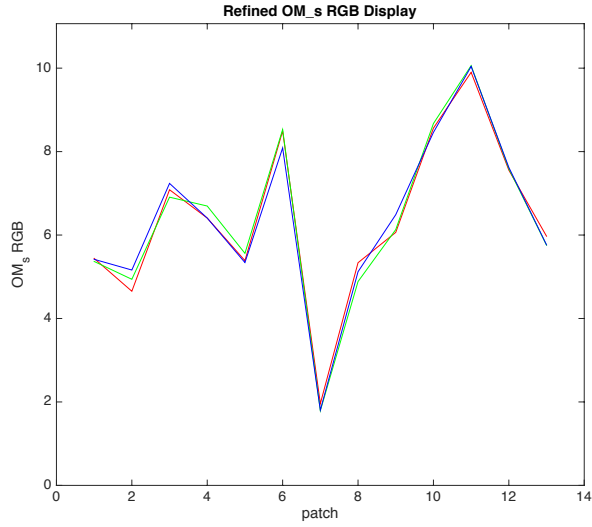


Figure 77. Measurements of 13 test stimuli for Experiment 3 across 3 test sessions - minimization of  $\Delta E$  versus Color-aid reference stimuli on Rec2020 Laser projector and RIT MPD

OM<sub>s</sub> for Laser versus RIT MPD (top row);  $\Delta E_{94}$  for Laser versus RIT MPD (middle row); histogram of observer preference to selection of RIT MPD in paired comparisons (bottom row)

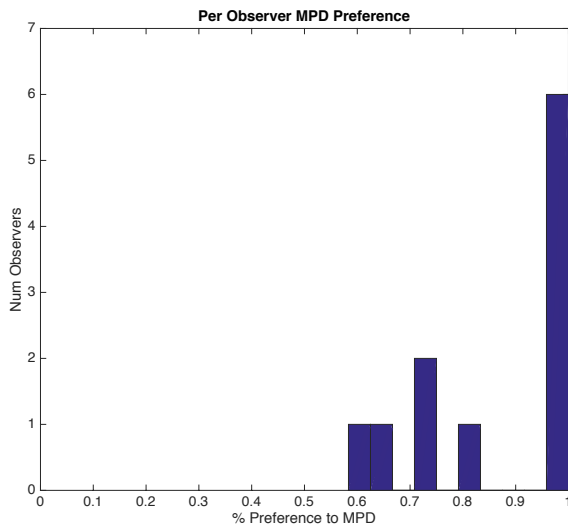
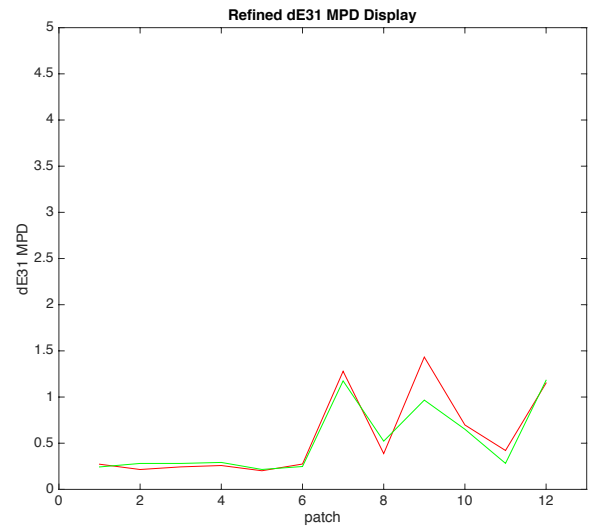
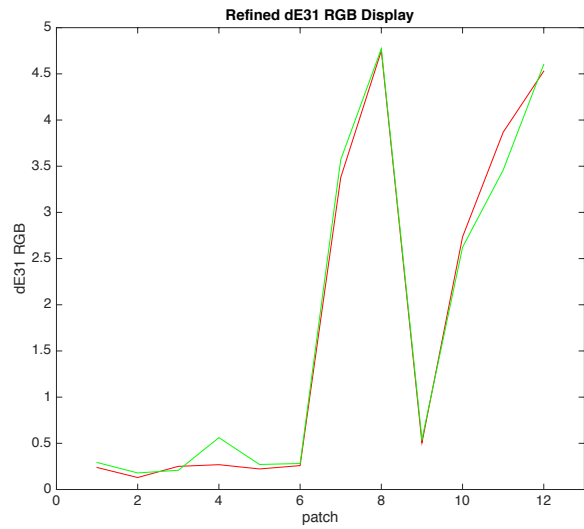
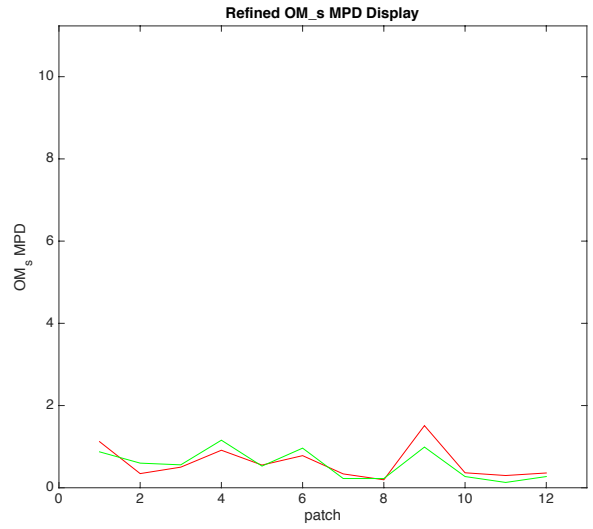
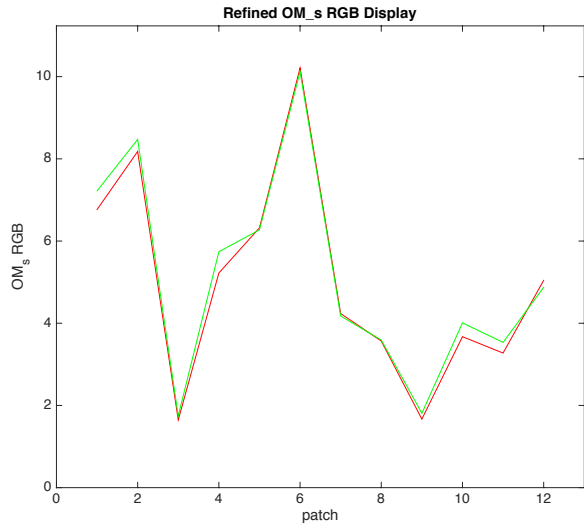


Figure 78. Measurements of 12 test stimuli for Experiment 4 across 2 test sessions - minimization of  $OM_s$  versus Color-aid reference stimuli on Rec2020 Laser projector and RIT MPD

$OM_s$  for Laser versus RIT MPD (top row);  $\Delta E_{94}$  for Laser versus RIT MPD (middle row); histogram of observer preference to selection of RIT MPD in paired comparisons (bottom row)

Particularly interesting in Experiments 3 and 4 are that several observers picked only the MPD, even for the cases where the laser and MPD showed identical matches to the reference stimuli according to the 1931 observer. Each commented at the end of their session that there must have been something wrong with their observations in that the laser-based system never seemed a good match to the Color-aid reference. Others commented that the position of the MPD nearer to the Color-aid reference in Figure 73 might have caused them bias in their selections. This was debunked in Experiment 1 where the light booth was positioned to the far left of the visual field as in Figure 73 for exactly half of the participants (14) and to the far right (adjacent to the three-channel sample port) for the remaining half. The mean observer preference to the MPD when it was nearer the lightbooth was 64% of color patch observations with a standard deviation across observers of 13%. The mean preference to the MPD when it was farther from the lightbooth stimuli than the three-channel display was actually higher at 72% with a standard deviation of 19%. There was thus no adjacency bias evident and the light booth was positioned only on the left for Experiments 2-4.

Figures 79-82 next show the preference to selection of the MPD in the forced-choice comparisons for every individual patch. These results are plotted against 5 different observer metamerism indices for each of the four experiments to assess where correlation is strongest. The models compared include  $OM_s$ ,  $OM_c$  and  $OM_h$ , the straight observer metamerism magnitude according to the Sarkar, CIE2006 and Heckaman CMF sets, respectively. Next are plots against simple 1931 standard observer color difference. Last is a plot versus the Sarkar CMF observer variability index,  $OM_{s,var}$  which is the calculated volume of error ellipsoids associated with the spread of observer match variability. For each plot point, the mean observer metamerism of the reproduced stimuli versus the Color-aid reference was computed for both the MPD and the associated three-channel display. Next the net difference by which the three-channel system's index exceeded the MPD's index in each metric was used for the plot's abscissa values. Most plot values were thus positive as the three-channel system underperformed the MPD in all permutations for nearly all of the observed stimuli. As the magnitude of this deficiency increases, it would be expected that the MPD would be more likely selected as a better match to the Color-aid reference in the paired comparison. It might also be expected that the response function should be sigmoidal, as the indices have been designed to reflect normal psychophysical threshold behaviors. Where there is no difference in observer metamerism index between MPD and three-channel system, the preference to the MPD should ideally be only 50%, representing the results of observer's guessing between two choices effectively similar in appearance.

Reviewing the three options for simple observer metamerism,  $OM_x$ , the CIE2006 and Heckaman CMF sets deliver very weak apparent correlation to MPD preference. This is understandable for the CIE variant as the experiment data was collected with a fixed field-of-view and the CMF candidates represent models of variable field-of-view (and age). The Sarkar set, though, does offer some reasonably consistent trending. Figure 83 shows all four experiment results plotted together with a sigmoidal curve fit as a function of  $OM_s$ . The weakest correlation of the five candidate metamerism indices comes from the 1931 standard observer color difference results, evident for each experiment individually as well as a combined plot, Figure 84. Sarkar-based observer variability,  $OM_{s,var}$ , is also a weak correlation, though this is somewhat expected as overall CMF population variability should not necessarily be directly relevant to the task of a forced-choice color match selection.

The 75% JND for preference to the MPD versus the three-channel systems compared in these experiments is an  $OM_s$  of 2.4. Composite plot sigmoidal trend lines for  $OM_c$  and  $OM_h$  yield significantly less definitive trending and are not shown here. This is particularly interesting as conclusions drawn using the particular indices were very similar to Sarkar-based indices modeled in Chapter 6. The present results suggest that the more explicit prediction of observer behavior is not as well correlated with CMF populations designed from those two vision models. No attempt was made to model MPD preference versus simple 1931 standard observer  $\Delta E_{94}$  as the signals in the domain of -1 to +1 color difference units are not monotonic. The reasonable predictions afforded by the Sarkar CMF set are encouraging. This observer metamerism index holds strong potential for models of observer satisfaction with color matches in cross-media applications. However, there also appears opportunity for further refinement of vision models used and metamerism indices designed to yield stronger correlation still. Also encouraging is the significant preference for the one-projector MPD to either of the three-channel systems here. The design objective for the system is validated by these results.

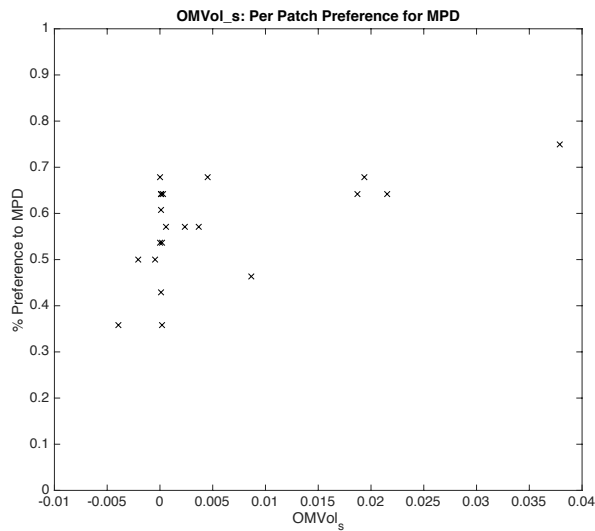
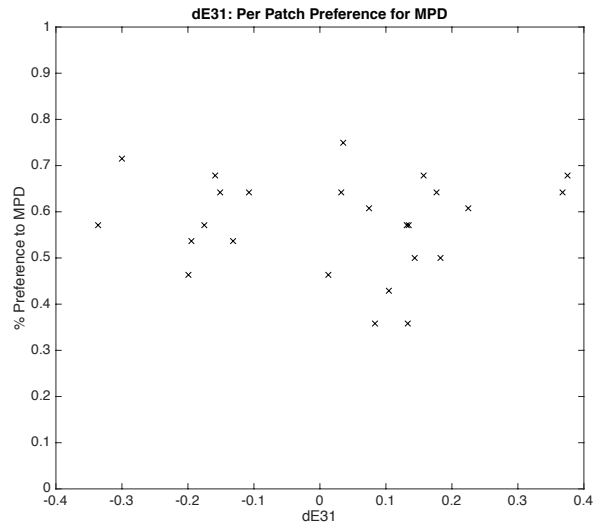
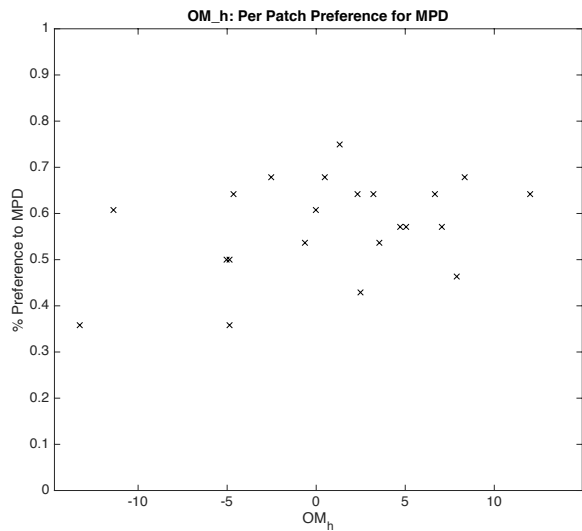
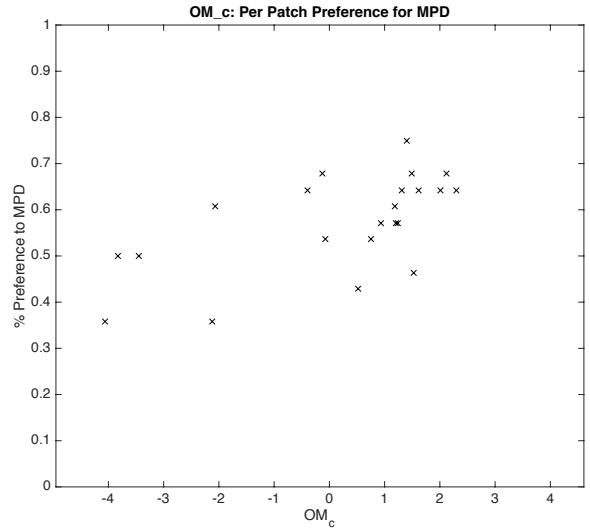
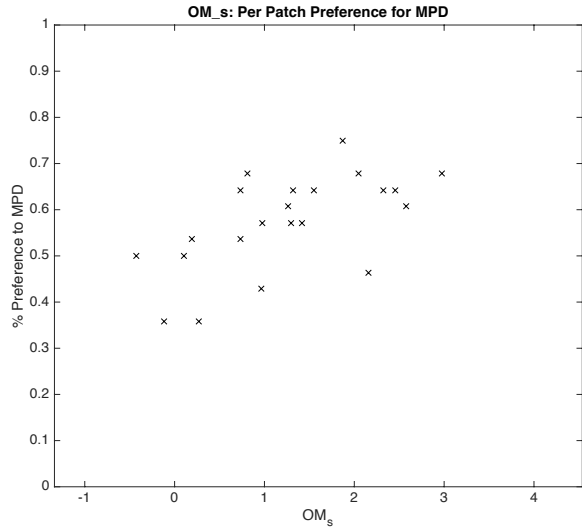


Figure 79. Measurements of forced-choice selection preferences per color patch for Experiment 1 - minimization of  $\Delta E$  versus Color-aid reference stimuli on Panasonic P3 projector and RIT MPD

Scaled against  $OM_s$ ,  $OM_c$ ,  $OM_h$ ,  $\Delta E_{94}$  (1931 2° standard observer) and  $OM_{s,var}$ , - in all cases, the numerical value shown on the x-axis is the net amount by which the color difference index for the three-channel display exceeds that for the RIT seven-channel MPD

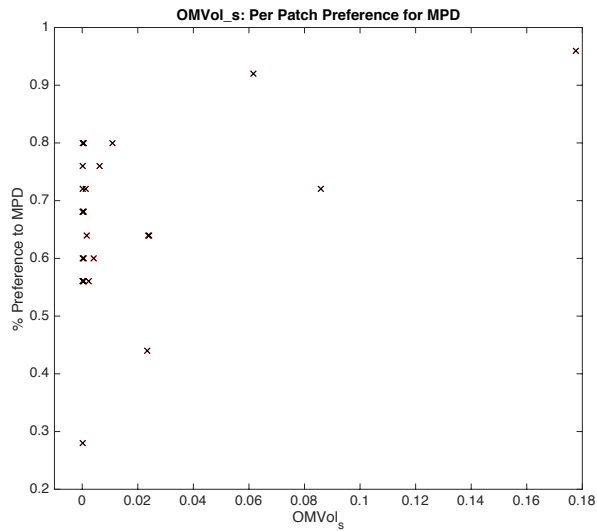
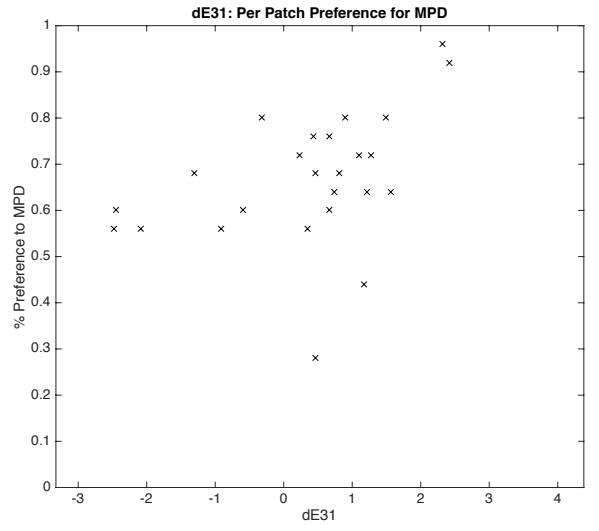
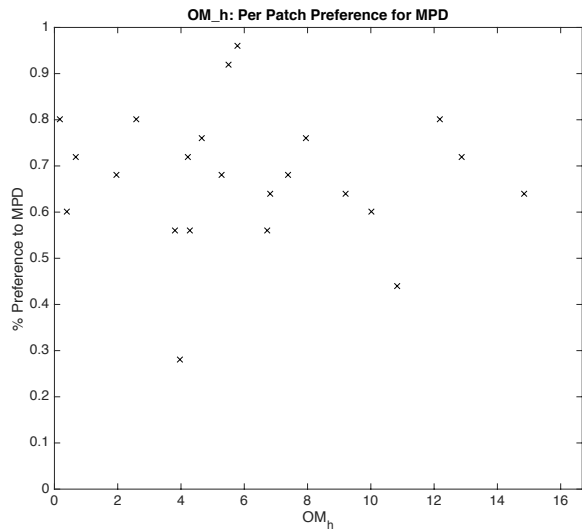
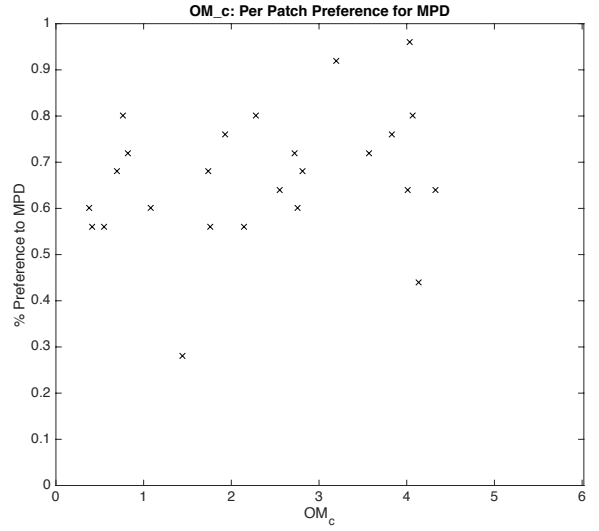
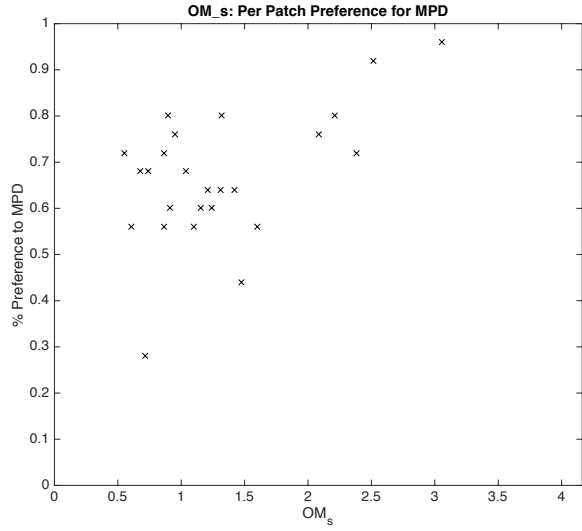


Figure 80. Measurements of forced-choice selection preferences per color patch for Experiment 2 - minimization of  $OM_s$  versus Color-aid reference stimuli on Panasonic P3 projector and RIT MPD

Scaled against  $OM_s$ ,  $OM_c$ ,  $OM_h$ ,  $\Delta E_{94}$  (1931  $2^\circ$  standard observer) and  $OM_{s,var}$ , - in all cases, the numerical value shown on the x-axis is the net amount by which the color difference index for the three-channel display exceeds that for the RIT seven-channel MPD

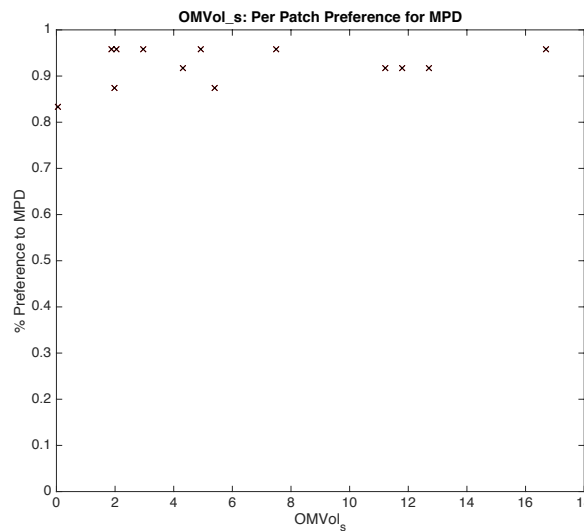
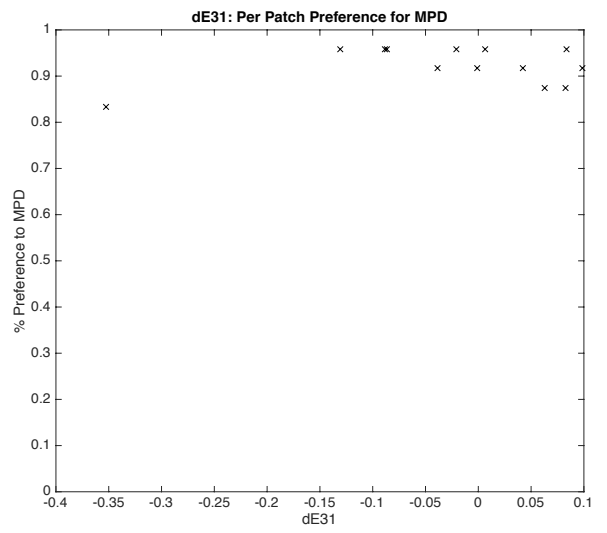
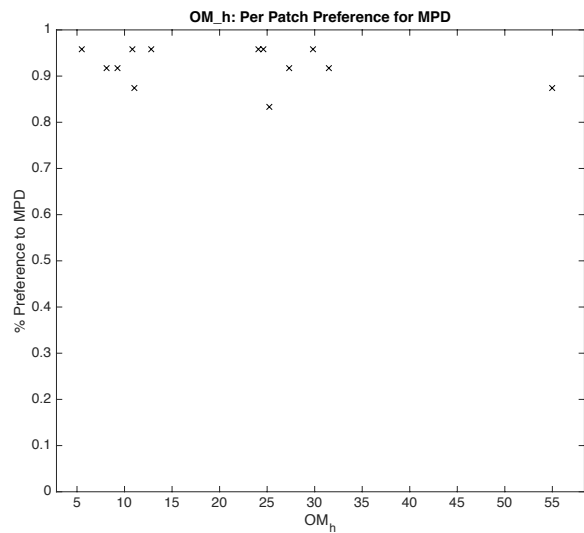
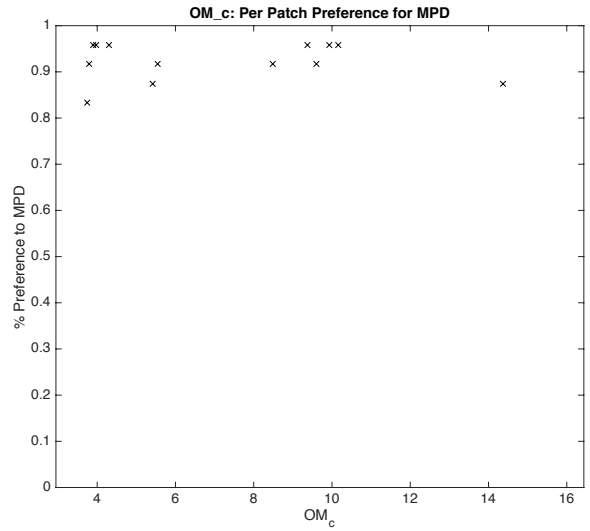
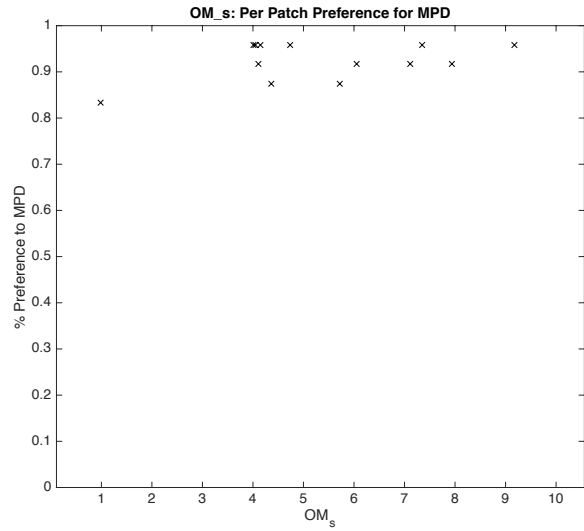


Figure 81. Measurements of forced-choice selection preferences per color patch for Experiment 3 - minimization of  $\Delta E$  versus Color-aid reference stimuli on Rec2020 Laser projector and RIT MPD

Scaled against  $OM_s$ ,  $OM_c$ ,  $OM_h$ ,  $\Delta E_{94}$  (1931 2° standard observer) and  $OM_{s,var}$ , - in all cases, the numerical value shown on the x-axis is the net amount by which the color difference index for the three-channel display exceeds that for the RIT seven-channel MPD

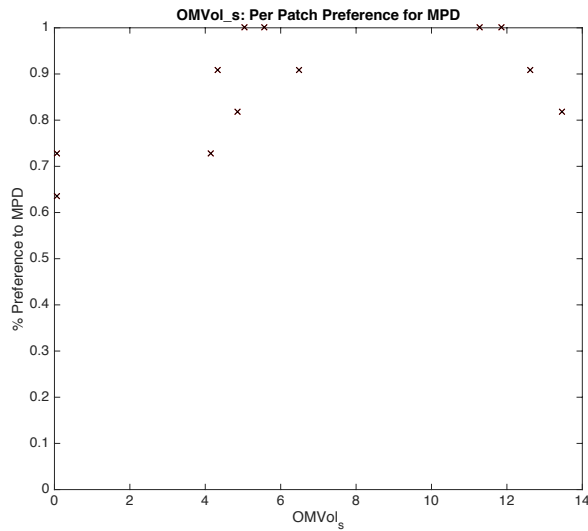
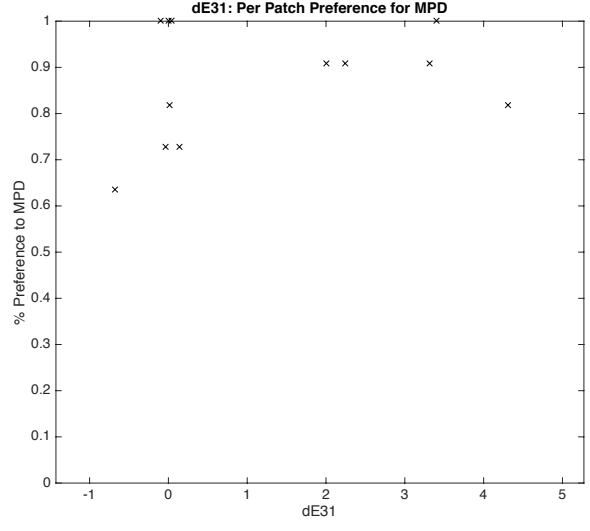
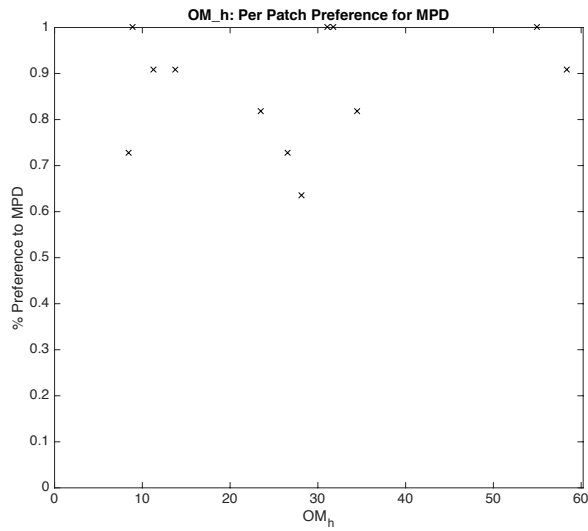
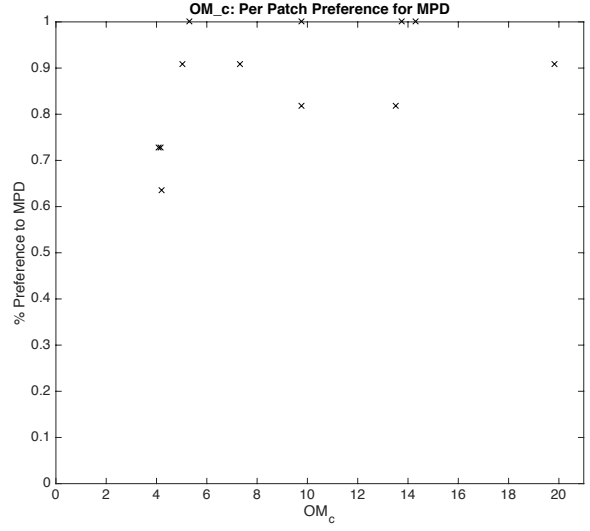
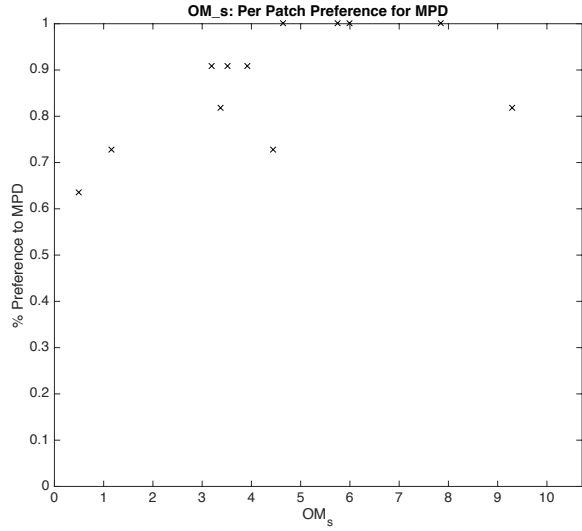


Figure 82. Measurements of forced-choice selection preferences per color patch for Experiment 4 - minimization of  $OM_s$  versus Color-aid reference stimuli on Rec2020 Laser projector and RIT MPD

Scaled against  $OM_s$ ,  $OM_c$ ,  $OM_h$ ,  $\Delta E_{94}$  (1931 2° standard observer) and  $OM_{s,var}$ , - in all cases, the numerical value shown on the x-axis is the net amount by which the color difference index for the three-channel display exceeds that for the RIT seven-channel MPD

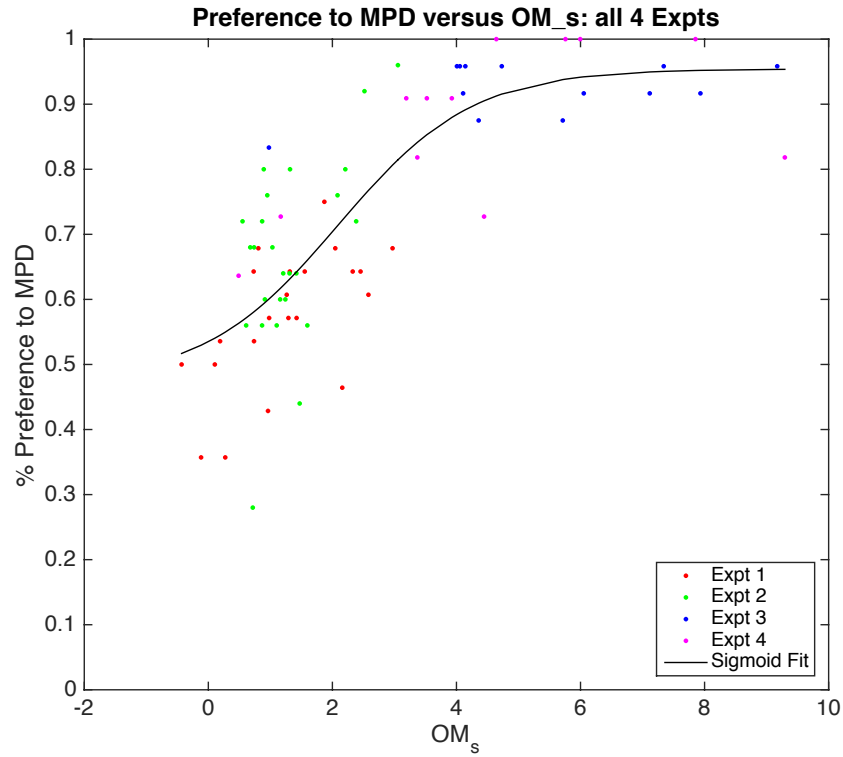


Figure 83. Combined RIT MPD selection preference from all four experiment permutations as a function of  $OM_s$

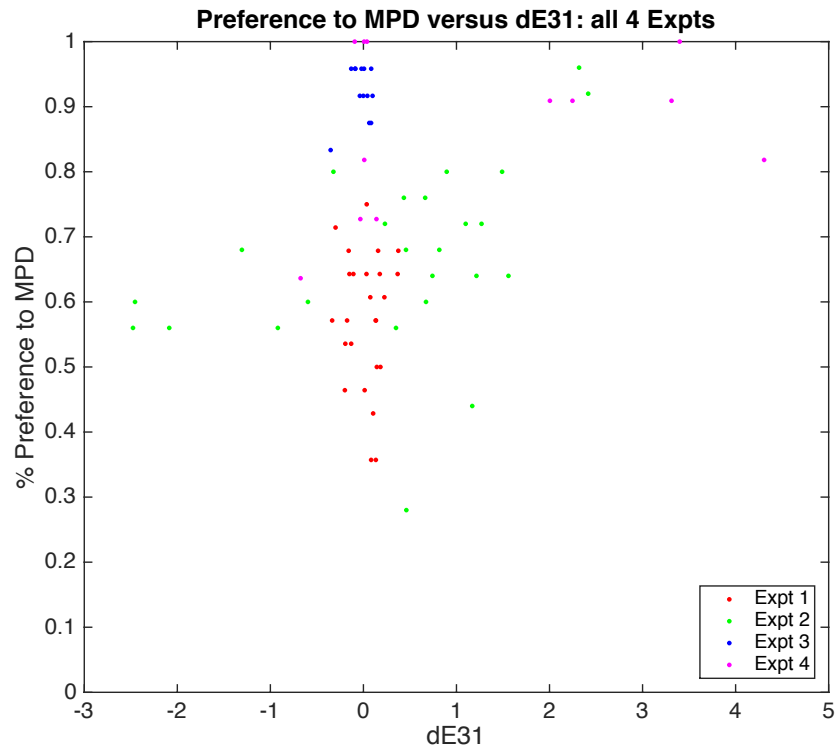


Figure 84. Combined RIT MPD selection preference from all four experiment permutations as a function of  $\Delta E_{94}$  (1931  $2^\circ$  standard observer)

## **Conclusions**

Models of observer metamerism based on CMF definitions promoted by Sarkar et al. have proven predictive of observer preference for color matching in mixed-spectra forced-choice comparisons. Further, issues of observer metamerism and variability suggested for highly monochromatic stimuli defined by ITU-R Rec. 2020 are real. Systems designed under these definitions are likely to deliver greatly exaggerated inconsistency of experience amongst cinema audiences. On the other hand, an intentionally engineered multiprimary display encompassing deliberate primary spectral design can enhance available color gamut and minimize observer metamerism in an optimized multispectral color management scheme.

## Chapter 9

---

### What We Have Learned

The evolution of digital motion picture technology has afforded tremendous advancements in image quality, content distribution and artistic options for contemporary filmmakers. For camera and display equipment, notable developments have emerged in image resolution and framerate, augmenting advancing techniques in computer-generated imagery, special effects and stereoscopic presentation. The field of color has also experienced more recent enhancements as equipment providers and creatives have both recognized the merit of expanded color gamut and improved dynamic range as tools for strengthening storytelling. But the expansion of spectral dimensionality in captured, manipulated and displayed color has garnered only minimal attention so far in the motion picture industry.

The inspiration to the preceding dissertation work follows from a single larger premise; the establishment of a full spectral workflow for motion picture applications. But for such a grand goal, smaller steps must be taken to allow for plausible and meaningful progress. Replacing the century-old paradigm of three-channel metameric color reproduction with a spectral solution is not easy. The science and engineering are difficult enough to do well. And this comes before the resulting implications to the cost, performance and viability of cinema equipment and workflows is even considered. If not for the human observer's constrained integration of visible energy into a finite number of response channels, the proper pathway for color imaging might have been spectral from the start. At the same time, simplifications from metamerism models allowed single-channel black-and-white systems to be somewhat trivially manipulated to deliver full color modulation in the earliest cinema systems. It is ironic, though understandable, that these paradigms risk restricting the consistency of the artist's intent in next-generation systems. Similarly, it is compelling that an aggressive push for bigger color in cinema may have yielded a rush to color standards which exacerbate variability in the color experience. The "more is better" approach simply cannot work if the foundational premise for universal trichromatic color in motion picture is flawed. From momentum in laser projection for the big screen to LED, quantum dots and others for the small, expanding color gamut without thinking of spectral intent and observer metamerism disregards our current understanding of diversity in natural human color vision.

This dissertation has delivered critical learning for the successful implementation of observer-invariant color in expanded gamut display. Novel contributions in four key areas summarize the ultimate value of this research.

*The saliency of emerging vision and Color Matching Function models is validated*

Contributions made show how models of human CMF variability across distributions of normal color behavior can be used to build indices of metamerism and observer variability, allowing researchers to visualize the consequence of specific spectral designs. Identification of Sarkar, et al.<sup>63</sup> CMF sets as predictive of real observer preferences in forced-choice metamerism experiments provides significant improvements beyond CIE standard observer protocols. This fundamentally challenges color calibration and color management paradigms in the cinema and television industries.

*Beware of emerging laser displays!*

This research has also shown where current trends in three-channel display towards more purely monochromatic emission risk worsening the variability of experience in rendered color content for cinema audiences. This is a significant departure from previous experiences with more traditional three-channel displays where broad spectral emission mitigated observer variability. When used to generate colorimetric matches to aim spectral stimuli under constraints of the 1931 2° observer, ITU-R Rec. 2020 laser primaries simply do not yield adequate color matches for a majority of color normal observers when contrasted with traditional broad-band multiprimary display. Motion picture colorists, cinematographers and directors should absolutely be concerned about the consistency of experience audiences can be expected to have interacting with images that have been painstakingly designed.

*Abridged MPD models can predict superior metamerism performance*

The RIT MPD designed and built for this research shows how abridged multiprimary projection can be optimized with preferred color-rendering properties to minimize failures of observer variability. The supporting optimization models conclude ideal spectral signatures as a function of primary count and permit a prediction of trade-offs between color gamut coverage and

metameric consistency. The constructed test bed will be capable of evaluating emerging color vision models, as well.

*The RIT MPD and associated Observer Metamerism indices deliver*

Finally, this research proves through practical experiments with real observers that a multiprimary display with correctly designed spectral signature does yield overwhelmingly preferred color consistency to a large-gamut laser system with only minimal sacrifice in the size of the reproducible color space. It also performs consistently better than current SMPTE431-compatible devices. Abridged multispectral system design is a feasible and reasonable stepping stone to a larger goal of full spectral color capture and display and one which carries significant value for artists in the cinema and television industries.

Multispectral imaging promises to expand useful color gamut in video applications in a controlled manner that enforces ultimate observer consistency. Extensions to application domains in visual effects, virtual cinematography, stereo cinema and enhanced creative color communication are just a few of the opportunities enabled by well designed camera and display systems and well researched observer models. Ultimately, industry demands for higher resolution, higher framerate and higher dynamic range are made in the spirit of enabling more accurate and more stunning visual experiences. Enhancing the color dimension must be an obvious objective in the same spirit of technology evolution. But a better understanding of observer variability and the demands of absolute spectral reproduction accuracy must be gained for establishing meaningful design tolerances. Otherwise, we risk chasing a spectral resolution goal based in blind specsmanship versus one rooted in meaningful science.



## Contributed Publications

The following summarizes journal publications and conference proceedings generated from this work.

### Journal Publications

“Modeling Observer Variability and Metamerism Failure in Electronic Color Displays,” *Journal of Imaging Science and Technology*, Vol. 58, Issue 3, November 2014

“Towards Higher Dimensionality in Cinema Color: Multispectral Video Systems,” *Motion Imaging Journal*, April 2013

### Conference Proceedings

“Observer Metamerism Models and Multiprimary Display Systems,” *Society of Motion Picture and Television Engineers Technical Conference*, Hollywood, CA (2015)

“Towards Standardizing a Reference White Chromaticity for High Definition Television,” *Society of Motion Picture and Television Engineers Technical Conference*, Hollywood, CA (2015) – co-author to M. Donato,

“Reducing Observer Metamerism in Wide-gamut Multiprimary Displays,” *Proc. Human Vision and Electronic Imaging*, San Francisco, CA (2015)

“Modeling Observer Variability and Metamerism Failure in Electronic Color Displays,” *Proc. Color Imaging Conference 22*, Boston, MA (2014)

“Towards Higher Dimensionality in Cinema Color: Multispectral Video Systems,” *Proc. Society of Motion Picture and Television Engineers Technical Conference*, Hollywood, CA (2012)

“Optimizing Spectral Color Reproduction in Multiprimary Digital Projection,” *Proc. Color Imaging Conference 19*, San Jose, CA (2011)

Invited Talks/Posters

“Navigating Big Color,” *Technology Summit on Cinema at NAB2015*, Las Vegas, NV (2015)

“Multispectral Digital Projection,” Rochester Institute of Technology College of Imaging Arts and Sciences Research Symposium, Rochester, NY (2014)

“Multispectral Video Capture,” *National Association of Broadcasters Trade Show*, Las Vegas, NV (2012)

“Multispectral Video Display and Observer Metamerism,” *National Association of Broadcasters Trade Show*, Las Vegas, NV (2011)

# Epilogue

---

## Potential Future Work

The constructed MPD system described in this dissertation should afford several opportunities for advanced application testing relative to typical cinema post-production workflows. There is also the issue of building the other components for a full multispectral imaging chain for motion picture content, including capture and post-processing. A summary of applicable color science questions and potential experiments for work beyond the defined research objectives of Chapter 2 permits a look into future directions in these topics.

First and foremost, there remains potential for revisiting statistical correlation between observer metamerism indices and psychophysical data summarized in Chapter 8. Some newer color vision models have emerged during the course of this dissertation work and deserve consideration. Asano, et al.<sup>88</sup>, for example, have built upon the work of Heckaman, et al.<sup>76</sup> with focus on observer classification and refined physiological modeling. Other models, too, are likely to surface as additional researchers offer their contributions.

And then there are specific industry-relevant experiments that may be beneficial in expanding the scope of observer variability research. As an example, current trends in enhanced colorimetric gamut in newer display devices offer viewers colors not previously experienced in cinema presentation. Presumably an enhanced spectral gamut from the inclusion of greater than three primaries with ancillary colorimetric gamut improvements does likewise. Identifying which generates a stronger value proposition when considering spectral accuracy and observer metamerism trade-offs is important and the answers may be different for content producers versus content consumers. Specifically, an artist who demands their work be interpreted in a certain way considering color may find merit in color correction systems that enforce spectral match and a reduction of observer metamerism. Or a consumer who seeks maximum color impact, regardless of the author's intent, may prefer the most saturated primaries available. These topics hit specifically on issues of encoding-referred versus output-referred color management. And, of course, manufacturers and standards bodies such as SMPTE will be concerned with system design complexity and the potential bandwidth overhead of the multispectral paradigm. With so many bits in the stream dedicated to pixel count and framerate, what room should be saved for color?

Second, as stated previously, a majority of spectral imaging research in the literature focuses on fully accurate reproduction of original stimuli. Giorgianni and Madden<sup>64</sup> have derived extensive system tone and color treatments that must be included to maintain appearance when viewing environment varies between capture and display. Adjustments are made for chromatic adaptation, absolute luminance level, system dynamic range and surround luminance factors among others. Consideration of these understood color appearance phenomena from a spectral perspective should be incorporated into algorithmic approaches for spectral rendering if the imaging systems are to be accepted for cinema applications. Further, observer metamerism paradigms may be relaxed when the intent of an artistic cinema workflow is to intentionally perturb reality. Practical comparison of content mastered on a traditional three-channel display and matched by wide gamut and multispectral systems can explicitly address the metamerism issue in the cinema post-production workflow where corrected color rather than scene color becomes the aim.

Finally, detectability thresholds in observer metamerism for the multispectral imaging system versus the traditional RGB systems provide for interesting study. Some color mastering workflows in cinema demand side-by-side metamerism be controlled while typical exhibition scenarios generate only single stimulus evaluations. Understanding observer behaviors in both modalities can quantify the issues of control demanded of new system designs, especially with the added dimension of high temporal variability in typical motion content.

Table 21 summarizes multispectral imaging chain components, color science questions and a select few experiments which are considered of interest in the continuation of this research.

Table 21. Advanced application questions and experiments

<p><b>Additional Spectral Imaging Chain Components</b></p>	<ul style="list-style-type: none"> <li>- Robust multispectral video capture systems built around paradigms of exact spectral estimation or minimized observer metamerism</li> <li>- Efficient image processing for rendering captured content to observer-invariant MPDs, including gamut mapping and management of rendering intent</li> <li>- Image compression and storage for high bandwidth spectral or multiprimary video streams; including focus on effective PCS paradigms</li> <li>- Spectral color correction tools for creative perturbation of captured multispectral content</li> </ul>
<p><b>Color Science Questions</b></p>	<ul style="list-style-type: none"> <li>- How do other emerging CMF models (such as from Asano, et al.) complement the studied work of CIE2006, Sarakar, et al. and Heckaman, et al.? Can refined metamerism indices yield even stronger correlation to collected data?</li> <li>- What is the general display preference of <math>K'</math>-channel multispectral imaging systems with reduced observer metamerism versus traditional three-channel wide gamut video systems (artists vs consumers, etc.)?</li> <li>- How does observer metamerism manifest in the context of artistic intent in color correction (what is level of concern for observer metamerism when accurate match to a real scene object isn't the objective)?</li> <li>- How should white balancing and color appearance phenomena be accommodated in spectral imaging workflows?</li> <li>- What is the single stimulus versus side-by-side detectability of observer metamerism for motion content and subsequent ramifications in above questions?</li> </ul>
<p><b>Example Application Experiments</b></p>	<ul style="list-style-type: none"> <li>- Perform visual observer metamerism experiments for three-channel wide gamut versus multispectral display system for goal of preferred color reproduction of high chroma imagery</li> <li>- Perform visual preference experiments for three-channel wide gamut versus multispectral display system for goal of accurate color reproduction of SMPTE431-based artistic content</li> <li>- Assess magnitude of observer metamerism as a function of viewing paradigm, single stimulus versus side-by-side</li> </ul>

# References

---

- <sup>1</sup> C Clark, D Stump, "The Status of Cinematography Today," SMPTE Motion Imaging Journal, September 2011
- <sup>2</sup> RS Berns, "The Science of Digitizing Paintings for Color-Accurate Image Archives: A Review," Journal of Imaging Science and Technology, July/August 2001
- <sup>3</sup> K Tomizawa, A Yoshida, K Nakamura, Y Yoshida, "QuintPixel: Multi-primary Color Display Systems," Proc. SIGGRAPH 2010 Emerging Technologies
- <sup>4</sup> D Hutchinson, "Introducing BrilliantColor Technology," Texas Instruments white paper
- <sup>5</sup> T Ajito, T Obi, M Yamaguchi, N Ohyama, "Expanded Color Gamut Reproduced by Six-Primary Projection Display," Proc. SPIE 3954, 130-137 (2000)
- <sup>6</sup> T Ajito, T Obi, M Yamaguchi, N Ohyama, "Multiprimary color display for liquid crystal display projectors using diffraction grating," Opt. Eng. **38**(11) (1999)
- <sup>7</sup> O Alexander et al. "Creating a Photoreal Digital Actor : The Digital Emily Project," IEEE European Conference on Visual Media Production (CVMP), Nov. 2009
- <sup>8</sup> M Fairchild, D Wyble, "Mean observer metamerism and the selection of display primaries," Proc. CIC15 (2007)
- <sup>9</sup> B Hill, "Color capture, color management and the problem of metamerism: does multispectral imaging offer the solution?" SPIE Vol 3963 (2000)
- <sup>10</sup> C Poynton, "Digital Video and HDTV: Algorithms and Interfaces," 2<sup>nd</sup> ed., Ch. 26, Morgan Kaufman (2012)
- <sup>11</sup> CIE, "Fundamental Chromaticity Diagram with Physiological Axes – Part 1," CIE Pub. 170-1:2006
- <sup>12</sup> M Yamaguchi, H Haneishi, H Fukuda, J Kishimoto, H Kanazawa, M Tsuchida, R Iwama, N Ohyama, "High-fidelity video and still image communication based on spectral information: Natural Vision system and its applications," SPIE Vol. 6062
- <sup>13</sup> K Ohsawa, T Ajito, Y Komiya, H Fukuda, H Haneishi, M Yamaguchi, N Ohyama, "Six Band HDTV Camera System for Spectrum-based Color Reproduction," Journal of Imaging Science and Technology, 48, 2 (2004)
- <sup>14</sup> M Pointer, "The gamut of real surface colours," Color Res. And Appl. 5, 3 (1980)
- <sup>15</sup> J Tajima, "Development and Analysis of 'Standard Object Color Space' Database (SOCS)," Proc. Of International Symposium on Multispectral Imaging and Color Reproduction for Digital Archives, Chiba, Japan (1999)
- <sup>16</sup> M Yamaguchi, M Mitsui, R Iwama, H Haneishi, N Ohyama, "Real-time video production using six-band HDTV camera and six-primary display," Proc. CIC12 (2004)
- <sup>17</sup> R Iwama, M Mitsui, M Yamaguchi, H Haneishi, N Ohyama, "Real-time multispectral and multiprimary video system," Proc. AIC '05

- 
- <sup>18</sup> M Yamaguchi, T Teraji, K Ohsawa, T Uchiyama, H Motomura, Y Murakami, N Ohya, "Color image reproduction based on the multispectral and multiprimary imaging: Experimental evaluation," SPIE Vol. 4663 (2002)
- <sup>19</sup> K Ohsawa, H Fukuda, Y Komiya, M Yamaguchi, N Ohya, "Spectrum-based color reproduction system for motion picture," SPIE Vol. 5008 (2003)
- <sup>20</sup> X Cao, H Du, X Tong, Q Dai, S Lin, "A Prism-Mask System for Multispectral Video Acquisition," IEEE Transactions on Pattern Analysis and Machine Intelligence (2011)
- <sup>21</sup> X Cao, X Tong, Q Dai, S Lin, "High Resolution Multispectral Video Capture with a Hybrid Camera System," IEEE Conference on Computer Vision and Pattern Recognition (2011)
- <sup>22</sup> J Hardeberg, H Brettel, F Schmitt, "Spectral characterization of electronic cameras," Proc. SPIE 3409 (1998)
- <sup>23</sup> J Hardeberg, "Filter Selection for Multispectral Color Image Acquisition," Proc. PICS Conference (2003)
- <sup>24</sup> PD Burns, RS Berns, "Image Noise and Colorimetric Precision in Multispectral Image Capture," Proc. CIC6 (1998)
- <sup>25</sup> RS Berns, LA Taplin, M Nezamabadi, Y Zhao, "Modification of a Sinarback 54 Digital Camera for Spectral and High-Accuracy Colorimetric Imaging: Simulations and Experiments," Rochester Institute of technology, Munsell Color Science Laboratory Technical Report (2004)
- <sup>26</sup> G Novati, P Pellegrini, R Schettini, "Selection of filters for multispectral acquisition using the Filter Vector Analysis Method," Proc. SPIE 5293 (2003)
- <sup>27</sup> J Tajima, M Tsukada, Y Miyake, H Haneishi, N Tsumura, M Nakajima, Y Azuma, T Iga, M Inui, N Ohta, N Ojima, S Sanada, "Development and Standardization of a Spectral Characteristics Database for Evaluating Color Reproduction in Image Input Devices," Proc. SPIE 3409 (1998)
- <sup>28</sup> O Kohonen, J Parkkinen, T Jaaskelainen, "Databases for Spectral Color Science," Color Research & Application, 31,5 (2006)
- <sup>29</sup> M Mohammadi, M Nezamabadi, RS Berns, LA Taplin, "A Prototype Calibration Target for Spectral Imaging," Proc. AIC '05 (2005)
- <sup>30</sup> M Mohammadi, M Nezamabadi, RS Berns, LA Taplin, "Spectral Imaging Target Development Based on Hierarchical Cluster Analysis," Proc. CIC12 (2004)
- <sup>31</sup> P Pellegrini, G Novati, R Schettini, "Training Set Selection for Multispectral Imaging Systems Characterization," Journal of Imaging Science & Technology, 48, 3 (2004)
- <sup>32</sup> R Schettini, G Novati, P Pellegrini, "Training set and filter selection for the efficient use of multispectral acquisition systems," Proc. CGIV (2004)
- <sup>33</sup> WK Pratt, CE Mancill, "Spectral estimation techniques for the spectral calibration of a color image scanner," Applied Optics, 15,1 (1976)
- <sup>34</sup> Y Murakami, T Obi, M Yamaguchi, N Ohya, "Nonlinear estimation of spectral reflectance based on Gaussian mixture distribution for color image reproduction," Applied Optics, 41, 23 (2002)

- 
- <sup>35</sup> P Urban, MR Rosen, RS Berns, "Spectral image reconstruction using an edge preserving spatio-spectral Wiener estimation," *J. Opt. Sci Am.*, 26, 8 (2009)
- <sup>36</sup> MJ Vrehl, HJ Trussell, "Color Correction Using Principal Components," *Col. Res. and App.*, 17, 5 (1992)
- <sup>37</sup> Y Zhao, RS Berns, "Image-based Spectral Reflectance Reconstruction Using the Matrix R Method," *Col Res & App*, 32, 5 (2007)
- <sup>38</sup> D Long and C Mondiek, "Towards Higher Dimensionality in Cinema Color: Multispectral Video Systems," *SMPTE Motion Imaging Journal*, April 2013
- <sup>39</sup> T Ajito, T Obi, M Yamaguchi, N Ohya, "Expanded color gamut reproduced by six-primary projection display," *SPIE Vol. 3954* (2000)
- <sup>40</sup> D Nystrom, "Multispectral Color Reproduction Using DLP," thesis, Linkopings Universitet (2002)
- <sup>41</sup> DC Hutchison, "Introducing BrilliantColor Technology," Texas Instruments DLP Division white paper
- <sup>42</sup> K Tomizawa, A Yoshida, K Nakamura, Y Yoshida, "Quintapixel: Multiprimary Color Display Systems," *Proc. SIGGRAPH* (2010)
- <sup>43</sup> T Ajito, T Obi, M Yamaguchi, N Ohya, "Multiprimary color display for liquid crystal display projectors using diffraction grating," *Opt Eng*, 38, 11 (1999)
- <sup>44</sup> T Ajito, K Ohsawa, T Obi, M Yamaguchi, N Ohya, "Color Conversion Method for Multiprimary Display Using Matrix Switching," *Optical Review*, 8,3 (2001)
- <sup>45</sup> H Motomura, "Color conversion for a multiprimary display using linear interpolation on equi-luminance plane method (LIQUID)," *Journal of the SID*, 11, 2 (2003)
- <sup>46</sup> F Konig, K Ohsawa, M Yamaguchi, N Ohya, B Hill, "A Multiprimary Display: Optimized Control Values for Displaying Tristimulus Values," *Proc. PICS* (2002)
- <sup>47</sup> H Kanazawa, M Mitsui, M Yamaguchi, H Haneishi, N Ohya, "Color conversion for multi-primary displays using a spherical average method," *Proc. CIC12*
- <sup>48</sup> D Kang, Y Kim, Y Cho, K Park, W Choe, Y Ha, "Color decomposition method for multi-primary display using 3D-LUT in linearized LAB space," *SPIE Vol. 5667* (2005)
- <sup>49</sup> Y Murakami, J Ishii, T Obi, M Yamaguchi, N Ohya, "Color conversion method for multi-primary display for spectral color reproduction," *J. Electronic Imaging*, 13,4 (2004)
- <sup>50</sup> T Uchiyama, M Yamaguchi, N Ohya, H Haneishi, "A Visual Evaluation of the Image Reproduced on a Multiprimary Display by Color Decomposition Based on Spectral Approximation," *J. of Imaging Science & Technology*, 49, 4 (2005)
- <sup>51</sup> B Hill, "Optimization of Total Multispectral Imaging Systems: Best Spectral Match versus least Observer Metamerism," *SPIE Vol. 4421* (2002)
- <sup>52</sup> D Tzeng, R Berns, "A Review of Principal Component Analysis and Its Applications to Color Technology," *Color Research and Application*, April 2005

- 
- 53 F Imai, R Berns, D Tzeng, "A Comparative Analysis of Spectral Reflectance Estimated in Various Spaces Using a Trichromatic Camera System," *Journal of Imaging Science and Technology*, July/August 2000
- 54 G Wyszecki, "Psychophysical investigation of relationship between normal and abnormal trichromatic vision," *Farbe* 1953:2:39-52
- 55 G Wyszecki, W Stiles, "Color Science," 2<sup>nd</sup> ed., Ch. 3, Wiley-Interscience (2000)
- 56 M Vrehl, R Gershon, L Iwan, "Measurement and Analysis of Object Reflectance Spectra," *Color Res & App*, 19 No.1 (1991)
- 57 D Long and MD Fairchild, "Optimizing Spectral Color Reproduction in Digital Projection," *Proc. CIC19* (2011)
- 58 F Konig, K Ohsawa, M Yamaguchi, N Ohya, B Hill, "A multiprimary display: discounting observer metamerism," *SPIE* 4421 (2002)
- 59 K Ohsawa, F Konig, M Yamaguchi, N Ohya, "Multiprimary display optimized for CIE1931 and CIE1964 Color matching functions," *SPIE* 4421 (2002)
- 60 A Sarkar, L Blonde, P Le Callet, F Autrusseau, P Morvan, J Stauder, "Toward Reducing Observer Metamerism in Industrial Applications: Colorimetric Observer Categories and Observer Classification," *Proc. CIC18* (2010)
- 61 A Sarkar, F Autrusseau, F Vienot, P LeCallet, L Blonde, "From CIE2006 Model to Improved Age-Dependent and Average Colorimetric Observers"
- 62 MD Fairchild, "Modeling Observer Metamerism through Monte Carlo Simulations," *OSA Annual Meeting, Rochester, NY*, 126 (1996)
- 63 M Fedutina, A Sarkar, P Urban, P Morvan, "(How) Do Observer Categories Based on Color Matching Functions Affect the Perception of Small Color Differences?"
- 64 E Giorgianni and T Madden, "Digital Color Management," 2<sup>nd</sup> ed., Ch. 4, Addison-Wesley (1998)
- 65 T Uchiyama, M Yamaguchi, H Haneishi, N Ohya, "A Method for the Unified Representation of Multispectral Images with Different Number of Bands," *J. of Imaging Science and Technology*, 48, 2 (2004)
- 66 L Ma, Z Shi, X Tang, "Lossless Compression of Multispectral Images using Spectral Information," *SPIE* 7494 (2009)
- 67 K Shinoda, Y Murakami, M Yamaguchi, N Ohya, "Lossless and lossy coding for multispectral image based on sRGB standard and residual components," *J. of Electronic Imaging*, 20, 2 (2011)
- 68 EA Day, L Taplin and RS Berns, "Colorimetric Characterization of a Computer-Controlled Liquid Crystal Display," *Col. Res. & App.*, 29,5 (2004)
- 69 R Alfvén and MD Fairchild, "Observer Variability in Metameric Color Matches Using Color Reproduction Media," *Col. Res. & App.*, 22,3 (1997)
- 70 D Wyble, RS Berns, "A Critical Review of Spectral Models Applied to Binary Color Printing," *Col. Res. & App.*, 25,1 (2000)

- 
- <sup>71</sup> WS Stiles and JM Burch, "NPL Color Matching Investigation: Final Report," *Optica Acta* 6, 1-26 (1959)
- <sup>72</sup> NI Speranskaya, "Determination of Spectrum Colour Coordinates for 27 Normal Observers," *Optics Spectrosc.* 7, 424-428 (1959)
- <sup>73</sup> CIE, "Special Metamerism Index: Change in Observer," CIE Pub. No. 80, Vienna (1989)
- <sup>74</sup> RS Berns, "Billmeyer and Saltzman's Principles of Color Technology," 3<sup>rd</sup> ed., Ch. 2 (2000)
- <sup>75</sup> P Morvan, A Sarkar, J Stauder, L Blondé, J Kervec and SK Hasan, "A Handy Calibrator for Color Vision of a Human Observer", IEEE International Conference on Multimedia and Expo (ICME), Barcelona, 2011
- <sup>76</sup> MD Fairchild and RL Heckaman, "Metameric Observers: A Monte Carlo Approach,": Proc. CIC21 (2013)
- <sup>77</sup> J Pokorny, VC Smith and M Lutze, "Aging of the Human Lens," *Applied Optics* 26, 1437-1440 (1987)
- <sup>78</sup> J Pokorny and VC Smith, "How Much Light Reaches the Retina?" in C.R. Cavonius (ed), *Colour Vision Deficiencies XIII, Documenta Ophthalmologica Proceedings Series*, 59, 491-511 (1997)
- <sup>79</sup> J Xu, J Pokorny, and VC Smith, "Optical Density of the Human Lens," *JOSA A* 14, 953-960 (1997)
- <sup>80</sup> RA Bone, JT Landrum and A Cains, "Optical Density Spectra of the Macular Pigment in Vivo and in Vitro," *Vision Research* 32, 105-110 (1992)
- <sup>81</sup> TT Berendschot and D van Norren, "Objective Determination of the Macular Pigment Optical Density Using Fundus Reflectance Spectroscopy," *Archives of Biochemistry and Biophysics* 430, 149-155 (2004)
- <sup>82</sup> A Stockman, LT Sharpe and CC Fach, "The Spectral Sensitivity of the Human Short-wavelength Cones," *Vision Research* 39, 2901-2927 (2000)
- <sup>83</sup> "Stockman and Sharpe Cone Fundamentals, 2-deg Fundamentals Based on Stiles and Burch 10-deg CMFs Adjusted to 2-deg," CVRL Functions, [www.cvrl.org](http://www.cvrl.org)
- <sup>84</sup> M Neitz and J Neitz, "Molecular Genetics of Color Vision and Color Vision Defects," *Arch Ophthalmol* Vol. 118, 691-700 (2000)
- <sup>85</sup> D Long and MD Fairchild, "Modeling observer variability and metamerism failure in electronic color displays," *J. Imaging Science and Technology* 58(3), (2014)
- <sup>86</sup> Sony Corporation White Paper, "Colour matching between OLED and CRT," v1.0, (Feb 15, 2013)
- <sup>87</sup> M Donato and D Long, "Towards standardizing a reference white chromaticity for HDTV," progress report to SMPTE ST/RP 2080 committee on measurement and calibration procedures for HDTV displays, (Nov 18, 2014)
- <sup>88</sup> Y Asano, MD Fairchild, L Blonde and P Morvan, "Observer Variability in Color Matching on a LCD monitor and a Laser Projector," Proc. CIC22 (2014)